Mechanistic Evaluation of Sulphide Scale Formation in the Oilfield

A thesis by

OKOCHA EMEKA CYRIL

Submitted for the Degree of

Doctor of Philosophy

Institute of Petroleum Engineering
Heriot Watt University
Edinburgh UK

March 2011

ABSTRACT

Scale deposits, such as more conventional sulphate and carbonate scales, impair oil and gas production and lead to problems such as production loss, equipment failure and additional expenditure. However, more recently the occurrence of sulphide scales (e.g. FeS, ZnS and PbS) is increasingly being reported. The mechanisms of formation and inhibition of sulphide scales in oilfield systems are not yet fully understood. This thesis presents a modelling, methodological and mechanistic study of sulphide scale (FeS, ZnS, PbS) formation and inhibition. A number of specific aspects relating to sulphide scaling are studied in this thesis, as follows: (i) Sulphide scale formation and the related mechanisms of inhibition by chemical scale inhibitors; (ii) the effects of commercial scale inhibitors (e.g. PPCA, DETPMP and other blends) on sulphide and mixed scale formation; (iii) the effect of THPS as a sulphide scale dissolver and the additional effect of brine composition (Ca^{2+} and Mg^{2+}) on its performance; (iv) the effect of scale inhibitors on the morphology of both $BaSO_4$ and $CaCO_3$ when co-precipitated with sulphide scales; (v) the effect of scale inhibitors on mixed sulphide scaling (e.g. ZnS/PbS etc.); (vi) a sulphide prediction model was also developed which gives a description of the sulphide precipitation interactions and this was tested against experiment.

These various experimental studies were carried out using an integrated combination of techniques such as a modified static bottle tests (performed in an anaerobic apparatus for some cases to avoid Fe^{2+} oxidation), dynamic static tests, particle size analysis, inductively coupled plasma (ICP), scanning electron microscopy (SEM) and energy dispersive X-ray analysis (EDX). These studies have enabled us to develop some new insights into the mechanisms of sulphide scale formation and inhibition in this work. For example, some of the specific contributions to the understanding of sulphide scale formation an d inhibition mechanisms, from this work are listed as follows:

- A number of predictions were made using a detailed sulphide model of experimental quantities such as final solution pH, saturation ratios (SR), mass of FeS etc. These predictions were compared directly with the experimentally measured quantities and excellent agreement has been found.
- A number of novel types of FeS inhibition behaviour have been observed and describes when treated with scale inhibitors e.g. some FeS solutions are found to become clear from black 24hrs after the scale inhibitor treatment.
- There is significant barite crystal distortion when co-precipitated with FeS, but no distortion is observed when barium sulphate co-precipitates with PbS and ZnS.
- Mg^{2+} has a profound effect on the ability of THPS to inhibit FeS and this work demonstrates that THPS is significantly enhanced by the presence of Mg^{2+} which has more effect than any other ions.
- $CaCO_3$ crystals deposit in bulk solution, rather than on the metal surface when co-precipitated with ZnS. The polymorphs of $CaCO_3$ form on the metal surface when co-precipitated with PbS.
- Mixed PbS and ZnS sulphide scale is found to be easier to inhibit than either scale individually.

ACKNOWLEDGEMENTS

I would like to start by thanking my supervisors Professor Ken Sorbie and Professor Eric Mackay for offering me the opportunity to come to Heriot-Watt University to study for this doctorate. Ken's guidance, patience, support and encouragement made this work possible. Eric deserves praise for his help in mentoring, guidance and provision of the motivation that has made my stay in Edinburgh more enjoyable.

I would like to express my sincere thanks to Petroleum Technology Development Fund of Nigeria (PTDF) for funding my PhD in Scotland. My gratitude also goes out to the FAST 3 JIP sponsors (Baker Petrolite, BP, BWA Water additives, Champion Technologies, Chevron, Clariant oil services, Conoco-Phillips, Halliburton, MI Swaco, Nalco, Petrobras, Petronas, REP, Rhodia, Saudi Aramco, Shell, Statoil Hydro and Total) for their input, financial support and the provision of samples for my research.

Many thanks go to the following people, Lorraine Boak for her guidance in the laboratory especially with the ICP, Dr Jim Buckman for his help in obtaining ESEM/EDAX images and data from the spindles and filter papers "*smellys*". I also would like to acknowledged Robin Shields and Mike Singleton for their help with the Malvern particle size analyzer. I will also like to thank Tom Clark and Thomas McGravie for their expertise in manufacturing and installing the Dynamic Static Vessel and other help in the laboratory.

My colleagues in the flow assurance and scale team (FAST) thanks for the company and great times we spent together they will be cherished. Heather O'Hara thanks for the administrative help.

Many thanks to my good friends, without whom life would be dull during the last three years: Craig Kerr, Miguel Freitas, Onos Iboje, Enrique Ibanez Iglesias, Sonia Marie Montero.

Special thanks go to my parents, brothers and sisters who encouraged and supported me throughout my stay in Europe.

Finally to my brother Rev Ray Okocha whose energy and thirst for knowledge I have surfed on for so many years "Daalu".

Dedication

To my Mother Lady Theresa Egondi Okocha

TABLE OF CONTENTS

LIST OF FIGURES

LIST OF TABLES

NOMENCLATURE AND ABBREVIATIONS

Quantities shown without units are dimensionless

Abbreviation	Meaning
a	Ionic activity / mol dm^{-3}
At%	Atomic percentage
DETPMP	Diethyltriaminepentakis(methyl phosphonic) acid
EDTA	Ethylenediaminetetra acetic acid
EDX	Energy-dispersive X-ray Spectroscopy
ESEM	Environmental Scanning Electron Microscope
Fe	Iron
FeS	Iron Sulphide
FW	Formation Water
G	Gibbs free energy / Joules mol^{-1}
g	Grammes
H_2S	Hydrogen Sulphide
ICP	Abbreviation of ICP-AES
ICP-AES	Inductively Coupled Plasma Atomic Emission Spectroscopy
IE	Inhibition Efficiency
k	Rate constant / $hours^{-1}$ or $hours^{-½}$ as indicated in the text
K	Dissociation Constant (equivalent to complexation constant)
K_{sp}	Solubility Product / mol^2 dm^{-6}
Kw	Ionic product of water

M	Moles per litre
m	Mass / grammes or metre (depending on context, as specified in the text)
MIC	Minimum inhibitor concentration / ppm
ml	Millilitres
μm	Micrometre
Mol	Moles
O_2	Oxygen
^oC	Degrees Celsius
P	Pressure
PbS	Lead Sulphide
pH	Potential of hydrogen, the absolute value of base-ten logarithm of the hydrogen ion activity in solution
pK_a	Absolute value of base-ten logarithm of acid dissociation constant
pK_c	Absolute value of base-ten logarithm of complexation constant
PPCA	Phosphino-polycarboxylic acid
ppm	Parts per million (weight / volume unless otherwise stated)
PQ	Performance Quotient
PVS	Poly Vinyl Sulphide
SI	Scale Inhibitor
SEM	Scanning Electron Microscope
SW	Sea Water
T	Temperature / ^oC unless stated as ^{o}Kelvin in the text
t	Time / Hours
THPS	Tetrakis (hydroxymethyl) phosphonium sulphate

Vs-Co	Poly (vinyl sulphonate ethyl acrylate)
W%	Weight Percentage
ZnS	Zinc Sulphide
%	Percentage
[]	Concentration in ppm

Greek Letter	**Meaning**
Γ	Amount adsorbed / mg L^{-1}
γ	Surface excess free energy / joules mol^{-1}
$\gamma_{\pm}$	Ionic activity coefficent
Δ	Difference in a quantity
ε	Electrical permittivity /
ζ	Zeta Potential / mV
η	Viscosity / centipoise
θ	Bragg diffraction angle / degrees
κ	/ m^{-1}
λ	Wavelength / m
μ	Chemical Potential / Joules mol^{-1}
ρ	Density / Kg m^{-3}
σ	Surface tension / Nm^{-1}
ϕ	Fractional porosity
Ω	Ohm

Chapter 1 Introduction

Chapter 1 introduces the sulphide scale problem and discusses the various forms of sulphide scales that occur associated with oil production. It also describes the sources of the sulphide scaling ions in these systems. The introduction also briefly explains how sulphide scaling differs from corrosion, souring and fouling problems and describes how such problems may merge as flow assurance challenges. Finally, the aims and objectives of the thesis are listed and a brief outline of the thesis is given.

1.1 Background to Oilfield Scale

Oil production decline due to mineral scale formation has been a persistent problem since the early days of the oil industry until the present day. The reservoir fluids present in petroleum producing formations are water (usually a brine), gas and oil. These fluids are usually in equilibrium at the time the reservoir is discovered. However, when a new well is drilled, completed and begins to flow the natural equilibrium is disturbed and this can lead to solids depositions including scale buildup along the production system.

Typically, oilfield scales are formed from different processes including.

a) Direct precipitation from the water that occurs naturally.
b) Interaction of two incompatible waters to form scale precipitates.

Sorbie and MacKay (2007)

Scale deposits impair the production formations deep in the reservoir, and they can also block downhole completion equipment. Mineral scale can also form in the near wellbore formation causing a reduction in porosity and permeability and in top side tubulars and equipment including production tubing, valves, pumps, separators, coalescers, heat exchangers and filters. These components can be completely coated with scale leading to failure along with various associated safety concerns. This scaling problem increases greatly as deeper, higher temperature wells are being brought into production, and as more conventional reservoirs become depleted along with the associated increase in water production. When primary production (initial production of oil, possibly co-produced with gas and reservoir formation water, from a production well under its own pressure) ceases, or as the oil reservoir matures, the reservoir initial pressure drops. At this point, secondary methods (water flooding, gas injection or a mixture of both) are engaged to increase the pressure thereby producing more hydrocarbon resources. With any produced aqueous fluids, the potential to form mineral scale becomes higher. Also, as produced fluids are brought to the surface, the pressure decreases and scale formation becomes more likely since the chemical equilibrium of the fluids is disturbed. This imbalance results in the produced brines becoming supersaturated with respect to

particular minerals as the mineral solubility changes with the variation in pressure, temperature and pH in the near wellbore region and production facilities.

The most common and economical secondary recovery method is water flooding. This involves the injection of water into the reservoir to maintain well pressure and also to directly displace the oil towards the production facilities. This is frequently used in offshore facilities with the preferred injection water being seawater. The water flood process will generate a huge volume of this injected and in situ brine as produced water and, depending on the produced brine composition and the thermodynamic conditions (pressure, P and temperature, T) in the production wells, precipitation and scaling can occur.

In the petroleum industry, scale can be deposited all along the water paths from injectors through the reservoir to the surface equipment. The related scale precipitation which occurs along the pathways varies in form and quantity depending on the produced brine compositions and the T and P conditions.

Economical consequences of oilfield scale formation are serious because of the reduction in oil and gas production and the costs of scale prevention and removal, and the associated deferred oil production cost. It is estimated that more than USD1.4 billion is lost to scale annually in the US alone, Frenier (2008) It is also reported that more than 4 million bbls of production maybe lost in the UK sector of the North Sea MacKay *et al* (2003). Scale may also be a safety risk if it causes malfunctions in safety valves and other components such as inflow control devices (ICDs).

1.2 Forms of Oilfield Mineral Scales

There are four types of scales associated with oilfield production which include Inorganic scales (sulphates, carbonates, sulphides), Organic scales (Asphaltenes, waxes), gas scales (Hydrate), and Soaps (Naphthenates) as shown in Figure 1.1.

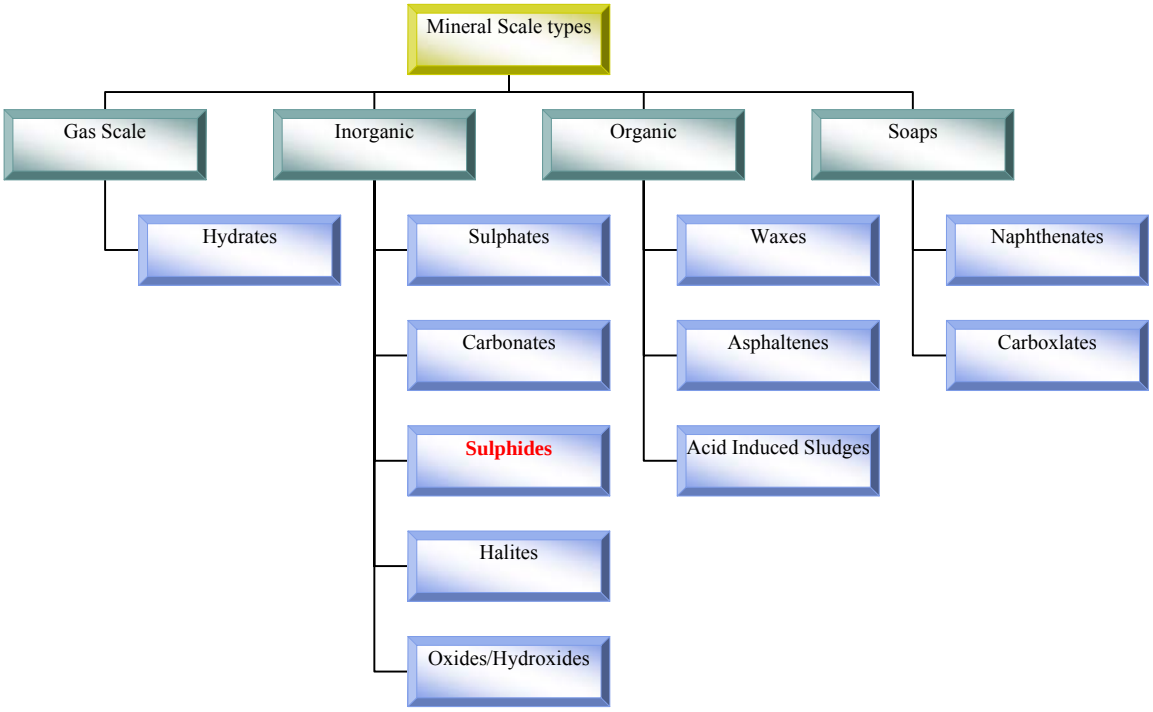

Figure 1.1 Schematic classifications of the various types of organic and inorganic 'scales' that are formed in the oilfield

1.3 Sulphide Scales Associated with Hydrocarbon Production

Sulphide scales are less common than sulphate and carbonate scales but they also cause significant production problems. Sulphide scales typically have a lower solubility than conventional sulphate and carbonate scales Przbylinski (2001). Sulphide scales are predominately iron sulphide, lead sulphide and zinc sulphide. The most common type of sulphide scale is iron sulphide. Iron forms a variety of binary compounds with sulphur in contrast to other sulphide scales (Pb, Zn) where predominantly single sulphide scales are formed. Many types of iron sulphides may form in H_2S rich environments, and these include a wide range of compounds from stoichiometric through to non stoichiometric compounds e.g. amorphous ferrous sulphide, mackinawite, cubic ferrous sulphides, smythite, greigite, pyrrhotite, troilite, and pyrite Nasr-El-Din *et al* (2001a) Nasr-El-Din *et al* (2001b) These will be discussed in more detail in Chapter 2.

Problems distinctively associated with sulphide scales in the oilfield are as follows:

- Increased frequency of corrosion failures
- Formation damage and pore plugging
- Valve and other safety equipments failure
- Reservoir souring
- Filter plugging due to the colloidal nature of some sulphides (e.g. FeS)

1.4 Sources of Sulphide Scaling Ions Associated with Oil Production.

There are several sources of iron, zinc, lead and sulphide ions in oil and gas reservoirs which lead to the formation of FeS, ZnS and PbS in these systems. The sources for Fe, Pb, and Zn ions include:

1. Reaction products of dissolution of formation minerals (Pyrite, Siderite, Sphalerite, galena) during connate and aquifer water contact during formation.
2. Dissolution of minerals (e.g. leaching of Fe^{2+}, Zn^{2+}, Pb^{2+} from rocks) by injected fresh or sea water, which is used for pressure support in the reservoir during production.
3. Ions (e.g.Zn^{2+} from Zinc Bromide, Zinc Chloride, lead oxide) from heavy brine completion fluids lost into the formation during drilling and work over operations.
4. Corrosion by-products from the production systems (e.g. Fe^{2+}, removed from metal surface) Jordan et al (2000); Collins and Jordan (2001) and Jordan *et.al* (2004).

Hydrogen sulphide gas is the most likely source of sulphide ions that result in the formation of iron, lead and zinc sulphide scale. In petroleum reservoirs, hydrogen sulphide may originate from three natural processes:

1. Bacterial sulphate reduction (BSR) that occurs at low temperatures up to 80 °C.
2. Thermal cracking of organic sulphur (decomposition of drilling compounds and corrosion inhibitors within heavy brines) compounds prevailing at higher temperatures.

3. Thermo chemical sulphate reduction (TSR) happening at temperatures exceeding 100 °C can also produce hydrogen sulphide gas or bi-sulphide ions. Mougin (2007)

Iron sulphide scale is also thought to be deposited by microbial enhanced corrosion or derived from the reaction of iron oxide from corrosion and hydrogen sulphide, a by-product of sulphate reducing bacteria (SRB) metabolism Collins and Jordan (2001).

1.5 Corrosion, Souring, Fouling and Sulphide Scale Interactions.

It is important here to distinguish between the interactions of corrosion, souring; fouling and sulphide scale deposition which, in production systems, can be closely related and one may be a precursor to another.

Corrosion is described as the destruction of a metal by chemical or electrochemical reaction with its environment American Electrochemical society (1946). The metal most commonly involved in oilfield applications is iron usually in the form of steel. Corrosion is the principal cause of damage to metals in wells and production facilities releasing [Fe^{2+}] into solution. These soluble [Fe^{2+}] reacts with components in the environment such as H_2S to form iron sulphide scale.

Souring is the presence of sulphur products particularly H_2S in association with petroleum fluids. The H_2S is generated from either a biogenic process or through an abiogenic process. The presence of H_2S in a production system can greatly accelerate corrosion in the system.

Fouling is the presence of organic or/and inorganic debris, microbial biomass, sand, corrosion products, scale and microbial materials in petroleum systems causing blockages and these can arise from both biological and non-biological sources. For example, a souring problem can easily be caused by microbial activities leading to corrosion of the steel leading to fouling conditions and sulphide scale deposition. Corrosion can occur in

the absence of H_2S leading to "sweet" CO_2 corrosion, oxygen corrosion, and electrochemical corrosion, Sulphide scales on the other hand occur mostly in the presence of H_2S. While sulphide scales mostly impair production, they can also act to help reduce or in some cases prevent the occurance of other adverse processes, for example FeS scale may in some cases act as a protective layer for steel against corrosion.

The actual mechanism of sulphide formation especially iron sulphide formation in high H_2S environments in oil production, is often quite complex. It is difficult to determine, whether the iron sulphide is formed by direct solid state reaction or precipitation or both. However, in this thesis, sulphide formation is mainly considered as a precipitation reaction from super-saturated brines.

1.6 Aim of this Thesis

The aim of this thesis is to improve our understanding of

(i) sulphide scale formation,

(ii) its interaction with other conventional scales,

(iii) its prevention, inhibition, and treatment.

There is a need to improve understanding of the sulphide scaling processes both in isolation (as single scales such as FeS or ZnS) and also in combination with other scales (barite and calcite). It is also necessary to develop better inhibitors to prevent and control sulphide deposition in oil and gas systems. This thesis touches on the sulphide scale inhibition, by investigating the behaviour of two commercially used scale inhibitors under a variety of conditions. These inhibitors, diethylenetriaminepentakis-methylphosphonic acid (DETPMP), phosphino-polycarboxylic acid (PPCA), were chosen because they represent different types of SIs (phosphones and polymers) routinely used to prevent sulphide scaling in oilfield installations. Their structures are shown in Figure 1.2. A test methodology to screen chemicals for sulphide scales is developed as part of the initial part of the study.

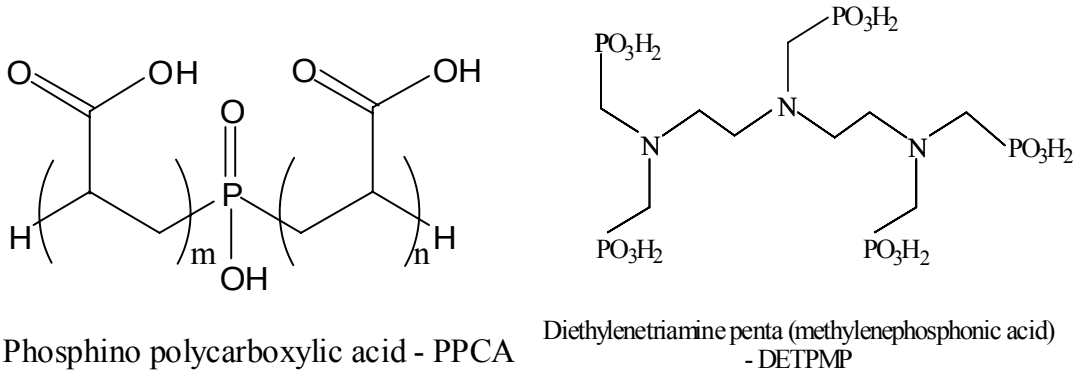

Phosphino polycarboxylic acid - PPCA

Diethylenetriamine penta (methylenephosphonic acid) - DETPMP

Figure 1.2 Structure of the PPCA and DETPMP scale inhibitors.

This thesis also explores role of stiochiometric sulphide dissolvers in complexing sulphide scale cations, the mechanisms to keep the cation in solution preventing the formation of sulphide scales. A dissolver for sulphide scales (particularly iron sulphide) is reported in this thesis in Chapter 5 and the influence of brine compositions in the complexing mechanisms. The dissolver known as Tetrakis Hydroxymethyl Phosphonium Sulphate (THPS), which has the structure shown in Figure 1.3, is discussed in detail in Chapter 5.

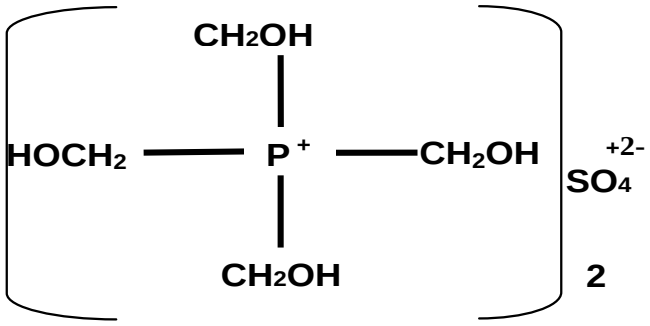

Figure 1.3 – THPS Chemical Structure

1.7 Structure of the Thesis

Chapter 1 (**Introduction)** introduces the sulphide scale problem, discusses the forms of sulphide scales that can occur and describes the sources of the sulphide scaling ions in oil production systems. How sulphide scaling differs from corrosion; souring and fouling

problems and areas where they merge as flow assurance challenges are also discussed. The aims and objectives of the thesis and a brief summary are also presented.

Chapter 2 (**Literature Review)** reviews the types of FeS/ZnS/PbS scale encountered in the oil and gas industry. The mechanism of FeS precipitation is described and a detailed review of the H_2S and solubility constants for FeS, ZnS, PbS reactions is presented. A summary of the methods for sulphide scale control in the oil and gas industry, the generic types of scale inhibitor and the mechanisms of inhibition action are given. THPS as an iron sulphide dissolver are reviewed in this chapter.

Chapter 3 (**Experimental Methods**) presents the experimental methods and procedures developed in this work and the rationale for their development. These experimental methods include a modified anaerobic static bottle test, Environmental Scanning Electron Microscopy (ESEM) application, Inductively Coupled Plasma (ICP) ion assays, Energy Dispersive X-ray analysis (EDX), particle size distribution analysis and dynamic beaker tests.

Chapter 4 (**Sulphide Modelling**) presents the complete sulphide formulation in an open sulphide model including the concentrations of sulfide species as $[H_2S]$ changes, final pH and resulting saturation ratios for the final metal sulphide (FeS).

Chapter 5 **(FeS Results)** presents results for the anaerobic static bottle test for different sulphide scale inhibitors (SIs). The performance of these sulphide inhibitors is categorized using both visual and ICP [Fe] results. Particle size measurements are also made and these results are presented for cases both with and without SI (PPCA and DETPMP). SI precipitation of [Fe] prior to FeS formation is also considered in this Chapter.

Chapter 6 **(THPS Results)** describes the dissolving/dispersing effects of THPS on [FeS]. The stability of THPS in various brine compositions is also examined. THPS performance in the presence of other sulphide scales (PbS, ZnS) is also studied, and how

inhibition is affected by mixed sulphide scales is described. This Chapter also describes the effect of $[Mg^{2+}]/ [Ca^{2+}]$ ratio on the inhibition of THPS and the influence of brine composition on THPS inhibition.

Chapter 7 **($BaSO_4$ /Sulphide Scale Interaction)** describes the morphological changes that occur in barite crystals when co-precipitated with sulphide scales. It also details the effect of two commercial scale inhibitors (PPCA and DETPMP) on barite scale, and mixed sulphide scale of FeS, ZnS and PbS.

Chapter 8 **($CaCO_3$ /Sulphide Scale Interaction)** introduces a novel dynamic beaker vessel technique to study $CaCO_3$—sulphide scale co-precipitation. This experimental approach can monitor the process of scale formation and deposition and is useful to understand the mechanism of scale formation and inhibition. $CaCO_3$ scale is formed both in the bulk solution and on the metal surface and both processes are studied and observations are reported on the morphology of scale crystal formation. The role of SI in the $CaCO_3$ crystal changes when co-precipitated with sulphide scales is also examined.

Chapter 9 **(Mixed ZnS-PbS Scales)** describes the interaction between ZnS and PbS in a mixed scaling system. Formation and inhibition mechanism for ZnS and PbS are first studied individually then together in a mixed scaling environment of distilled water (DW) and in various brine compositions.

The conclusions and recommendations for the future work are presented in Chapter 10.

Chapter 2 Literature Review

This Chapter contains a survey of published work on sulphide scales relevant to this thesis. Topics reviewed include a discussion of the solubility constants for hydrogen sulphide and sulphide scales FeS, PbS, and ZnS. Various prevention and treatment regimes for sulphide scales are also reviewed. The effects of generic and proprietary scale inhibitors on sulphide scales are reported, and the use of THPS in treating sulphide scale, especially FeS, is surveyed. This Chapter also covers the prediction of sulphide scale, the development of test methodologies, and the removal of sulphide scales both in the laboratory and the field. These studies show the difficulty in sulphide prediction, sulphide SI/dispersant product screening, sulphide treating and inhibition compared with more conventional inorganic scales.

2.1 Introduction and General Review of Sulphides Scales

The mineralogy, mineral chemistry and geological occurrence of sulphide minerals have been well researched particularly because of their economic and environmental importance. The compositional variations of the major sulphide minerals are well characterized. However, information on sulphide scale formation, prevention, control and interaction with other scales in oilfield brine is still scarce and patchy. Oilfield sulphide scales were sometimes referred to as "exotic scales", implying that they did not occur very often. However, this industry view has recently changed and sulphide scales (especially FeS) are seen as actually being quite common due to their occurrence. The literature review here deals with the parameters that influence sulphide formation and inhibition in the oil industry. Through experimental analysis and observed field studies, the fundamental theory of sulphide formation is described. Several of the most widely used methods of treatment and inhibitor performance testing for sulphides as well as some novel applied field techniques are reviewed. The importance of sulphide mineral formation in the environment as a sink for heavy metals in addition to its significance in sulphur geochemical cycle is also well reviewed. The environmental implications of sulphide in acid mine drainage (AMD) is well known, (Matlock 2002; Johnson 2005; Akcil 2006) and the industrial uses of metal sulphide in metallurgy and mining have also been widely studied (Lewis 2010).

2.2 Types of Sulphide Scales

2.2.1 Forms of Iron Sulphide

There are seven known forms of Fes that have been indentified and these ranges from stoichiometric FeS_2, Pyrite and Marcasite, through a range of non-stoichiometric compounds. These non-stoichiometric minerals range from Pyrrhotite, $Fe_{1-x}S$ and greigite(Fe_3S_4), which have an excess of sulphur over iron, through to stoichiometric FeS, troilite, (Lee 2004) and to metal rich (sulphur deficient) Mackinawite (FeS_{1-x}). Troilite, stoichiometric FeS, is a rare mineral, formed in nature under strongly reducing conditions, (Evans 1970; Kostov 1982; Harmandas 1998). One such reducing environment is in swamps, where anaerobic bacteria can reduce sulphate to sulphide. Table 2.1 shows FeS polymorphs with their thermodynamic solubility products summarized. The different forms of FeS have created complex problems in the field, where different FeS products have precipitated at different points in the

production process, thereby requiring quite different treatment programs. (Ball 1984; Nasr-El-Din *et al.* 2001a; Nasr-El-Din *et al.* 2001b) .

Name	Formula	Expression	Ksp
Amorphous	FeS	$\alpha Fe^{2+}\ \alpha S^{2-}$	1.44×10^{-17}
Troilite	α-FeS	$\alpha Fe^{2+}\ \alpha S^{2-}$	6.17×10^{-17}
Pyrrhotite	$Fe_{0.98}S$	$\alpha Fe^{2+}\ \alpha S^{2-}$	2.70×10^{-19}
Mackinawite	FeS	$\alpha Fe^{2+}\ \alpha S^{2-}$	2.88×10^{-18}
Greigite	Fe_3S_4	$\alpha^3 Fe^{2-}\ \alpha^4 S^{2-}$	2.99×10^{-55}
Pyrite	FeS_2	$\alpha Fe^{2+}\ \alpha S_2^{2-}$	8.51×10^{-26}
Marcasite	FeS_2	$\alpha Fe^{2+}\ \alpha S_2^{2-}$	8.65×10^{-26}

Table 2.1 Thermodynamic solubility products of various iron sulphides polymorphs at 25°C (Harmandas 1998)

It has been suggested that FeS can transform from one form to another depending on physical conditions (Luther 1991). This transformation may add a further complication to FeS scale treatment programs as the FeS may transform from an easier to a more difficult to inhibit scale. The kinetics of FeS transformation specifically from FeS to pyrite was investigated by Rickard (Rickard 2001), he suggested that the presence of trace organics can determine the stoichiometry and oxidation state of the iron sulphide product formed. Studies by Rickard (Rickard 1974; Rickard 1975) have shown the formation of iron mono-sulphides from goethite and soluble sulphide, and their subsequent further reaction with sulphur to form pyrite. It has been demonstrated that the transformation of pyrrhotite to pyrite (FeS_2) does not occur directly (Schoonen 1991). Marcasite (FeS_2) (a polymorph of pyrite), or a mixture of marcasite and pyrite, is commonly found as the replacement product for pyrrhotite in a supergene environment. The structure of various FeS polymorphs and how the formation of clusters subsequently lead to their transformation is reviewed by Rickard (Rickard 2005). These results have several implications for oil and gas production since these transformations may be affected by the production processes as reservoir fluids are brought to the surface.

2.2.2 Forms of Zinc Sulphide

Zinc sulphide is insoluble in aqueous solution with a solubility product of 2×10^{-25}. There are two forms of Zinc sulphide which are of interest to the petroleum industry; sphalerite (ZnS) commonly called zinc blend and wurtzite (Zn, Fe)S. Figure 2.1 shows the tightly knit structure of zinc sulphide while Figure 2.2 shows the structure of wurtzite, although other forms such as Mátraite and Rudashevskyite (iron (II) analogue of sphalerite) are known polymorphs that also exit in nature. It is important to note that in the context of "exotic" oilfield scales, there have been reports of the occurance of Smithsonite ($ZnCO_3$) (Ramsay Jr. 1964; Carney 1974 ; Fu 2009) which can also cause flow disruptions. However in the context of this thesis ZnS is the form referred to and no other polymorphs was considered, although in the mixed scale studies reported here there is the possibility of wurtzite formation.

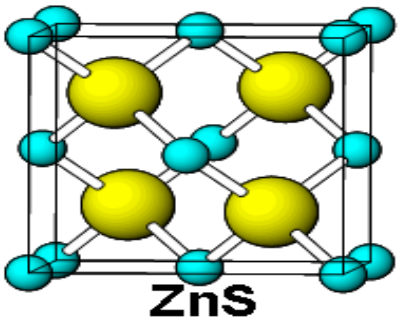

Figure 2.1 ZnS structure (Skinner 1961)

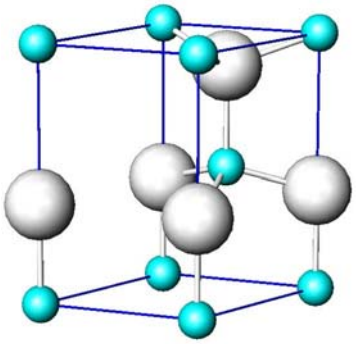

Figure 2.2 Wurtzite structure (Xu 1993)

2.2.3 Lead Sulphide.

Lead sulphide has been known for some time to cause production problems in the oil and gas industry (Jordan 2000; Worden 2000; Al-Masri 2005; Godoy 2005; Lopez 2005; Hitchon 2006; Oriski 2007). PbS has the lowest solubility of the sulphide scales having a Ksp of 3×10^{-29} at 25°C (Vaughan 2005). Compared to the other sulphide scales, lead sulphide is not known to have polymorphs, however anglesite ($PbCO_3$) and PbO have also been reported to impair petroleum process (Hitchon 2006). Figure 2.3 shows the lead sulphide atomic structure showing the position of lead and sulphur atoms.

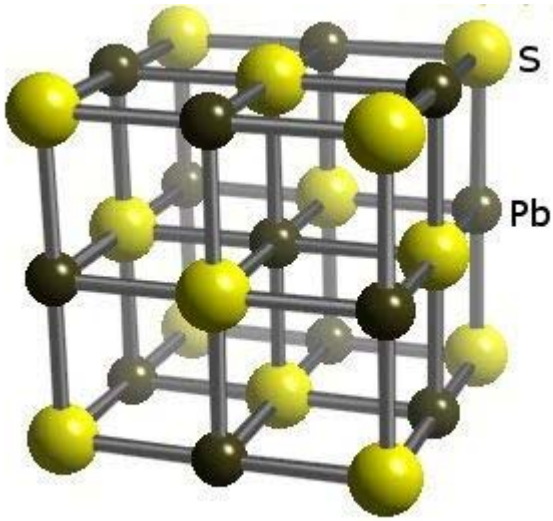

Figure 2.3 PbS structure showing the position of Pb and S atoms (Ramsdell 1925)

2.3 Mixed Sulphide Scales

2.3.1 Mississippi Valley Type Petroleum Formation Brines.

Mixed sulphides occur naturally in commingled brines, where ZnS, PbS occur together, or ZnS, FeS and PbS occur in the same field, depending on the formation rock compositions. The brine compositions leading to ZnS and PbS formation are of interest in the context of this thesis. Mississippi Valley-type brines, commonly referred to as MVTs, are petroleum field brines, carrying lead-zinc concentrations ranging from trace amounts to large economic ore deposits. The most abundant minerals in MVTs are sphalerite ZnS and galena PbS (the ores of zinc and lead respectively). Several other minerals are found in substantial quantities, such as quartz, calcite, and dolomite. MVT type petroleum brines are found throughout the world, the largest and most intensely studied are in North America. They are usually characterized by the following,

1) Low-temperature formation (50°-200°C, but usually 100°-150°C).
2) Epigenetic (forming after) emplacement within restricted dolstone or limestone strata of sedimentary basins (i.e. stratigraphically controlled).
3) Precipitation from highly saline brines.
4) The presence of calcite and/or Ouorite gangue mineralization (Leach 1993; Misra 1999; Leach 2001; Rakovan 2006; Sangster 1995).

Recent researches on petroleum basin brines have shown a close genetic relation between oil brines and mineralizing fluids of Mississippi Valley Type (MVT) deposits. The genetic models of the MVT deposits generally involve formation waters (Na–Ca–Cl rich) migrating from sedimentary basins during times of tectonic extension. (Carpenter 1974; Kharaka 1987; Leach 2001; Giordano 2002)

2.3.2 Mixed Scale Formation in MVT Petroleum Related Brines.

It is well known that some petroleum-related brines contain measurable quantities of base metals (Pb-Zn), (Hartog 2002) which routinely co-precipitated with calcium carbonate as sulphides when the right conditions prevail (Carpenter 1978; Kharaka 1986a; Kharaka 1986b; Giordano 2002). Field evidence shows that these brines typically have between [Pb] and [Zn] in the range of ~1-250mg/L (Kharaka 1987; Jordan 2000; Oriski 2007). However, higher levels of Pb-Zn have been reported to up to 575mg/L for Pb and Zn respectively (Giordano 2002). The impact of sulphide-$CaCO_3$ co-precipitating has not been reported, or discussed. Chapter 8 shows results of $CaCO_3$ co-precipitating with sulphide scale (ZnS and PbS), the objective of this study is to examine the $CaCO_3$ crystals formed both in bulk and on a metal surface, and the impact sulphide-$CaCO_3$ co-precipitating will have on scale treatment programs.

2.4 Solubility and Thermodynamics of Sulfides in Aqueous Solutions

2.4.1 Solubility and Thermodynamics of Hydrogen Sulphide in Aqueous Solutions

Investigation into thermodynamics and equilibrium constants of the hydrogen sulphide system have been carried out by many workers in research fields, such as geology, oceanography, sedimentology, water treatment and corrosion control. (Berner 1967; Doyle 1968; Rickard 1969; Deshmukh 1980; Vorholz 2002). Some authors have investigated the equilibrium constants of the hydrogen sulphide system by conducting experiments or using theoretical thermodynamic models, in order to calculate the concentrations of sulphide species (Weiss 1970; Douabul 1979; Roberts 1985; Carroll 1989; Suleimenov 1994). When hydrogen sulphide dissolves in the water solution, the vapour-liquid equilibrium of hydrogen sulphide is described as

$$H_2S_{(g)} \xleftrightarrow{K_{H_2S}} H_2S_{(aq)} \qquad (1.1)$$

Then we have the dissociation of hydrogen sulphide and dissociation of HS^- ion:

$$H_2S^-(aq) \xleftrightarrow{K_1} H^+(aq) + HS(aq) \quad (1.2)$$

$$HS^-(aq) \xleftrightarrow{K_2} H^+(aq) + S^{2-}(aq) \quad (1.3)$$

Wei (Wei 2006) gives a good comparison and summary of the literature for hydrogen sulphide solubility constants by several authors (Weiss 1970; Douabul 1979; Roberts 1985; Carroll 1989; Suleimenov 1994; Nordsveen 2003).

$$K_{H2S} = \exp\left[-41.0563 + 66.4005\left(\frac{100}{T_k}\right) + 15.1060\ In\left(\frac{T_k}{100}\right)\right] \quad \text{(Weiss1970)}$$

$$K_{H2S} = 10\left[\frac{3898.56}{T_k} - 12.4914\ InT_k + 0.00831109\ T_k + 82.7622\right] \quad \text{(Roberts 1985)}$$

(Carroll 1989)

$$K_{H2S} = \frac{10}{\exp\left[-3.3747 + 072437T_k - 1.10765\times10^{-4}T_k^2 - \frac{1549.159}{T_k} + 0.144237InT_k\right]}$$

$$K_{H2S} = 10^{\left[-634.27 + 0.2709T_k - 011132\times10^{-3}T_k^2 - \frac{16719}{T_k} - 2619\log T_k\right]} \quad \text{(Suleimenov 1994)}$$

$$K_{H2S} = 10^{\left[-0.71742672 - 0.01214542T_c + 5.6659982\times10^{-5}T_c - 8.1902716\times10^{-8}T_c^3\right]} \quad \text{(Nordsveen 2003)}$$

Where T_k is the temperature in Kelvin and T_c is temperature in Celsius

Wei (2006) observed a good match was made by four of the five equations listed above. Carroll's equation (Carroll 1989) was found to be higher than the equations presented by Weiss (Weiss 1970), Roberts (Roberts 1985) and Suleimenov (Suleimenov 1994). Several authors gave equations that were developed to calculate the first dissociation constant at different temperatures, among which the equation proposed by Suleimenov (Suleimenov 1997) is widely employed by other researchers to calculate the sulphide species in the hydrogen sulphide system and found to be around 6.99.

$$K_1 = 10^{782.43945 + 0.361261T_k - 1.6722\times10^{-4}T_k^2 \frac{20565.7315}{T_k} - 142.741722\ InT_k} \quad \text{(Suleimenov 1997)}$$

Wei (Wei 2006) also compares the equations for the first dissociation constant at different temperatures and results from different authors matched up with one another.

However, calculations for the second dissociation constant proved to be more difficult to match up and a wide range of values have been reported; unlike the first dissociation constant, the values for the second dissociation constant are far apart. However the values measured of $K_2 = 10^{\left[\frac{31286}{T_k} + 94.9734\ InT_k - 0.097611\ T_k - \frac{2.17087\times10^6}{T_k} - 607.722\right]}$ (Ellis and Giggenbach 1971; Giggenbach 1971) is used. In this thesis the values of K_1 and K_2 used at 25°C are given below

$$K_1 = \frac{[HS^-][H^+]}{[H_2S]} = 6.99 \quad (1.4)$$

$$K_2 = \frac{[S^{2-}][H^+]}{[HS^-]} = 17.4 \quad (1.5)$$

2.4.2 Solubility and Thermodynamics of FeS of in Aqueous Solutions.

The equilibrium constants for the iron sulphide system have been investigated in various research fields, such as geology, oceanography, sedimentology, water treatment, and corrosion studies. It is noted that using two different expressions of HS^- and S^{2-} leads to a significant difference of the calculated solubility limits. Several authors have calculated different forms of FeS, using both $[HS^-]$ and S^{2-} based expressions. Values for different FeS forms range are as follows; Amorphous FeS 1.14×10^{-3}, 1.36×10^{-17} (Berner 1967) (Morse 1987) mackinawite 2.86×10^{-4}, 1.50×10^{-4}, 2.83×10^{-18} (Berner 1967; Morse 1987; Benning 2000) pyrrhotite 1.32×10^{-19} (Berner 1967). Equations 1.6-1.9 show the complete FeS formation equations which are essential to make a complete prediction model; this is explained in chapter 4 leading to a sulphide prediction model.

The Sulphide System	**Notations**	
$H_2S^-_{(aq)} \xleftarrow{K_1} \rightarrow H^+_{(aq)} + HS^-_{(aq)}$	$K_1 = \frac{x_2 x_3}{x_1}$	(1.6)
$HS^-_{(aq)} \xleftarrow{K_2} \rightarrow H^+_{(aq)} + S^{2-}_{(aq)}$	$K_2 = \frac{x_2 x_4}{x_3}$	(1.7)
$H_2O_{(aq)} \xleftarrow{K_1} \rightarrow H^+ + OH^-$	$K_{ow} = x_2 \times x_6$	(1. 8)

$$Fe^{2+} + S^{2-} \leftarrow \xrightarrow{Ksp_1} \rightarrow FeS_{(s)} \qquad K_{sp} = x_4 \times x_5 \quad (1.9)$$

x_1= [H_2S], x_2= [H^+], x_3= [HS^-], x_4= [S^{2-}], x_5= [Fe^{2+}], x_6= [OH^-], x_7= [FeS]

2.4.3 Solubility and Thermodynamics of ZnS across pH Range and Temperature

Considerable data on ZnS solubility is available from the literature. Earlier results (Glixelli 1907; Barnes 1959; Barnes 1960; Barnes *et al.* 1964; Barnes 1966; Barnes 1967; Barnes *et al.* 1969; Barrett 1982) to more recent data (Daskalakis 1993; Ronngren 1993; Tagirov 2007, 2010) all show that the solubility of ZnS increases with temperature over the whole pH range. These studies show that Zn speciation varied with increasing temperature in solution, as the pH changed from 2 to >8, with Zn^{2+}(pH,<3), Zn $(HS)_2$ (pH,3-4.5), $Zn(HS)_3$, (pH,5-8) and ZnS (HS^-) (pH,>8) Tagirov et al. (2007). Tagirov and Steward (2007) determined the stoichiometry and stability of Zinc sulphide complexes from 25°C to 250°C at different pressures. They were able to calculate Zn speciation based on a model valid for sulphide solutions over a wide range of geologically important temperatures and pressures (to 500 °C and 2-150 bars). In a study that investigated the formation of ZnS from aqueous solution, Luther (Luther III 1999) suggested that the formation of ZnS was a stepwise process. This theory was corroborated by Peters *et. al* (1989) who observed that ZnS first forms as an amorphous structure before transforming into a stable form.

2.4.4 Solubility and Thermodynamics of PbS

Investigations into the solubility of PbS have been carried out by in researchers in various fields, such as geology, mineral exploration research, oceanography, and sedimentology. Barrett et.al (1982, 1988) calculated PbS solubilities over a range of salt concentrations from 1 to 5M NaCl and from 25°C to 300°C, and they suggests that PbS solubility increases as brine salinity increases. ZnS and PbS solubility were compared and ZnS is found to be 30-100 times more soluble than PbS Collins and Jordan (2001)

2.5 Prediction of sulphide Scales.

Although the sulphates are independent of pH, there is a strong pH dependence on the solubility of sulphide scales. This makes prediction of sulphide scales more

complicated than the prediction of sulphates because all the sulphide species which form over the entire pH range must be taken into account. It may also include the organic acids and other acids present. Proprietary models have been developed to predict FeS, ZnS and PbS precipitation, but this are usually field and operator specific, Commercial codes which run sulphide scale precipitation are listed below. However, the codes are not open and the precise formulations cannot be seen. In Chapter 4 a full sulphide model is detailed with the formulations and validated with experimental results. Other known models have been reported including those by Bahadori (Bahadori *et al.* 2006), they proposed a correlation equation to predict ferrous iron (Fe^{2+}) deposition (pH 4.5-7.5) in oil desalting plants disposal waste waters; this is in good agreement with practical data at different hydrogen sulphide concentration.

The limited number of codes that run PbS and ZnS is due to the low solubility of this scales, that means whenever the ions are detected, and the right environment (H_2S) persists the sulphide scale is expected to form.

Code Name	Publisher	Conventional scales	Sulphide
Multiscale.	Norwegian University of Science and Technology	$CaCO_3$, $BaSO_4$, $SrSO_4$, $FeCO_3$.	FeS
PHREEQC	USGS	$CaCO_3$, $BaSO_4$, $SrSO_4$, $FeCO_3$.	FeS, ZnS, PbS
ScaleChem	Oil Systems	$CaCO_3$, $BaSO_4$, $SrSO_4$, $FeCO_3$.	FeS
DownHole SAT	French Creek	$CaCO_3$, $BaSO_4$, $SrSO_4$, $FeCO_3$.	FeS
Scale2000	BRGM	$CaCO_3$, $BaSO_4$, $SrSO_4$, $FeCO_3$.	FeS,
Scale Soft Pitzer	Rice University	$CaCO_3$, $BaSO_4$, $SrSO_4$, $FeCO_3$.	FeS, ZnS

Table 2.2 Scale prediction software showing the scales that can be predicted.

2.6 Sulphide Scale Prevention, Inhibition Control Measures

Sulphide scales have been reported much more frequently in the last decade and more fields cases are being reported around the world were sulphide scale is the dominate scale challenge (Jordan *et al.* 2000; Collins 2001; Nasr-El-Din *et al.* 2001a; Nasr-El-Din *et al.* 2001b; Przybylinski 2001b, 2003; Jordan 2004).

There are two basic approaches to mitigating scale deposition in the oil industry.

The pro-active preventative approach usually comprising of:

a) Filters/scavengers to strip away scaling ions (SO_4, H_2S for seawater).
b) Scale inhibitors (SI).

The reactive approach usually comprising of:

a) Chemical dissolvers/dispersants.
b) Mechanical/physical removal.

Prevention is *usually* cheaper and better than cure and this also applies in oil and gas production. The key to sulphide scale control like any other scale lies in having a good prediction of the sulphide scale occurrence, and/or, having preventative mechanism in place to avoid the problem.

The reactive approach which include the removal of sulphide scale, like conventional scale is expensive due to the deferred hydrocarbon production during treatment. Mechanical and chemical means are still routinely used to control and treat scaled systems, although these are usually regarded as short term solutions or "reactive" scale control. Leal et.al (2007) describes a systematic approach to remove iron sulphides in gas wells using both a mechanical device (fluidic oscillator) and a sulphide phosphonate dissolver in the Ghawar field. Table 2.3 shows several reactive means deployed for scale removal. Other mechanical measures include, preening, particulate blasting, scraping, brushing, hydrojetting of pipe work and valves, pipeline pigging, routine valve movements, mechanical cleaners, and explosives to rattle pipes. Mechanical removal is possible if there is access but it does require regular repeat treatments. Chemical measures include the application of acid washes, chelating agents, corrosion inhibitors, polymer based scale inhibitor. Chemicals have been known to chelate, disperse, and inhibit sulphide scale depending on their specific mechanism. It is usually more effective than mechanical removal, however the risk of

corrosion, personnel safety, and complications from HT/HP wells can be considerable.

Chemical Methods	**Mechanical Methods**
Acid washes,	hydrojetting of pipe work and valves
Chelating agents,	pipeline pigging, mechanical cleaners
Dissolvers	Wiping, particulate blasting, scraping, peening
Dispersants/SI	routine valve movements, explosives to rattle pipes

Table 2.3 Sulphide scale removal methods

2.6.1 Sulphide Scale Inhibition

The more effective or proactive scale control is by scale inhibition. Scale inhibitors are water/oil soluble chemicals that prevent or retard the nucleation of and/or crystals growth of inorganic scales. There are several classes of SIs that have been used to inhibit sulphide scaling including phosphates/polyphosphates (Collins 2001), phosphate-ester, phosphonates, organic amino-phosphates, and organic-polymers (Sorbie 1991a; Sorbie *et al.* 1992; Sorbie *et al.* 1995; Sorbie *et al.* 2000). They have different functions and interact with the formation and scale in various ways. However due to the low solubility of sulphide scales most SI mentioned here would not act as stoichiometric SIs. Sulphide scales usually require more than ten times the dosage for sulphate inhibition (Kelland 2009). Nasr-El-Din and Al-Humaidan (Nasr-El-Din *et al.* 2001b) describes a downhole squeeze treatment to mitigate iron sulphide deposition, a combination product comprising of THPS, a corrosion inhibitor, and a surfactant.

2.6.2 Sulphide Scale Inhibitor Deployment

There are a number of different ways for applying Sulphide SIs in the field either into the formation or downhole environment.

(i) Squeeze treatment

(ii) Continuous injection

(iii) Solid or encapsulated SI

The standard method for scale inhibitor application is by "squeezing" the chemical into the rock matrix which is producing the water stream. This method can also be applied when dealing with sulphide scales. The idea is to protect the near wellbore area and some of the tubulars from scale deposition. In a squeeze treatment, the SI is pumped into the well. When production is brought back on line after a squeeze, the inhibitor gradually desorbs from the rock grains and remains dissolved in the produced waters, which prevents scaling until the concentration falls to a level that is too low to be effective. The length of time required for inhibitor concentration in the produced water to fall below this minimum effective inhibitor concentration (MIC) is known as the squeeze lifetime. Obviously, long lifetimes are desirable in order to minimise the number of treatments, so reducing treatment and deferred oil costs. Lopez et al.(2005) squeezed a polymeric SI to a well in the Gulf of Mexico, where it proved to be effective in stopping a mixed (ZnS & PbS) sulphide scales. For a simple treatment where inhibitor is adsorbed on the rock surface in the pore space, the rate of chemical return depends on the slope of the adsorption isotherm. The velocity of return of the inhibitor concentration element of concentration c is denoted v_c, and is given by Equation 1.10.

$$v_c = \frac{v}{1+\frac{\rho}{\phi}\left(\frac{\partial \Gamma}{\partial C}\right)_C} \tag{1.10}$$

where v is the velocity of the produced water, ϕ is the rock porosity, ρ is the rock density, Γ is the mass of inhibitor adsorbed per unit mass of rock and C is inhibitor concentration in terms of mass per unit volume (Sorbie 1991b)

The SI can also be injected by continuous treatment (Heath 2009). This is usually applied to injection well and is the method of choice for sulphide scales. It is often applied to protect pipelines and tubular and topside systems. Corrosion is a major concern when low pH fluids (which many SI's) are pumped through steel tubing and pipelines, this tend to accelerate iron release increasing corrosion. A corrosion inhibitor (CI) compatible with the SI is usually pumped together to ensure the

integrity of the tubular and pipelines (Fleming *et al.* 2003; Ragulin *et al.* 2004; Poggesi 2001).

Solid or encapsulated scale inhibitor is usually used when water or aqueous fluid is to be avoided. It is also applied with fracturing liquids. The idea is to place/trap these SI particles into pores, which slowly releases its contents into the produced water when production begins (McRae *et al.* 2004). This method has been employed to control sulphide deposition in some producing fields (Jordan *et al.* 1999; Bourne *et al.* 2000; Przybylinski 2003).

2.6.3 Sulphide Scale Experiments and Testing of Sulphide Inhibitors.

Inhibition studies on sulphide scales involve a range of experimental procedures ranging from static bottle tests, tube blocking experiments through to techniques such as ICP to detect sulphide cations and straightforward visual observations. Several authors have detailed procedures where dynamic tube blocking tests were used to test the efficacy of selected sulphide scale inhibitors. For example, Lopez (Lopez 2005) detailed a procedure for testing zinc and lead sulphide inhibitors in which cation and anion brines of non-oxidising salts were mixed after nitrogen sparging for several hours until the oxygen concentration is 0.050ppm in an anaerobic environment, using ascorbic acid as an oxygen scavenger. Przbylinski (Przybylinski 2001a) used a different method of oxygen exclusion to perform iron sulphide scaling tests, which included using sealed serum glass bottles and air tight syringes for solution transfer. Przbylinski (Przybylinski 2001a) Collins and Jordan (Jordan 2000; Collins 2001; Jordan *et al.* 2004) (Przybylinski 2001a) and Kaplan (Kaplan 1992) used test procedure similar to the standard static bottle test procedures. In some cases, e.g. Przbylinski (Przybylinski 2003) relied on visual determination of iron sulphide formation as ferrous sulphide is black. ZnS and PbS can also be determined by visual test, this method have also been employed by Chen (Chen 2010), although it should be noted that that it is much harder to detect low concentrations of zinc and Lead sulphide. Jordan (Jordan *et al.* 2000) described a fluid turbidity method for the measurement of suspended scale solids by measuring light intensity (using a baseline of 450nm) to determine scale inhibitor performance, Kaplan (Kaplan 1992) also used this method (turbidity measurements) when determining the ability of chemicals to disperse zinc scales. Collins and Jordan (Collins 2001) used bottle tests to determine the relative

performances of sulphide scale inhibitors and chelating agents. (Dyer *et al.* 2006), (Przybylinski 2001a) used both tube blocking procedure and a simple but effective static test to determine the efficacies of lead and zinc sulphide inhibitors in an anaerobic environment. The results were a combination of the followings visual observations (including digital images), % transmittance (UV spectrophotometer λ =450nm), sample of test solution taken and quenched in 5% nitric acid and analysed by ICP.

2.6.4 Sulphide Scale Dispersants, Chelates and Dissolvers

There are several dissolvers that have been known to prevent or control sulphide scaling. Acids such as Nitrilotriacetic acid (NTAA) have been used to sequester [Fe] thus preventing FeS formation (Taylor *et al.* 2003) although it has been shown to decompose at high temperatures (>150°C).

Chelating agents such as EDTA and DTPA have been used to form water soluble stable complex with the sulphide cations, thus preventing the formation of sulphides scales (Collins 2001). Dispersants are common in the petroleum industry such as Tetrakis Hydroxymethyl Phosphonium Sulphate (THPS). They are usually used as a biocide in the petroleum industry to control the influence of sulphate reducing bacteria. THPS has been known in the oil industry as a non oxidizing broad based biocide. Its use has expanded in the oil industry since its ability as an FeS dissolver was discovered. Results of our THPS experiments are discussed in Chapter 5.

THPS is a non-foaming biocide classed as a non-oxidizing agent in the oil industry which is readily biodegradable and has no potential to bio-accumulate. THPS has the structure shown in Figure 2.4 and it degrades in the environment to THPO (Tris Hydroxymethyl Phosphine oxide) and bishydroxymethyl Phosphonic acid (BMPA) (WHO 2000) which is classified as a non hazardous material. Figure 2.5 shows the reaction between [Fe] and THPS and the chelating process where [Fe] is sequestered from an aqueous solution in a mannich-like reaction described by (Jefferey 2000).

THPS is usually formulated as a biocide or optimized as a dissolver (although in general they will all do both to some extent). Indeed, because the mechanisms of SRBs production of H_2S and subsequent FeS deposition are intimately related, then

FeS control is often viewed within the oil industry as falling within "biocidal treatment programme". Therefore, the field design of a THPS application would in practice take a more "holistic" view of the SRB/FeS problem because of the close coupling between these cause and effect phenomena. Some authors, Videla (Videla 2002) explores THPS in the context of bio-corrosion. In this thesis it is assumed that the THPS products acts purely as a dissolver, assuming then that the FeS were abiotically generated (which can occur).

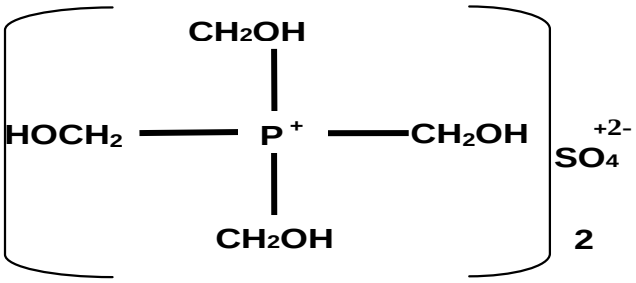

Figure 2.4 – THPS Chemical Structure

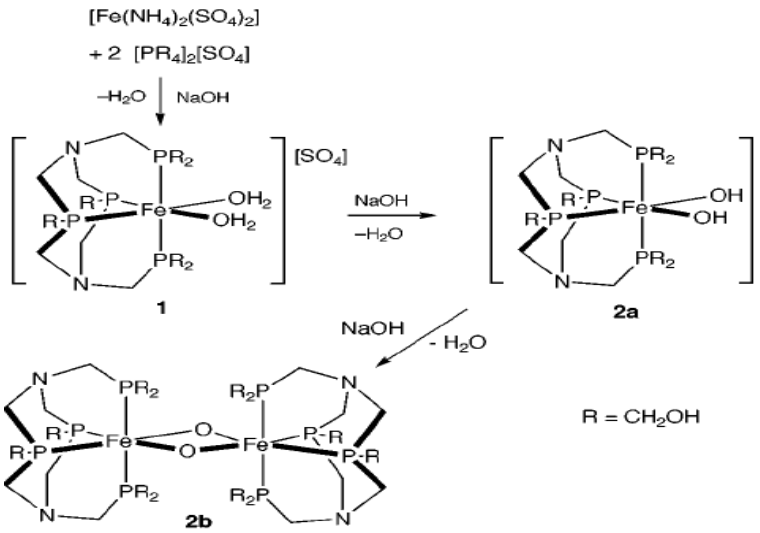

Figure 2.5 Schematic showing THPS and Fe reaction forming a water soluble complex. (Jefferey 2000)

2.6.5 THPS Use as Iron Sulphide Dissolver.

There is an increasing interest in biocides which form water soluble complexes since these compounds are capable of acting both as a biocide and as an [Fe] metal

dissolver. THPS is an example of novel chemistries that show promising results not only in the laboratory test but also in field conditions, (Downward 1997; Fidoe 2002; Gilbert 2002.; Talbot 2005; Jefferey 2000) Jefferey et.al (Jefferey 2000) describes how THPS aids FeS dissolution, They suggest that a Mannich-like condensation reaction occurs which chelates the [Fe] ion separating it from the H_2S- thereby taking it from the reaction.

THPS is preferred to acid washes in sulphide removal because

(i) They show efficient dissolution of iron based scales at low concentrations.

(ii) They do not evolve significant amounts of H_2S and.

(iii) They are very eco-friendly, as described above.

Other dispersants used in the oil industry includes Acrolein, which have been used as a mixed iron sulphide scale dissolver-H_2S scavenger combination product (Acrolein). It was applied in a West Texas field as described by Salma (2000). That study stated that the Acrolein product was cheaper than THPS, and it was applied at lower concentrations, Acrolein is known for its toxicity and its application comes with specific hazards.

2.6.6 THPS squeeze

Rincon (Rincon 2004) describes the squeezing of THPS to three different formations in Eastern Venezuela with varying reservoir characteristics including high GOR, high water cuts, heavy and semi-heavy crude with varying degree of souring. He observed that the THPS applied did not cause any change in permeability or cause formation damage and surprisingly caused an increase in production and an expected reduction in the H_2S by more than 60%. Nasr-El-Din and AL-Humaidan (2001) and (Nasr-El-Din *et al.* 2001b) describes a downhole squeeze treatment to mitigate iron sulphide deposition, a combination product comprising of THPS, a corrosion inhibitor, and a surfactant were applied.

2.7 Field Cases of Sulphide Scales in Association with Conventional Scales.

PbS and ZnS scales were unexpectedly encountered in a HP/HT field in the UK sector of the North Sea, (Oriski 2007) where the scale prediction before field development showed a potential for $CaCO_3$ and NaCl based on water taken during DST. However production restrictions were observed a year into production where Pb, Zn, ions

appeared in the DST samples obtained. A new prediction with the Pb and Zn ions indicated a PbS and ZnS scale problem and this was taken into consideration and an inhibitor was selected. The selected scale inhibitor was not poisoned by the sulphide scales but it did very little in preventing or treating the sulphide scales, the PbS and ZnS were attributed to temperature. Collins and Jordan (2001) described a similar occurance were sulphide scale caused massive restriction in the HP- hydrocyclones and separators. A low molecular weight scale inhibitor was optimized to control sulphide deposition via a continuous injection line, and the SI concentration was increased to 30ppm. Dyer et.al (2006) describes the selection and testing of sulphide scale inhibitors used in Elgin and Franklin fields in the UK sector of the North Sea. Przybylinski (2001) described a field that historically had a calcium carbonate problem but over time developed a high PbS and ZnS scaling problem. Despite an increase in the original scale inhibitor concentration that was used for the calcium carbonate to 300ppm, it did not get better. A subsequent change in scale inhibitor at a higher concentration of 400ppm reduced the sulphide scale and brought it under control. Lopez *et. al.* (2005) describe the selection process and testing of sulphide scale inhibitors suitable for both PbS and ZnS using the anaerobic dynamic tube-blocking test. This was used in a field in Mobile bay, Gulf of Mexico. Lehmann and Firouzkouhi (Lehmann 2008) describe a treatment that deactivates iron sulphide, reducing the particle size and facilitating the transport of the scale with produced water preventing scale deposition on production systems. Jordan *et. al.* (2004) describes a combined sulphide scale inhibitor/hydrogen sulphide scavenger treatment that reduces the level of hydrogen sulphide whilst controlling calcium carbonate scaling in an HT/HP, high salinity field. Jordan *et. al.* (2000) described a similar sulphide scaling case where a careful assessment of the water chemistry was not carried out in a UK sector and a Norwegian sector of the North Sea, resulting in very high values of PbS and ZnS scales. These sulphide scales caused severe productions problems especially in the HP/LP hydrocyclones, HP/LP separators and pipelines.

A polymer based scale inhibitor for the expected sulphate and carbonate scales was applied at a higher MIC (25-30ppm than would have been necessary for the sulphate scale 2-5ppm) to control the sulphide scales.

2.8 pH Effect on Sulphide Scale Deposition.

pH is a major controlling factor in sulphide precipitation, the pH controls the crystallinity, composition, grain size, and final product (Schoonen 1991) Antonio et al. (Antonio 2000) suggests that the pH of the system affects the amount of iron sulphide precipitate produced, he presented data that indicates that aqueous H_2S, in its fully protonated state, is only weakly reactive with Fe^{2+} and does not facilitate Fe–S precipitation. As the pH increases, the amount of H_2S and the amount of precipitate also increases. The sulphide pH relationship is clearly expressed and explained in the sulphide model developed in Chapter 4 of this thesis and its significance in sulphide prediction.

Chapter 3 Experimental Methods

This chapter contains details of all the experimental procedures used in the course of this study. It also provides details of brine preparation methods, standard and modified anaerobic static efficiency tests, particle size analysis experiments. Anaerobic static tests for FeS studies and dynamic beaker tests are also described. A comprehensive list of the various brine compositions used in this thesis is given in the order which they appear in the thesis.

3.1 Brine Preparation

Most of the experiments performed in the course of this thesis were carried out in an aqueous medium. No actual field brines were used. Instead, all brines were prepared in the laboratory from distilled water and mineral salts supplied by VWR. Brines were prepared in 1, 5, 10 or 20 litre batches depending on the amount required for each experiment. When required in 1 litre samples, brines were prepared by weighing the correct amounts of the required salts and dissolving in approximately 750mls after the salts are fully dissolved, the volume is topped up to 1 litre. This also applies to the 5 litre and 10 litre batches. If a 10 or 20 litre batch was required, the correct amounts of the relevant salts were weighed into a bucket and dissolved in a volume of distilled water equal to three quarters of the final volume. The solution was stirred with an overhead motorized propeller. When dissolution was complete, some of the solution was placed in a 5 litre graduated flask and topped up to the mark with distilled water. This was done twice or four times and the 5 litre portions were combined in a plastic barrel, giving the target solutions in the final 10 or 20 litre mixture. Degassing is achieved by placing the solution in a conical flask, with a magnetic rod placed inside. The flask is placed on a stirrer at mid speed and connected to a vacuum pump till the air bubbles are completely purged.

3.1.1 Hydrogen Sulphide Preparation

Due to the toxicity and potential danger involved in handling hydrogen sulphide (H_2S) gas and H_2S containing liquid, the hydrogen sulphide used in this thesis was introduced as aqueous H_2S. This was achieved by dissolving sodium sulphide (Na_2S) in distilled water or brine as the test conditions required, no H_2S gas or liquid-H_2S was used in these experiments. Brine preparation, nitrogen sparging and degassing involving H_2S were carried out in the fume cupboard to limit exposure to the H_2S. An H_2S monitor system with two alarm sensors was installed in the laboratory to detect H_2S gas leaking, a portable H_2S gas monitors was always worn while the other was attached outside the fume cupboard to catch H_2S gas leaks during experiments with H_2S. The detection limit

was set at 0.1ppm with beeps and alarms set to go off (continuous ringing sound) at 1ppm.

3.2 Scale Inhibitors and Dissolvers

Polyphosphonocarboxylic acid (PPCA) and Diethylene triamine pentamethylene phosphonic acid) (DETPMP), two common commercial scale inhibitors used in the oil and gas industry, are investigated extensively in this study. The inhibitors were provided by Biolab-BWA. The molecular weight of PPCA is ~3800g/mol and the activity is 42%. The molecular weight of DETPMP is 573g/mol and the activity is 45%. The structures of PPCA and DETPMP are shown in Chapter 1. Other scale inhibitors were tested in this study, many of them were proprietary chemicals and their general chemical make-up is given in Table 4.1 of Chapter 5.

Chapter 6 describes an extensive study on THPS, which is a well known industrial chemical used mainly for its biocidal properties. However, it has also been used for its ability to chelate iron thereby removing FeS. THPS works synergistically in blends with a range of different chemicals, this blends enhances THPS effectiveness either as a biocide or FeS dissolver. The structure of THPS is shown in Chapter 1.

3.3 Static Efficiency Tests

3.3.1 Buffer Solution

Some of the static efficiency tests were carried out at a fixed pH. This was achieved by buffering the test solutions with a mixture of acetic acid and sodium acetate. In order to have adequate buffering capacity, the pK_a of a buffer must be within one pH unit of the target pH. The acetate anion has a pK_a value of 4.75, so this system is suitable for the task. Buffer was prepared by dissolving 68.0 g of sodium acetate trihydrate and 2.50 ml of glacial acetic acid in distilled water to make 500 ml of solution in a graduated flask. Buffer solutions were tested by mixing with seawater and formation water in the volume ratio used in the tests, and the pH of the resultant mixture was measured with a freshly calibrated pH meter. Buffer solutions were accepted if the pH value of this mixture was between 5.3 and 5.5.

3.3.2 Quenching Solution

The purpose of the quenching solution was to halt any forming precipitate (e.g. FeS, $BaSO_4$, PbS etc.) in a given test. When a sample of the test solution is mixed with this high ionic strength concentrated inhibitor solution, all further precipitation is halted. This preserves the Ba, Fe, Pb, or Zn ion concentration reached at the time of sampling, effectively taking a "snapshot" of the scaling reaction at that time. This is "freezing" of the brine composition is achieved because the quenching solution contains much more inhibitor than the amount required to halt the scaling. The polymer, poly vinly sulphonate (PVS), was chosen for use in this quenching solution because of its high calcium tolerance. Quenching solutions were prepared in 5 litre batches by dissolving 28.55 g potassium chloride with 5 g of a PVS-containing inhibitor in distilled water and making up to the mark in a graduated flask. This produced a solution with 3000 ppm K^+ and 220 ppm PVS. The quenching solution was adjusted in to the range pH 8.0 - 8.5 by addition of concentrated sodium hydroxide. Unpublished work carried out at Heriot Watt has demonstrated that this quenching solution halts all barium precipitation, so that concentrations remain stable for more than two weeks.

3.3.3 Modified Static Efficiency Tests Using Anaerobic Nitrogen Glove Box

Inhibitor stock solutions with an active concentration of 10000 ppm were prepared by weighing the correct amount of inhibitor into a Teflon cup and mixing with distilled water. A further 1000 ppm concentration was made for some SI's because of the smaller quantities received from the vendor. The stock solutions and brines were then filtered through a 0.45 μm nitrocellulose membrane, and filter stock solutions were diluted with filtered seawater in a graduated flask to reach the target inhibitor concentration, typically in the range 0 - 5000 ppm (these high levels will be explained in the thesis). Using a measuring cylinder, 10ml, 100ml portions of formation water and seawater were measured into 100 ml and 250 ml polyethylene or glass bottles as appropriate; respectively, 0.2 ml or 2 ml of acetate buffer was pipetted into each portion of formation water (in the case of buffered experiments). This 50:50 mixing ratio was used in every

test reported in this thesis. All tests were performed in duplicate. Bottles were numbered, and every even number was the duplicate of the preceding odd number, i.e. 1 and 2 were duplicates, 3 and 4 were duplicates etc. A pair of duplicates containing no inhibitor, the blank tests, was included in every batch. The separate brines samples were mixed in strict numerical order by pouring formation water into seawater, or scaling brines as the case permits. After 2 and 20 two hours had passed, samples were taken in strict numerical order by removing a 1 ml aliquot of test mixture with a pipette and mixing with 9 ml quenching solution in a 10 ml test tube; after the tube was capped to prevent evaporation and contamination, the tubes are capped and inverted repeatedly to promote mixing.

During all the FeS experiments, the tests were performed as described above, but with an additional "oxygen (O_2) reduction" regime. These near anaerobic tests were performed in the nitrogen glove box in Figure 3.1. A strict oxygen reduction regime was developed with the sole aim of keeping the amount of (O_2) as low as possible between 0-20ppb. This procedure begins immediately after the salts are dissolved in water as stated above, the regime includes the following:

- Using Fe stable salts such as Ammonium iron (II) sulphate $(NH_4)_2SO_4FeSO_4.6H_2O$ commonly known as Mohr's salt.
- Degassing the brines to achieve 0-20ppb (checked using dissolved O_2 test kits)
- Nitrogen sparging of the SI, and brines for more than 1hr, finishing off by placing a nitrogen blanket over the solutions before sealing with the top.
- All experiments were performed in nitrogen glove box as shown in Figure 3.3 filled with O_2 free nitrogen gas unless indicated in the case of Pb and Zn only experiments.

In the course of these studies, O_2 levels of between 0-20 ppb were usually achieved before brine mixing, and these levels were maintained throughout the tests because the tests were performed in the nitrogen glove box.

Figure 3.1 Nitrogen glove box where all the sulphide studies are performed.

3.3.4 Analysis of Samples and Data Processing

The initial scaling cation (Ba, Fe, Pb, Zn) concentration at the beginning of the test was measured indirectly by preparing a control solution. Control solutions were made by mixing 5 ml formation water (scaling solution) with 90 ml quenching solution in a 100 ml graduated flask. After mixing, 5 ml of seawater (scaling solution) was added and the mixture was topped up to the mark with quenching solution and mixed again. Mixing in this way prevented any ion loss by ensuring that incompatible waters were only mixed in the presence of a large excess of quenching solution. The mixing ratio 1:1:18 FW: SW: Quench mirrors that used when 1 ml of 50:50 test solution is mixed with 9 ml quenching solution.

Ion concentrations in the quenched solutions from inhibited tests, blank tests and control samples were analysed by Inductively Coupled Plasma - Atomic Emission Spectroscopy

(ICP-AES). Matrix-matched standards and zeros were run between every 8 to 12 samples in each batch of ICP analysis. The measured ion concentrations in the zero (pure quenching solution) and the standard (quenching solution of a known ion concentration) give an estimate of the analytical error at the time of measuring. The raw data were then corrected by applying the formula shown in Equation 3.1, where s and z are the mean measured ion (in this case Iron) concentrations in the standard and the zero solutions, *t* is the actual concentration in the standard and *f* is the dilution factor.

$$[Fe]_{corrected} = \left(\frac{s-z}{t}\right)([Fe]_{raw} - z)f \tag{3.1}$$

These corrected barium concentrations were then used to calculate the inhibition efficiency for each duplicate using Equation 3.2, where the subscripts t, b and i denote test, blank and initial, respectively. An average of each duplicate was reported as the final efficiency, if no iron is lost from the inhibited solution, $[Fe]_t = [Fe]_i$ and efficiency = 100%, but if the inhibitor has no effect at all $[Fe]_t = [Fe]_b$ and efficiency = 0%.

$$\%Efficiency = 100 \times \frac{[Fe]_t - [Fe]_b}{[Fe]_i - [Fe]_b} \tag{3.2}$$

Inhibition efficiency is generally positive, it can be possible for this quantity to be *negative* at certain points in time.

3.4 Scanning Electron Microscopy (SEM) and Energy Dispersive X-ray Analysis System (EDX)

The Philips XL30 Scanning Electron Microscope (SEM), as shown in Figure 3.2, is used for electron microscopy. An electron beam is scanned across a sample surface. When the electrons strike the sample, a variety of signals are generated, and it is the detection of specific signals that produces an image or a sample's elemental composition.

Figure 3.2. Scanning Electron Microscopy

The Phoenix Energy Dispersive X-ray Analysis system (EDXA), with a UTW detector and LEAP+ technology was incorporated into the SEM. All elements down to the atomic number of boron can be detected, including the light elements carbon, nitrogen and oxygen. Both qualitative and quantitative analysis is available, as well as the mapping of up to 15 elements at a time. EDXA analysis is capable of producing high quality elemental data at a fast rate.

Scanning Electron Microscopy (SEM) has long played a central role in structural characterisation for flow assurance samples. When a sample is examined with an electron beam, three signal types can be created: secondary electrons, backscattered electrons and X-rays. Secondary electrons are sample electrons ejected after interaction with the primary electrons of the beam. These have low energy (less than 50 eV), and thus escape from shallow areas within the sample, resulting in the best imaging resolution. Back-scattered electrons (BSE) are primary beam electrons which have left the sample due to static collisions. They have energies from 50 eV up to the accelerating voltage of the beam. Because of their higher energy, they have higher specific volumes of interaction,

thus lower resolution. SEM works by bombarding the surface of a material with a beam of electrons and detecting both secondary electrons or BSEs since X-rays provide poor spatial resolution compared to these types. A virtual image is constructed from the signals emitted by the sample and the resolution of SEM instruments is the measure of the smallest feature observable by the apparatus specified by Å or nm ranges. This is typically set by the size of the spot formed by the beam on the sample surface. In SEM, magnifications are decoupled from depth of field and are determined by the size of the beam scan. This is the main advantage over conventional transmission light microscopy. Because of the need for high vacuum and extensive sample preparation with SEM, the environmental scanning electron microscopy (ESEM) mode of operation is often preferred in solid characterisation studies. High vacuums are a requirement for correct beam focusing to avoid the effects of ignitable gases due to the high voltages employed. Thus, only samples that are vacuum tolerant and conductive may be used in SEM.

However in **Environmental** SEM (ESEM), no prior specimen preparation is required and even wet samples can be analysed. A multiple pressure limiting apparatus separates the sample chamber from the beam column. The column remains at high pressure, while the chamber sustains pressures of at least 4.6 Torr (Philips, 1996). Gas flow controls the pressure in the chamber and this is usually comprised of inert species. Gas ionisation in the sample chamber eliminates the charging effects typically seen with non-conductive samples and this is used to amplify the secondary electron signal which is measured in the ESEM detector (Philips, 1996). Sample coating is often required in ESEM to aid in conductivity/contrast and to avoid destabilizing sensitive samples. However, one disadvantage of a coating, whilst enhancing the surface detail of the sample is the masking of internal structures (Philips, 1996). Most ESEM apparatus have in-built EDAX capabilities to make use of the energy produced as a result of the incidence of the primary electron beam. The EDAX detectors measure the quantity of emitted X-rays as a function of energy, which is characteristic of the element from which it is emitted. But EDAX provides only an elemental composition of the exact surface spot of the sample being analysed. Thus it becomes important to perform a surface scan of the sample under scrutiny. However, one of the advantages over XRF or elemental analysis is that EDAX

can focus on different sample areas and help identify multiple contaminants. One of the most undesired effects during an EDAX analysis is the interference of skirt X-rays. These are produced from electrons scattered by gas molecules. The effect can be minimized by correct adjustments of the distance and angle between the X-ray detector and the sample. Elements with atomic numbers from that of beryllium to uranium can be detected due to low X-ray intensity. The minimum detection limits vary from about 0.1 wt% to a few percent depending on the element and matrix. ESEM/EDAX was performed using an XLM Philips model in this thesis, operated with nitrogen. The objective was to obtain both soap morphology and elemental composition information. Copper and aluminium standards were used to verify the correct EDAX instrument operations. Gold coating was not used owing to reasonable sample stability under vacuum and to avoid any interference from the potential absorption of gold. The beam energy was 20 keV. Three different measurements were carried out on each sample, thus atomic and weight percentages represent the average of these values. An EDAX spectrum of the stub holder used to place the samples in the gas chamber was also acquired to determine background interference.

3.5 Dynamic Beaker Tests—Calcium Carbonate Surface & Bulk Deposition

A Perspex vessel was built to simulate the formation of calcium carbonate scale deposition by CO_2 loss. The principle is that, as CO_2 is lost from supersaturated brine, $CaCO_3$ scale will be formed in the bulk and on the metal surface of the spindle. The spindle is non-rotating hence a magnetic stirrer was used to accelerate scale formation in the dynamic beaker test to the surface of the spindle. Calcium carbonate scales were deposited from the scale forming solution to the active surface of stainless steel (UNS S31603). During the experiments, an insulating tape (black tape) around the electrode ensured that only the end surface is the electrochemically active surface. On the active surface of the electrode, the deposition takes place and it is the only surface analysed by the ESEM as discussed in Chapter 7. With the development of the experiments, the pH is allowed to drift freely during the experiments (as technically it should in the CO_2 degassing process). The composition of the scaling solution changes in this study

depending on the aim of the experiments. The vessel and the spindles were always polished to a fine degree after the end of an experiment making sure it was initially clear of all scale.

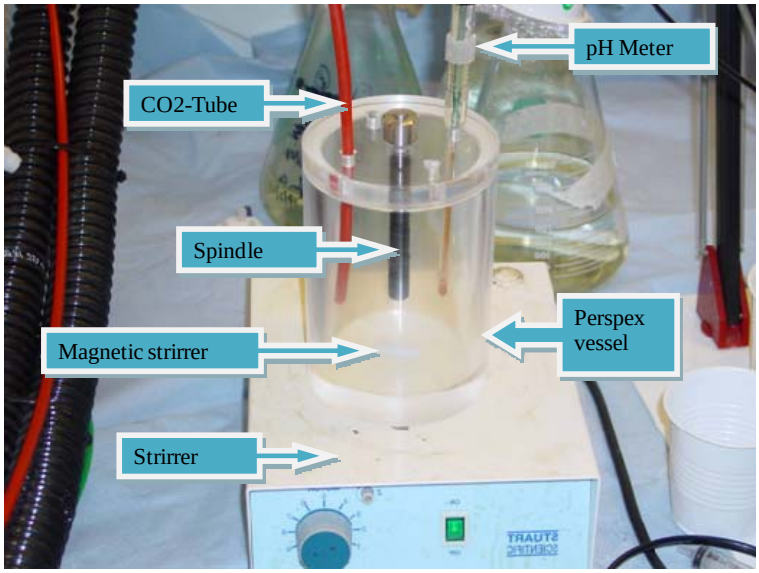

Figure 3.3 Dynamic beaker vessel for calcium carbonate/sulphide deposition tests**.**

3.6 Particle Size Measurement

The iron FeS particle size distribution was determined using a Malvern Mastersizer 1000 Particle Size Analyzer; this machine uses the principle of laser diffraction to determine the particle size of the FeS described in Chapter 4. The technique of laser diffraction is based around the principle that particles passing through a laser beam will scatter light at an angle that is directly related to their size.

3.6.1 Malvern Instrument Settings Used for FeS particle Size Experiments

The settings for FeS particle size measurements using the Malvern Mastersizer was fairly simple and easy to follow. The Machine was left to warm-up for 30mins before the start of the experiment; the instrument parameters used in this thesis are as follows:

Presentation - Std

Focal Length - (type in lens type)*

Beam Length - 2.2nm

Data Storage - Not working

Kill Data - Always set to zero

The alignment was performed automatically by the machine, however the background count and obscuration (0.1 - 0.3) is set manually.

*Table of Lens Types for different particle sizes

Size	Lens Type
1.2 - 600µm	300mm
0.5 - 180µm	100mm
0.1 - 80µm	45mm

3.7 THPS Concentration (ppm) Determination

Chapter 5 of this thesis reports work on THPS interactions with FeS, PbS and ZnS, in different brine compositions. In order to determine the active concentration of THPS before and after the experiments an industry standard test developed by LaMotte Company was used and the procedure can be found in LaMotte instructional archives.

http://www.lamotte.com/pages/common/pdf/instruct/8776.pdf

3.8 Brine Compositions

3.8.1 FeS Formation Using the Forties Formation

A range of brine compositions were used in different experiments throughout the thesis. A comprehensive list is provided here, with brines listed in the order in which they appear in the thesis.

Chapter 5 describes static efficiency tests carried out using modified synthetic Forties Formation water and synthetic North Sea Seawater. The formation brine is modified by the addition of iron to the brine composition although it is not present in these quantities in the original formation water. The Seawater was also modified by the addition of the sulphide ion leaving the other ions at the same concentrations as found in standard

synthetic North Sea Seawater. Compositions and nomenclature are shown in Table 3.1. THPS study in Chapter 5 was carried out using the brine compositions in Table 3.2 and 3.3, whilst Table 3.2 represented mild scaling system; Table 3.3 represents a severe scaling system. The brine composition in Table 3.3 is modelled after Miller formation which has a high concentration of iron about 175ppm. The high [Fe] represents a case for severe FeS and $FeCO_3$ deposition as Miller field also contains about 28% mol CO_2 (Lu 2008). Table 3.4 is the brine analogues composition for the $BaSO_4$-sulphide studies in Chapter 6. Experimental studies in Chapter 7 used the brine composition in Table 3.5.

Table 3.1 Brine Composition for Forties FW and SW used in Experiments described in Chapter 5

All concentrations in milligrams per Litre

Ion	Forties FW	North Sea Seawater
Sodium	31275	10887
Calcium	2000	428
Potassium	739	1368
Magnesium	654	460
Barium	269	0
Strontium	771	0
Sulphate	0	2960
Chloride	52360	19766
sulphide	0	100
Iron	100	0

Table 3.2 Composition of Low Salinity NaCl Brine Analogues used in Experiments reported in Chapter 6

All concentrations in milligrams per Litre

Ion	Low FW1	Low FW2	Low FW 3	Low FW4	North Sea Seawater
Sodium	10000	10000	10000	10000	10000
Calcium	735	0	735	0	428
Magnesium	105	105	0	0	1368
Iron	175	175	175	175	0
sulphide	0	0	0	0	500
Chloride	17028	15727	16721	15421	19062

Table 3.3 Compositions of Miller FW and SW Analogues used in Experiments in Chapter 6				
All concentrations in milligrams per Litre				
Ion	Miller FW A	Miller FW B	Miller FW C	North Sea Seawater
Sodium	27080	27080	27080	10890
Calcium	735	735	0	428
Potassium	1340	1340	1340	1368
Magnesium	105	105	0	460
Barium	775	0	0	0
Strontium	180	0	0	0
Sulphate	0	0	0	2965
Iron	175	175	175	0
sulphide	0	0	0	500
Chloride	45127	44581	42975	19027

Table 3.4 Compositions of Miller FW and SW Analogues used in Experiments in Chapter 6					
All concentrations in milligrams per Litre					
Ion	Miller FW 1	Miller FW 2	Miller FW 3	Miller FW 4	North Sea Seawater
Sodium	27080	27080	27080	27080	10890
Calcium	735	0	735	0	428
Potassium	1340	1340	1340	1340	1368
Magnesium	105	105	0	0	460
Barium	775	775	775	775	0
Strontium	180	180	180	180	0
Sulphate	0	0	0	0	2965
Iron	175	175	175	175	0
sulphide	0	0	0	0	500
Chloride	45127	43827	44821	43521	19027

Table 3.5 Compositions of Nelson FW and SW Analogues used in Experiments in Chapter 7

All concentrations in milligrams per Litre

Ion	Miller FW 1	SW1	Miller FW 2	SW2	Miller FW 3	SW3
Sodium	31275	10890	31275	10890	31275	10890
Calcium	2000	428	2000	428	2000	428
Potassium	654	1368	654	1368	654	1368
Magnesium	739	460	739	460	739	460
Barium	268	0	268	0	268	0
Strontium	771	0	771	0	771	0
Sulphate	0	2960	0	2960	0	2960
Iron	0	100	0	0	0	0
Zinc	0	0	0	0	0	250
Lead	0	0	0	100	0	0
sulphide	500	0	500	0	500	0
Chloride	54173	20133	54173	20133	54173	20133

Table 3.6 Compositions of Nelson FW and SW Analogues used in Experiments in Chapter 8

All concentrations in milligrams per Litre

	Forties Formation Water Analogues							
Ion	A1	A2	A3	A4	A5	A6	A7	Seawater
Sodium	10000	10000	10890	10890	10890	10890	10890	10000
Calcium	1163	1163	428	428	428	428	428	0
Potassium	1340	1340	1368	1368	1368	1368	1368	0
Magnesium	1473	1473	460	460	460	460	460	0
Zinc	0	0	250	250	0	250	250	0
Lead	0	100	0	100	100	0	100	0
HCO3	0	0	0	0	0	0	0	2520
sulphide	0	0	0	0	500	500	500	0
Chloride	22989	22989	22989	22989	22989	22989	22989	15421

3.9 Summary

The brine compositions used in this thesis were chosen to best replicate field production conditions as closely as possible. An attempt was also made to simulate the worst case scenarios by using high concentrations of sulphide in the brines (over 200 ppm). The impact of using such high concentrations means that all the sulphide scales capable of forming are formed and precipitate out, even in mixed multiple sulphide scenarios. This chapter presents a detailed list of the precise brine compositions used throughout this thesis.

Chapter 4: Sulphide Scale Prediction and Its Relation Scale to Test Design

This chapter presents a detailed description of the sulphide model, leading to the prediction of saturation ratios and masses of the formed sulphide scales, final solution compositions, pH etc. The equilibrium equations for the sulphide system are derived and solved in a manner in which they are compared directly with the experimentally measured quantities. The actual Saturation Ratios (SRs) (e.g. SR = $[Fe^{2+}][S^{2-}]/K_{spFeS}$) are calculated for the various experiments and the prediction model is used directly to the design the details of the sulphide scaling experiment in the blank solutions. A number of calculated examples are presented and some key predictions of the sulphide scaling model are tested experimentally and agreement between the predictions of the model and the experiments are very good.

4.1 Background and Introduction

The ability to correctly predict the occurance and severity of oilfield scales during the life time of producing fields is of great importance to oil production companies. Sulphide scale deposits have been reported where sour reservoirs are being produced and/or in wells in deeper, higher temperature reservoirs (Alnes 2009).

Iron sulphide scale has been the most common of the oilfield sulphide scales to date and this has posed a number of problems in field and storage facilities (Alnes 2009). Commercial prediction codes have been developed which predict various oilfield scales, although only a few of these codes can predict sulphides scales. In Chapter 2, a list of the codes and the scales which they are able to predict is given in Table 2.2. However, these codes are not "open" and the precise formulation of the sulphide equations cannot be seen.

In addition, it may not be possible or easy to simulate the exact process in which the sulphide scaling experiments are performed. The subsequent chapters of this thesis will present a description of how simple experiments can be carried out to test inhibitors which will help to prevent or disperse sulphide scales. This procedure requires that FeS be produced (or ZnS or PbS) in blank (uninhibited) tests in a systematic manner at given saturation ratios (e.g. SR = $[Fe^{2+}][S^{2-}]/K_{spFeS}$). For iron sulphide, for example, the 2 component solutions of the scaling mix are described as follows:

Solution A containing the Fe^{2+} ions at a given concentration and at a given pH; and

Solution B containing a certain concentration of Na_2S as a source of "sulphide ion" (actually $[H_2S]$, $[HS^-]$ and $[S^{2-}]$).

Solution B is quite alkaline since H_2S is a very weak acid but NaOH is a strong alkali. On mixing of Solutions A and B, a precipitate or colloidal dispersion of FeS forms and the resulting solution has a certain final pH which is measured. The mixed solution (A + B) has some initial Scaling Ratio (SR) of FeS (or PbS or ZnS) which in the final equilibrium solution will be SR = 1

and a certain mass of sulphide scale will form. The final solution also has some final composition (of [Fe^{2+}], H_2S], [HS^-] and [S^{2-}]), pH etc.

In this chapter, the chemical equilibrium equations for FeS prediction is revisited, which are strongly coupled to the H_2S and pH in solution. The equilibrium equations for the sulphide system are derived and solved in a manner in which can be compared directly with the experimentally measured quantities in Solutions A and B described above. The model shows how the actual Saturation Ratios (SRs) are calculated for the various experiments and the prediction model can be used directly to design the details of the sulphide scaling experiment in the blank solutions. Thus, when inhibitors are applied, it is been used in systems which are well characterised in terms of SR. A number of calculated examples are presented and some key predictions of the sulphide scaling model are tested experimentally. This chapter reveals that agreement between the model predictions and the experiments are very good.

4.2 The Sulphide Scaling Equations

4.2.1 The Sulphide- Metal System

The sulphide scaling equations are bound up with the overall fate of H_2S and metal cation (Fe^{2+}, Zn^{2+} and/or Pb^{2+}) in an oilfield produced brine. The chemical equations for the sulphide-metal system (using iron as example) are as follows:

1. $H_2S_{(aq)} \rightleftharpoons H^+ + HS^-$ $\qquad K_1 = \dfrac{x_2.x_3}{x_1}$

   $x_1 \qquad\qquad x_2 \quad x_3$

2. $HS^- \rightleftharpoons H^+ + S^{2-}$ $\qquad K_2 = \dfrac{x_2.x_4}{x_3}$

   $x_3 \qquad\qquad x_2 \quad x_4$

3. $Fe^{2+} + S^{2-} \rightleftharpoons FeS_{(s)}$ $\qquad K_{sp1} = x_5.x_4$

   $x_5 \quad x_4 \qquad\qquad x_7$

4. $H_2O \rightleftharpoons H^+ + OH^-$ $\qquad K_w = x_2.x_6$

   $x_2 \quad x_6$

Where the following notation for the concentrations of the seven (7) species in the system have been used:

Notation	Species
x_1 =	$[H_2S]_{(aq)}$
x_2 =	$[H^+]$
x_3 =	$[HS^-]$
x_4 =	$[S^{2-}]$
x_5 =	$[Fe^{2+}]$
x_6 =	$[OH^-]$
x_7 =	$[FeS]_{(s)}$

Note that there are 7 unknowns in the system at equilibrium but four (4) equilibrium equations (Eqns. 1 to 4 above), and hence 3 more equations are required. These are, as usual, the normal 2 mass balances (for S and Fe) and 1 charge balance equation as follows:

5. $Total\ Sulphur\ (M),\ X_S = x_1 + x_3 + x_4 + x_7$

6. $Total\ Fe\ (M),\ X_{Fe} = x_5 + x_7$

7. $Total\ Charge\ (M),\ C = x_2 - x_3 - 2x_4 + 2x_5 - x_6$

Thus, Equns. 1 – 7 define the sulphide metal system exactly in that there are seven (7) equations in seven (7) unknowns. In summary, the full sulphide model is shown below:

Summary of the Sulphide-Iron Scaling System

Equilibrium Equations

1. $H_2S_{(aq)} \rightleftharpoons H^+ + HS^-$ $\quad K_1 = \frac{x_2.x_3}{x_1}$

   x_1 $\quad x_2$ $\quad x_3$

2. $HS^- \rightleftharpoons H^+ + S^{2-}$ $\quad K_2 = \frac{x_2.x_4}{x_3}$

   x_3 $\quad x_2$ $\quad x_4$

3. $Fe^{2+} + S^{2-} \rightleftharpoons FeS_{(s)}$ $\quad K_{sp1} = x_5.x_4$

   x_5 $\quad x_4$ $\quad x_7$

4. $H_2O \rightleftharpoons H^+ + OH^-$ $\quad K_w = x_2.x_6$

   x_2 $\quad x_6$

Mass Balances (Sand Fe)

5. *Total Sulphur* (M), $X_S = x_1 + x_3 + x_4 + x_7$

6. *Total Fe* (M), $X_{Fe} = x_5 + x_7$

Charge Balance

7. *Total Charge* (M), $C = x_2 - x_3 - 2x_4 + 2x_5 - x_6$

For a set of known (measured or literature) equilibrium constants K_1, K_2, K_{sp1} and K_w, and input total amounts of sulphur (X_S), iron (X_{Fe}) and charge (C), the above 7 equations can be solved numerically to give the equilibrium state of the system i.e the equilibrium values of the unknowns x_1 to x_7. These equations have been solved numerically and this sulphide model has been coded in VBA within an Excel spreadsheet. The actual reduced equations which are solved and an outline of our solution strategy are given in Appendix A of this chapter. The equilibrium constants K_1, K_2, K_{sp1} and K_w used in these sulphide scaling calculations have been taken from the literature. There is some uncertainty on the exact values of some of these constants but recommended values have been given (Myers 1967; Flaschka 1980; Day 1991; Benning 2000; Wei 2006) The actual numbers used are summarised in Table 4.1.

Eq. Constant	Reaction	Recomm-ended value	Range reported	Literature References
K_1	$H_2S \rightleftarrows H^+ + HS^-$	9.632×10^{-8}	1.333×10^{-8} 9.632×10^{-8}	Flaschka *et al* (1980), Day and Underwood (1991), Wei 2006
K_2	$HS^- \rightleftarrows H^+ + S^{2-}$	$\sim 1.00 \times 10^{-17}$	1.148×10^{-12} 1.00×10^{-19}	Weast (1991), Myers (1967)
K_{sp1}	$Fe^{2+} + S^{2-} \rightleftarrows FeS_{(s)}$	1.29×10^{-19}	1.36×10^{-17} 1.29×10^{-19}	Morse *et al* 1987, Berner 1967, Helgeson (1969)
K_{sp2}	$Zn^{2+} + S^{2-} \rightleftarrows ZnS_{(s)}$	2.03×10^{-25}	2.03×10^{-25} 3.00×10^{-23}	Daskalakis et al 1993; Ronngren *et al* 1993; Tagirov *et al* 2007.
K_{sp3}	$Pb^{2+} + S^{2-} \rightleftarrows PbS_{(s)}$	3.80×10^{-28}	4.0×10^{-28}	Barnes 1960; Barrett and Anderson 1982
K_w	$H_2O \rightleftarrows H^+ + HO^-$	1.00×10^{-14}	1.00×10^{-13} 1.00×10^{-14}	Anderegg (1967), Lucas (1967)

Table 4.1: Equilibrium constants (T = 20°C) for the sulphide system in Eqns. 1 – 7.

4.2.2 Base Case Numerical Solution of Sulphide Equations

Suppose a specific mixture of sulphide (from Na_2S) and iron (as Fe^{2+}) in two solutions are mixed them together. This would give a specific mixture composition in which the total sulphur (X_S) would be known (in whichever form - [H_2S], [HS^-] and [S^{2-}]) and the total iron (X_{Fe}) and the total charge (C). The equations of the full sulphide model can be solved using equations (Eqns. 1 – 7 above) to obtain the composition of the final equilibrium solution (i.e. x_1 to x_7). As an example: if the following composition of the initial solution by defining the aqueous [H_2S] and the [Fe^{2+}]:

$x_{10} = [H_2S]_{aq}$ = 1.0000E-03M (34.1ppm)
$x_{10} = [Fe^{2+}]_{aq}$ = 3.0000E-02M (1675.5ppm)

and it is known that these were present in distilled water ([H^+] = [OH^-] = 1E-07 M). Solving the equation set for the sulphide model will result in the following solution:

Converged solution z1, z2				
z1 = x2			pH	
= [H+]=	6.14691E-06	M	5.21	
z2 = x5				
[Fe2+]=	2.99982E-02	M	1675.40	ppm
Back substitute to obtain ..				
x4 =[S2-]	4.30025E-18	M		
x3=[HS-]	2.64333E-06	M		
x1=[H2S]	9.95606E-04	M		
x6=[OH-]	1.62683E-09	M		
x7 =[FeS]	1.75098E-06	M		
Mass FeS per Litre				
=	1.53936E-01	mg		
		after		
Sp_FeS =	1.00000E+00	pptn.		
	4.07204E+11	before pptn..		

This is an exact numerical solution for the 7 equilibrium equations and several issues should be noted for this equilibrium composition, as follows:

(i) the final pH = 5.21 and is on the acidic side and would be expected since H_2S in water is weakly acidic;

(ii) a tiny amount of the iron is missing ([Fe^{2+}] goes from 1675.5ppm to 1675.4ppm) and the missing Fe turns up as the ~0.15mg of FeS;

(iii) although a very small amount of FeS forms, it is at a very high Saturation Ratio (SR) of ~4.07E11 – this is hugely higher than the SR seen for $BaSO_4$ indicating that this FeS scale is occurring at more severe SR levels;

(iv) given the very high SR levels, it is difficult to predict what levels of sulphide scale inhibitors (SI) that may be required to disperse this small amount of FeS. This is the function of the inhibitor tests which are described and carried out in the sulphide studies of this thesis.

Solving the above equations as they stand does not model how the actual sulphide inhibition experiments i.e. by mixing 2 solutions (A and B), as described above are performed. The procedure used to design and analyse these experiments is given in the following section.

4.2.2 The Fe Solution (Solution A) + The Na_2S System (Solution B)

As noted above, the actual experimental procedure for forming FeS (or other sulphides) in our inhibitor testing is not to set the $[H_2S]$ and $[Fe^{2+}]$ levels in distilled water. Hence, the sulphide prediction in Section 4.2.2 does not reflect what is done in the actual experiments. Instead, to predict what happens in our experiments, it should be recognised that the process takes two solutions as follows:

Solution A - containing the Fe^{2+} ions at a given concentration and at a given pH; and

Solution B - containing a certain concentration of Na_2S as a source of "sulphide ion" (actually $[H_2S]$, $[HS^-]$ and $[S^{2-}]$).

Solution A requires no calculation and it is specified completely by simply inputting $[Fe^{2+}]$ and pH (and therefore $[H^+] = 10^{-pH}$). An example of a Solution A composition is as follows:

Input SOLUTION A		
X2 = [H+]=	2.5119E-07	M
pH =	**6.6**	
x1 = [H2S]	0.0000E+00	M
x3 =[HS-]=	0.0000E+00	M
x4=[S2-]=	0.0000E+00	M
x5=[Fe2+]=	**3.5810E-05**	M
[Fe2+]ppm=	**2**	
x6=[OH-]=	3.9811E-08	M
x7=[FeS]s=	0	M
Fraction A=	**0.5**	
Charge =	7.1832E-05	

Note that there is no sulphur (S) in Solution A – the only species with non-zero concentrations are the Fe^{2+}, H^+ and OH^- ions. On the other hand, Solution B is the source of sulphur which is added as the salt Na_2S (i.e. as S^{2-}). However, this sulphide ion (S^{2-}) will re-speciate in water to

give an alkali solution, governed by Eqns. 1, 2 and 4 in the sulphide system above (no Fe equation); that is, the Na_2S solution is described solely by the equations:

Summary of the Na_2S System

1. $H_2S_{(aq)} \rightleftarrows H^+ + HS^-$ $\quad K_1 = \frac{x_2.x_3}{x_1}$

   x_1 $\quad x_2$ $\quad x_3$

2. $HS^- \rightleftarrows H^+ + S^{2-}$ $\quad K_2 = \frac{x_2.x_4}{x_3}$

   x_3 $\quad x_2$ $\quad x_4$

4. $H_2O \rightleftarrows H^+ + OH^-$ $\quad K_w = x_2.x_6$

   x_2 $\quad x_6$

Mass Balances (Sand Fe)

5. *Total Sulphur* (M), $X_S = x_1 + x_3 + x_4$

Charge Balance

7. *Total Charge* (M), $C = x_2 - x_3 - 2x_4 - x_6$

Therefore, to predict the pH of Solution B, the above system of 5 equations (equilibria + mass + charge balance equations) must be solved. An example of this is shown below where the initial input sulphide ion concentration is 20ppm (which gives $[S^{2-}]$ = 6.2375E-04 M) in neutral brine or distilled water.

Converged SOLUTION B (from above)

X2 = [H+]=	1.6029E-11	M
pH =	10.795	
x1 = [H2S]	1.0379E-07	M
x3 =[HS-]=	6.2365E-04	M
x4=[S2-]=	3.8907E-10	M
x5=[Fe2+]=	0	M
[Fe2+] ppm =	0	
x6=[OH-]=	6.2386E-04	M
x7=[FeS]s=	0	M
Fraction B=	**0.5**	
Charge =	-1.2475E-03	

(-2 * S2-_orig)

Note that the sulphide does indeed greatly re-speciate with nearly all of the S ending up as the $[HS^-]$ ion with only tiny amounts of $[H_2S]_{(aq)}$ and $[S^{2-}]$ being formed. The process also leads to a fairly alkaline solution being formed since the higher negative charge ultimately appears as OH^- ions, as expected since the sulphide ion is a weak base.

The blank solution for a sulphide inhibition test is made by adding together Solutions A and B. Before reacting, the initial composition of this A+B mixture is given by the *average* composition as shown below for the 2 example solutions above.

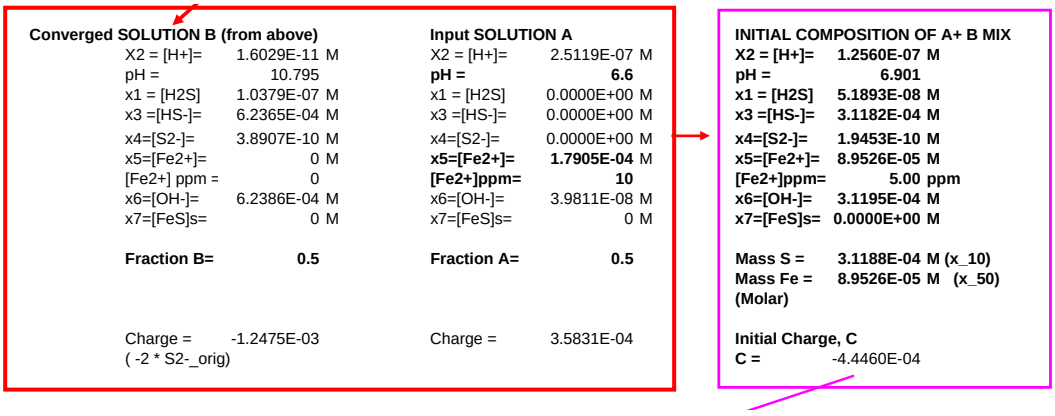

Converged SOLUTION B (from above)			**Input SOLUTION A**		
X2 = [H+]=	1.6029E-11	M	X2 = [H+]=	2.5119E-07	M
pH =	10.795		**pH =**	**6.6**	
x1 = [H2S]	1.0379E-07	M	x1 = [H2S]	0.0000E+00	M
x3 =[HS-]=	6.2365E-04	M	x3 =[HS-]=	0.0000E+00	M
x4=[S2-]=	3.8907E-10	M	x4=[S2-]=	0.0000E+00	M
x5=[Fe2+]=	0	M	**x5=[Fe2+]=**	**1.7905E-04**	M
[Fe2+] ppm =	0		**[Fe2+]ppm=**	**10**	
x6=[OH-]=	6.2386E-04	M	x6=[OH-]=	3.9811E-08	M
x7=[FeS]s=	0	M	x7=[FeS]s=	0	M
Fraction B=	**0.5**		**Fraction A=**	**0.5**	
Charge =	-1.2475E-03		Charge =	3.5831E-04	
(-2 * S2-_orig)					

INITIAL COMPOSITION OF A+ B MIX		
X2 = [H+]=	**1.2560E-07**	**M**
pH =	**6.901**	
x1 = [H2S]	**5.1893E-08**	**M**
x3 =[HS-]=	**3.1182E-04**	**M**
x4=[S2-]=	**1.9453E-10**	**M**
x5=[Fe2+]=	**8.9526E-05**	**M**
[Fe2+]ppm=	**5.00**	**ppm**
x6=[OH-]=	**3.1195E-04**	**M**
x7=[FeS]s=	**0.0000E+00**	**M**
Mass S =	**3.1188E-04**	**M (x_10)**
Mass Fe =	**8.9526E-05**	**M (x_50)**
(Molar)		
Initial Charge, C		
C =	-4.4460E-04	

In the example above, a 50:50 mix of Solutions A and B is taken and the average initial composition is as given. The mixture has effectively 10ppm sulphide + 5ppm iron (obviously half the values in the individual solutions in a 50:50 mix). However, this solution is ***not*** at equilibrium, it simply provides us with the total masses of S and Fe and the effective charge of the changing ions (ions that do not change such as Na^+ and Cl^- are neglected; the total charge in an actual solution is of course zero). These are then used in the full sulphide model (Eqns. 1 -7 above) to predict the final equilibrium composition of the fluid which in this case is as follows:

Back Substitution to obtain all species ..

Converged solution z1, z2

z1 = x2			pH	
= [H+]=	4.49739E-11	M	10.35	
z2 = x5				
[Fe2+]=	2.61041E-09	M	1.46E-04	ppm

Back substitute to obtain ..

x4 ={S2-]	4.94175E-11	M	Total S (M)	
			3.1188E-04	
x3=[HS-]	2.22250E-04	M		
x1=[H2S]	1.03773E-07	M		
x6=[OH-]	2.22351E-04	M		
			Total Fe (M)	
x7 =[FeS]	8.95229E-05	M	8.9526E-05	
Mass FeS				
per Litre =	7.87032E+00	mg		
Sp_FeS =	**1.00000E+00**	**after pptn.**		
	6.21286E+10	**before pptn..**		

Several points can be noted from this result:

(i) the pH of the final solution is quite alkaline (pH = 10.35);

(ii) because there is an excess of S, virtually all of the iron is consumed (forms FeS) – the final $[Fe^{2+}]$ is tiny, as is $[H_2S]$.

(iii) the FeS readily appears because the solubility product of FeS is so low (K_{sp1}=1.29x10^{-19}) – the Saturation Ratio (SR) = ~6.29x10^{10}. The solution is greatly oversaturated despite the very low initial concentrations of iron (5ppm) and sulphide (10ppm) in the initial mix.

4.3 Experimental Confirmation of Sulphide Prediction Models

4.3.1 Predicted vs. Experimental Na_2S (Solution B) pH Values

In this section, results are presented which test the accuracy of the sulphide prediction model discussed above. Firstly, test the model on the simple solution of Na_2S (in brine or distilled water) where no FeS forms (Solution B). This is described by the solution of Eqns. 1, 2 and 4 with values of K_1, K_2 and K_w in Table 4.1, as discussed above. Figure 4.1 and 4.2, show the

measured pH for a series of Na_2S solutions in distilled water compared with the direct predictions from the model. The same data is presented on these two figures but Figure 4.2 shows the sulphide concentration axis with a log scale so that the lower concentration pH results are clear. The agreement between predicted and experimental pH values for concentrations above 1ppm is excellent. This is encouraging since it shows the model is sufficiently quantitatively accurate for test design purposes.

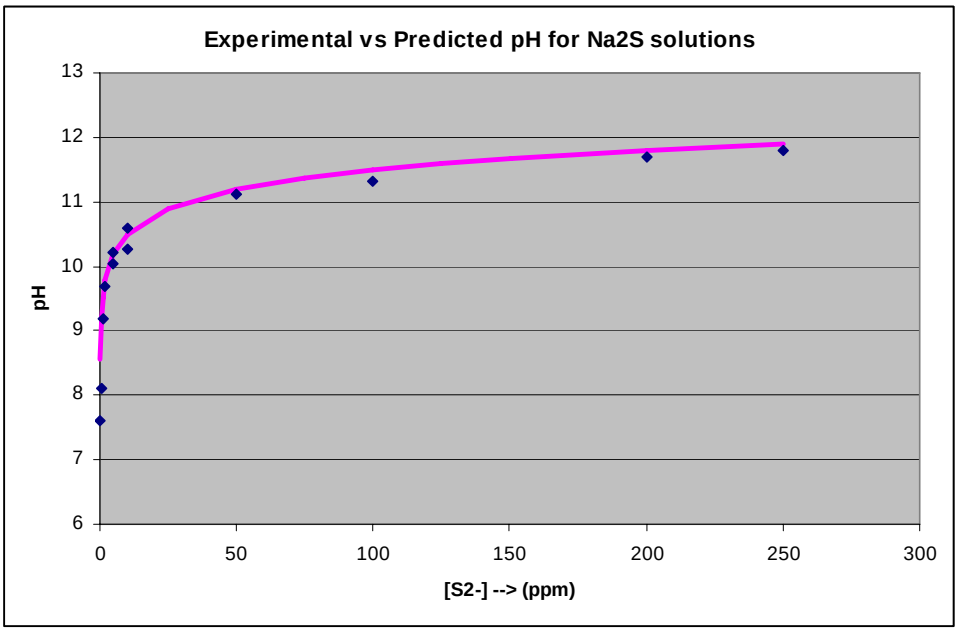

Figure 4.1: Comparison of the measured and predicted pH values for a range of Na_2S solutions (0 – 250 ppm).

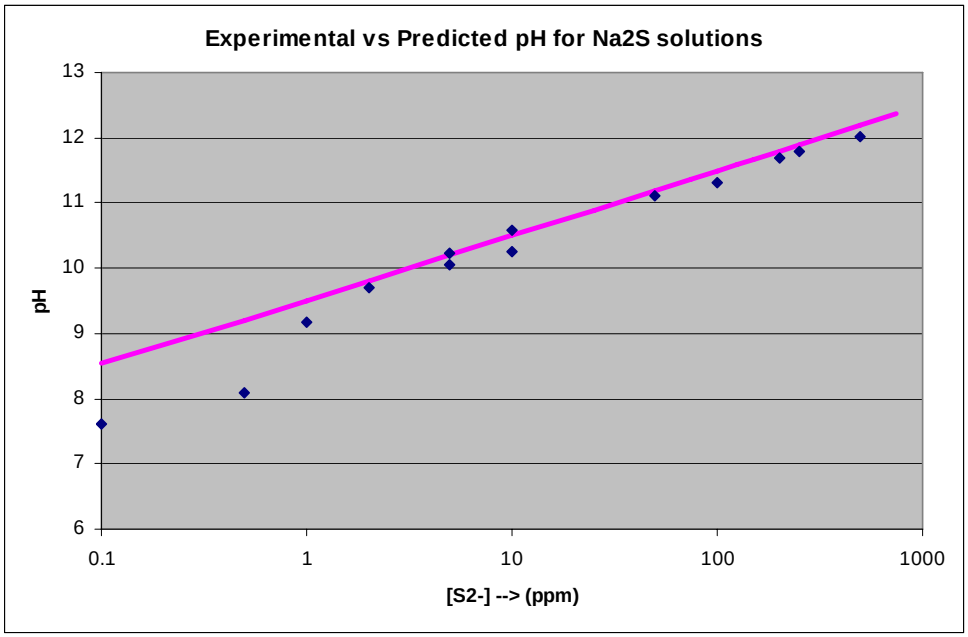

Figure 4.2: Comparison of the measured and predicted pH values for a range of Na_2S solutions.

4.3.2 Predicted vs. Experimental pH Values for the Full Solution A+B Experiments

In this subsection results are presented of how accurate the model can predict the final pH of the Solution A + B experiments. A number of solutions with the varying compositions was made:

Solution A		**Solution B**			50:50 A+B	
[Fe2+]	**pH**	**[Na2S] or [S2-]**	**Predicted [S2-] pH**	**Experimental [S2-] pH**	**Predicted FeS pH**	**Experimental FeS pH**
1ppm	6.70	1ppm	9.495	9.21	8.93	8.43
1ppm	6.70	5ppm	10.19	10.44	9.84	9.59
1ppm	6.70	10ppm	10.494	10.80	10.17	10.20
5ppm	6.41	1ppm	9.495	9.21	8.31	8.18
5ppm	6.41	5ppm	10.19	10.44	9.51	9.35
5ppm	6.41	10ppm	10.494	10.80	10.05	9.98
10ppm	6.13	1ppm	9.495	9.21	8.10	8.11
10ppm	6.13	5ppm	10.19	10.44	8.46	8.22
10ppm	6.13	10ppm	10.494	10.80	9.82	9.56

Graphical plots of experimental FeS solution final pH results vs. the model predicted pH results is presented in Figure 4.3. The pH results are found to match within experimental error. Note that the pH was measured in duplicate and the reproducibility is very good. Figures 4.4 and 4.5 show the graphical plots of predicted FeS precipitate and the experimental FeS precipitate collected and measured after mixing solution A+B. These results indicate that the model is accurate in predicting sulphide SR, precipitated mass and final pH of sulphide solutions.

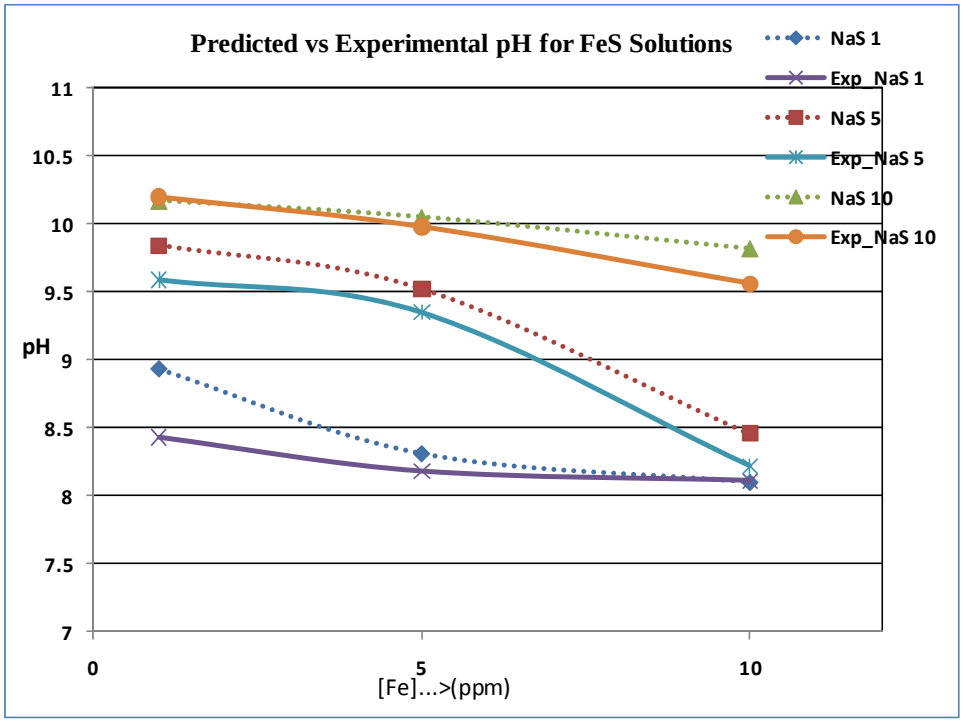

Figure 4.3: Comparison of the measured and predicted pH values for a range of FeS solutions

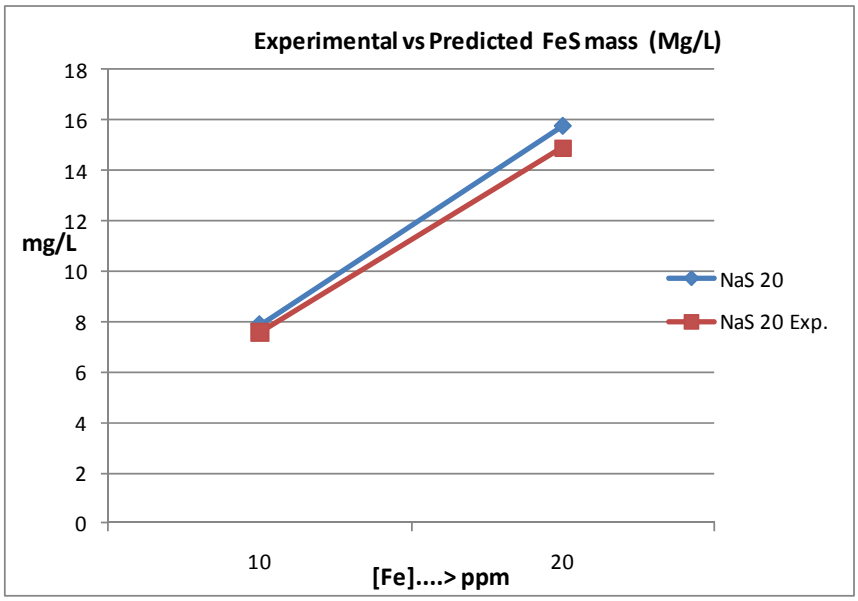

Figure 4.4 Comparison of the measured and predicted mass for a range of FeS solutions

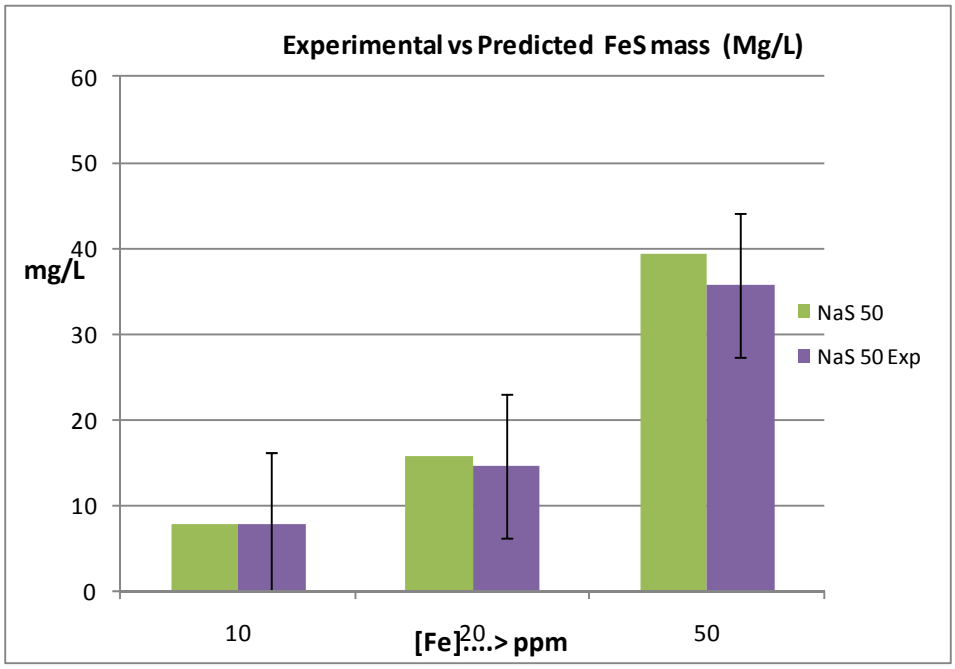

Figure 4.5 Comparison of the measured and predicted mass for 50 ppm [S^{-2}] for a range of FeS solutions

4.3.3 The Fixed pH Sulphide-Iron System

It is known that in most reservoirs, the pH is stabilized within a fairly narrow margin and it tends not to fluctuate very widely. In this subsection, results representing a case where the pH is fixed and the calculations are presented for a [Fe^{2+}] = 5ppm case. Results for the soluble [Fe^{2+}] vs. pH are shown in Figure 4.6 and it is seen that above about pH ~6, all the FeS in the system precipitates out. The full calculation and associated derivation are shown in Appendix A of this thesis. In the fixed pH case, $[H^+]$ is given a specific value, denoted as $[H^+] = \bar{x}_2$ which creates a solvable quadratic equation. Although and FeS case is shown in this example, the model can equally work for ZnS and PbS scales.

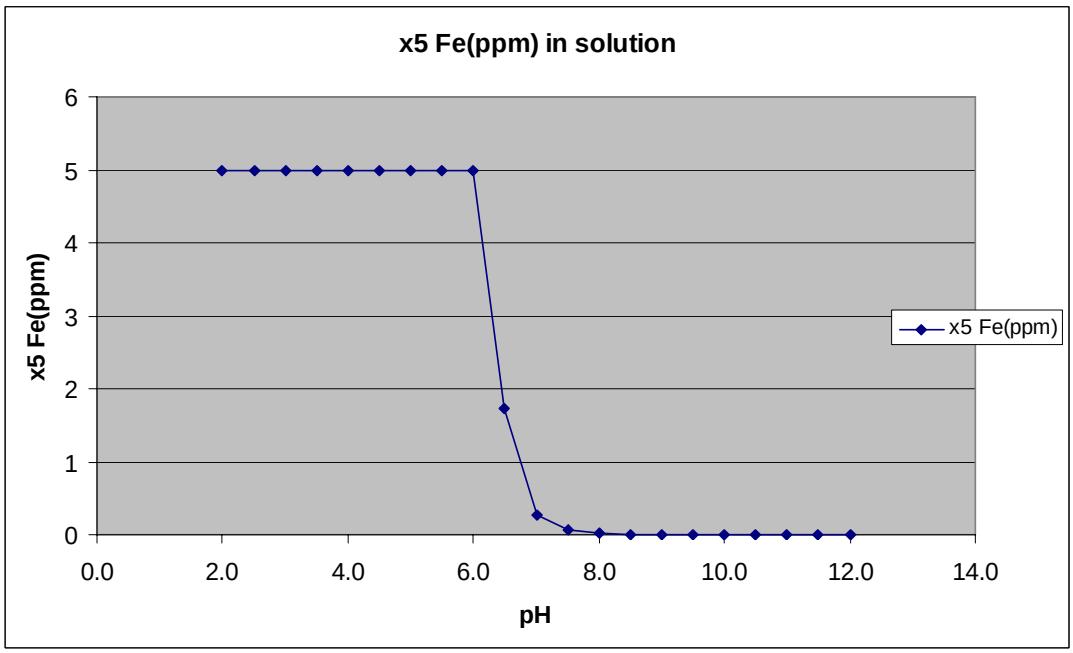

Figure 4.6 Plot of the iron concentration as a function of pH for the data above.

4.4 Discussion and Conclusions

A metal/sulphide model has been developed from the equilibrum equations obtained from the literature. The sulphide model is produced by solving 7 equilibrium equations involved in sulphide (FeS, ZnS, PbS) scale formation. The equations include, $[H_2S]$, $[HS^-]$, $[H_2O]$, [FeS], $\sum[S]$, $\sum[Fe^{2+}]$ and $\sum$charge balance equations. The numerical solution for the 7 equilibrium equations was determined using the Newton-Rhapson numerical method (see Appendix A). The sulphide model is capable of predicting accurately H_2S, and FeS Saturation Ratio (SR). Excellent agreement has been observed between the results from the sulphide prediction model, particularly the final solution pH and the precipitated mass of FeS, and laboratory experiments. The sulphide prediction model has been applied mainly to the FeS system in this work. However, this is the most difficult sulphide to validate experimentally because of the various possible oxidation states of iron (Fe II and Fe III). The ZnS and PbS systems do not have this oxygen concern and, since these scales also have a much lower K_{sp} than FeS, the model can easily be applied to these scales.

Chapter 5 Characterisation and Mechanisms of Scale Inhibitor (SI) for FeS Inhibition

This chapter presents results from anaerobic static bottle tests on a range of different sulphide scale inhibitors (SIs). Performance of sulphide inhibitors is categorized using both visual and ICP [Fe] results. The results show different inhibition mechanisms employed by the SIs, and the effect on FeS formation. The particle size of FeS was determined and the results are presented for cases both with and without SI (PPCA and DETPMP). SI co-precipitation of [Fe] prior to FeS formation is also studied in this chapter.

5.1 Introduction

The work discussed in this Chapter characterises the ways in which generic scale inhibitors (SI) for sulphate/carbonate or sulphide scales perform in the presence of iron sulphide (FeS) scales. Central to the work discussed here is the fact that different SI types (phosphonates and polymers) inhibit scales in slightly different ways. The aim of this study is to group the observed sulphide inhibition patterns into categories by examining their performance in simple (FeS) sulphide scaling systems. The effect that SI type has on the particle size of FeS will also be examined. The results will also throw some light on the mechanisms of sulphide inhibition.

5.2 Experimental Setup for the Commercial Scale Inhibitors

A number of commercial scale inhibitors were used in the sulphide scale inhibition efficiency testing program. These SIs varied in composition and specificity, and several of them were *not* intended for use against FeS scale; some were designed more to prevent Pb/ZnS scales and a coded list of these products is given in Table 5.1 The performance of each of the SIs was measured using static efficiency tests as described in Chapter 3, sampled at 2 and 22 hours after mixing. Tests were buffered to pH 6.8 using acetic acid/sodium acetate solution, and a 50:50 volumetric ratio of sulphide scaling water was used in all cases, as detailed in Chapter 3. These waters were prepared using distilled water by dissolving accurately weighed amounts of the relevant salts in a fixed volume of solution. Strict anaerobic condition was maintained during the experiment as described in Chapter 3. The SIs were initially tested over the lower concentration range (as usually applied for sulphate/carbonate scales) 10, 50, and 100ppm for a 50ppm FeS mix (as shown in Experiment 1). Subsequently, the SI concentration was increased to 100, 150 and 200ppm (as shown in Experiment 2) for the same FeS solution concentration.

5.3 Visual Observation and Static Results for Generic Phosphonate and Polymeric Scale Inhibitor

The initial experiments were performed using DETPMP representing the phosphonate group of SIs, and PPCA representing the polymer group of SIs. The aim was to use these SIs as "bench marks" with which several sulphide SIs were to be *"categorised"*. Figure 5.1 shows the inhibition efficiency for the DETPMP (phosphonate) for $BaSO_4$ with the visual observations and conditions. Note that the efficiency reduces with an increase in [SI] from 50 to 200ppm for the 2hr time while there is a reduction in efficiency at 22hrs. This can be attributed to the FeS interference/poisoning of the SI. At 22hrs, the Blank samples (at 10 and 50pppm) show a settling/separation to the bottom of the bottle of the formed FeS. Figure 5.2 shows the inhibition efficiency for PPCA for $BaSO_4$ and its accompanying visual observations. Note the higher efficiencies of the SI at the 2hr time compared with the DETPMP but this is not reflected in the visual observations. At 22hrs the efficiencies do drop but they are noticeably higher than for the DETPMP. FeS is observed to have settled at the base of the sample bottles, as shown in Figure 5.2. These experiments demonstrated that the primary inhibition mechanism of the SI (DETPMP and PPCA) is unaffected by the presence of FeS. The SIs inhibition mechanism continues to retain all it functions even though it is in a suppressed form.

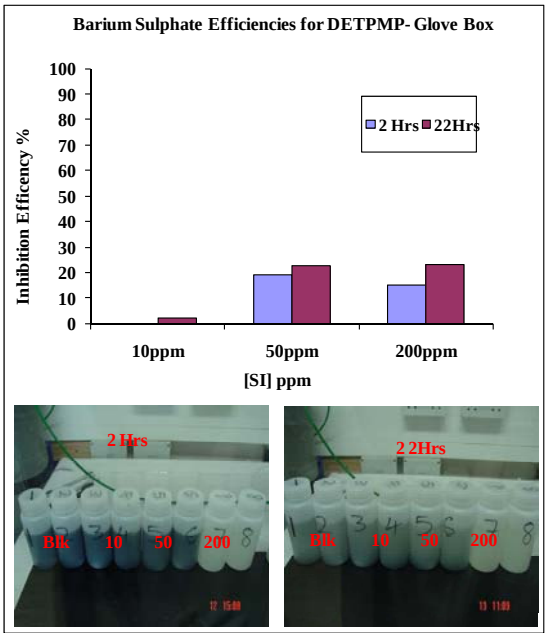

Figure 5.1 $BaSO_4$ Efficiencies for DETPMP

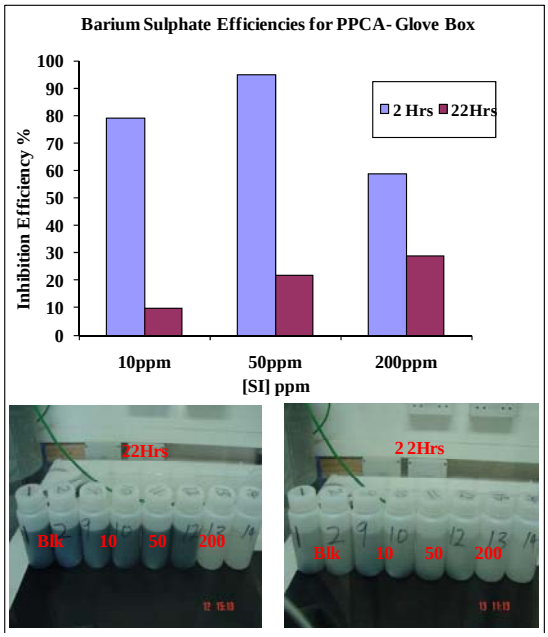

Figure 5.2 BaSO4 Efficiencies for PPCA

5.3.1 Visual Observation and Static Results for Various Commercial Scale Inhibitor Types

The visual observations and the fate of the iron in solution ([Fe]) in a $BaSO_4$/FeS mix are used to categorise the SIs that were tested for their performance with FeS. Two identical experiments were carried as described in Chapter 3 but with increasing concentration of SI. The first experiment was carried out at 10, 50, and 100ppm SI concentration, while the second experiment was carried out at 100, 150, and 200ppm SI concentration. A summary of both sets of results (low and high [SI] – Experiments 1 and 2) for each species in turn is shown in Figures 5.3 - 5.15. Each of these Figures shows the final [Fe] vs. the initial [SI] at 2 and 22 hours at the top, and below this an image of the actual test samples is shown for Experiments 1 and 2 at 2 and 22 hours.

5.3.2 Iron Sulphide Scale Inhibitor Visual Characterisation

The inhibition behaviour of some SIs tested against FeS in the field was reported (Przybylinski 2001). However no distinctive behaviour(s) was reported or characterised, also specific SI types were not given in that study. Table 5.1 below summarises the observed behaviour for each SI

type tested for the FeS scaling system in this work. The visual results for these SIs can be grouped together; as they react in the same way to the FeS, as follows:

Behaviour type A - Black solution when scaling waters are mixed and remain black (e.g. blank).

Behaviour type B - Black solution when scaling waters are mixed which then clarify within 24 hours.

Behaviour type C - Clear solution when scaling waters are mixed and stay clear.

One plausible theory for the change from black FeS solution to a clear solution (Behaviour B) may be that of delayed activation of the SI due to *kinetics*, as the SI made more contact with the FeS it got to a point when the SI self activated and chelated the [Fe] breaking the FeS bond. Another theory may be the change of the SI functionality to a *ligand/chelate* compound caused by the presence of the FeS, this behaviour was not noticed for ZnS or PbS.

5.3.3 Iron sulphide scale inhibitor characterisation using [Fe] from ICP results

The SIs showed two distinct behaviour based on the [Fe] measured on the ICP. The results indicate that the phosphonate, phosphonic acid, and Phosphate Ester SIs displayed similar behaviour in the presence of FeS. While the polymeric SI group displayed similar behaviour. Broadly, it appears that phosphonate based products behave somewhat differently to polymeric sulphide inhibitors (with a few exceptions) as follows:

Phosphonate products A, B, C, E and H appear to show a lower "dip" in [Fe] at [SI] = 10ppm which is *lower* at 2 hrs and *increases* at 22hr and then inhibition is observed at higher [SI]; the phosphonate exception is **product D**.

Polymeric products I, F, L, M, and K appear to show high [Fe] over the whole [SI] range and the iron level uniformly decreases at 24 hr; the polymeric exceptions are **products N and G.** Direct links between the types of behaviour that are observed in the sulphide inhibition tests (A, B, and C) and the corresponding solution [Fe] results are qualitative and reproducible results.

SI Code	Chemical Description	Observed Behaviour
A	Phosphonate (DETPMP)	10ppm type A, 50-100ppm type B, 150-200ppm type C
B	Phosphonic acid	10ppm type A, 50-100ppm type B, 150-200ppm type C
C	Phosphonic acid	10-100ppm type A, 150ppm type B, 200 type C
D	Phosphonic acid	10-100 type A, 150ppm type B, 200ppm type C
E	Phosphonic acid	10-100 type A, 150ppm type B, 200ppm type C
F	Co-polymer	10-150 type A, 200ppm type B
G	Co-polymer	10-100 type A, 150-200ppm type B
H	Phosphate Ester	10-50ppm type A, 100-150 type B, 200ppm type C
I	Unknown	10-150ppm type A, 200ppmtype B
K	polymer	10-150 type A, 200ppm type B
L	Unknown	10-150 type A, 200 type B
M	Polyacrylate	10-50 type A, 100-150 type B, 200ppm type C
N	Unknown	10-100 type A, 150 type B, 200ppm type C

Table 5.1: List of Commercial Scale Inhibitor tested.

5.3.4 Scale Inhibitor Testing Summary

Figure 5.3 shows the visual effects of SI A (DETPMP) on FeS at 2 and 22hours after mixing and this graph shows the fate of [Fe] for both experiments. This Figure indicates that the SI is effective from 100mg/L. The 3 SI behaviours (A, B and C) can also be observed as the [SI] is increased. At 50ppm, it shows the transition point between the inhibition and non-inhibition displayed by the partial separation of the FeS into a clear (inhibited) section and a black (uninhibited) section. The graph shows a drop in the [Fe] at 10ppm which was consistent for all of the phosphonate based SIs except N and G (undeclared chemistry as at the time of testing). Figure 5.4 shows the visual effects of SI B (a phosphonic acid based SI) on FeS at 2 and 22hours after mixing where the figure shows the fate of [Fe] concentration for both experiments. The SI B also appears to have a MIC of 100ppm. The drop in [Fe] at 10ppm is also observed. Figure 5.5 shows the result for SI C (a phosphonic acid based SI) similar to SIs A and B. In this experiment, the point to note is the clarity of the solutions after 22hours. This Figure also indicates that the chemical is effective at concentration of 150mg/L, which indicates that SI C is less effective than SIs A and B. The graph shows the fate of [Fe], and it shows the drop in [Fe] at 10ppm similar to A and B. Figure 5.6 shows the visual effects of SI H, (a phosphonate ester based SI) on FeS at 2 and 22hours after mixing. The Figure indicates that the chemical is effective at concentrations from 150 ranging to 200mg/L, again less effective than SI A, with the drop in [Fe] at 10ppm, and the behaviours A,B,C can also be observed. In Figure 5.7, the Figure shows the visual effects and fate of [Fe] for SI G (a copolymer based SI). This experiment shows the 150 and 200ppm solutions clarifying at 22hours. Although labelled as a co-polymer, it performed similarly to the phosphonates, although clarification (behaviour B) occurred only at 150ppm and 200ppm. Figure 5.8 shows the concentrations at which FeS is inhibited by SI E (a phosphonic acid based SI) and the concentration at which it clarifies after 22hours. In this experiment only 200ppm SI solution can inhibit the FeS formation. Figure 5.8 shows that there is a clarifying effect at 150ppm but the chemical is effective at concentration of 200mg/l, behaviours A, B and C is also clearly observed. Figure 5.9 shows the visual effects of SI L (a polymer based SI) on FeS and this Figure indicates that the chemical is not effective at the tested concentrations although a clarifying effect is noted at 200ppm. The graph indicates a constant

[Fe] as the [SI] increases without a drop in concentration. Figure 5.10 shows the visual effects on FeS by SI N (a polymer based SI). It indicates that the chemical is effective at concentrations ranging from ~150ppm to 200mg/L. It shows a drop in [Fe] at 10ppm similar to the phosphonates SIs. Figure 5.11 shows the visual effects of SI M (a Polyacrylate SI) on FeS and this Figure indicates that the chemical is effective at concentrations at 200mg/L and the graph shows a constant level of [Fe] across the [SI]. Figure 5.12 shows the visual effects on FeS by SI D (a phosphonic acid based SI) and the fate of [Fe] and this Figure shows that the chemical is effective at concentration of 200mg/L. Figure 5.13 shows the visual effects on FeS by SI I (chemistry unknown) and the fate of the [Fe]. In this experiment, the chemical (I) is ineffective at all SI concentrations. Figure 5.14 shows the visual effects of SI K (a polymer based SI) on FeS. In this experiment there is no clear inhibition shown by SI K, however there is a change in coloration at 200mg/L after 22hrs, indicating that the chemical is reactive at concentrations of <200mg/L. Figure 5.15 shows the visual effects of SI F (co-polymer based SI). From this experiment it is evident that the chemical is not a suitable iron sulphide inhibitor, although the [Fe] remained unchanged across the [SI] range, these clarification mechanisms were reported by Okocha *et al* (2008). FeS inhibition by SIs of phosphate, polymer and mixed chemistries is accomplished but at differing concentrations and mechanisms based on the chemistries. The SIs retains their primary inhibition mechanisms as it engages with FeS, resulting in three behaviour patterns observed visually for most of the SIs tested, the fate of [Fe] during the experiments can also be categorized based on the SI chemistries.

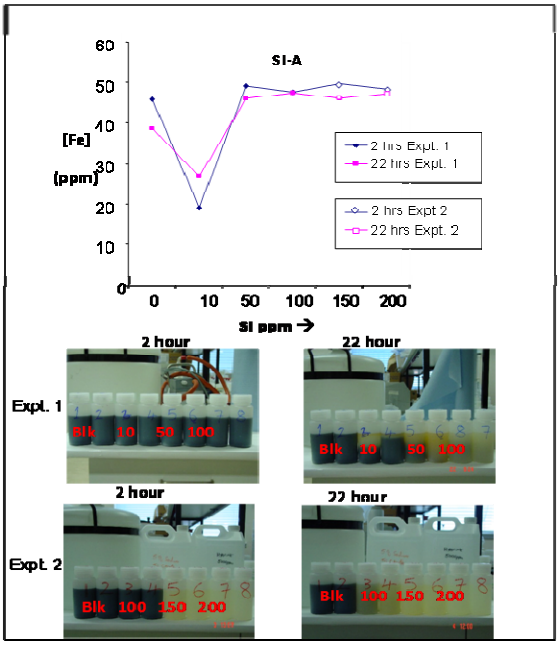

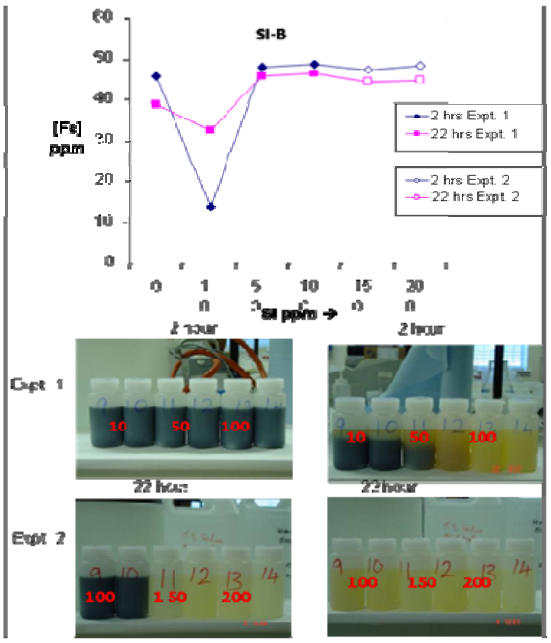

Figure 5.3 SI A on FeS; and graph of [Fe] fate. **Figure 5.4 SI B** on FeS; and graph of [Fe] fate.

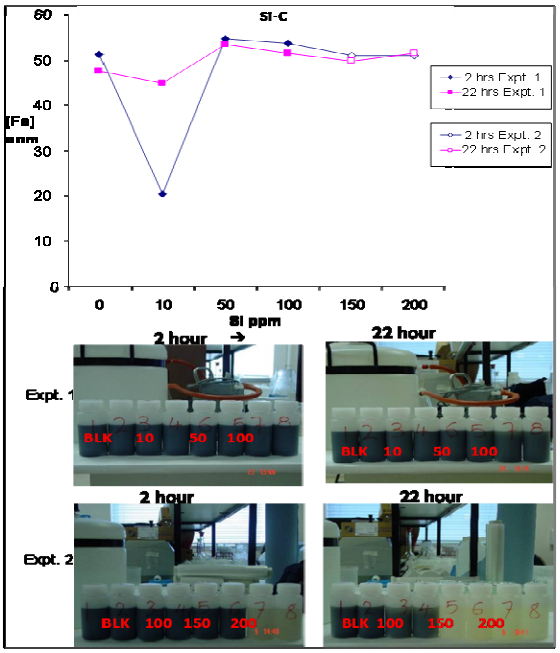

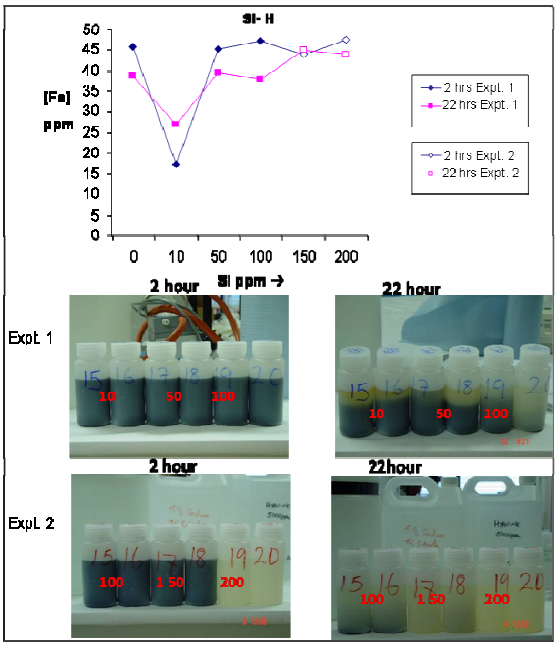

Figure 5.5 SI C on FeS; and graph of [Fe] fate. **Figure 5.6 SI H** on FeS; and graph of [Fe] fate.

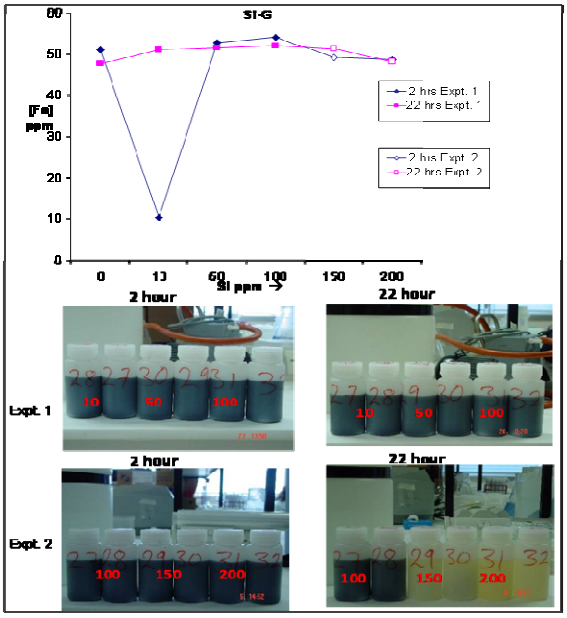

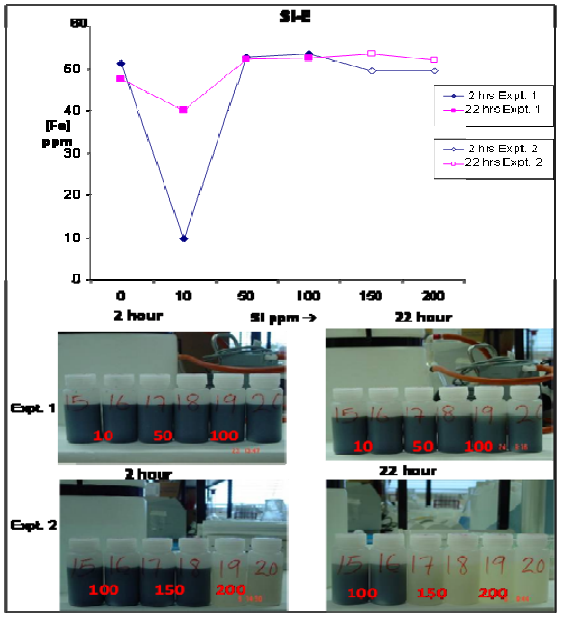

Figure 5.7 SI G on FeS; and graph of [Fe] fate. **Figure 5.8 SI E** on FeS; and graph of [Fe] fate.

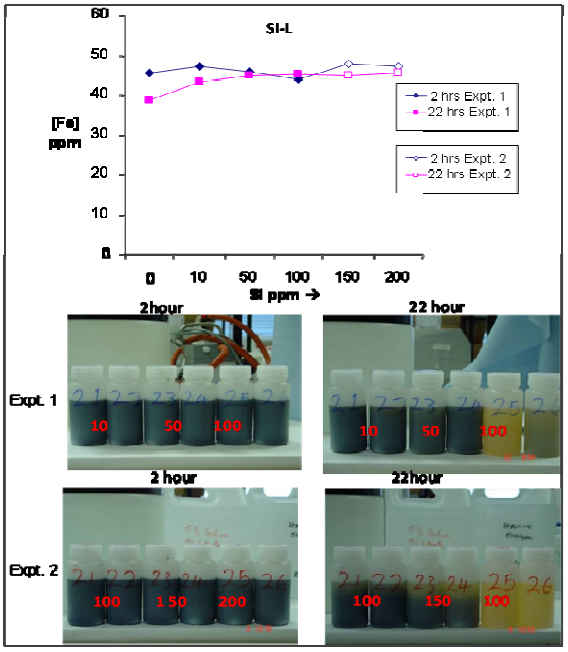

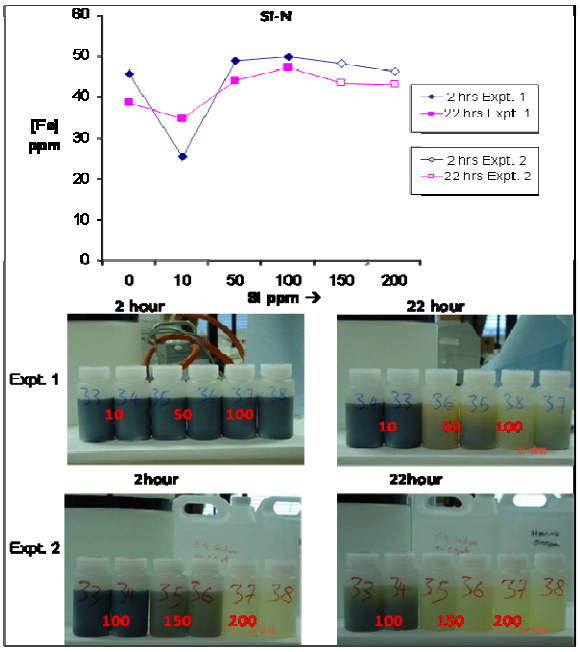

Figure 5.9 SI L on FeS and graph of [Fe] fate. **Figure 5.10 SI N** on FeS; and graph of [Fe] fate.

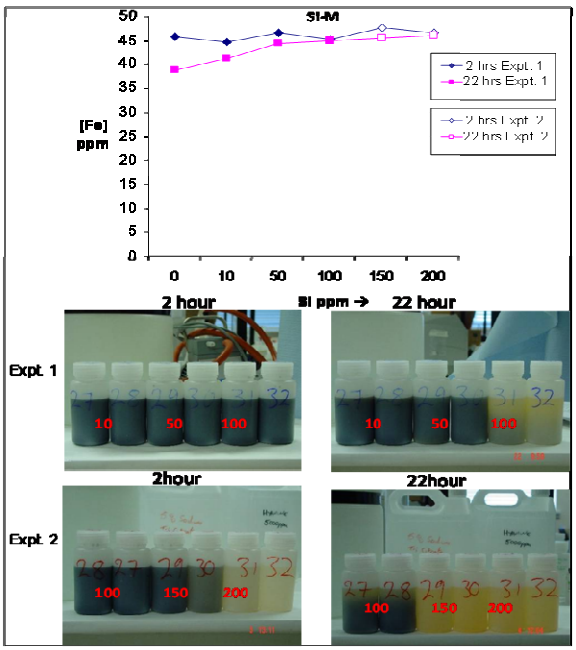

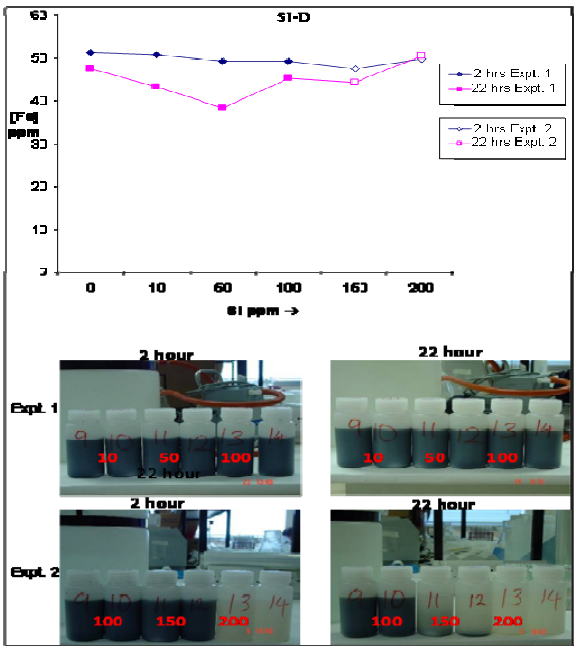

Figure 5.11 SI M on FeS; graph displays [Fe] fate. **Figure 5.12 SI D** on FeS; and graph of [Fe] fate.

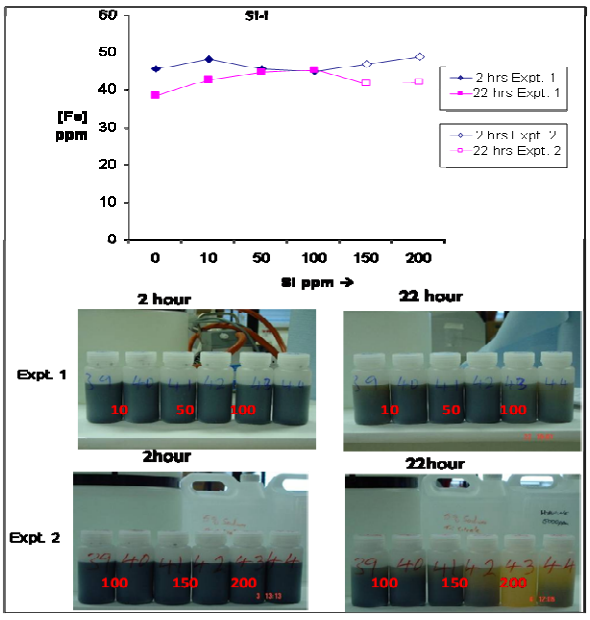

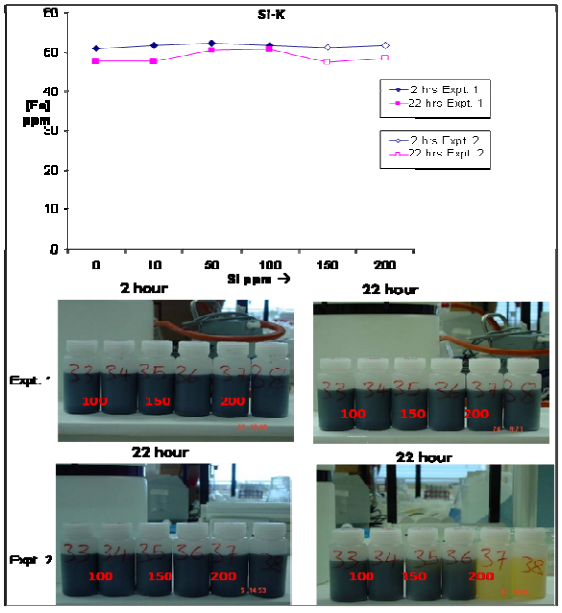

Figure 5.13 SI I on FeS; and graph of [Fe] fate. **Figure 5.14 SI K** on FeS; and graph of [Fe] fate.

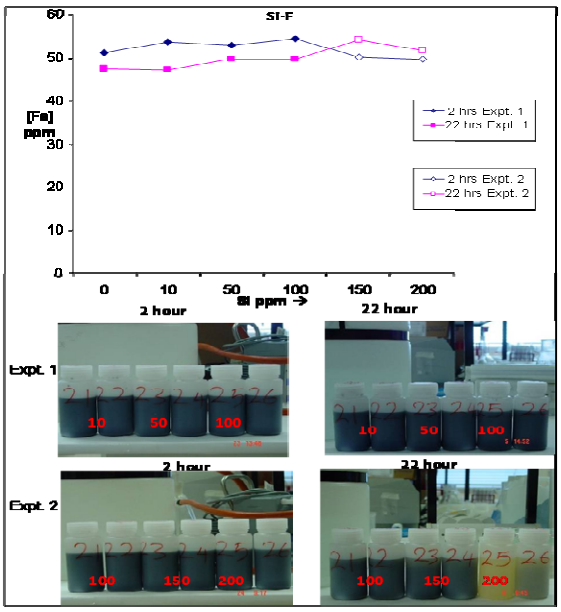

Figure 5.15 SI F on FeS; and graph of [Fe] fate.

5.4 Precipitation of [Fe] by SIs — (New Mechanism in FeS Formation)

There are several factors that can influence the process of FeS scale inhibition. As discussed briefly in the introduction and in more detail in the literature review, these factors have been studied in specific conditions, usually by isolating the variable of interest. A major mechanism used to prevent sulphide scaling (especially FeS) is to chelate the scale-forming cation (Fe^{2+}) via sequestration. This mechanism forms ionic complexes usually with organic inhibitors, making the iron less available to form scale. A new inhibition mechanism is observed based on experiments shown in Figures 5.16-5.19, the mechanism indicates that SIs caused the precipitation of [Fe] or vice versa. The blank (uninhibited) solutions show no decrease in the [Fe] but the inhibited solutions show a slight drop in [Fe]. Figure 5.16 shows the precipitation of iron by DETPMP across a range of concentrations up to 200ppm, for [Fe] of 5mg/L, the figure indicates a gradual drop in available [Fe] in the solution of ~10% from 0 to 200ppm. Figure 5.17 shows the precipitation of iron by SI PPCA for [Fe] of 5mg/L, the Figure also indicates a drop of available [Fe] of ~10% from 0 to 200ppm. Figures 5.18 and 5.19 shows the precipitation of iron 10mg/L which indicates a drop of ~20 %, this increase suggest a maximum limit for [Fe] sequestering per mg/l of applied SI.

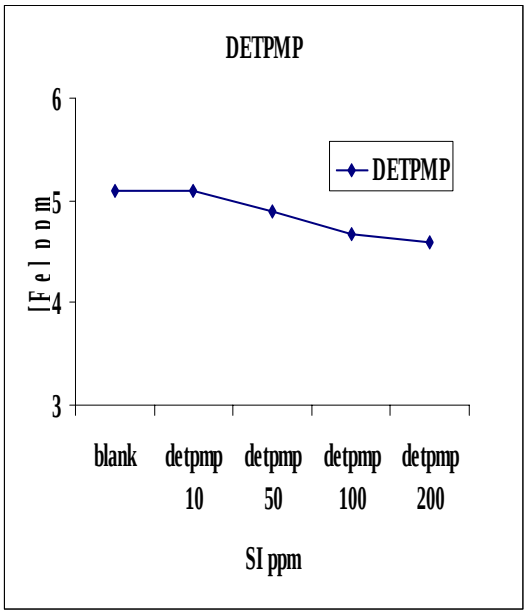

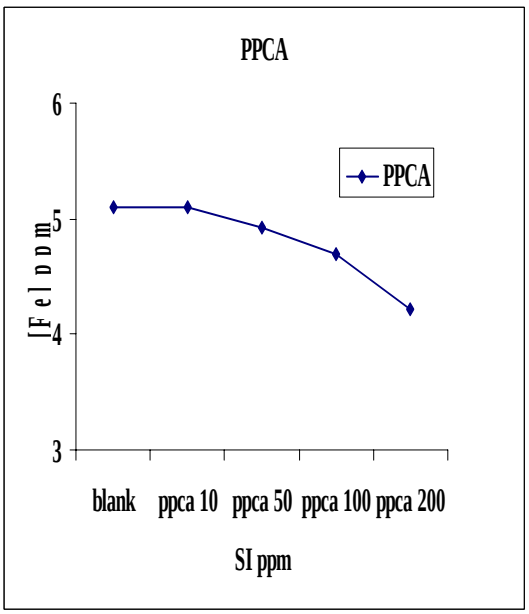

Figure 5.16 DETPMP/$FeSO_4$ mix (50ppm). **Figure 5.17** PPCA/$FeSO_4$ mix (50ppm)

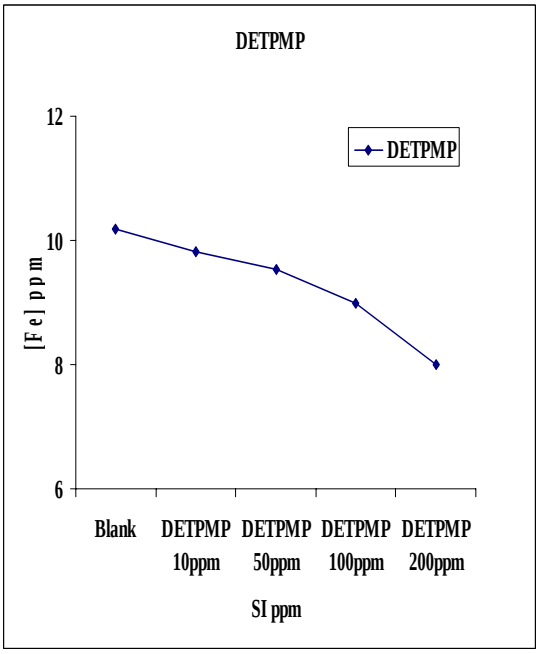

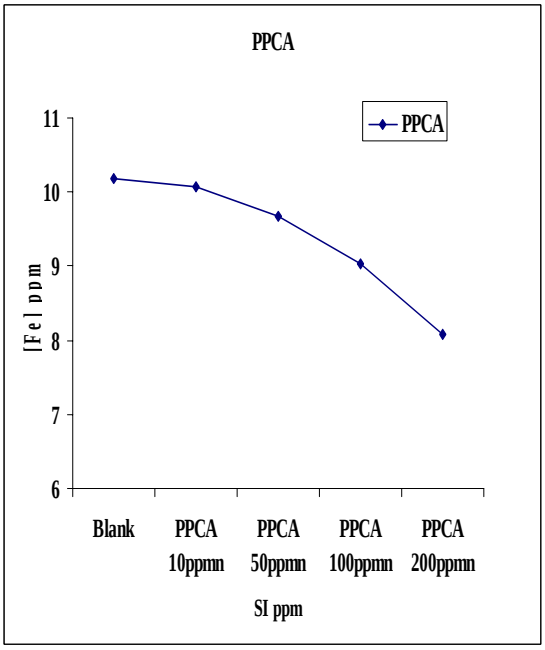

Figure 5.18 DETPMP/$FeSO_4$ mix (100ppm) **Figure 5.19** PPCA/$FeSO_4$ mix (100ppm).

From the results shown in Figures 5.16-5.19 it is evident that the [Fe] concentration is dropping out of solution as the SI is mixed with the scaling cation, Figures 5.18 and 5.19 displays a similar trend as shown above for both SIs.

5.5 FeS Particle Characterization Study- Filter Blocking Experiments.

The actual mechanism of sulphide formation especially iron sulphide formation in H_2S environment in oil production is still unclear. It is difficult to determine whether the iron sulphide is formed by direct solid state reaction, by ion combination and precipitation or by both mechanisms. However, in this thesis, sulphide formation is considered as a precipitation reaction from (FeS) super-saturated brine. In order to investigate any effect SI will have on colloidal FeS, it is important to study the formation mechanisms from nucleation to growth of the FeS particles and the impact of SI on the growth mechanisms.

5.5.1 Gravity Flow Test for FeS Using a 0.1 µm Filter.

To help elucidate the effect of SI on FeS formation and growth, a gravity flow test was performed using a burette filled with FeS at various [SI] (DETPMP) with a 0.1µm filter at its tip to demonstrate subtle changes to the solution which would not be observed by simple visual inspection. Figure 5.20 shows the untreated (blank) and treated [SI] across a range concentrations, plotted against time (minutes), with pictures of the related filters at the end of the experiment. This Figure indicates that the blank sample took the longest to reach the 5ml mark indicating a larger blocking effect than for the treated samples. This implies that the untreated FeS sample had larger particles that hinder the flow of the solution compared to the treated (SI) solutions. The Figure also shows the degree of coloration in the filters immediately after the experiments, with decreasing coloration as the [SI] increased suggesting a dispersal effect with the SI. The Figure also indicates no difference between the treated samples (including a clear solution [200ppm]) suggesting a uniform effect by the [SI] on the FeS irrespective of [SI. Although the 200ppm SI solution was actually clear, it took the same time to filter through as the 10 – 100ppm SI solutions indicating that, despite the clarity of the solution, it did contain FeS particulates (of size ~0.5µm). This emphasis the problem of using visual inspection for FeS

inhibition determination mentioned above. It is possible to assume the clear solution had no particulates and was completely inhibited, but this was not the case.

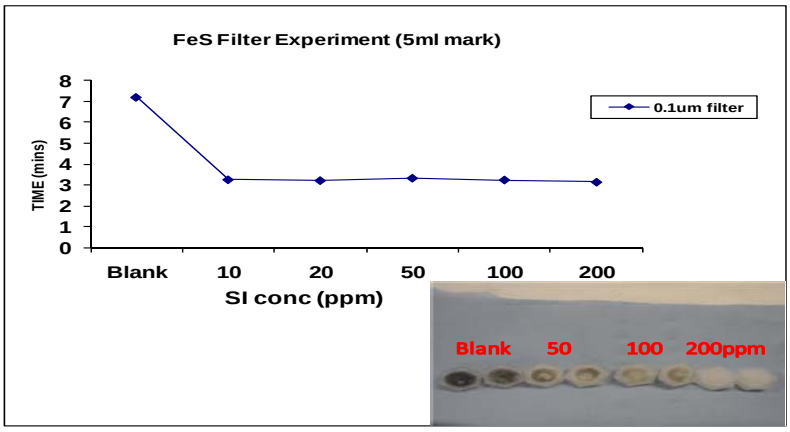

Figure 5.20 FeS gravity test to 5ml mark using 0.1µm filter

5.6 Particle Size Experiments.

5.6.1 DETPMP on FeS Particle Size.

In order to further elucidate the results from the filter experiments, the particle size in the FeS solutions was determined using the light scattering method (Malvern mastersizer 1000) described in Chapter 3. Figure 5.21 shows the particle sizes in microns (µm) of a blank solution and different concentrations of SI (DETPMP) up to 200ppm. The results from the figure shows a large particle size of up to ~300µm for the blank solution (untreated), compared to the other samples with varying concentrations of SI. The particle size of the treated samples were much smaller, ranging from 0.16 - 0.27 µm at its largest. These particle sizes are similar to the particle size of very fine sand. It is important to note that **visually the samples appear the same**, i.e **black** apart from the samples containing 200 ppm SI.

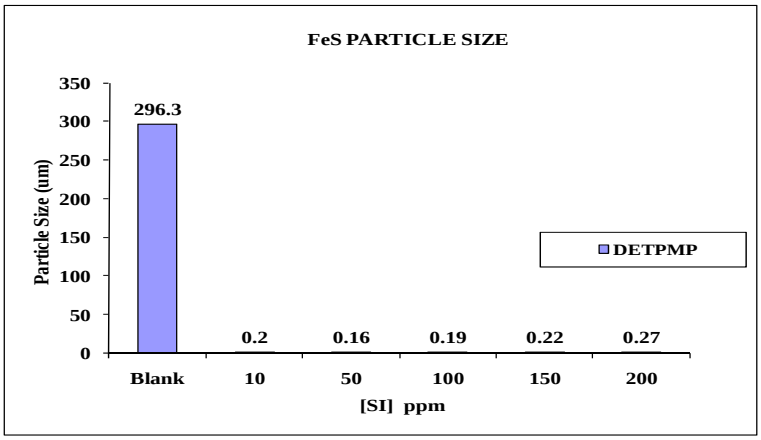

Figure 5.21 Particle size with DETPMP [SI].

5.6.2 PPCA on FeS Particle Size

Figure 5.22 shows the particle sizes in micron (μm) with a blank (untreated) solution for a range of concentrations of SI (PPCA). The huge difference in particle size observed here between the untreated FeS solution and the treated FeS solution is similar to that in the DETPMP experiment. The 150-200ppm solutions although measured did not form black FeS and remained clear throughout the experiment. These results are in accord with the filter experiments, confirming the suggestion that the particle size of the untreated solution FeS (blank) is larger than the treated samples, hence these solutions blocked the filter faster, i.e., taking a much longer time to reach the 5ml mark on the burette. These results suggest that the uninhibited FeS has a rapid nucleation reaction and continued to grow through a crystal growth mechanism. For the *inhibited* case (for both phosphonates and polymeric SIs), the nucleation stage still occurs and colloidal FeS forms, however the subsequent crystal growth of these colloidal particles is strongly retarded by ***all*** of the inhibitors tested, even at fairly low SI concentrations.

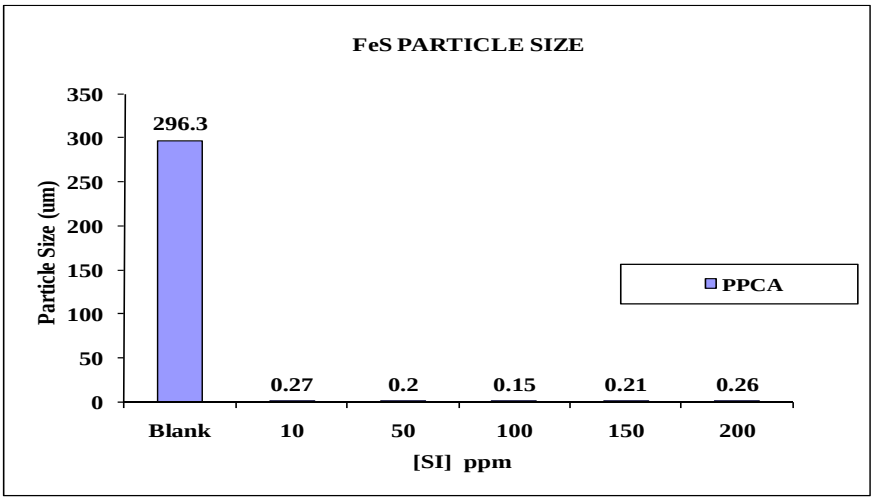

Figure 5.22 FeS Particle size with PPCA [SI].

5.6.3 Effects of [SI] Mix Regime on the FeS Particle Size.

The chelation of some [Fe] prior to the formation of FeS can reduce the amount of available [Fe] which then combines with the aqueous H_2S. The mixing regime which results in the chelation of some [Fe] occurs when the [SI] is added to the scale forming cation (NH_4FeSO_4) and then mixed with the NaS (see Chapter 3) to form the FeS solution as shown in Figures 5.16 – 5.19. Figures 5.23—5.24 show the treated FeS particle size data without including the untreated FeS data; these Figures include particle size data for PPCA and DETPMP for two [SI] mixing regimes. The objective of these experiments (mixing regimes) was to study the effect on the particle size of the resultant FeS using two [SI] mixing regimes. The results show that [SI] mix regime do not affect the reduction in particle size caused by the [SI] as observed in the experiments. The result indicates that the particle size is lower in the 2hrs time than in the 22hours sample time for both mixing regimes and SIs. Also, an average FeS particle size of 0.2 µm is observed for both mixing regimes and SIs. Note that the colloid sizes for PPCA and DETPMP is less than 0.5µm for both mix solutions and SIs.

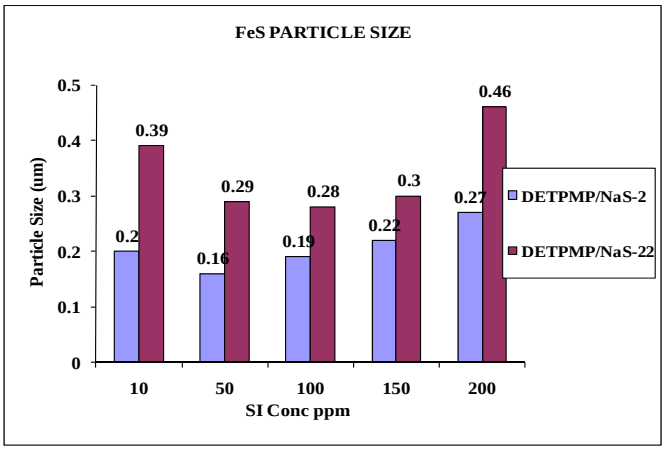

Figure 5.23 FeS Particle size with DETPMP ([SI]/NaS mixing regime) at 2 and 22hours.

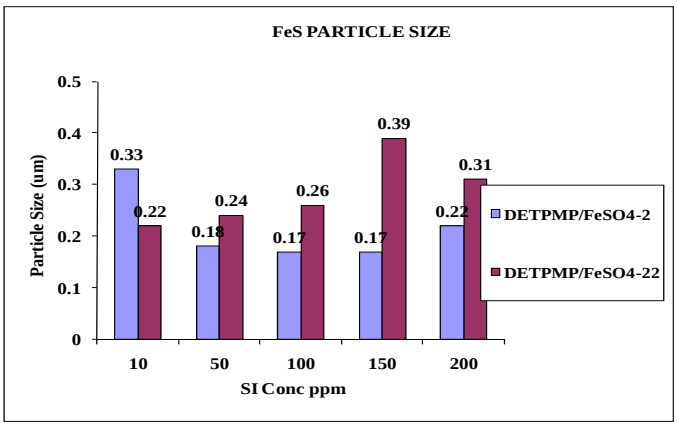

Figure 5.24 FeS Particle size with DETPMP ([SI]/$FeSO_4$ mixing regime) at 2 and 22hours.

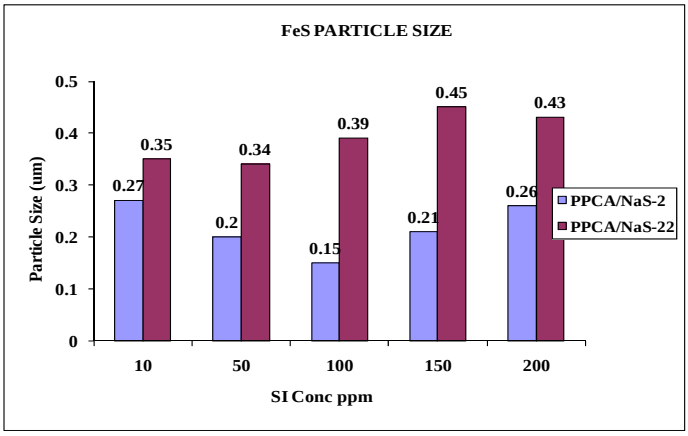

Figure 5.25 FeS Particle size with PPCA ([SI]/$FeSO_4$ mixing regime) at 2 and 22hours.

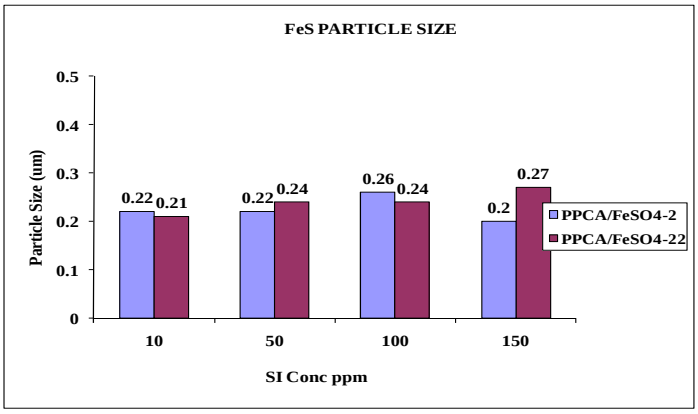

Figure 5.26 FeS Particle size with PPCA ([SI]/$FeSO_4$ mixing regime) at 2 and 22hours.

5.6.4 Effects of Low (Sub-Stoichiometric) Levels of Scale Inhibitor [SI] on FeS Particle Size.

In order to determine the transition point between the treated and untreated solutions, the [SI] concentrations must be reduced to below sub-stoichiometric levels. The transition point here is the cut-off points where the [SI] concentrations do not significantly reduce the particle to the level seen in Figures 5.21 - 5.26. This study is a continuation of the experiments on the effects of [SI] on FeS particle size with varying [SI] of DETPMP and PPCA, whilst comparing the data with the particle size of the untreated FeS as shown in Figure 5.27. Recall that the untreated FeS had an average particle size of ~350µm, which was significantly higher than the treated FeS cases (~0.5µm). Figures 5.28 shows data for [SI] in the range 1–10ppm and these results indicates that such low concentration levels of DETPMP are still clearly capable of reducing FeS particle size below 0.5µm. These SI concentrations are at well sub-stoichiometric levels and these results are very similar to those in Figures 5.21, 5.23, and 5.24. Figure 5.29 shows data indicating that 1-10ppm of PPCA is also capable of reducing the FeS particle size to below 0.5µm, very similar to data in Figures 5.22, 5.25, and 5.26. The data also shows a gradual increase in particle size from 10ppm to 1ppm which is consistent with the reduction in [SI]. The observed results are therefore very similar to the results from previous experiments using higher amount of [SI] for both PPCA and DETPMP.

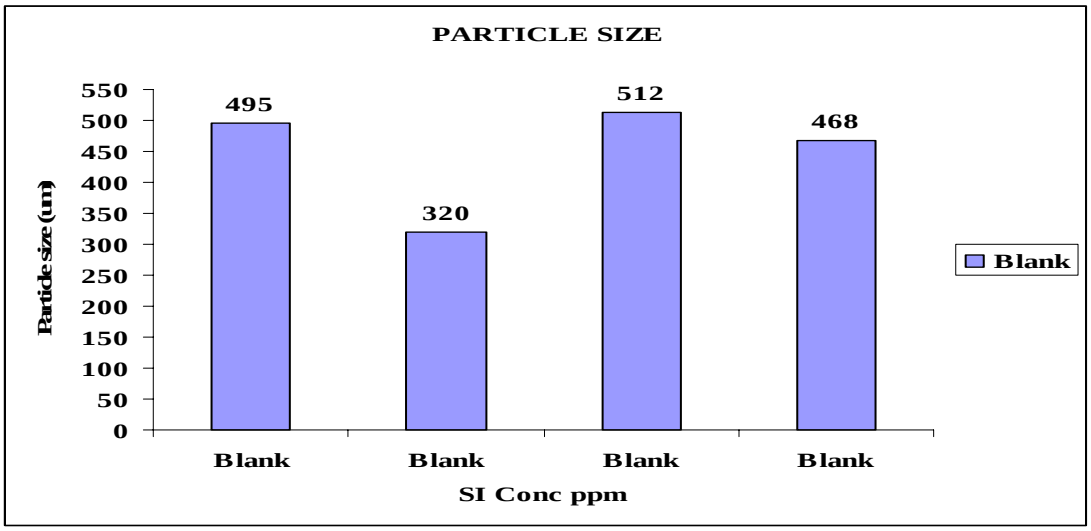

Figure 5.27 Particle sizes of the untreated FeS (Blank) for Figures 5.28-5.33.

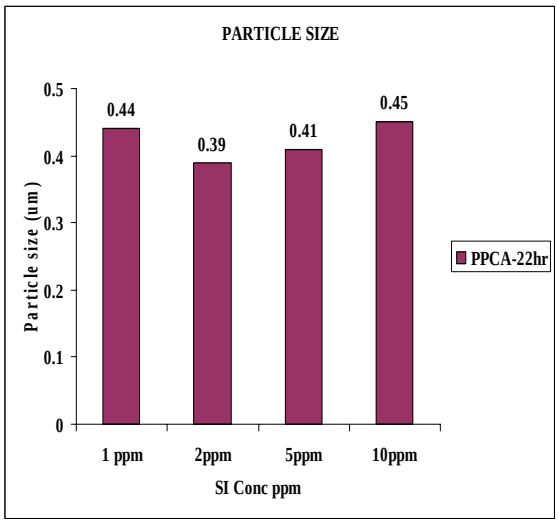

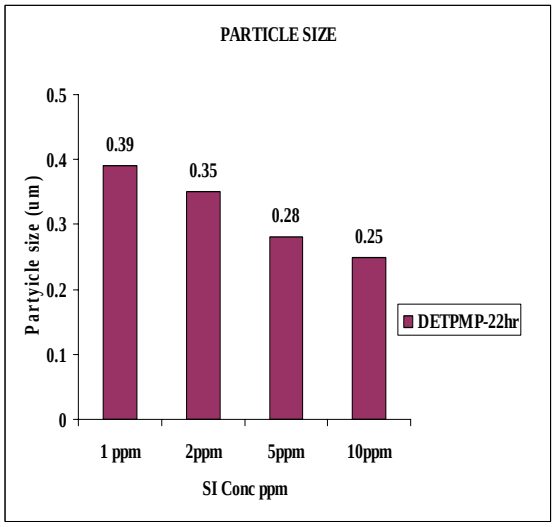

Figure 5.28 Particle size for FeS with PPCA. **Figure 5.29** Particle size for FeS with DETPMP.

In order to determine the transition point where the SI no longer affected the FeS particle size, the [SI] concentration was further reduced to the [SI] range 0.125ppm – 1 ppm and results from these experiments are shown in Figures 5.30-5.33. An increase in the particle size is observed as a result of the further reduced [SI] from 1ppm to 0.0125ppm. Figure 5.30 shows the particle size of FeS with varying [SI] of PPCA at 2hrs. Results show a small rise in the particle size at

0.5ppm (4.83µm) compared to the 1ppm case but this increase is more noticeable at 0.125ppm with an increase in particle size to 73µm. This increase in particle size in 0.125-0.5ppm is still much less than the particle size of the untreated (blank) FeS which is usually around ~300µm. Figure 5.31 shows FeS particle size at 22hrs which is consistent with results in Figure 5.30 at 2hrs, indicating that sampling time has little impact on the particle size.

Figure 5.32 shows the particle size of FeS with varying [SI] of DETPMP in the lower SI concentration range, 0.125 ppm to 1ppm. There is a noticeable increase in the particle size from 0.5 to 0.125ppm DETPMP. The figure shows that 0.5 ppm of DETPMP produces a particle size of 1.1µm, whereas a 0.25ppm SI concentration gives an FeS particle size of ~8.42µm. There is a more noticeable increase at 0.125ppm of DETPMP with an increase to 72µm. This increase in particle size seen in 0.5-0.125 ppm is still less than the particle size of untreated (blank) FeS which is usually >300µm as shown in Figure 5.27.

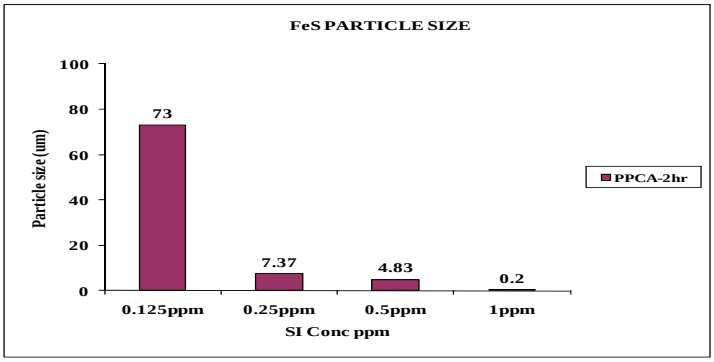

Figure 5.30 Particle size for FeS with PPCA at reduced of 0.125-1ppm at 2hrs.

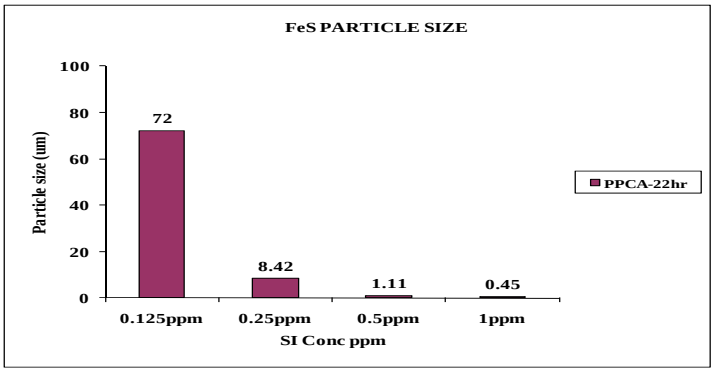

Figure 5.31 Particle size for FeS with PPCA at reduced of 0.125-1ppm at 22hrs.

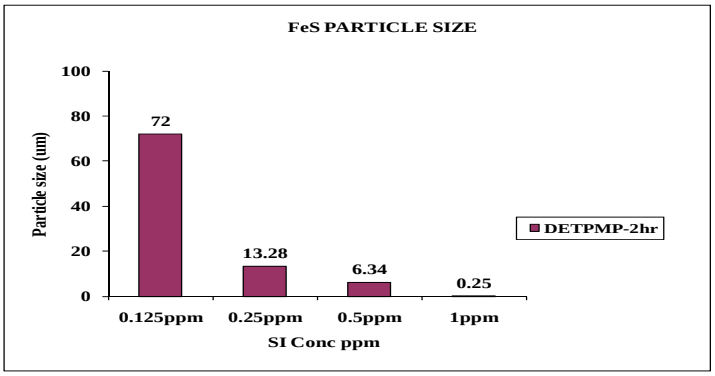

Figure 5.32 Particle size for FeS with PPCA at reduced of 0.125-1ppm

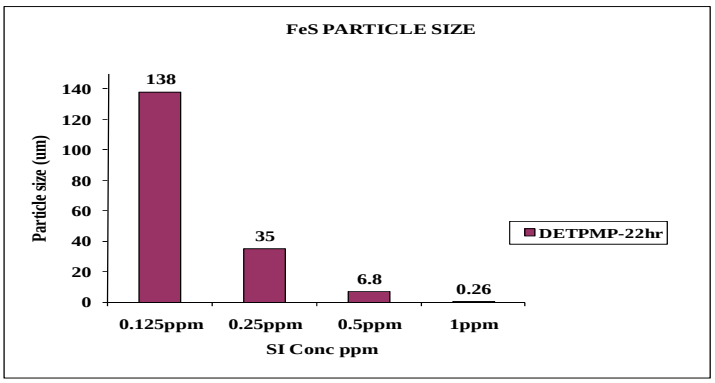

Figure 5.33 Particle size for FeS with PPCA at reduced of 0.125-1ppm.

5.7 Effects of [SI] on the Particle Size of FeS in the Presence of Crude Oil.

The impact of crude oil on the particle size was assessed using the same techniques described in Chapter 3 and which produced the above results. The crude oil chosen is also an emulsion forming crude to simulate a difficult field FeS scaling case scenario. Figure 5.34 shows the untreated FeS (no SI) of several particle size results for FeS in the presence of crude oil. The results show an average of ~380µm these results are in accord with the results observed in the non-crude samples. Figures 5.35-5.36 show particle size with various [SI] at sub-stoichiometric values for DETPMP and PPCA. The difference between the blank and the treated case is quite significant but the low [SI] did not reduce the FeS particle sizes to the levels observed in the samples which did not contain crude oil. This could be as a result of several factors including

lesser amount of [SI], emulsion interference or an oil sheen effect. In all cases, there is a consistent blank (untreated) result which validates the experiment and the result from the treated (with SI) samples indicates that the SI was involved in the actual reduction of the FeS particle size. The system has to be kept under vacuum or oxygen free to prevent the FeS from oxidizing and turning into ferric iron. It is important to note that the FeS formed here was synthetic and hence may not be the same size formed by microbial sources.

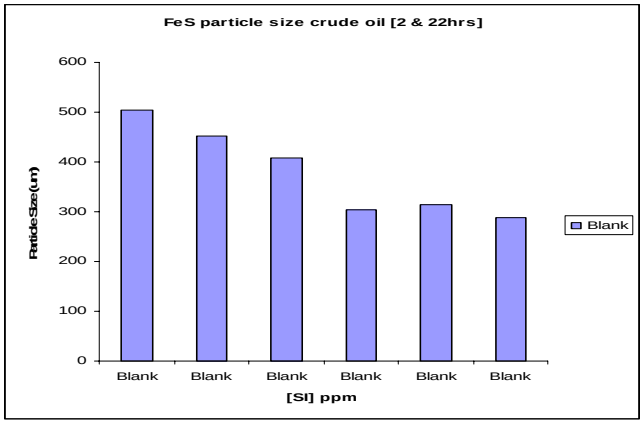

Figure 5.34 Particle size for blank FeS formed in the presence of crude oil.

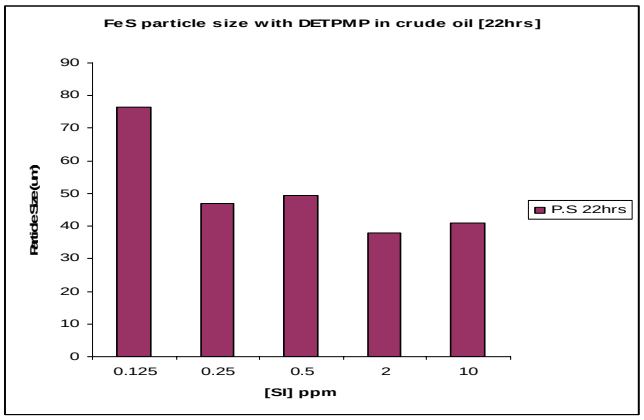

Figure 5.35 Particle size of FeS with [SI] of DETPMP formed in the presence of crude oil.

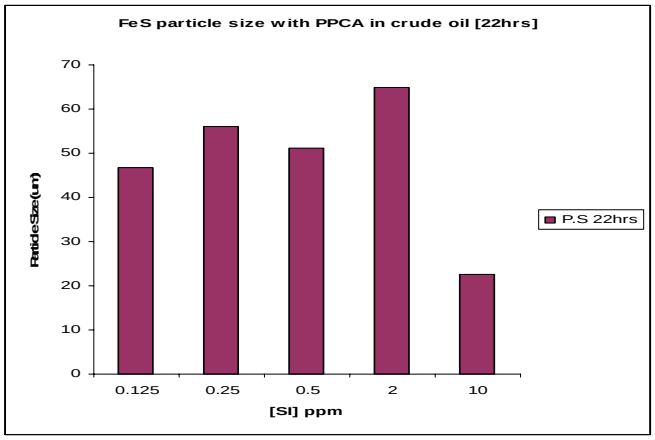

Figure 5.36 Particle size of FeS with [SI] of PPCA formed in the presence of crude oil.

5.8 Summary and Interim Conclusions on the FeS Formation Mechanisms

The results presented above provide a set of detailed, wide ranging but essentially qualitative observations on FeS formation, FeS inhibition and the factors affecting these. However, several new findings on the FeS formation and inhibition mechanisms are described here which have not previously been reported, as follows:

1. New categorization of the range of SI behaviour types are presented as they interact with FeS based on three visual observations; A—black, B—black initially then turning clear, and C—clear.
2. A precipitation mechanism is described here when SI and [Fe] mix thereby reducing the [Fe] available for the formation of FeS.
3. Both phosphonate and polymer based SIs have a profound effect on the particle size of FeS; the particle size is reduced from >300µm in the blank to less than 0.3µm in the SI treated solutions. This is observed for ***all*** the SIs studied.

In the oil industry these results will have immediate consequences in scale treatment programs and on the characterization of FeS scale inhibitors based on their interaction with FeS. This will provide useful information in scale inhibitor selection. The precipitation experiments indicate

that there is a correlation between [SI] concentration and the amount of [Fe] that is available prior to FeS precipitation thus giving a better prediction on the severity of FeS scale. The experiment showed that although there was a drop in available [Fe] in the system it was still capable of forming FeS and this may have quite profound consequences in water management of oilfield waters.

To understand the particle size experimental results, we should consider both bulk precipitation and scaling (colloidal) in the treated system. FeS is formed immediately as soon as the two solutions are mixed due to the high super-saturation. The FeS formed in the blank solution has a final particle size about that of coarse sand (~300μm) which could block filters, separators and other production equipment. The treated systems ***look like*** the untreated system but the actual sizes of the colloidal FeS has been greatly reduced from their original size to about ~0.5μm and this is observed for ***all*** the SIs in Table 5.1. This reduced particle size should save on equipment downtime and prolong the life of filters. Similar results were obtained when the particle size was measured in the presence of crude oil, the untreated (No SI) and treated (No SI) visually were similar to the previous study without crude oil as shown above.

Chapter 6 THPS Studies - Interactions of THPS with Sulphide Scales

Tetrakis (hydroxymethyl) phosphonium sulphate (THPS) is a widely applied biocide in the petroleum industry which was also found to be of great use in removing/dispersing iron sulphide deposits. This chapter presents experimental results using THPS which reveal certain characteristics in the inhibition and dispersal of sulphide scales in different brine and salinity compositions. The efficiency of THPS in preventing/dispersing FeS in mixed sulphide scales systems is also explored in this work. A synthetic high salinity FW brine similar to the Miller field was used for majority of the test cases reported here. This brine composition contains a mixture of several scaling ions including barium, strontium and iron, creating a complex field scaling condition.

In particular, the following 3 aspects of the application of THPS have been studied:

(i) The stability of THPS and its effects on sulphide inhibition/dissolution.

(ii) The efficiency of THPS for FeS in mixed (Zn, Pb) sulphide scaling systems.

(iii) The influence of [Ca] and [Mg] on the efficiency of THPS at MIC threshold.

Detailed experimental results from static inhibition efficiency tests for four different commercial THPS based products are reported here.

6.1 Introduction

The use of tetra kis (hydroxymethyl) phosphonium sulfate (THPS) in the petroleum industry has been widely reported (Nasr-El-Din 2001; Gilbert 2002.) Traditionally, THPS research has concentrated on assessing its use as biocide to prevent or control micro-organisms that cause souring of oilfield fluids. Recently studies have shifted to highlighting the use of THPS as an FeS dissolver and its increased use in the inhibition and dispersion of FeS. In this chapter, modified static bottle tests are used to assess THPS in various scaling systems. The results from these tests help to develop an understanding of dispersal mechanism employed by THPS for FeS in different scaling systems, including a mixed sulphide scaling scenario that is encountered in real field conditions. The prime purpose of these studies was to elucidate the efficacy, stability and performance of THPS, either as a scale inhibitor (SI), as a dissolver or as a synergistic chemical in preventing sulphide scaling in various scenarios (Nasr-El-Din 2001; Gilbert 2002.)

6.2 Experimental Details for the THPS Stability Experiments

It has been reported that fresh THPS stock solutions should be made up daily when carrying out test work. To test the stability of our THPS solution, we tested their efficiency at FeS dispersal after seven days of ageing using 1% THPS solutions. These FeS scale formation experiments were carried out at 20^{o}C in a modified static bottle test system, sampled at 22hrs for each aged THPS solution; in all of these stability tests, a 50:50 volumetric ratio of seawater and synthetic Miller FW was used, as described in Chapter 3. Synthetic brines were prepared using distilled water by dissolving accurately weighed amounts of the relevant salts in a fixed volume of solution. Four brines compositions were used, based on Miller FW and Synthetic North Sea seawater, and are labeled analogues FW, A, B and C respectively, as shown in Table 6.1. The FW A analogue contained sodium chloride, iron and barium chloride at the same concentrations as conventional Miller brine, together with calcium or magnesium chloride. The FW B analogue does not contain barium and strontium but had the other ions at the same concentrations; this represents a mix where other scaling is not present such as in hydro-

testing of pipelines. Finally, the FW C analogue did not contain barium, strontium, calcium or magnesium ions but the other ions were maintained at the same concentrations, simulating filtered injection water. The seawater analogue contained sodium chloride and sodium sulphate at the same concentrations as conventional synthetic seawater and added sulphide simulating a sour system. Also, ICP was used for monitoring the Fe ion concentration during the experiments. The test brine used modified Miller FW, and simulates sulphide scaling at different brine compositions by the addition and removal of other ions not found in the original Miller brine. Four THPS based products were used in this study, although it was not known which of the products reported in this chapter were optimized either as a biocide, FeS dispersant or both. The THPS stability experiments were conducted using FeS that was spontaneously precipitated by mixing 10ml of modified Miller FW brine A/B/C and 10ml of North Sea water. The Table 6.2 shows the THPS products information given by the suppliers.

Table 6.1 Compositions of Miller FW and SW Analogues used in Experiments in Chapter 6

All concentrations in milligrams per Litre

Ion	Miller FW A	Miller FW B	Miller FW C	North Sea Seawater
Sodium	27080	27080	27080	10890
Calcium	735	735	0	428
Potassium	1340	1340	1340	1368
Magnesium	105	105	0	460
Barium	775	0	0	0
Strontium	180	0	0	0
Sulphate	0	0	0	2965
Iron	175	175	175	0
sulphide	0	0	0	500
Chloride	45127	44581	42975	19027

Table 6.2 THPS product details given by suppliers				
THPS	XA	X B	XC	XD
Supplier	Rhodia	Rhodia	Rhodia	Clariant
Biocide	Unknown	Unknown	Unknown	Unknown
FeS dissolver	Unknown	Unknown	Unknown	Unknown

6.3 Stability of the THPS Solutions prior to Mixing

6.3.1 Aims and Design of Experiments

In order to understand the mechanisms of THPS dispersing FeS in brine, a series of jar test experiments was conducted. The reported short shelf life of THPS (Zhao 2008) prompted the test to verify the stability of the THPS products at various brine compositions. The THPS based products were prepared at 1% concentration which was close to the reported values where degradation of mixed THPS in seawater was observed. The THPS based products were mixed and kept in the fume cupboard where they were exposed to oxygen and natural light. All the THPS products were tested by diluting them to 3000ppm; this is the known value for a 100% inhibition at the high scaling brine of Miller FW: Seawater at 50:50, the test was carried out for a period of three weeks (21days).

6.3.2 Results for the THPS Stability Tests

Figures 6.1-6.4 shows the Inhibition efficiencies in percentage (I.E %) using analogue Miller FW A and Seawater. This simulates a 50:50 mix of Miller FW and Seawater for the four THPS based products. The figures show that the THPS products were active for up to 3 weeks after mixing to 1% concentration. In general, the I.E % samples did not fall below 95% for the worst performing test sample and no notable changes in behaviour during the testing period were observed (either by visual inspection or by ICP analysis). There was **no** difference except for sample XB which fell from 100% to 95% in the first 24hrs but remained at ~95% for the next two weeks. In addition to the ICP and visual test, an additional test was carried out to determine the [THPS] concentration by using

iodine solution method described in Chapter 3. This was done using the starch indicator LaMotte assay kit (CODE 8776) which employs a titration method to calculate [THPS] concentration in which the solution turns blue-black indicating the presence of active THPS during the test time. The experiment indicates that the THPS products do not show degradation due to exposure to UV, oxidation, hydrolysis or photo-degradation.

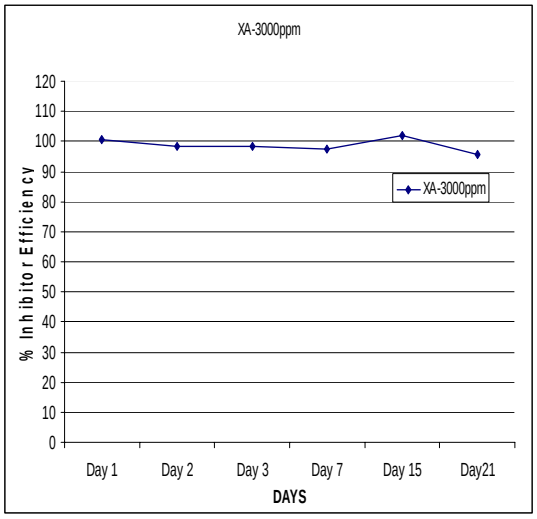

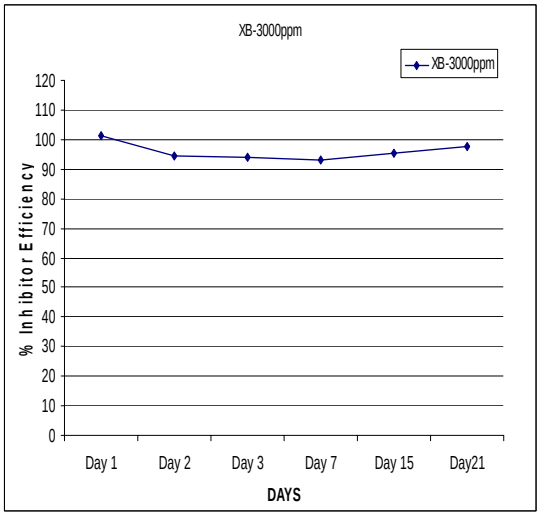

Figure 6.1 % I.E for THPS XA for 3 weeks. **Figure 6.2** % I.E for THPS XB for 3 weeks

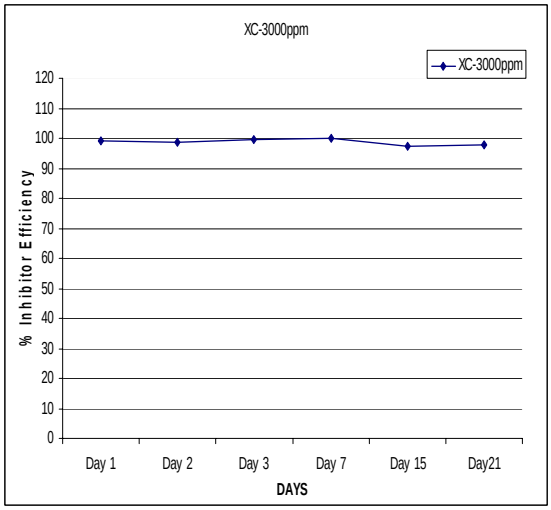

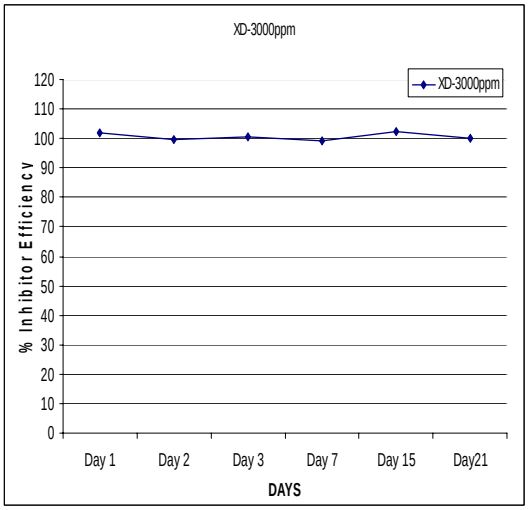

Figure 6.3 % I.E for THPS XC for 3 weeks. **Figure 6.4** % I.E for THPS XD for 3 weeks.

From Figures 6.1 - 6.4 above, it is evident that the 1% THPS was still active and effective against freshly synthesised FeS. We note that, under the conditions used in this work, the THPS products appear to be quite stable over a 3 week period.

6.3.3 Stability of the THPS without other Scaling ions (No [Mg] [Ca] [Ba] [Sr])

Figures 6.5 - 6.8 shows the inhibition efficiencies in percentage (I.E %) using analogue Miller FW B and Seawater. This simulates a 50:50 mix of Miller FW and Seawater for the four THPS based products over time (21days) in the absence of other scaling ions of barium and strontium. No significant drop in efficiency was recorded during the testing period. The result indicates that other scaling ions (Ba and Sr) do not affect the stability of THPS over 3 weeks. The figures also show data with Miller FW C which did not contain [Ca] and [Mg] ions in addition to Ba and Sr. The data clearly indicates that the inhibition efficiency during the test period did not diminish with the efficiency being maintained throughout the test period. In addition to the ICP and visual observations, the [THPS] was also assayed by using the iodine solution/starch indicator LaMotte kit described above. Results in Figures 6.5 to 6.8 show that the long term stability of THPS is not affected by the brine composition in Miller FW B.

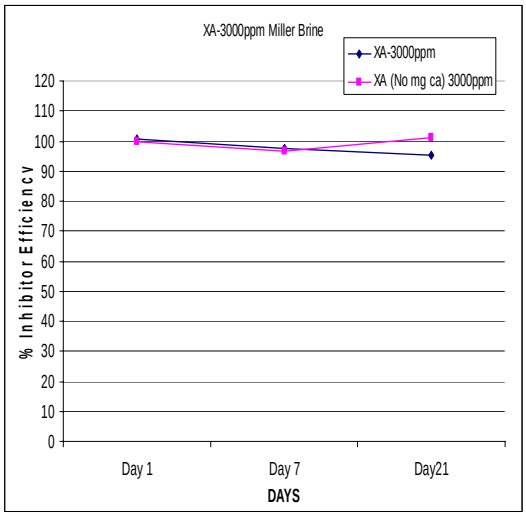

Figure 6.5 THPS XA I.E% for 3 weeks.

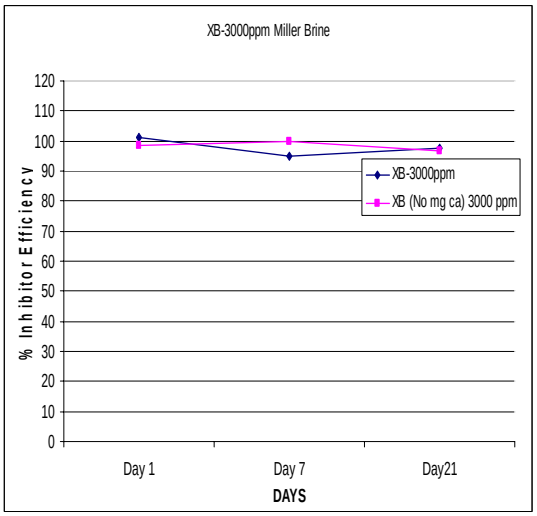

Figure 6.6 THPS XB I.E% for 3 weeks.

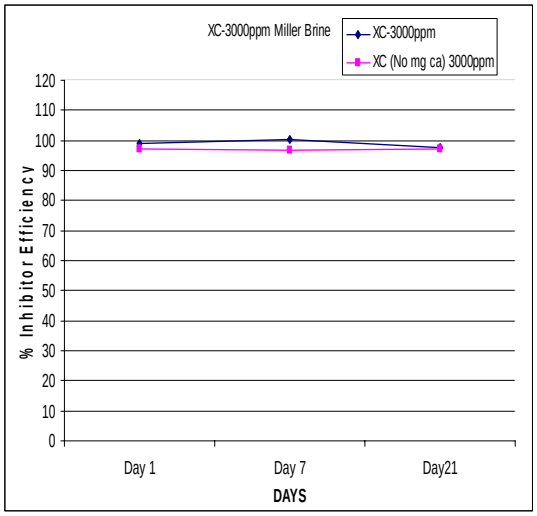

Figure 6.7 THPS XC I.E% for 3 weeks.

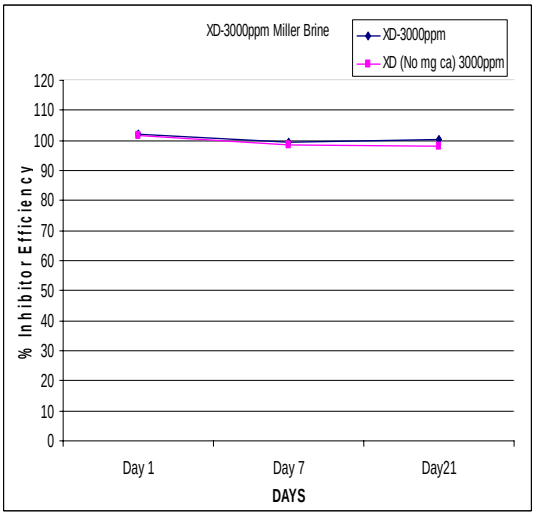

Figure 6.8 THPS XD I.E% for 3 weeks.

6.4 THPS Efficacy in Low Salinity Brine.

6.4.1 Aims and Design of Experiments

In order to investigate the efficacy and inhibition mechanisms of the THPS based products in a simple brine scaling system, without interference from other ions, a simple NaCl and FeS system keeping the iron concentrations from Miller brine unchanged was made. The aim of this study is to compare and contrast the THPS products performance in simple brine system and better understand THPS inhibition mechanism. The study then proceeds to examine the role of both [Mg] and [Ca] ions more systematically in the inhibition mechanism of THPS in a simple brine system. The brine compositions used is presented in Table 6.3; Analogue FW 1 contains 10000ppm sodium chloride, which is relatively low compared to real oilfield FW brines, and 175ppm of iron as in the base case Miller FW. Analogue FW 2 contains both magnesium and calcium at concentrations similar to the Miller FW in addition to sodium chloride and iron. Analogue FW 3 contains calcium with sodium and iron ions, while FW 4 contains magnesium with sodium chloride and iron. THPS concentrations of 1000, 1500 and 3000ppm was tested at 2 and 22hrs but with only the 22hrs data is presented below. The NSSW composition changes according to the experiment reflecting the final brine composition.

Table 6.3 Composition of Low Salinity NaCl Brine Analogues used in Experiments reported in Chapter 6					
All concentrations in milligrams per Litre					
Ion	Low FW1	Low FW2	Low FW 3	Low FW4	North Sea Seawater
Sodium	10000	10000	10000	10000	10000
Calcium	0	735	735	0	428
Magnesium	0	105	0	105	1368
Iron	175	175	175	175	0
sulphide	0	0	0	0	500
Chloride	15421	17028	16721	15727	19062

6.4.2 THPS Efficacy in Low Salinity Brine Results.

Figures 6.9 to 6.12 show visual and ICP results for the THPS experiments performed using low salinity brine made up of NaCl and FeS forming ions only. The results show inhibition efficiencies of [Fe] sampled at 22hrs after mixing, and visual results of the sample bottles which gave a quick and qualitative indication of the THPS performance. Figures 6.9 show the visual and ICP results for THPS XA, this indicates that 1000ppm and 1500ppm did not prevent the formation of FeS, but at 3000ppm, THPS XA was able to completely prevent the formation of FeS. Figure 6.10 shows the result for THPS XB which appears to be quite similar to the THPS XA results with 3000ppm effectively preventing the formation of FeS, while the 1000 and 1500ppm did not prevent FeS formation. Figure 6.11 show the visual images and the [Fe] inhibition efficiency of THPS XC, and the results indicate that at 1500ppm there was 50% inhibition efficiency and complete inhibition at 3000ppm. Figure 6.12 shows the results of THPS XD, the visual and the [Fe] inhibition efficiency indicates that at 1500ppm there was ~75% inhibition efficiency and complete inhibition at 3000ppm. The results from the Figures 6.9 to 6.12 showing both the inhibition efficiencies (percentage) and visual images of the THPS based products indicate that at 3000ppm all the THPS products were capable of keeping the [Fe] in solution preventing the formation of FeS in a low salinity brine, with THPS

XC and THPS XD out performing XA and XB. The MIC across all the THPS products is about 3000ppm, and may be ~1500ppm for THPS XD.

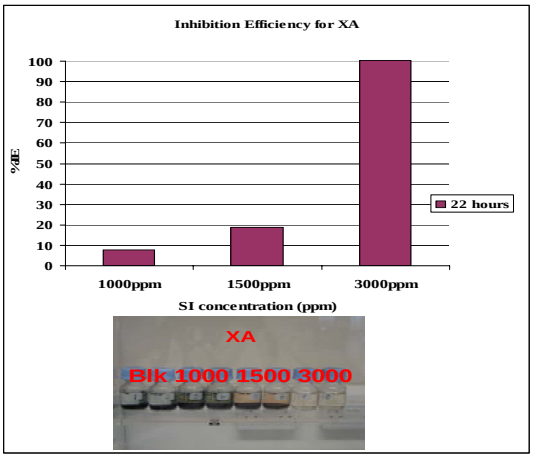

Figure 6.9 %I.E of XA for Fe in NaCl

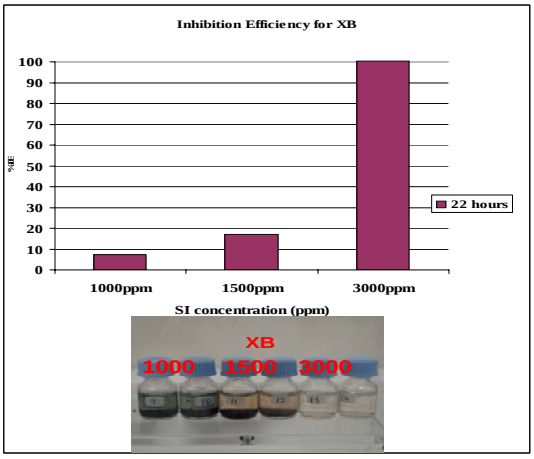

Figure 6.10 %I.E of XB for Fe NaCl.

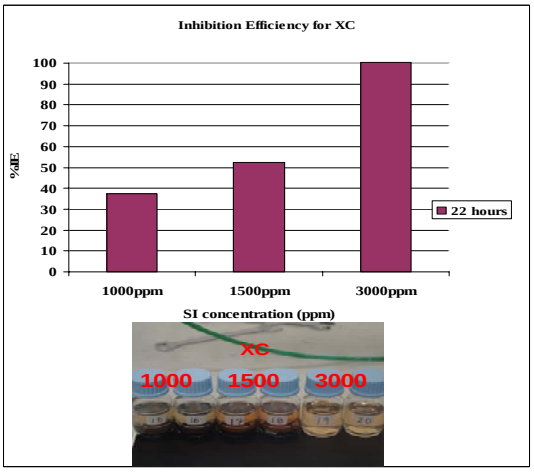

Figure 6.11 % I.E of XC for Fe in NaCl.

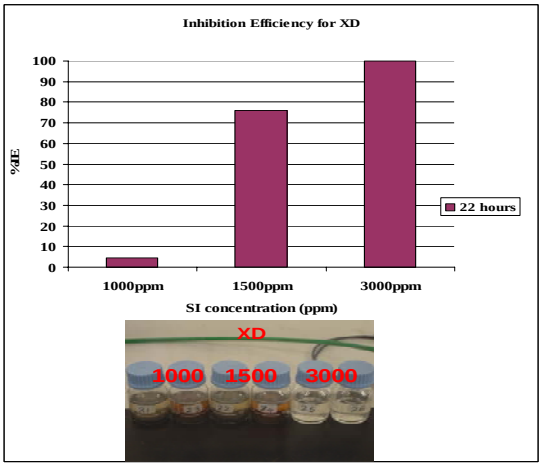

Figure 6.12 % I.E of XD for Fe NaCl.

6.4.3 Influence of Calcium and Magnesium on THPS Efficacy in Low Concentration Brine

Results from Figures 6.13 to 6.16 show the effect on THPS efficiency of the inclusion of magnesium and calcium to the brine. The addition of the ions can be seen to dramatically improve the THPS performance across the board. The magnesium and calcium concentration is similar to Miller FW and North Seawater (Low FW 2 and Seawater) as

shown in Table 6.2. Figure 6.13 show the visual and inhibition efficiency results for THPS XA, indicating improved performance across the test range. [THPS] in the range 1000-3000ppm, achieved 100% efficiency compared to Figure 6.9 which showed that only 3000ppm was able to keep the [Fe] in solution and prevent the formation of FeS. Figure 6.14 shows the visual and inhibition efficiency results for THPS XB, demonstrating clear improvement across the THPS concentrations tested; the 1000ppm THPS solution, which previously in Figure 6.10 was not capable of preventing FeS formation, is able to hold the [Fe] in solution. Note that this resulted in a slight red coloration of the brine, but this became clear as the THPS concentration increased. Figures 6.15 and 6.16 showed an improved performance for THPS XC and XD respectively with all concentrations achieving 100% efficiency. The data show an increase in IE for all the THPS samples indicating that [Mg] and [Ca] do have a significant impact on THPS efficiency.

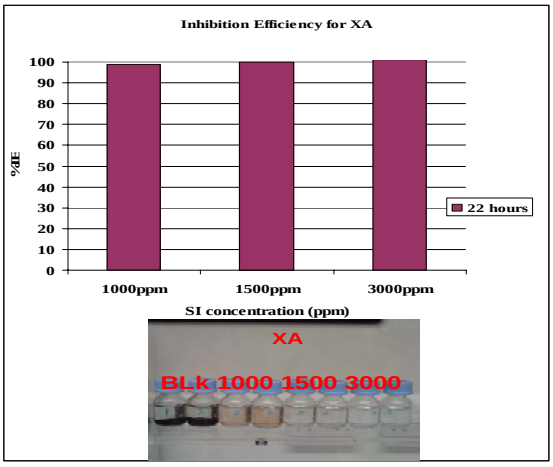

Figure 6.13 % I.E of XA for Fe in NaCl.

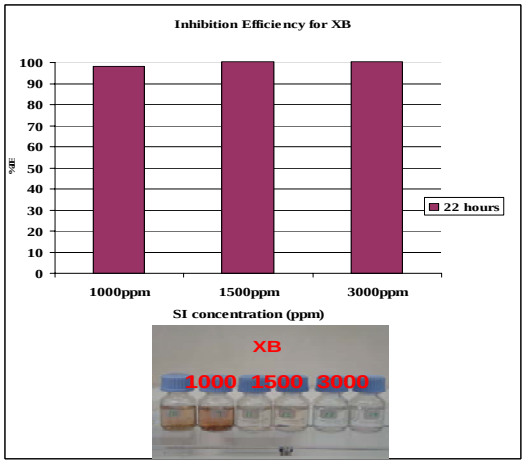

Figure 6.14 % I.E of XB for Fe NaCl

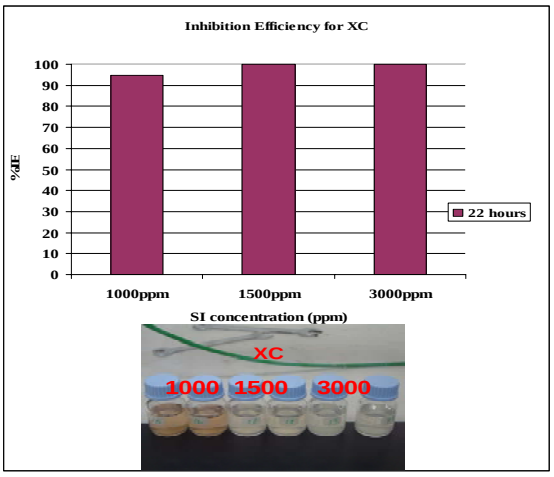

Figure 6.15 % I.E of XC for Fe in NaCl.

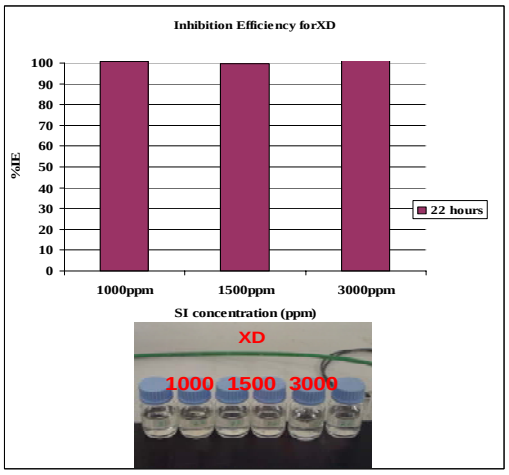

Figure 6.16 % I.E of XD for Fe NaCl.

Figures 6.17 to 6.20 show both the visual and inhibition efficiencies of THPS products in low salinity brine with added [Mg] and [Ca] similar to seawater and Miller brine compositions, but at reduced THPS concentrations of 250ppm and 500ppm. The results in Figures 6.13 to 6.16 prompted the re-examination of the effects of reducing the THPS concentrations to determine a new MIC for the THPS chemicals. However, the results show that a reduction in THPS concentrations was not able to keep the [Fe] in solution as shown in Figures 6.17 to 6.20, and this was observed for all of the THPS products. The THPS performance was still poor despite the increase in [Mg] and [Ca] suggesting this improved efficiency phenomenon noticed in Figures 6.13 to 6.16 is at or near MIC threshold.

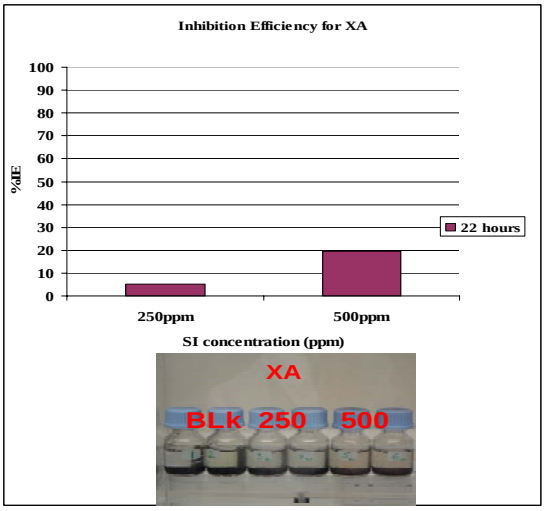

Figure 6.21 %IE of XA for Fe in NaCl.

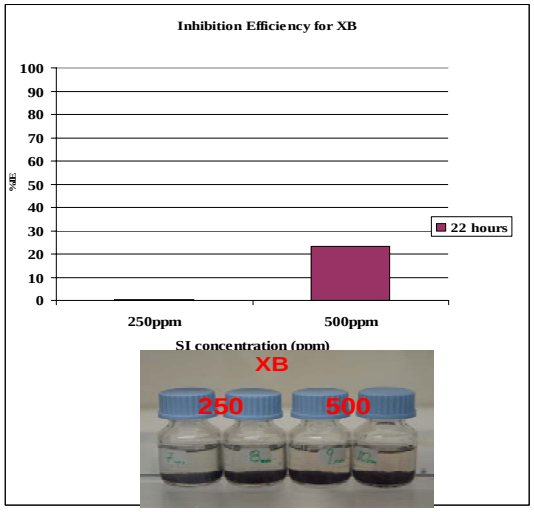

Figure 6.22 %IE of XB for Fe NaCl.

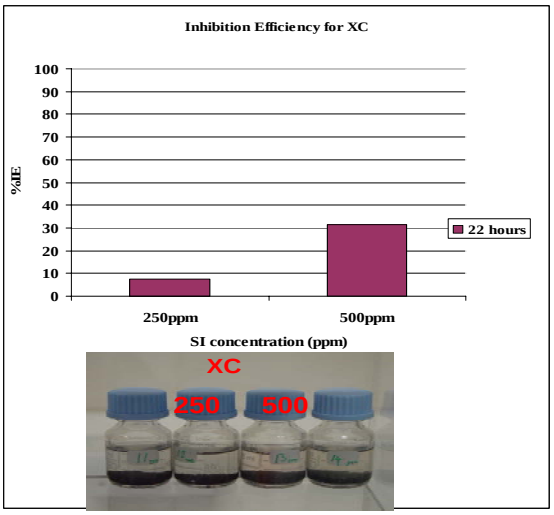

Figure 6.23 %IE of XC for Fe in NaCl.

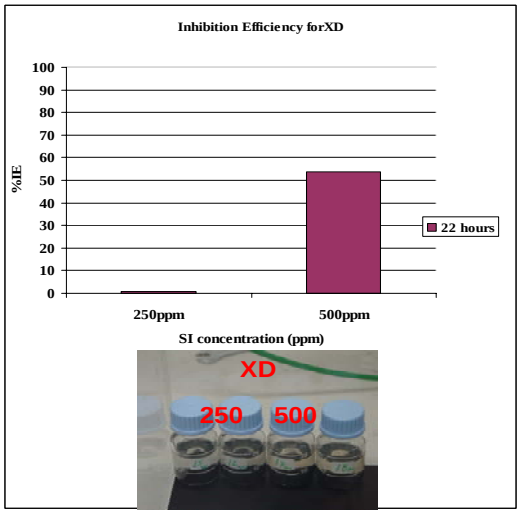

Figure 6.24 %IE of XD for Fe NaCl.

Figures 6.25 to 6.28 show both the visual and inhibition efficiency data of the analogue brine Low FW 3 and seawater mix. The mixture represents THPS products in low salinity brine with added [Ca] similar to seawater and Miller brine compositions, but with the [Mg] removed. The results showed a drop in the inhibition efficiency compared to [Ca] and [Mg] experiments, which is highlighted in Figures 6.13 to 6.16. The results were similar to the NaCl only experiments, as shown in Figures 6.9 to 6.12, where complete

inhibition was achieved at 3000ppm, although it should be noted that THPS XD at 1500ppm achieved over 90% efficiency.

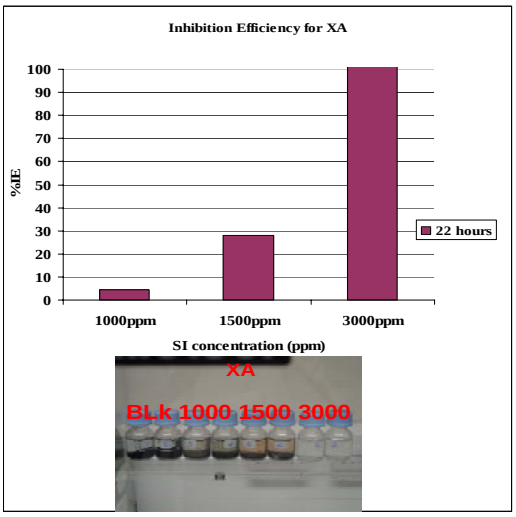

Figure 6.25 %I.E of XA in NaCl+ [Ca].

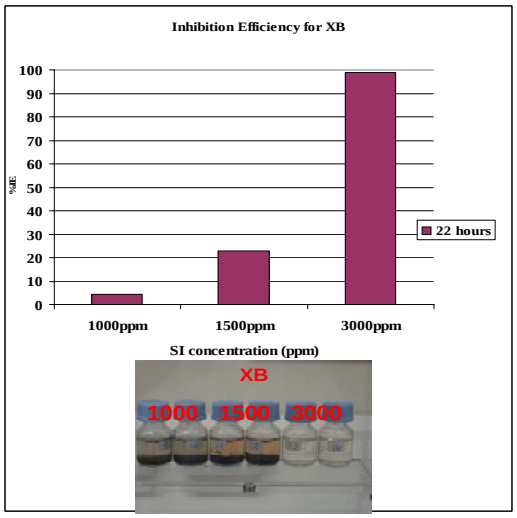

Figure 6.26 %I.E of XB in NaCl+ [Ca].

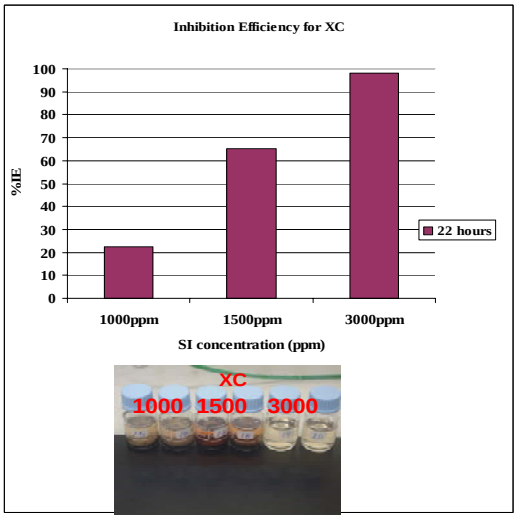

Figure 6.27 %I.E of XC in NaCl +[Ca].

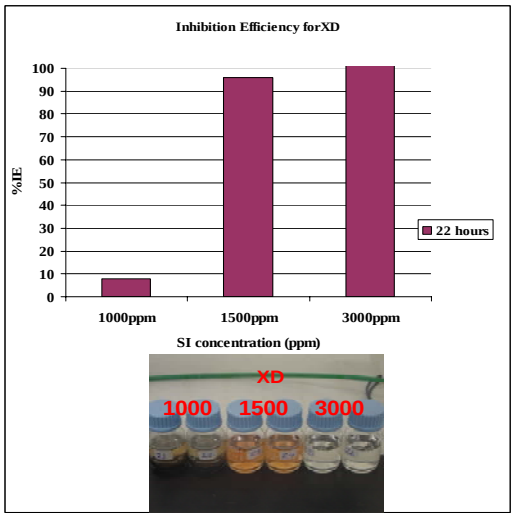

Figure 6.28 %I.E of XD in NaCl + [Ca].

Figures 6.29 to 6.32 show the visual and inhibition efficiency data for THPS products in analogue FW 3 and seawater mix representing low salinity brine with added [Ca] similar to seawater and Miller brine compositions, with [Mg] present. There was a drop in IE compared to the NaCl [Ca] + [Mg] case but less than the NaCl + [Ca] only. Figure 6.29

indicates that the MIC has shifted to 1500ppm for XA, XB while XC and XD have MIC of 1000ppm. The results indicate that [Ca] does play a role in enhancing the efficiency of THPS but it may not have a major effect alone compared to when the both [Mg]+[Ca] are present in the mix. These results point to the active role [Mg] play in enhancing THPS efficiency.

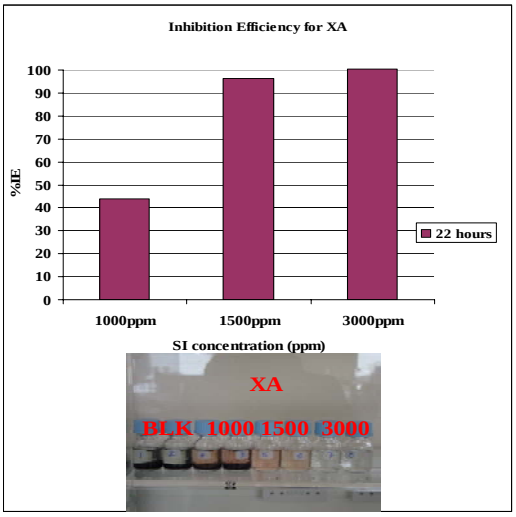

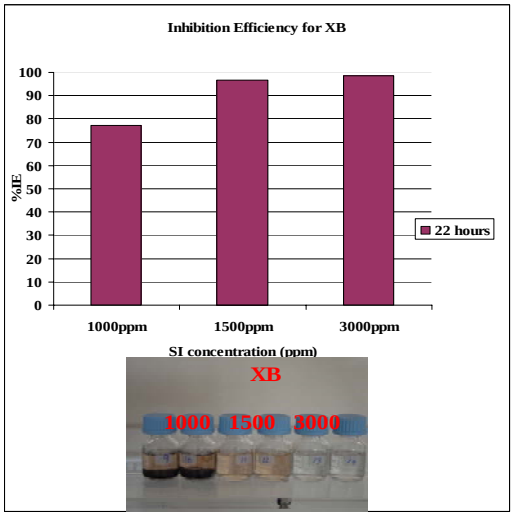

Figure 6.29 %I.E of XC in NaCl + [Mg]. **Figure 6.30** %I.E of XD in NaCl + [Mg].

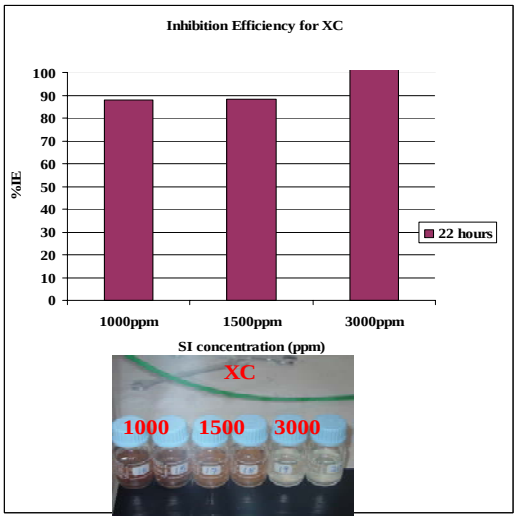

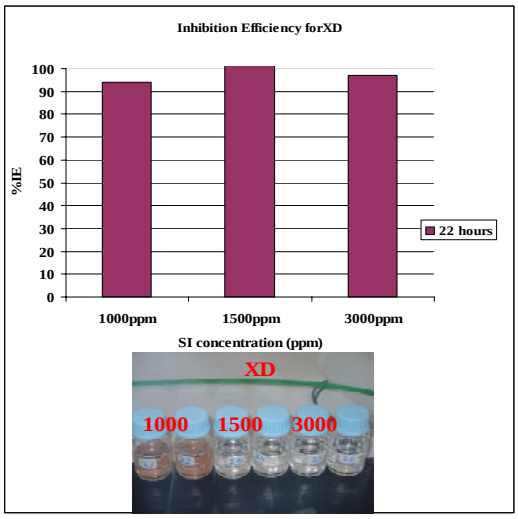

Figure 6.31 %I.E of XC in NaCl + [Mg]. **Figure 6.32** %I.E of XD for Fe NaCl + [Mg].

6.5 THPS Efficacy in High Salinity Brine

6.5.1 Aims of Study and Experiment Design.

The Miller Field scaling tendency was reported as being very severe for $BaSO_4$ and FeS since it produced 200ppm of H_2S Garland (1993). The rationale for using Miller brine in these experiments was to evaluate the effectiveness of the THPS products against high salinity brine for FeS in the presence of other scaling ions such as $BaSO_4$ and $SrSO_4$. The influence of calcium and magnesium on THPS efficiency reported on simple brine, will be explored using brine analogues M1 to M4 compositions in Table 6.4

Table 6.4 Compositions of Miller FW and Seawater Analogues

All concentrations in milligrams per Litre

Ion	M1	M 2	M 3	M 4	North Sea Seawater
Sodium	27080	27080	27080	27080	10890
Calcium	735	0	0	735	428
Potassium	1340	1340	1340	1340	1368
Magnesium	105	0	105	0	460
Barium	775	775	775	775	0
Strontium	180	180	180	180	0
Sulphate	0	0	0	0	2965
Iron	175	175	175	175	0
Sulphide	0	0	0	0	500
Chloride	44021	42415	42721	43715	19026

6.*5.2 THPS Efficacy for Miller Brine-Sea Water Type Formation Mix*

Figures 6.33-6.36 show the inhibition efficiency and visual results for the THPS products in a 50:50 mix ratio, using analogue M1: seawater mixture. The THPS concentrations were 500, 1000 and 1500ppm, for all THPS experiments. The THPS products displayed better performance at 2hrs than the 22hrs results for 500 and 1000ppm concentrations, from the figures it can be seen that 1500ppm XC and XD did inhibit FeS formation at 2 and 22hrs. XA and XB did inhibit FeS but at 2hours only and results dropped off a little at 22hrs, showing it was at the borderline of inhibition. These concentration values were the bench mark values for all future tests and sensitivity studies.

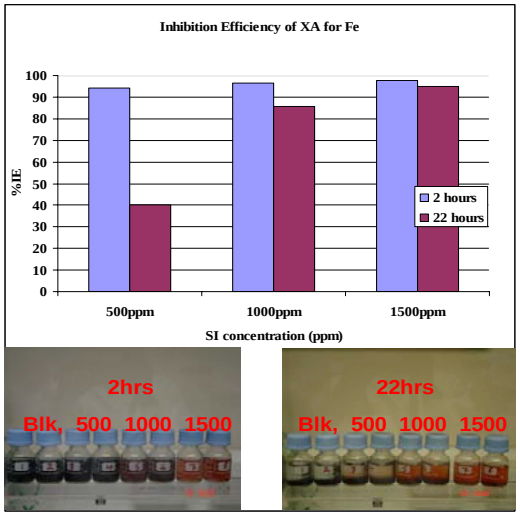

Figure 6.33 I.E% of XA in Miller brine.

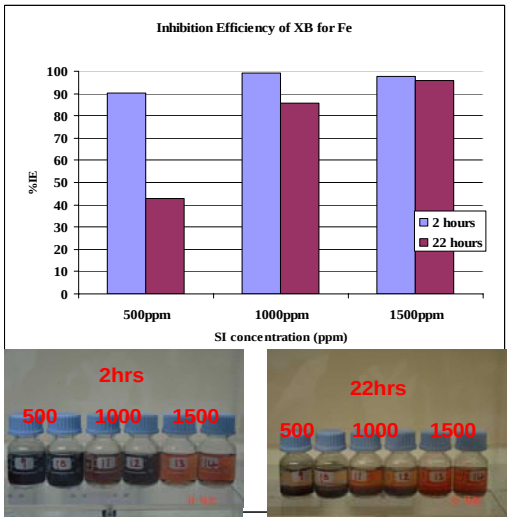

Figure 6.34 I.E% of XB in Miller brine.

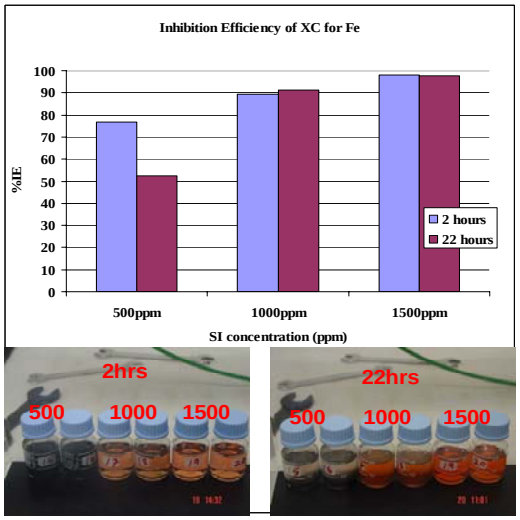

Figure 6.35 I.E% of XC in Miller Brine.

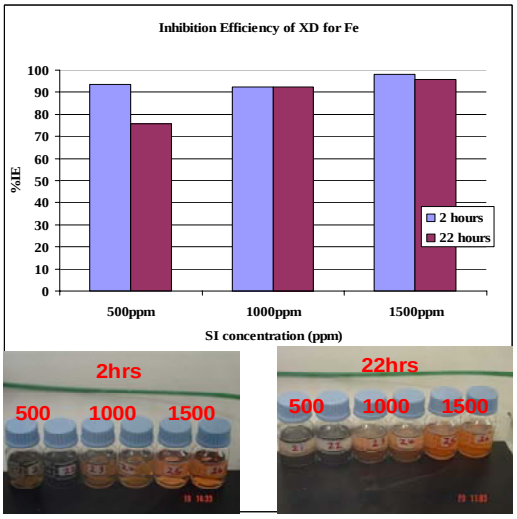

Figure 6.36 I.E% of XD in Miller Brine.

6.5.3 Influence of Calcium and Magnesium on THPS Efficacy in High Salinity Brine.

The influence of [Ca] and [Mg] on the performance of scale inhibitors has been well documented (Graham et al. 1997; Boak et al. 1999) (Gutjahr *et al.* 1996), (Sorbie *et al.* 1993). However, there have been no reported results on the influence of divalent ions on the efficiency of THPS. The aim of this study was to investigate the influence (if any) of [Ca] and [Mg] on THPS. Figures 6.37 - 6.40 show the inhibition efficiency results at 22hrs for the THPS products using Miller FW analogues mix. Figure 6.37 shows the

results for the analogue mix of M2 and Seawater; it indicates that at [1500] there was complete inhibition of FeS. However, when the [Ca] and [Mg] in both the seawater and in Miller formation brine was taken out using M3 and Seawater analogue mix, as shown in Figure 6.38, there was a significant drop in inhibition efficiency across the [THPS] range. This behaviour is consistent with the results obtained from the low salinity brine experiments. When only all of the [Ca] using M4 and seawater analogues was taken out there seems to be no change at or near the MIC levels in [1500] as shown in Figure 6.39, but at [500] and [1000] the results were lower than the M1 analogue in Figure 6.37. Figure 5.40 shows the IE when [Mg] was removed and this reveals the most significant drop during the study with all [THPS] performing badly. The results from the study suggest that [Mg] has a much more pronounced effect on THPS efficiency than [Ca]. The theory proposed here is that the Mg^{2+} ion combines with the phosphonium ion to form a complex which performs as an enhanced ligand, enabling more [Fe] to be held in solution. Brine salinity does not affect the Mg^{2+} ion ability to form the complex shown in the low and high salinity experiments.

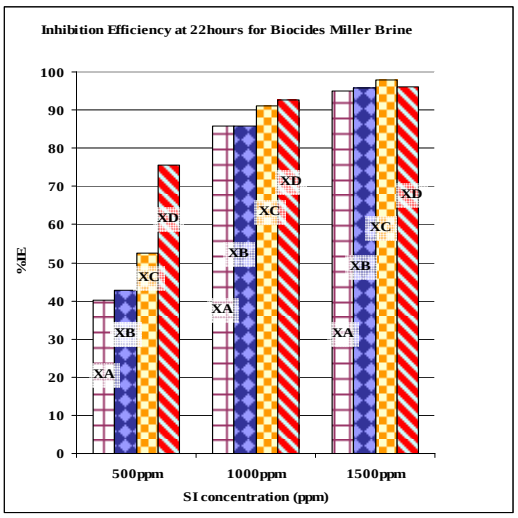

Figure 6.37 I.E% of THPS (Miller Brine).

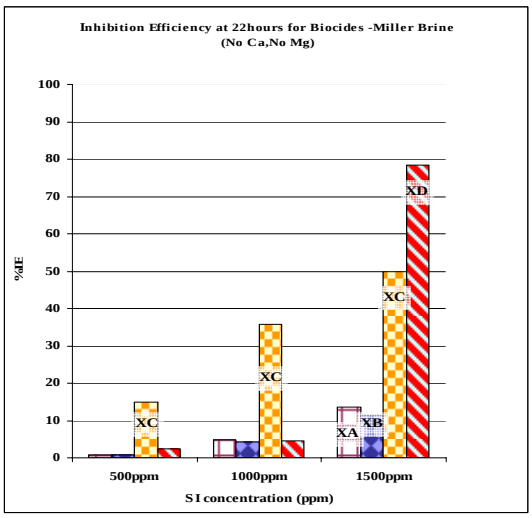

Figure 6.38 IE% of THPS with No Ca & Mg.

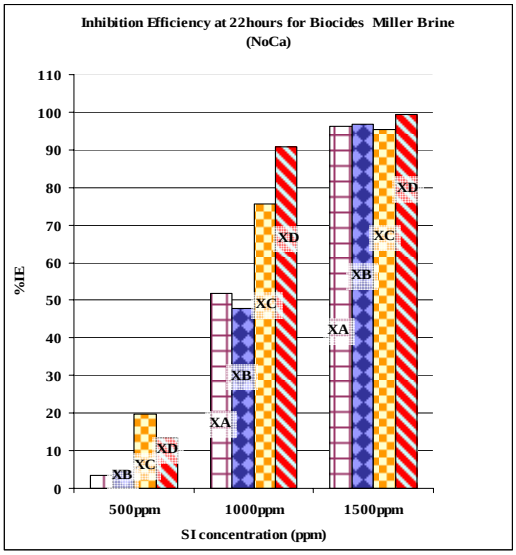

Figure 6.39 I.E% of THPS with No Ca.

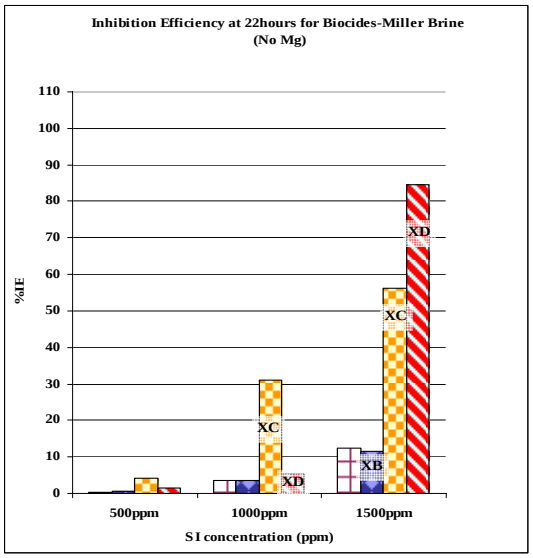

Figure 6.40 I.E% of THPS with No Mg.

6.6 Influence of Mixed Scaling Systems (FeS/PbS/ZnS) on THPS Efficacy.

6.6.1 Aims and Design of the Experiment

The purpose of this study was to investigate the effects of a severe mixed sulphide scaling system in high salinity brine on THPS. The ability of THPS to chelate iron preventing FeS formation has been proven, but its effect on other sulphides such as lead and zinc has not been reported. The experiments were conducted using brine analogues compositions as shown in Table 6.5. The results showing both visual and ICP results indicate that the performance of the THPS products in inhibiting FeS, ZnS and PbS depending on the brine analogue mix. Figures 6.41 to 6.44 show the inhibition efficiency performance of THPS products - the visual images are at 2 and 22hrs.

Table 6.5 Compositions of Miller FW and Seawater Analogues

All concentrations in milligrams per Litre

Ion	Miller FW 1	Miller FW 2	Miller FW 3	Miller FW 4	North Sea Seawater
Sodium	27080	27080	27080	27080	10890
Calcium	0	735	0	0	428
Potassium	1340	1340	1340	1340	1368
Magnesium	105	0	0	0	460
Barium	775	775	775	775	0
Strontium	180	180	180	180	0
Sulphate	0	0	0	0	2965
Iron	175	175	175	175	0
lead	100	0	100	100	0
Zinc	0	250	250	0	0
Sulphide	0	0	0	0	500
HCO_3	0	0	0	2520	
Chloride	43827	44821	43520	43520	19027

6.6.2 THPS Efficacy in Mixed Sulphide Scaling of FeS and PbS

Figures 6.41 to 6.44 show the visual and inhibition efficiency data for THPS products in analogue Miller FW 1 and seawater mix. This brine mix represents a high salinity brine in mixed FeS and PbS scaling. The THPS concentrations were tested at 1000, 2000 and 3000ppm. Figures 6.41 to 6.44 show that the presence of PbS did *not* affect the ability of THPS to inhibite FeS, for all THPS products; on the other hand, the THPS products could not prevent the PbS formation even at 3000ppm. As the data indicates, the presence of lead sulphide does impact negatively on the effectiveness of THPS for FeS inhibition. Note that THPS has never been proposed as a PbS dispersant by either its manufacturer or supplier companies.

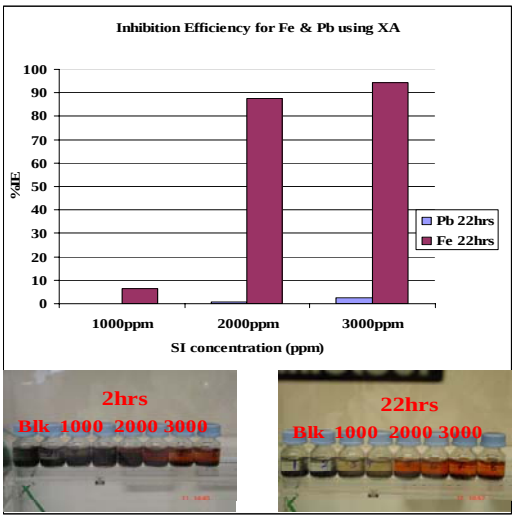

Figure 6.41 I.E% of THPS XA

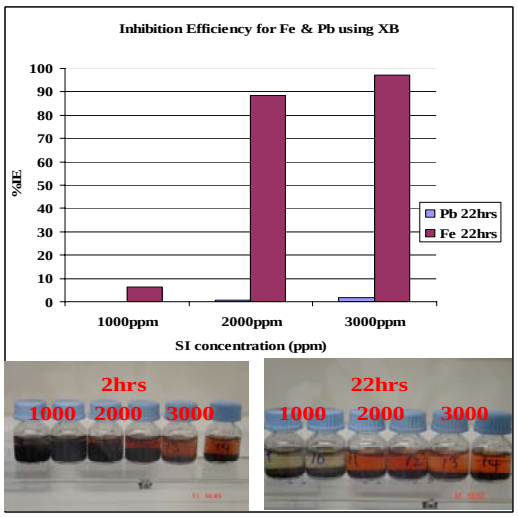

Figure 6.42 I.E% of THPS XB

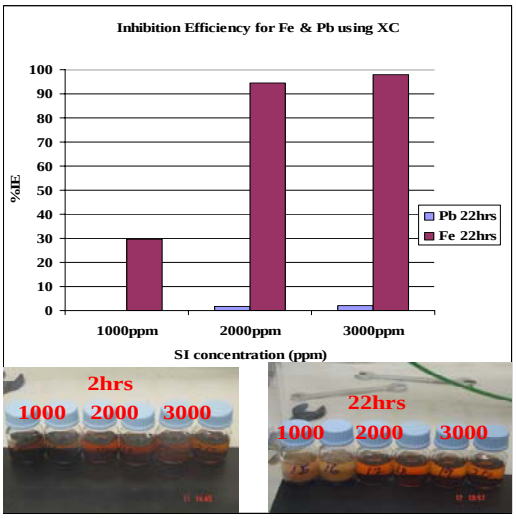

Figure 6.43 I.E% of THPS XC.

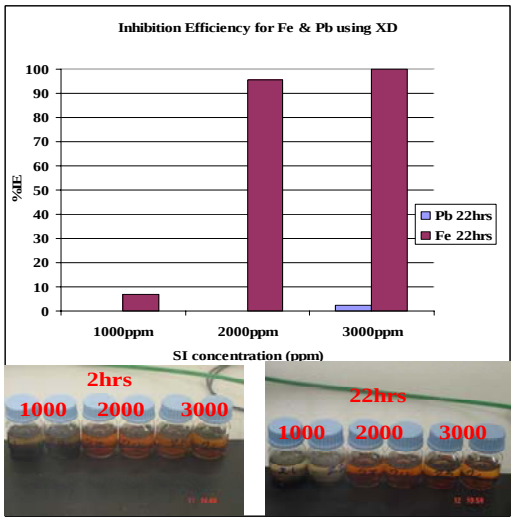

Figure 6.44 I.E% of THPS XD.

6.6.3 THPS Efficacy in Mixed Sulphide Scaling of FeS and ZnS

Results in Figures 6.45 to 6.48 show the THPS products inhibition efficiencies for FeS in the presence of ZnS. The experiments were conducted using analogue Miller FW 2 with Seawater, at THPS concentrations of 500ppm, 1000ppm, and 1500ppm. THPS XA and XB had performed badly with just over 50% efficiency, while XC and XD showed a slightly better performance to FeS but had no effect on the ZnS.

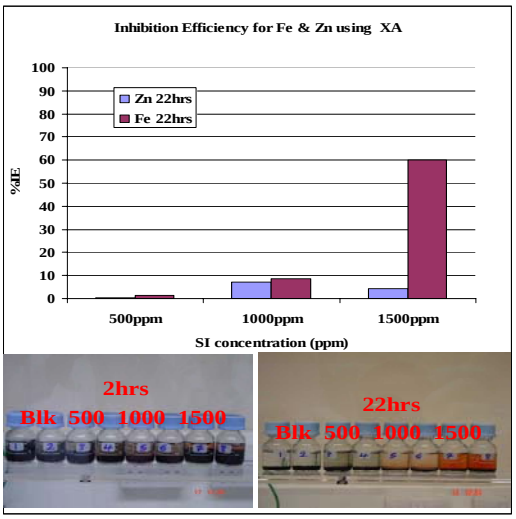

Figure 6.45 I.E% of THPS XA.

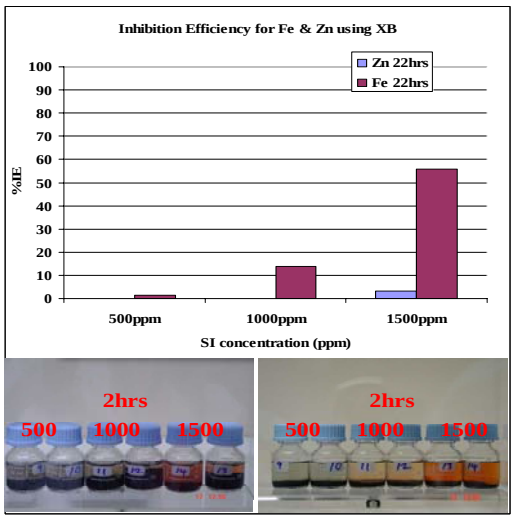

Figure 6.46 I.E% of THPS XB.

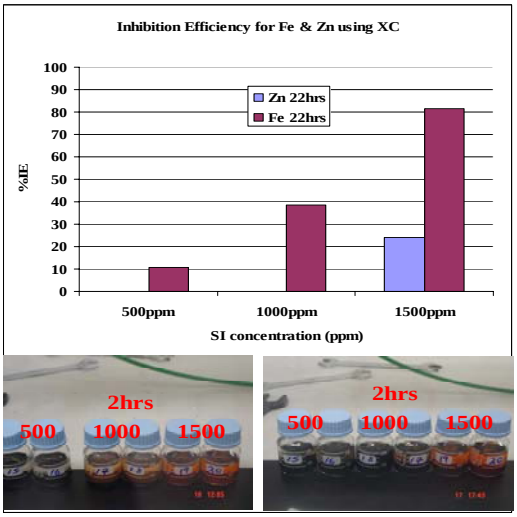

Figure 6.47 I.E% of THPS XC.

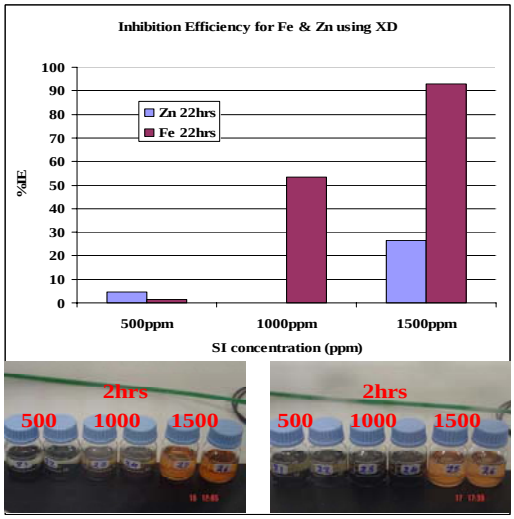

Figure 6.48 I.E% of THPS XD.

6.6.4 THPS Efficacy in Mixed Sulphide Scaling of FeS, ZnS and PbS

Figures 6.49 to 6.52 show the THPS products inhibition efficiency results using analogue Miller FW3 and Seawater. This mix represents Miller brine in the presence of ZnS, PbS and FeS. The THPS products were tested at 1500ppm, 2000ppm and 3000ppm concentrations. Results in these figures indicate that Fe was held in solution across the all THPS concentrations, the ZnS efficiency improved as the THPS concentrations was

increased, the PbS efficiency was below 5% even at 3000ppm. Overall, we can conclude that the THPS products did not inhibit the ZnS or PbS from forming.

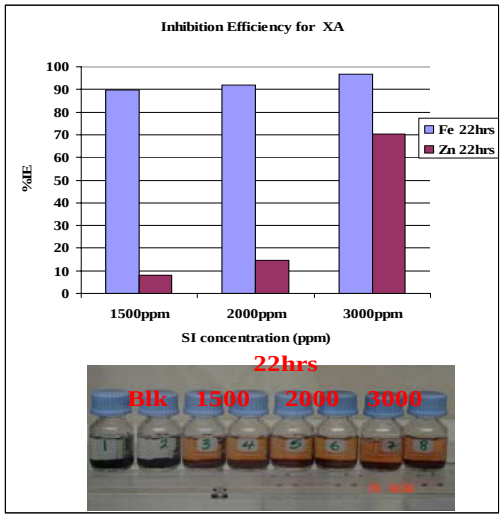

Figure 6.49 I.E% of THPS XA.

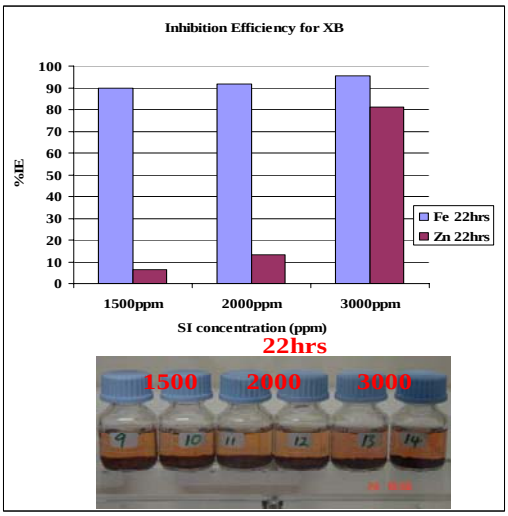

Figure 6.50 I.E% of THPS XB.

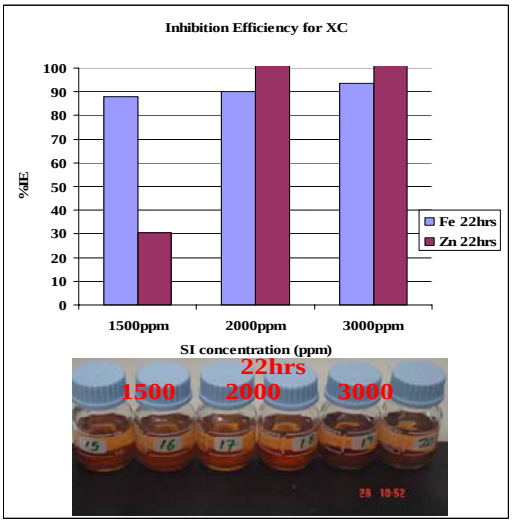

Figure 6.51 I.E% of THPS XC.

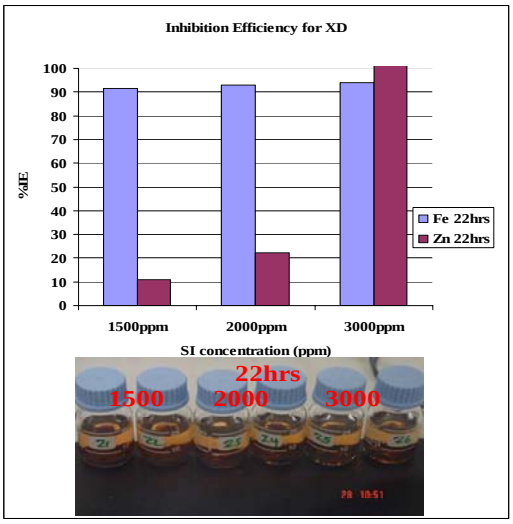

Figure 6.52 I.E% of THPS XD.

6.7 THPS Efficacy in Mixed Sulphide Scaling of FeS and $FeCO_3$

The efficacy of THPS in dealing with FeS and $FeCO_3$ was also investigated. The $FeCO_3$ was formed by adding $NaHCO_3^-$ to the brine, as described experimentally in Chapter 3. The bicarbonate was added to the seawater to prevent self scaling of the Miller FW 4.

Figures 6.53 to 6.56 show the IE% results for all four tested samples with XC performing better than the other tested products. Figure 6.53 presents data from product XA showing a diminished IE% for [2000] which was not the case for FeS. Similarly, product XB also displayed a significantly diminished IE% for [2000] and [3000] respectively which was contrary to earlier experiment for FeS.

However, Product XC did not show diminished IE% as shown in Figure 6.55 for $FeCO_3$ and performed in a similar manner as it did for FeS. This confirms the FeS study results in Figure 6.37, that product XC was overall the best performing ***dissolver*** product in this study at low concentration. Figure 6.56 shows data from product XD which also showed diminished IE for [2000] which did not occur for the FeS only case. This may be caused as a result of $FeCO_3$ formation. The reduced performance of XA and XB at 2000ppm as shown in figure 6.53 and 6.54 have been caused by the presence of $FeCO_3$.

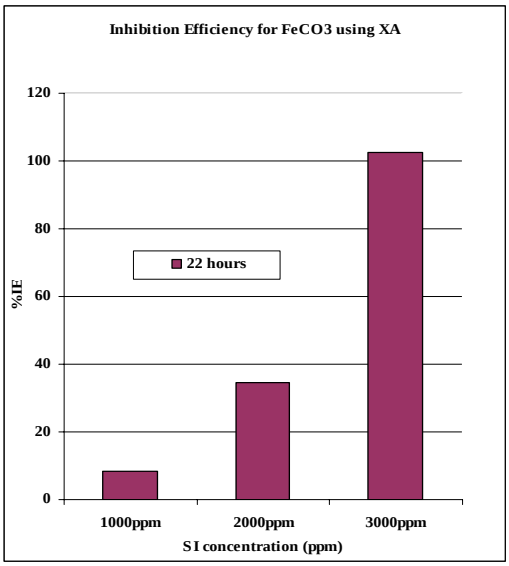

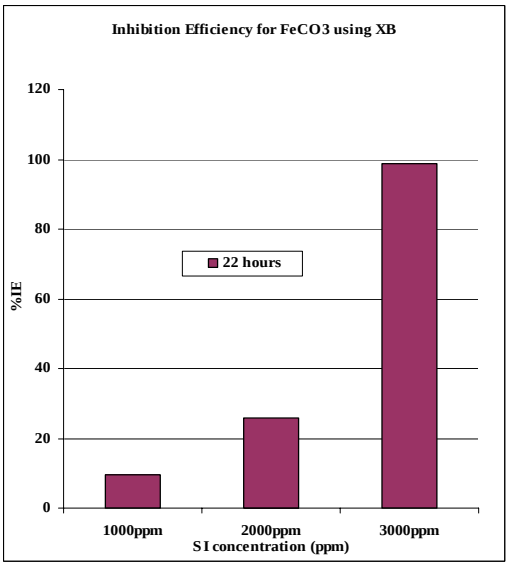

Figure 6.53 I.E% of THPS XA for $FeCO_3$ **Figure 6.54** I.E% of THPS XB for $FeCO_3$

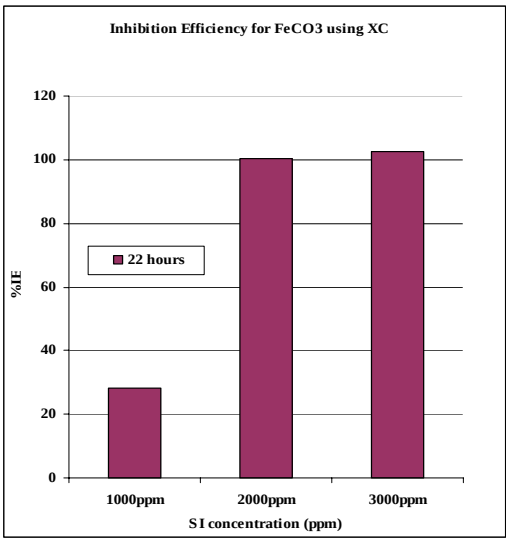

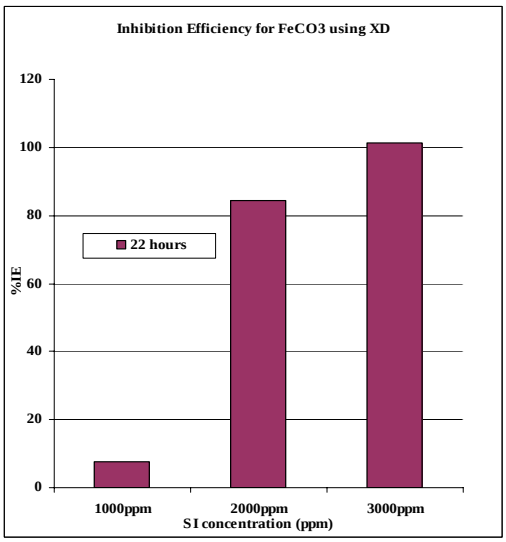

Figure 6.55 I.E % of THPS XC for $FeCO_3$ **Figure 6.56** I.E % of THPS XD for $FeCO_3$

The design of THPS dissolvers for specific scales and microbial conditions is essentially a "balancing act" between keeping the microbial count down and holding the iron in solution. However, it must again be remembered that this particular THPS formulation was probably optimised as a dissolver rather than as a biocide. The pH values for the $FeCO_3$ study were reduced; this pH reduction in the THPS solutions may also contribute to the dissolution of the Fe in these experiments.

6.8 Summary and Conclusions

6.8.1 Stability of 1% THPS.

In this study, it was demonstrated that the four tested THPS products were still active up to three weeks after mixing and were capable of dissolving FeS and FeCO3 without being degraded or losing efficacy. This work shows that of the 4 tested THPS products, 3 products XA, XC and XD were still performing above 98% with one product performing below 95% after 24hrs but this maintained ~94% performance level for the test period of three weeks.

This test suggests that THPS can be active in dissolving FeS and FeCO3 after being exposed for more than 2 weeks. The effect of residual [THPS] in dissolving FeS in

storage and process facilities can be predicted or modelled as [THPS] remains constant. Furthermore mixing and storage of THPS can occur in separate places other than the point of application this is especially useful in facilities with little storage capacities or which require constant dosage.

6.8.2 Influence of [Mg] on THPS in Low/High Salinity Brines

[Mg^{2+}] has a profound effect on the efficiency of THPS on FeS. The presence of Mg^{2+} ions significantly increased the THPS performance in both high and low salinity brines. FeS formation at near the MIC (threshold) conditions was inhibited by the addition of Mg^{2+} ions in the brine mix (Low or High salinity) compared to the brines without Mg^{2+} ions where FeS formation was observed indicating THPS inefficiency.

This is the first time that the effect of divalent ions on THPS performance for FeS formation has been investigated and reported. These results suggest that THPS performance is enhanced by Mg^{2+} ions but that brine salinity did not significantly affect this mechanism.

6.8.3 Influence of Mixed Sulphide Scales on THPS Efficiency.

The presence of mixed sulphide scales of PbS and ZnS co-precipitating with FeS do not affect the efficacy of THPS in dispersing FeS formation. THPS products tested were unsuccessful in inhibiting PbS and ZnS in a mixed or single sulphide system indicating that only FeS is the only sulphide scale that THPS is capable of inhibiting. These results imply that only FeS is *targeted* by THPS and conditions such as salinity and other scaling activities do not poison THPS, unlike some SIs that are poisoned by the presence of other ions or scaling activities.

Chapter 7 Morphology of ($BaSO_4$) Crystals Generated in Sulphide Scaling.

7.1 Introduction and Experimental Aims

Sulphide scales may be formed along with barium sulphate ($BaSO_4$) by various brine mixing processes in the field. The barite solubility product is, log Ksp = -9.96 (Blount 1977), making it a very insoluble mineral which is resistant to both chemical treatments and mechanical techniques. However, when low solubility sulphide scales are formed in association with $BaSO_4$, this leads to a more complex mixed mineral deposition and is more challenging to study. These two scales will interact and, although the system is rather complex, some interesting features and observations emerge. In early work examining the presence of defects in barite, Mellor (1922) showed that in a system of barium sulphate precipitated in the presence of a small amount of impurity of a Pb^{2+} ion, recent works by Okocha and Sorbie (2010) also supports this theory. Substitution takes place where the Pb^{2+} ion will uniformly replace some of the barium ion sites in lattice; hence resulting in a non-morphological change, i.e. solid solution. However, this transformation will only take place at very high temperatures (Butler 1971). The substitution can actually play an important role in inhibition by altering the physical and geometrical attributes of the host crystal lattice**.**

Synthetic Forties formation water and North-Sea seawater were used in this study as described in Chapter 3. The aims of this study are to investigate and observe:

1. The formation of sulphide scales in the final brine.
2. The formation of $BaSO_4$ in the brine mixture.
3. The performance of scale inhibitors (SIs) in the $BaSO_4$ / sulphide scaling system.
4. The fate of sulphide cation and Ba in the system with varying concentrations of [SI].

The Barium crystals formed in the experiments are also examined using the ESEM and EDAX technology described in Chapter 3. The morphology of the $BaSO_4$ crystals formed in the blank (no inhibitor) cases is compared with (a) the $BaSO_4$ crystals formed when sulphide scales are present, and (b) the $BaSO_4$ crystal forms which occur during scale inhibition/dissolution.

7.2. Effects of FeS on Barium Sulphate Formation and Inhibition.

7.2.1 Barium Sulphate Formation in the Absence of Sulphide Scale (Base Case).

Figure 7.1 shows the $BaSO_4$ crystals formed along with the EDAX results from the Forties FW and seawater 50:50 mix. The figure shows several prominent planes of $BaSO_4$ such as the (002) and (210) planes. These planes are characterized as being the main surfaces of $BaSO_4$ as they were representing the peaks with the highest intensity according to Hartman (Hartman 1989) and Van der Leeden (Van Den Leeden 1995). The (002) and (210) planes are the dominant planes of barium sulphate in order to maintain the equilibrium form of the rhombohedral structure of barite crystals, as shown in Figure 7.2. Other planes can also be identified such as the (200) and (211) planes in Figure 7.1.

The EDAX quantification show that $BaSO_4$ is the mineral formed with over 86% atomic distribution with NaCl making up the remainder.

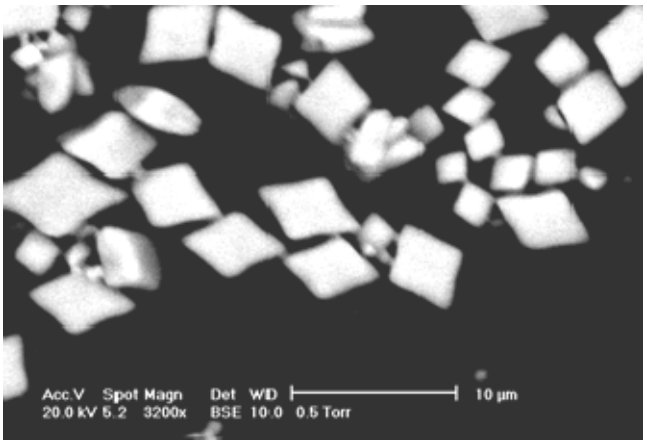

Element	Wt %	At %
O K	35.5	67.2
NaK	3.77	4.97
SrL	8.79	3.04
S K	12.95	12.23
ClK	4.42	3.78
K K	0.71	0.55
CaK	1.42	1.08
BaL	32.42	7.15
Total	100	100

Figure 7.1 ESEM and EDAX results showing the morphology of $BaSO_4$ crystals

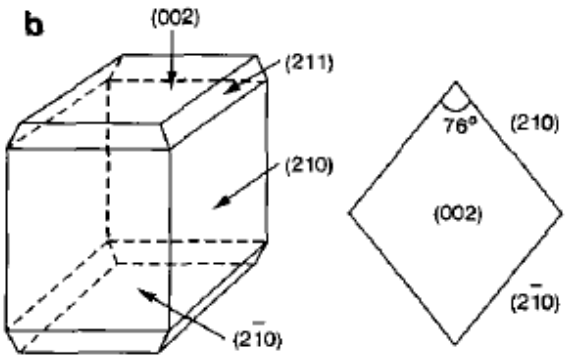

Figure 7.2 Rhombohedral structure of barite (Van der Leeden and Van Rosmalen, 1983)

7.2.2 Barium Sulphate Formation in the Presence of H_2S (Base Case).

Figures 7.3 shows the $BaSO_4$ crystals formed with the Forties FW and seawater 50:50 mix brines in the presence of aqueous sulphide (i.e. just sodium sulphide). The Seawater in this experiment contains sodium sulphide. Figure 7.3 show that the crystal structure is very similar to that in Figure 7.1, thus, indicating the sulphide ions have very little or no effect on the morphology of the barite crystals.

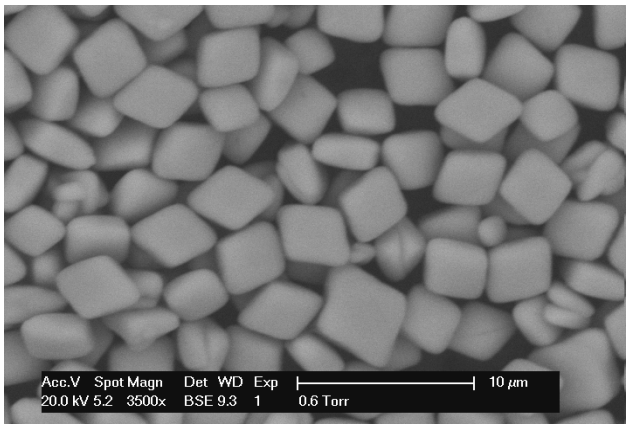

Element	Wt %	At %
C K	2.08	5.73
O K	30.19	62.46
SrL	11.58	4.37
S K	14.03	14.49
ClK	2.62	2.45
K K	0.58	0.49
CaK	1.08	0.89
BaL	37.84	9.12
Total	100	100

Figure 7.3 $BaSO_4$ crystals ESEM and EDAX results formed in the presence of H_2S.

7.2.3 Anaerobic FeS Formation (Base Case).

In order to understand the effect of the FeS on the $BaSO_4$ crystals, it is necessary to study the composition of the FeS in DW, as shown in Figure 7.4. A simple solution of iron (100ppm) in DW, was mixed with sodium sulphide in DW (50:50 mix). The solutions before mixing were treated using the method described in Chapter 3 for removing oxygen before mixing in a Nitrogen filled glove box. The EDAX quantification shows the ratio (%) of the FeS which suggests that the FeS formed is pyrrhotite. The pyrrhotite group of FeS is defined by the general formula of $Fe_{1-x}S$ it has several polymorphs including Fe_7S_8 called Pyrrhotite 4C. The transition of FeS to different polymorphs has been described in Chapter 2 where we have discussed the impact which different FeS forms have on the severity and control of FeS scale occurance.

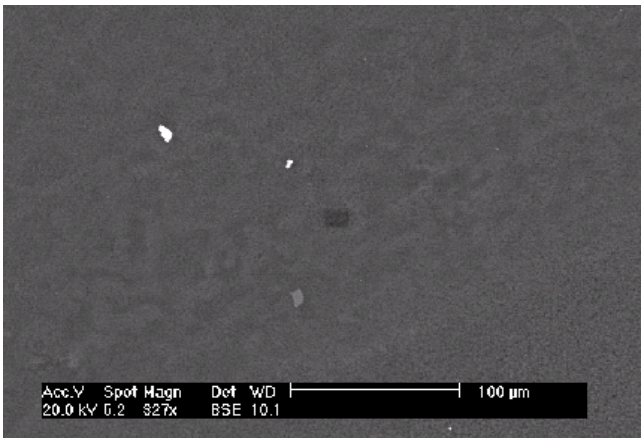

Element	Wt %	At %
S K	43.46	57.25
FeK	56.54	42.75
Total	100	100

Figure 7.4 ESEM image of FeS produced in anaerobic condition with EDAX results showing the atomic % distribution in suggesting the FeS formed is Pyrrhotite $Fe_{(1-x)}S$. As shown above, the resulting picture is dark with basically nothing to see (please note that the white and grey spots are noise in the ESEM figure)

7.2.4 Barium Sulphate Formation in the Presence of Fe.

Figure 7.5 shows the $BaSO_4$ crystals formed using brines of Forties FW and seawater with the addition of iron to the FW. The figure also shows the EDAX quantification from the. 50:50 mix. The figure shows the $BaSO_4$ crystals formed have four-pointed star shapes, compared to the rhombohedral structure obtained in Figure 7.1. These $BaSO_4$ four-pointed star crystals have, one long axis and a short axis. The figure indicates clearly that there is an effect on the barite crystal shape as [Fe] interacts with the $BaSO_4$ formation. The EDAX quantification, however, does not show incorporation of the iron in the lattice of the produced $BaSO_4$ crystals.

Having iron present in the brine produced a change in $BaSO_4$ morphology. However, changing the amount of iron present did not have a large effect since crystals precipitated from 100ppm [Fe] and 500ppm [Fe] are similar in shape. When iron was present, four-pointed star crystals of $BaSO_4$ were obtained. However, although the crystal morphology was altered by the shape, the $BaSO_4$ crystals texture remained unchanged as "*flat-faced with smooth surface*".

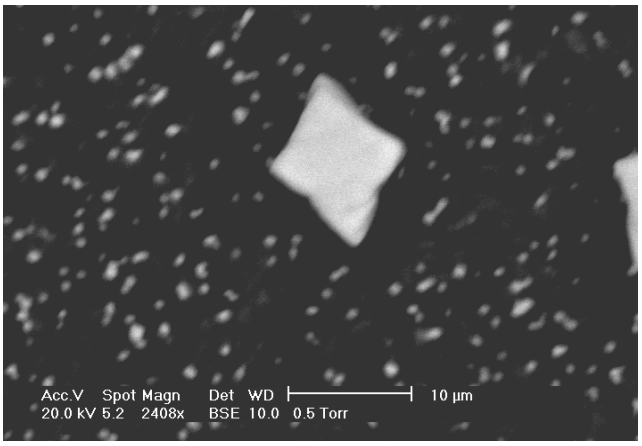

Element	Wt %	At %
O K	30.59	61.62
NaK	5.07	7.1
SrL	8.75	3.22
S K	13.45	13.52
ClK	5.28	4.8
K K	0.52	0.43
CaK	1.36	1.1
BaL	34.98	8.21
Total	100	100

Figure 7.5 ESEM and EDAX showing the morphology of $BaSO_4$ crystals in the presence of iron.

7.2.5 Barium Sulphate Formation in the Presence of FeS.

Figure 7.6 shows $BaSO_4$ crystals that were formed in the presence of co-precipitating FeS. The $BaSO_4$ crystals, which were co-precipitated at the same time as the FeS, display lattice distortions. These distortions are significant and, as the gross crystal morphology is affected, there appears to be growth along the crystal lattices giving it a bi-pyramid shape as shown in Figure 7.6. Figure 7.7 shows the FeS sludge as it adheres to the $BaSO_4$ crystals. The EDAX quantification in Figure 7.6 indicates the presence of a type of iron sludge around the $BaSO_4$ crystals. Figure 7.8 shows a closer view of $BaSO_4$ crystal when co-precipitated with FeS in which the distortions of the crystal lattice is dramatic, going from a standard $BaSO_4$ rhombohedral shape to a bi-pyramidal shape with rounded ends. There also appears to be growth along the crystal lattices enhancing the bi-pyramidal shape. This indicates that FeS causes extensive distortion to the $BaSO_4$ crystal lattice. The EDAX analysis shows that the crystal is $BaSO_4$.

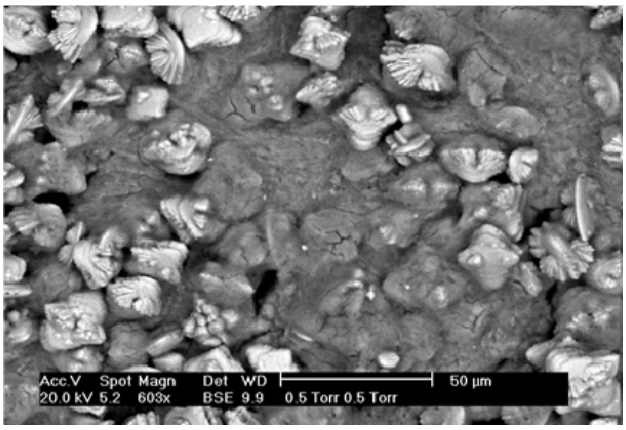

Element	Wt %	At %
O K	13.31	38.01
NaK	4.06	8.07
SrL	13.17	6.87
S K	15.06	21.46
ClK	5.49	7.07
K K	0.45	0.53
CaK	1.48	1.68
BaL	45.53	15.14
FeK	1.44	1.18
Total	100	100

Figure 7.6 ESEM image of $BaSO_4$ crystals co-precipitated along with FeS.

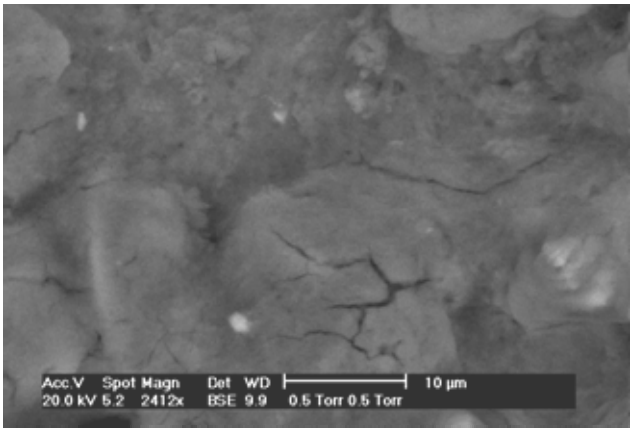

Element	Wt %	At %
O K	10.18	19.77
NaK	20.73	28.02
MgK	1.74	2.22
SrL	4.79	1.7
S K	14.27	13.83
ClK	28.75	25.2
CaK	1.67	1.29
BaL	5.95	1.35
FeK	11.91	6.63
Total	100	100

Figure 7.7 ESEM image and EDAX of $BaSO_4$ crystals co-precipitated along with FeS.

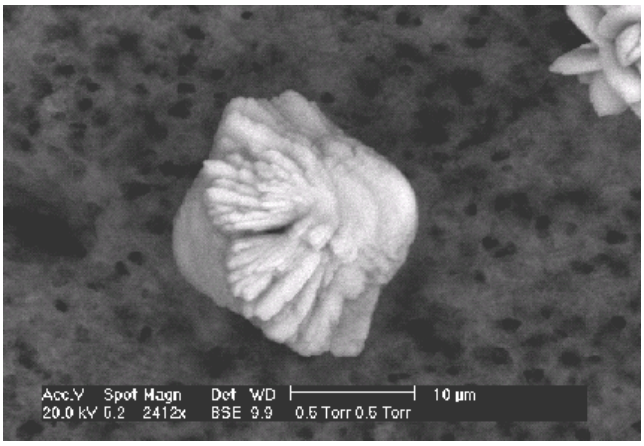

Element	Wt %	At %
O K	13.31	38.01
NaK	4.06	8.07
SrL	13.17	6.87
S K	15.06	21.46
ClK	5.49	7.07
K K	0.45	0.53
CaK	1.48	1.68
BaL	45.53	15.14
FeK	1.44	1.18
Total	100	100

Figure 7.8 ESEM image and EDAX of $BaSO_4$ crystals co-precipitated with FeS

7.2.6 Barium Sulphate-FeS Co-precipitation in the Presence of DETPMP.

Figures 7.9 to 7.10 show the effects of [SI] concentration on the $BaSO_4$ crystals when co-precipitated with FeS. The experiments were performed with initial DETPMP concentrations of 10 ppm, 50 ppm, and 200 ppm in the mixed brines. The crystals formed in the 10ppm SI case (Figure 7.9) are rounded-flat, thin mostly "tablet-like" crystals. The crystals formed from the 50ppm SI brine (Figure 7.10) appear like two half-moon spheres, indicating a breaking or splitting of the tablet-like crystals into two spheres, a groove was frequently observed on the surface of the spheres, giving them a peach-like appearance. Others appear narrow in the middle with growth emanating radially from a central isthmus. In this case, the extent of growth was highly uniform in all directions, making the twin ends of these crystals spherical, as shown in Figure 7.10. This was also observed by Laing et al. (2006) where he stated that these distortions was caused by the SI and could be as a result of the crystals growing as two halves radiating from a central isthmus, which then met and completed the sphere. In summary, as the SI concentration is increased, the shape of the crystals becomes more tablet-like (10ppm) then double-spherical (50ppm). As expected there were no FeS and $BaSO_4$ crystals formed at 200ppm of SI, i.e the mix brine remained clear. Note that as the SI was increased from 10 to 50ppm, the FeS sludge gets increasingly lighter and weighs less on the $BaSO_4$ crystals formed even although the solution still appear black and it is visually different from the untreated blank case.

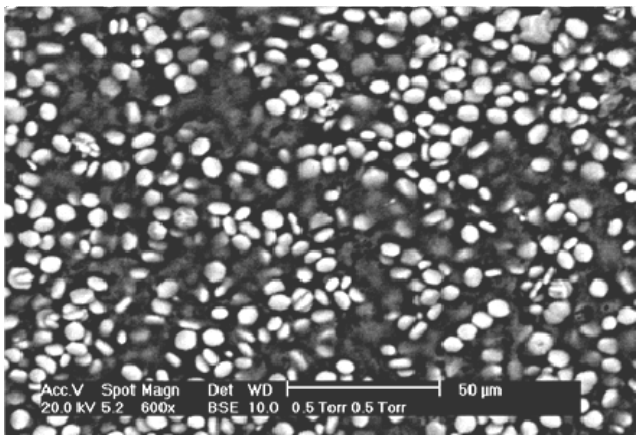

Element	Wt %	At %
O K	16.51	28.47
NaK	21.42	25.7
MgK	2.4	2.72
S K	11.49	9.89
ClK	31.82	24.76
CaK	2.01	1.38
FeK	14.34	7.08
Total	100	100

Figure 7.9 ESEM image and EDAX of $BaSO_4$ crystals in 10ppm DETPMP.

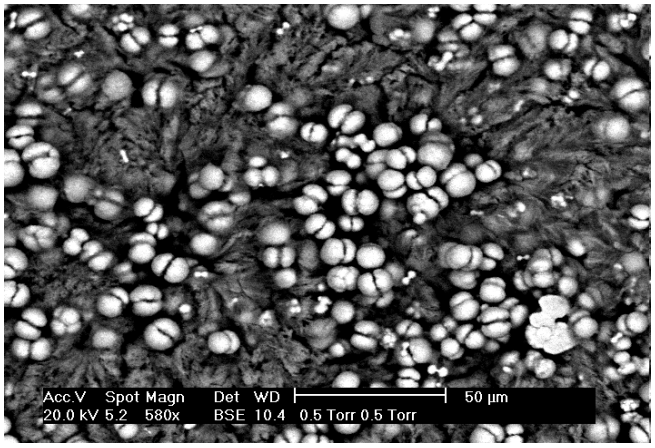

Element	Wt %	At %
O K	7.82	14.38
NaK	28.97	37.1
MgK	1.26	1.53
SrL	0.98	0.33
S K	8.16	7.49
ClK	39.81	33.07
K K	0.7	0.52
CaK	1.35	0.99
BaL	3.82	0.82
FeK	7.14	3.77
Total	100	100

Figure 7.10 ESEM image and EDAX of $BaSO_4$ crystals in 50ppm DETPMP.

7.2.7 Barium Sulphate-FeS Co-precipitation in the Presence of PPCA.

Figures 7.11 to 7.13 shows $BaSO_4$ crystals formed in the presence of the scale inhibitor, PPCA. The PPCA treated samples differed from those of the DETPMP in that the crystals are more spherical, around 10µm in diameter, and they appear to have rough surfaces, as if several crystals have been merged together. As the PPCA concentration was increased from 10ppm to 50ppm, the $BaSO_4$ crystals reduce and more *rough boulders*-like crystals appear as shown in Figure 7.13. The solution appeared the same with no difference between the 10ppm and the 50ppm solutions. As expected, the 200ppm PPCA solution did not form FeS or $BaSO_4$ crystals.

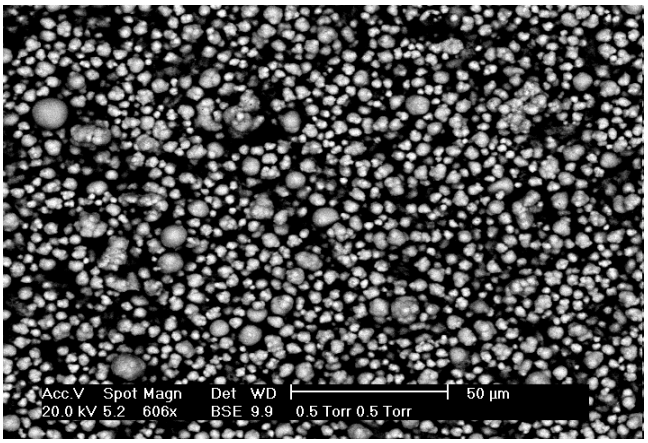

Element	Wt %	At %
O K	25.86	50.08
NaK	11.46	15.44
MgK	0.42	0.54
SrL	14.9	5.27
S K	13.53	13.07
ClK	10.04	8.77
K K	0.41	0.32
CaK	1.5	1.16
BaL	20.65	4.66
FeK	1.24	0.69
Total	100	100

Figure 7.11 ESEM image and EDAX of $BaSO_4$ crystals in 10ppm PPCA.

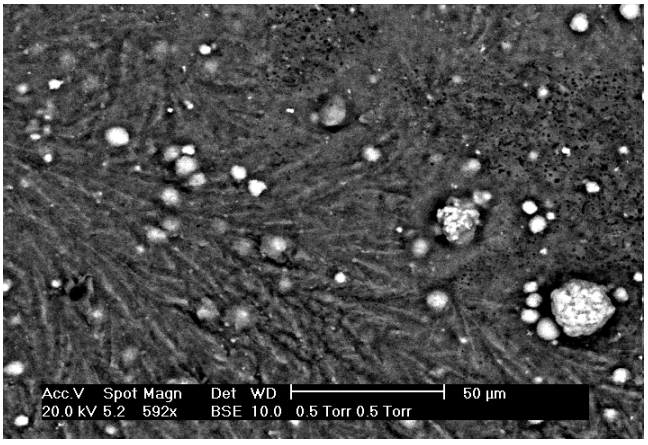

Element	Wt %	At %
C K	30.98	48.31
O K	18.37	21.5
NaK	14.62	11.91
MgK	1.44	1.11
SrL	0.85	0.18
S K	3.33	1.94
ClK	25.8	13.63
CaK	1.45	0.68
BaL	1.65	0.23
FeK	1.51	0.51
Total	100	100

Figure 7.12 ESEM image and EDAX of $BaSO_4$ crystals in 50ppm PPCA.

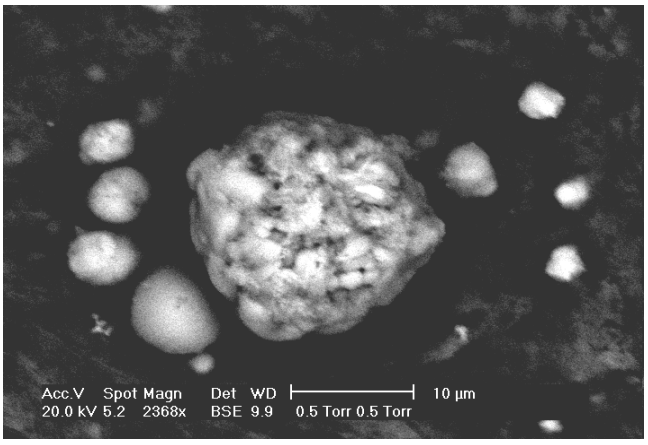

Element	Wt %	At %
C K	30.98	48.31
O K	18.37	21.5
NaK	14.62	11.91
MgK	1.44	1.11
SrL	0.85	0.18
S K	3.33	1.94
ClK	25.8	13.63
CaK	1.45	0.68
BaL	1.65	0.23
FeK	1.51	0.51
Total	100	100

Figure 7.13 Close-up of ESEM image and EDAX of $BaSO_4$ crystals in 50ppm DETPMP.

7.3. Effects of ZnS on Barium Sulphate Formation and Inhibition.

7.3.1 Barium Sulphate Formation in the Presence of Zn.

Figure 7.14 shows $BaSO_4$ crystals formed in the presence of zinc using brines described in Chapter 3. The same regular $BaSO_4$ shape of rhombohedral structure is formed in these solutions indicating that the presence of zinc does not cause any changes in the $BaSO_4$ crystal morphology. The size and shape of the crystal are consistent with those formed in the base case (FW + SW only). EDAX quantification shows that zinc ions were not incorporated into the $BaSO_4$ crystal lattice.

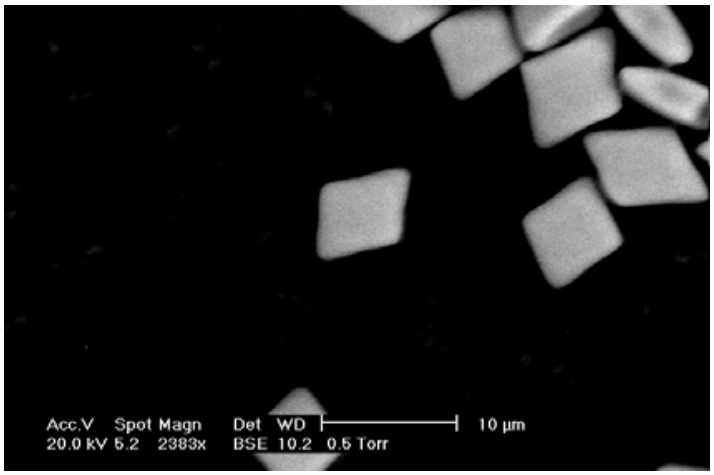

Element	Wt %	At %
C K	7.24	19.04
O K	23.95	47.32
NaK	3.62	4.98
SrL	7.22	2.61
S K	12.41	12.23
ClK	3.95	3.52
CaK	1.29	1.01
BaL	40.32	9.28
Total	100	100

Figure 7.14 ESEM image and EDAX quantification of $BaSO_4$ crystals in the presence of Zinc.

7.3.2 Barium Sulphate Formation in the Presence of ZnS

Figure 7.15 shows $BaSO_4$ crystals co-precipitated with zinc sulphide. These crystals exhibit similar shape and size as the regular rhombohedral $BaSO_4$ crystals, i.e. the morphology of the $BaSO_4$ crystal is unaffected by the white flocc-like ZnS that is prominent in the brine mix. The ZnS-$BaSO_4$ mix appears as a white colloid with flocculent precipitate floating in the brine. The EDAX quantification indicates the presence of zinc as seen in the figure as the white flocculent mass over the $BaSO_4$ crystal. The zinc ion shown in the EDAX quantification is probably from the ZnS mass around the $BaSO_4$ crystal rather than Zn actually being incorporated into the $BaSO_4$ crystal lattice. It should be noted here that ZnS precipitation only usually generates a harder gritty precipitate and this is described further in Chapter 9. The ZnS-$BaSO_4$ crystal mix appears more of a gel-like mix than as a hard, gritty precipitate as described in Chapter 9.

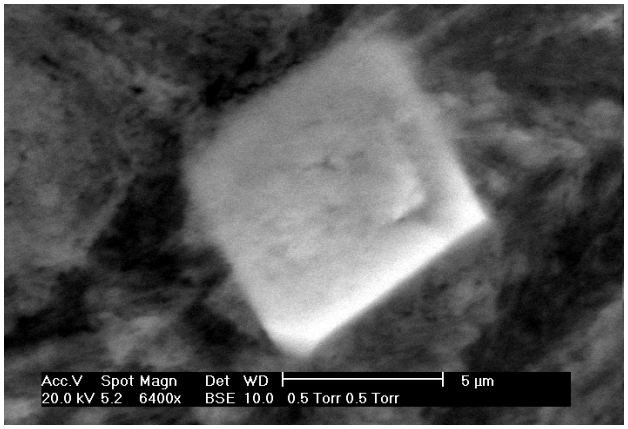

Element	Wt %	At %
O K	21.9	53.59
SrL	9.11	4.07
S K	16.13	19.68
ClK	6.15	6.79
K K	0.68	0.68
CaK	1.29	1.26
BaL	40.98	11.68
ZnK	3.76	2.25
Total	100	100

Figure 7.15 ESEM image and EDAX of $BaSO_4$ crystals co-precipitated along with ZnS

7.3.3 Barium Sulphate-ZnS Co-precipitation in the Presence of DETPMP

Figures 7.16 to 7.17 show the $BaSO_4$ crystals formed when co-precipitated with ZnS in the presence of DETPMP. The experiments were performed with initial DETPMP concentrations of 500 ppm and 3000 ppm, in the mixed brines. There was no change in the morphology of the $BaSO_4$ crystals until SI concentrations of 500ppm were used for the brine mix. The $BaSO_4$ crystals formed were star shaped with the edges eroded and the mid sections having some outcroppings that had eroded peaks. The surface was uneven and narrow protrusions appear in the mid axis of the crystals. As the SI concentration is increased to 3000ppm, the $BaSO_4$ crystals became more rounded and crystals appeared to be growing as two halves radiating from a central isthmus, which then met and completed the sphere or "peach shaped" object. The high concentration of SI used in this experiment reflects the effect of ZnS on the scale inhibitor. Normally at this high concentration of SI, no $BaSO_4$ crystals are expected to form. Visually the brine solution became lighter as the SI concentration was increased. The EDAX quantification shows that zinc was present around the $BaSO_4$ crystals but it was difficult to separately analyze the barite formed because both precipitates appeared as white flocculent masses.

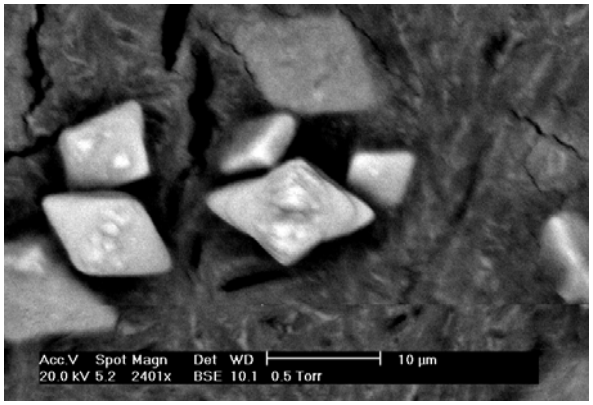

Element	Wt %	At %
O K	23.54	56.44
SrL	7.9	3.46
S K	15.4	18.43
ClK	5.59	6.05
K K	0.73	0.72
CaK	1.58	1.51
BaL	42.84	11.97
ZnK	2.43	1.43
Total	100	100

Figure 7.16 ESEM image and EDAX of $BaSO_4$ crystals co-precipitated with ZnS in 500ppm DETPMP

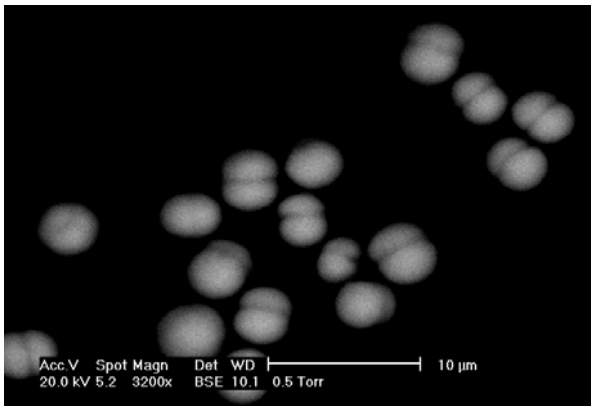

Element	Wt %	At %
C K	23.79	43.78
O K	28.57	39.47
NaK	2.77	2.66
SrL	2.81	0.71
S K	8.6	5.92
ClK	2.84	1.77
CaK	0.45	0.25
BaL	26.93	4.33
ZnK	3.24	1.1
Total	100	100

Figure 7.17 ESEM image and EDAX of $BaSO_4$ crystals co-precipitated with ZnS in 3000ppm DETPMP

7.3.4 Barium Sulphate-FeS Co-precipitation in the Presence of PPCA.

Figures 7.18 to 7.19 show the $BaSO_4$ crystals formed when co-precipitated with ZnS in the presence of PPCA. The SI concentrations used in the experiments were the same as in the DETPMP experiments (500ppm and 3000ppm). Similar crystal structures as in the DETPMP experiments were observed with the PPCA. Figure 7.18 shows the $BaSO_4$ crystals co-precipitated with ZnS in the presence of 500ppm of PPCA. The crystal form of the $BaSO_4$ was as four pointed stars, with small protrusions in the mid axis, similar to Figure 7.16. The surface texture is uneven and small irregular protrusions appear on the crystals. The ZnS textures on the other hand appeared to be thinner/lighter than those in the DETPMP experiment. This could

imply that the PPCA was more effective for the ZnS than the DETPMP. Figure 7.18 shows $BaSO_4$ crystals co-precipitated with ZnS in the presence of 3000ppm of PPCA. This shows a massive degradation of the $BaSO_4$ crystals to small spheres with smooth surfaces. EDAX quantification data indicate the presence of zinc, but it is not clear if this is incorporated into the crystal lattice, or whether the ZnS sludge around the $BaSO_4$ crystals contributes to the total zinc measured by EDAX in the system.

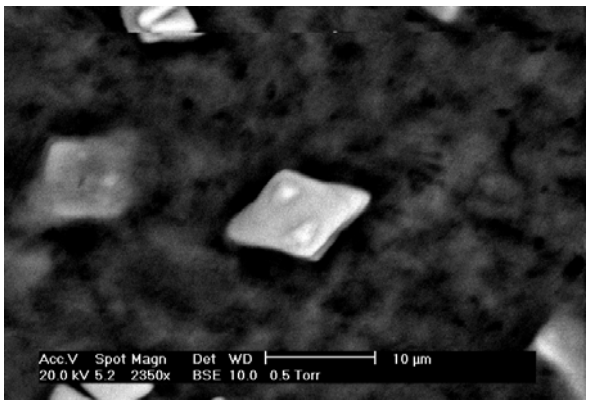

Element	Wt %	At %
O K	12.25	26.65
MgK	2	2.87
SrL	2.08	0.82
S K	15.86	17.21
ClK	36.32	35.66
K K	0.88	0.79
CaK	2.22	1.93
BaL	3.75	0.95
ZnK	24.64	13.12
Total	100	100

Figure 7.18 ESEM image and EDAX of $BaSO_4$ crystals co-precipitated with ZnS in 500ppm PPCA

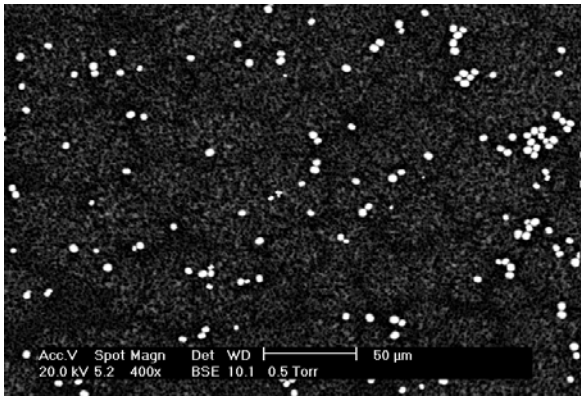

Element	Wt %	At %
O K	8.82	20.14
MgK	1.65	2.47
SrL	2.52	1.05
S K	13.97	15.92
ClK	41.73	43.02
K K	0.72	0.68
CaK	2.07	1.89
BaL	3.83	1.02
ZnK	24.69	13.81
Total	100	100

Figure 7.19 ESEM image and EDAX of $BaSO_4$ crystals co-precipitated with ZnS in 3000ppm PPCA

7.4 Effects of PbS on Barium Sulphate Formation and Inhibition.

7.4.1 Barium Sulphate Formation in the Presence of Pb.

Figure 7.20 show the precipitated $BaSO_4$ in the presence of lead using the brine compositions described in Chapter 3. The crystals formed are unchanged from the $BaSO_4$ classic rhombohedral shape obtained in Figure 7.1 indicating that lead ions do not alter the shape, size and formation of $BaSO_4$ crystals.

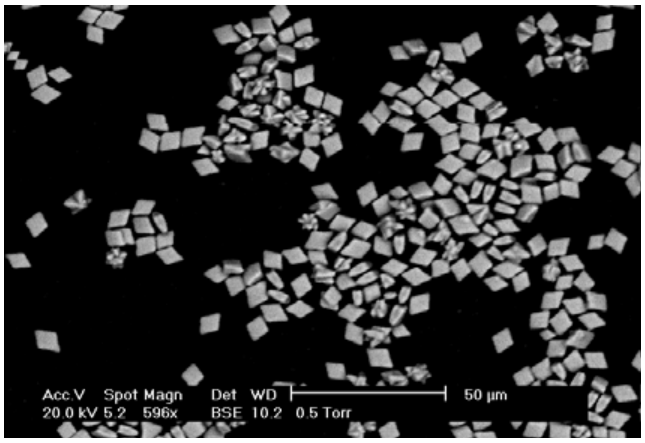

Figure 7.20 ESEM image of $BaSO_4$ crystals in the presence of lead.

7.4.2 Barium Sulphate Formation in the Presence of PbS

Figure 7.21 show $BaSO_4$ crystals co-precipitated with PbS. The $BaSO_4$ crystals formed are four-pointed star shapes with one long axis and one short axis and these were similar to the crystals produced in Figure 7.3. The surface texture of the crystals overall is smooth and there is a grainy, or gritty PbS precipitate which accompanies the $BaSO_4$ crystals which is unlike the white flocculent-fluffy ZnS precipitate. The EDAX data show the presence of lead, most likely from the lead sulphide sludge mix rather than from Pb incorporation within the $BaSO_4$ crystal lattice.

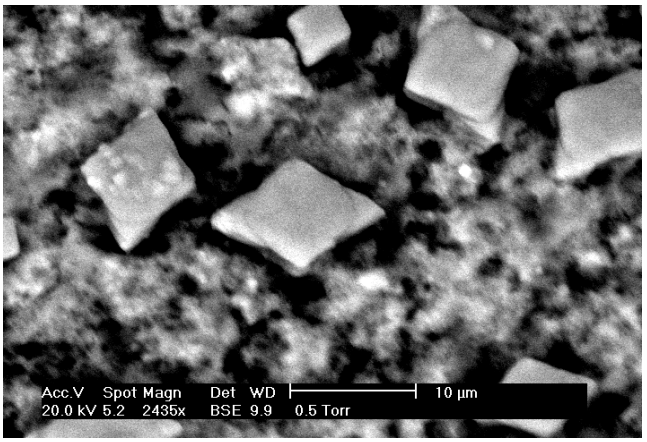

Element	Wt %	At %
O K	12.06	46.52
NaK	5.37	14.43
SrL	4.38	3.08
ClK	8.11	14.12
BaL	6.44	2.9
PbL	63.63	18.96
Total	100	100

Figure 7.21 ESEM image and EDAX quantification of $BaSO_4$ crystals co-precipitated with PbS.

7.4.3 Barium Sulphate-FeS Co-precipitation in the Presence of PPCA.

Figure 7.22 shows the $BaSO_4$ crystals formed when co-precipitated with PbS in the presence of 3000ppm PPCA. These $BaSO_4$ crystals are rounded spheres that have groves in the middle and the sizes vary and they appear similar to the crystals formed in Figures 7.10 and 7.17. The surface texture of the crystals overall is smooth but there appears to be a grainy or gritty PbS precipitate which accompanies the $BaSO_4$ crystals which is unlike the white flocculent ZnS precipitate. The EDAX quantification data indicates the presence of Pb ions, most likely coming from the PbS sludge. $BaSO_4$ crystal formation in the presence of DETPMP was not assessed.

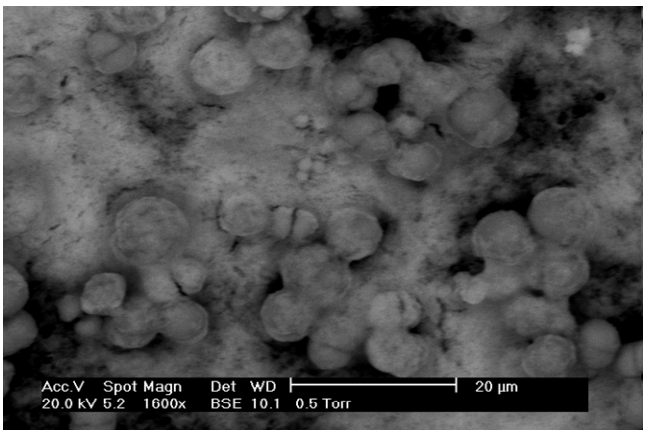

Element	Wt %	At %
O K	9.14	26.91
NaK	11.13	22.8
MgK	1.27	2.46
SrL	2.15	1.16
S K	6.74	9.9
ClK	17.5	23.25
CaK	1.15	1.35
BaL	5.1	1.75
PbL	45.79	10.41
Total	100	100

Figure 7.22 ESEM image and EDAX quantification of $BaSO_4$ crystals co-precipitated with PbS in the presence of 3000ppm PPCA.

7.5 Effects of $BaSO_4$ Co-precipitation in Mixed PbS and ZnS Scaling System.

7.5.1 Barium Sulphate Formation in Mixed Sulphide Scales (PbS [50] and ZnS [50]).

A variety of $BaSO_4$ crystal habits were obtained simply by altering the brine compositions for the mixed sulphide scaling brines, as described in Chapter 3. Figure 7.23 shows the ESEM and EDAX data for $BaSO_4$ crystals formed in mixed scaling composition of PbS [50ppm] + ZnS [50ppm]. The $BaSO_4$ crystals formed from the mixed sulphide composition remains unchanged from the regular rhombohedral shape seen in Figure 7.1 although there are a few crystals that had distortions in the mid sections of the crystals. The sludge mix of PbS and ZnS was powdery and covered the $BaSO_4$ crystals with the crystals appearing to be embedded in the sludge. Figure 7.23 shows the ESEM image and EDAX data of $BaSO_4$ crystals indicating no distortions or inclusions of Pb and/or Zn ions into the $BaSO_4$ crystals lattice.

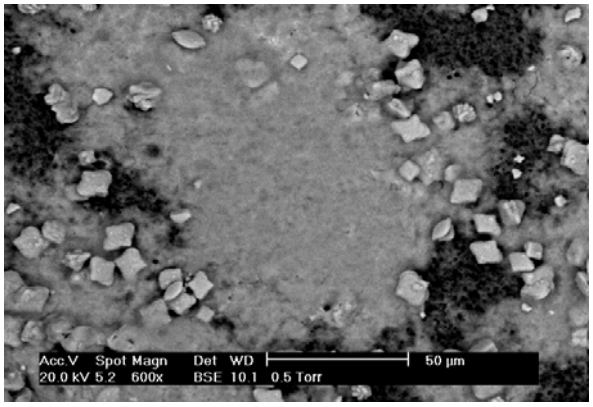

Element	Wt %	At %
O K	13.44	27.43
NaK	19.13	27.17
MgK	1.93	2.6
SrL	1.63	0.61
S K	4.94	5.03
ClK	31.37	28.89
CaK	2.32	1.89
ZnK	7.02	3.51
PbL	18.21	2.87
Total	100	100

Figure 7.23 ESEM image and EDAX of $BaSO_4$ Crystals co-precipitated with mixed ZnS [50] and PbS [50] EDAX shows quantification of the associated sludge.

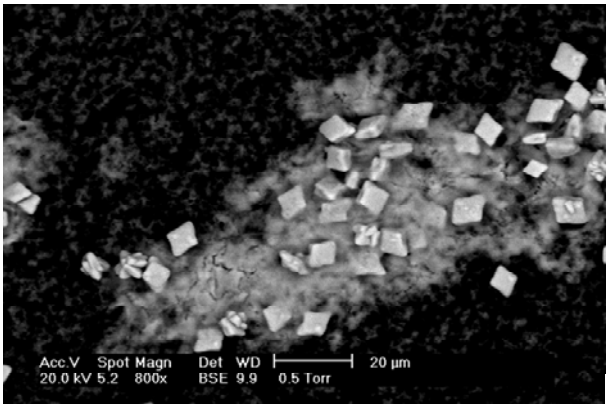

Element	Wt %	At %
O K	24.42	52.5
NaK	8.28	12.38
SrL	9.36	3.67
S K	13.35	14.32
ClK	7.08	6.87
CaK	1.38	1.19
BaL	36.13	9.05
Total	100	100

Figure 7.24 ESEM image and EDAX of $BaSO_4$ crystals co-precipitated with ZnS and PbS

7.5.2 $BaSO_4$ Formation in Mixed Sulphide Scales (PbS and ZnS) in the Presence of PPCA

Figure 7.25 shows the $BaSO_4$ crystals formed in a mixed sulphide scaling brine in the presence of 3000ppm of PPCA. The concentrations of Pb and Zn in the brines were the same as in Figures 7.23–7.24. The scales which are formed are uniformly spherical and <10 µm in diameter but with a groove often being observed on the surface of the spheres as shown in Figures 7.10, 7.17 and 7.13. The sulphide mixed sludge however is a fluffy gel-like flocculent mass which covers the distorted crystals. The EDAX data show both Pb and Zn ions similar to the EDAX data in Figure 7.23

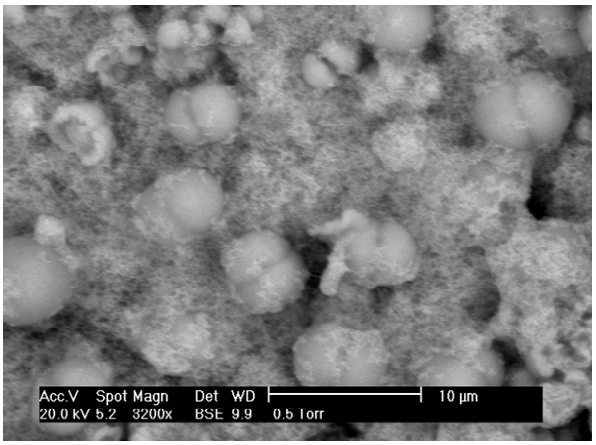

Element	Wt %	At %
O K	4.88	10.81
NaK	24.12	37.19
MgK	0.78	1.13
SrL	1.13	0.46
S K	5.87	6.49
ClK	35.39	35.39
CaK	1.29	1.14
ZnK	7.69	4.17
PbL	18.87	3.23
Total	100	100

Figure 7.25 ESEM image and EDAX of $BaSO_4$ crystals co-precipitated along with PbS [50] and ZnS [250] in the presence of 3000ppm PPCA.

7.5.3 Barium Sulphate Formation in Mixed (PbS [50] and ZnS [250]) Sulphide Scales

Figure 7.26 shows $BaSO_4$ crystals co-precipitated with PbS [50ppm] + ZnS [250ppm] and the differences in the appearance of the crystals are evident i.e. the hue of the crystals is unlike those observed in Figure 7.24 (PbS [50ppm] + ZnS [50ppm]) and the crystal morphology appears to be coated in a white (shining) outer coat. However, the crystal lattices appear to be unaffected as shown in Figure 7.23. The sulphide sludge appears to strongly adhere to the outer surface of the crystals creating a reflective surface and the EDAX data shows a similar quantification with Pb and Zn ions prominently featured.

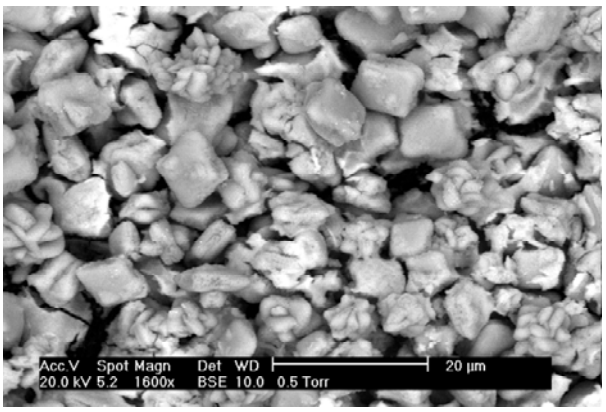

Element	Wt %	At %
O K	19.38	57.32
SrL	14.45	7.8
S K	10.77	15.89
CaK	0.86	1.02
BaL	26.18	9.02
ZnK	4.98	3.61
PbL	23.38	5.34
Total	100	100

Figure 7.26 ESEM image and EDAX data showing $BaSO_4$ Crystals co-precipitated with mixed ZnS and PbS [50]:[250] (No SI).

7.5.4 $BaSO_4$ Co-precipitation with Mixed Sulphide Scales (PbS [50] and ZnS [250]) in the Presence of PPCA.

Figures 7.27 to 7.29 show the effects of PPCA concentration (3000ppm) on the $BaSO_4$ crystals and also on the PbS+ZnS. When the SI is introduced, the shape of the crystals is significantly distorted compared with (PbS [50] + ZnS [50] + [SI]). Note PbS + ZnS sludge appears to be floc-like, as shown in Figure 7.25 and the $BaSO_4$ crystals appear extremely distorted compared to the untreated blank case. This change can probably be attributed to the [Zn^{2+}] since this was not observed in the PbS [50] + ZnS [50] + [SI] case. These anomalous crystal formations could be as a result of the crystallization of a complex salt, (due to the excess Zn^{2+}) either separately or as a mixture of complex crystals.

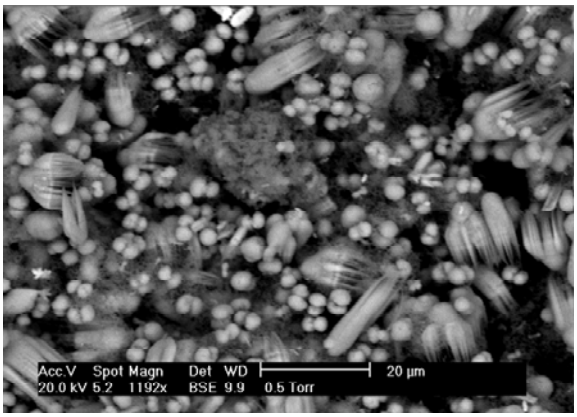

Element	Wt %	At %
O K	12.71	43.99
SrL	11.54	7.29
S K	13.82	23.85
CaK	0.77	1.06
BaL	18.73	7.55
ZnK	8.49	7.19
PbL	33.94	9.07
Total	100	100

Figure 7.27 ESEM image and EDAX of $BaSO_4$ crystals co-precipitated along with PbS [50] and ZnS [250] in the presence of 3000ppm PPCA.

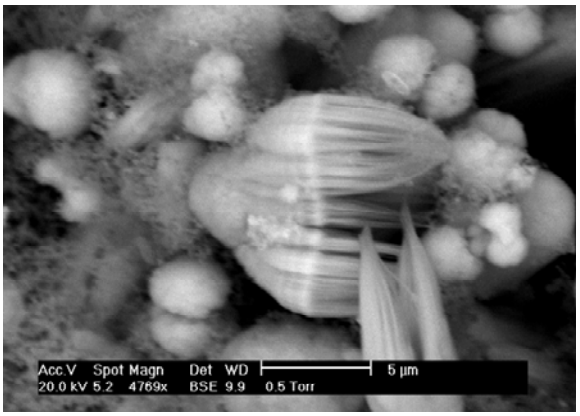

Element	Wt %	At %
C K	23.15	51.36
O K	16.68	27.78
SrL	6.4	1.95
P K	0.63	0.55
S K	10.51	8.73
K K	0.41	0.28
CaK	1.64	1.09
BaL	38.69	7.51
ZnK	1.88	0.77
Total	100	100

Figure 7.28 Zoom view of the ESEM image of distorted $BaSO_4$ crystals with EDAX data of **Figure 7.27**

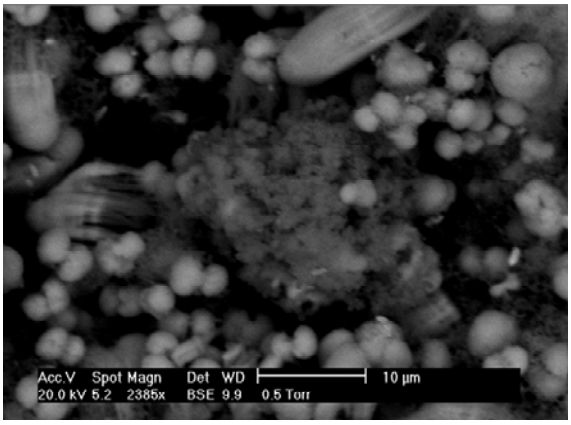

Element	Wt %	At %
C K	37.97	64.27
O K	20.18	25.64
MgK	0.72	0.6
SrL	1.98	0.46
S K	4.09	2.6
CaK	2.42	1.23
BaL	16.19	2.4
ZnK	5.64	1.75
PbL	10.81	1.06
Total	100	100

Figure 7.29 Zoom view of Figure 6.25 showing ESEM image of distorted $BaSO_4$ crystals and sulphide sludge along with corresponding EDAX data of **Figure 7.27**

7.6 Summary and Conclusions

The morphology of precipitated barite crystals is significantly affected by presence of iron sulphide scale. The barite is changed from a standard $BaSO_4$ rhombohedral shape to a bi-pyramidal shaped crystal with frayed edges. This distortion is as a result of the presence of FeS on the crystal lattice of $BaSO_4$ when it is co-precipitated with FeS. Zinc sulphide and lead sulphide on the other hand, do not affect the morphology of barite crystals when these sulphate/sulphide scale co-precipitate. The SI type was also shown to have an influence on the morphology of precipitated barite crystals.

Table 7.1 presents a summary of the data found in this Chapter. Crystal habits were found to be sensitive to changes in brine chemistry. DETPMP is known as a crystal growth inhibitor and it affected barite crystals in a different manner when co-precipitated with FeS, with many crystals having a round smooth surface and a groove in the middle, as did PPCA which is classed as a nucleation inhibitor. The barite crystals formed when co-precipitated with FeS in the presence of PPCA were round with rough surfaces, with large concentrations of the crystals being fused together as larger "boulder like" aggregates.

Barite crystals co-precipitated with ZnS or PbS show similar morphology, in the absence or presence of scale inhibitor. The barite crystal remains unchanged when co-precipitated with ZnS or PbS, and the barite crystals obtained when formed in the presence of scale inhibitor are quite similar in morphology. The morphology of precipitated barite crystals in a mixed sulphide scaling system is unchanged from the usual rhombohedral shape in a blank un-inhibited condition, when SI is added the barite crystals are eroded much like the case of ZnS and PbS. However, when the [Zn] is increased the barite scales formed in the presence of scale inhibitors are significantly distorted. This suggests that [Zn] ions significantly enhance the impact of SI on $BaSO_4$ crystals.

Table 7.1 Summary of $BaSO_4$ Morphology Results

	SI	$BaSO_4$ Crystal Morphology	Comment
Blank BaSO4	NO	Rhombohedral crystal structure	Base case for Study
BaSO4-[H_2S]	NO	No change to $BaSO_4$ structure	
BaSO4-[Fe]	NO	Slight change in basic $BaSO_4$ crystal structure	Rhombohedral $BaSO_4$ crystal to Four pointed star structure
BaSO4-FeS	NO	Significant distortion to $BaSO_4$ crystal structure to a Bi-pyramidal structure	Black colloidal FeS adhere to the $BaSO_4$ distorted crystals
BaSO4-[Zn]	NO	No change to $BaSO_4$ structure	
BaSO4-[Pb]	NO	No change to $BaSO_4$ structure	
BaSO4-ZnS	NO	No change to $BaSO_4$ structure	ZnS Colloid formed
BaSO4-PbS	NO	Slight change in crystal structure	Rhombohedral $BaSO_4$ crystal to Four pointed star structure
BaSO4-Blank	Yes	Eroded crystals in <10ppm (SI)	N/A
BaSO4-FeS	Yes	Eroded crystals in ~10ppm (SI)	PPCA/DETPMP caused significant deformation to the crystals at low [SI]
BaSO4-PbS	Yes	Eroded crystals in >1000ppm (SI)	Bigger eroded spheres formed by PPCA
BaSO4-ZnS	Yes	Eroded crystals at >100ppm (SI)	White Flocculent ZnS covering $BaSO_4$
BaSO4-ZnS+PbS	Yes	Eroded crystals at >100ppm (SI)	Significant distortion with increased [Zn]

Chapter 8 Influence of Sulphide Scales on the Morphology of $CaCO_3$ Scale Deposited on Metal Surface and in Bulk Solution

8.1 Introduction

The precipitation of calcium carbonate ($CaCO_3$) has been widely studied in the literature (Hasson *et al.* 1968; Bradley 1973; Chibowski 1980; Chong *et al.* 2001). Traditionally, studies of scale formation have concentrated on assessing precipitation from the bulk solution in laboratory jar tests. More recent research has focused on surface deposition using an integrated approach combining synchrotron XRD with electrodeposition (Kazmierczak *et al.* 1982; Liang *et al.* 1997; Mirotchnik *et al.* 1997; Morizot *et al.* 1999; Kohler *et al.* 2001; Zhang *et al.* 2001; Kjellin 2003). There have been recorded field examples where calcium carbonate scales occur with sulphide scales (Leach 1993, 2001; Hein 2006; Oriski 2007) In this chapter, the impact of carbonate/sulphide co-precipitation in bulk and on metal surfaces is demonstrated. The mechanistic understanding of $CaCO_3$ co-precipitation with sulphide scales has not been well documented or discussed. The relationship between bulk precipitation and surface deposition of the mixed carbonate and sulphide scales is examined here. Carbonate reservoirs represent an increasingly important source of oil production, with 50% to 70% of the remaining reserves in the world estimated to be in carbonate formations. Both carbonate and sulphide scale problems have been reported when water is produced from carbonate reservoirs and the use of scale inhibitors to control this problem is relatively common.

8.2 Experimental Design and Details

Experiments were carried out in a 500ml vessel at 20°C in beaker with a magnetic stirrer to accelerate bulk precipitation. $CaCO_3$ was precipitated spontaneously by mixing 150ml brine A with 150 ml brine B. The composition varied according to the sulphide scale being formed in association with the $CaCO_3$ scale. The influence of PbS and ZnS on $CaCO_3$ bulk and surface deposition has been studied. Tables 8.1 to 8.8 shows the brine compositions used in the study.

8.3 Brine Compositions

The brine compositions used are listed in the order in which they appear in the thesis. Table 8.1 shows the brine composition for the base case of $CaCO_3$ formed in the bulk and on the surface of the metal spindle. Table 8.2 gives details of the brine composition for $CaCO_3$ formed in the presence of H_2S both in bulk and on the metal surface. This is the base case used to determine the influence of H_2S on the formation of $CaCO_3$. Tables 8.3 and 8.4 show the brine compositions for $CaCO_3$ formed in the presence of Zn (Table 8.3) and Pb (Table 8.4). Table 8.5 gives the brine composition for the case where $CaCO_3$ is co-precipitated with ZnS, while Table 8.6 details the brine composition for the case where $CaCO_3$ is co-precipitated with PbS. Table 8.7 gives the brine compositions for cases where CaCO3 is formed in the presence of Pb-Zn (simulating MVT brines – see Chapter 3). Table 8.8 shows the brine compositions for the case where $CaCO_3$ is co-precipitated with ZnS and PbS similar to brines in MVT formations.

Composition of brine used in $CaCO_3$ bulk and surface deposition		
All concentrations are in mg/L		
Ion	Brine 1	Brine 2
Na	10000	10000
Ca	1163	0
Mg	1473	0
K	1340	0
Cl	22989	12491.8
HCO_3	0	2520

Table 8.1 Showing the brine composition for the base case of $CaCO_3$ crystals deposition

Composition of brine used in $CaCO_3$ bulk and surface deposition		
All concentrations are in mg/L		
Ion	Brine 1	Brine 2
Na	10000	10000
Ca	1163	0
Mg	1473	0
K	1340	0
Cl	22989	12491.8
HCO_3	0	2520
S	0	500

Table 8.2 Showing the brine composition for $CaCO_3$ deposition formed in the presence of H_2S.

Composition of brine used in $CaCO_3$ bulk and surface deposition		
All concentrations are in mg/L		
Ion	Brine 1	Brine 2
Na	10000	10000
Ca	1163	0
Mg	1473	0
K	1340	0
Cl	22989	12491.8
HCO_3	0	2520
Zn	250	0

Table 8.3 showing the brine composition for $CaCO_3$ deposition formed in the presence of Zn.

Composition of brine used in $CaCO_3$ bulk and surface deposition		
All concentrations are in mg/L		
Ion	Brine 1	Brine 2
Na	10000	10000
Ca	1163	0
Mg	1473	0
K	1340	0
Cl	22989	12491.8
HCO_3	0	2520
Pb	100	0

Table 8.4 Showing the brine composition for $CaCO_3$ deposition formed in the presence of Pb.

Composition of brine used in $CaCO_3$ bulk and surface deposition		
All concentrations are in mg/L		
Ion	Brine 1	Brine 2
Na	10000	10000
Ca	1163	0
Mg	1473	0
K	1340	0
Cl	22989	12491.8
HCO_3	0	2520
Zn	250	0
S	0	500

Table 8.5 Showing the brine composition for $CaCO_3$ co-precipitated with ZnS.

Composition of brine used in $CaCO_3$ bulk and surface deposition		
All concentrations are in mg/L		
Ion	Brine 1	Brine 2
Na	10000	10000
Ca	1163	0
Mg	1473	0
K	1340	0
Cl	22989	12491.8
HCO_3	0	2520
Pb	100	0
S	0	500

Table 8.6 Showing the brine composition for $CaCO_3$ co-precipitated with PbS.

Composition of brine used in $CaCO_3$ bulk and surface deposition		
All concentrations are in mg/L		
Ion	Brine 1	Brine 2
Na	10000	10000
Ca	1163	0
Mg	1473	0
K	1340	0
Cl	22989	12491.8
HCO_3	0	2520
Pb	100	0
Zn	250	0

Table 8.7 showing the brine composition of $CaCO_3$ deposition in the presence of Pb+Zn.

Composition of brine used in $CaCO_3$ bulk and surface deposition		
All concentrations are in mg/L		
Ion	Brine 1	Brine 2
Na	10000	10000
Ca	1163	0
Mg	1473	0
K	1340	0
Cl	22989	12491.8
HCO_3	0	2520
Pb	100	0
Zn	250	0
S	0	500

Table 8.8 Showing the brine composition for $CaCO_3$ co-precipitated with ZnS and PbS.

8.4 Experimental Results and Discussion

8.4.1 Base Case ($CaCO_3$ Crystal Formation)

In order to investigate the influence of sulphide co-precipitation with $CaCO_3$ it is important to establish the base case of precipitated $CaCO_3$ crystals in bulk and on the active metal surface. Bulk $CaCO_3$ precipitation was carried out using the method described in Section 8.3 with the brine composition listed in Table 8.1. Figures 8.1 to 8.4 show the ESEM images and EDAX elemental quantifications for the $CaCO_3$ crystals formed on the active metal surface. The classic trigonal rhombohedral crystal shape is clearly seen. Figures 8.5 and 8.6 show the $CaCO_3$ crystals formed in the bulk solution with the corresponding EDAX quantification. The crystals formed on the metal surface at 24 hours are between 10 and 20μm in size. In the bulk solution, the size of the crystals in the bulk precipitate is less than 5μm. The size of these $CaCO_3$ crystals is measured when the experiment was carried out for 2hrs to allow for fewer crystals to be deposited on the metal surface. Figures 8.7 and 8.8 show the $CaCO_3$ crystals deposited on the metal surface and in bulk solution, and these figures show fewer crystals deposited on the metal surface at 2hrs. The crystals formed in bulk, appear similar to those in Figure 8.5 with the

crystals aggregating together as a $CaCO_3$ mass. The experiment clearly shows that the precipitate formed in the bulk is different to the deposit formed on the metal surface, which is in agreement with findings by other authors (Chen 2005; Hasson D. 1996). The magnetic stirrer was kept rotating for the duration of the experiment and this may have hindered the development of the $CaCO_3$ crystals. The EDAX quantification shows that $CaCO_3$ was formed on the metal surface and in the bulk solution. The [Fe] data was from the metal surface and not from the brine.

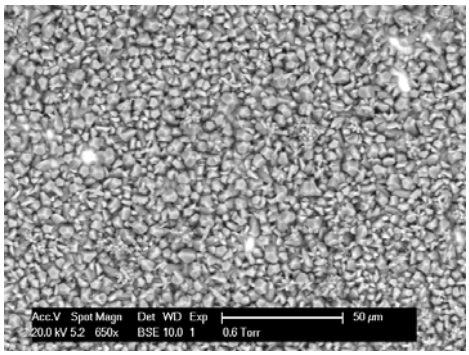

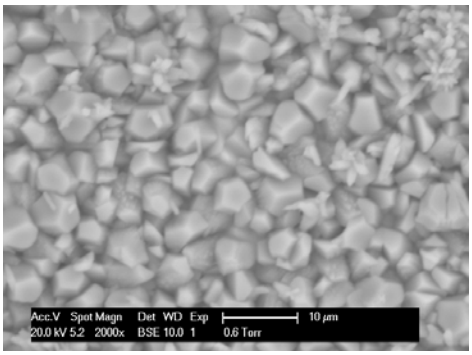

Figures 8.1-8.2 showing $CaCO_3$ crystals on the metal surface at 50µm and 10µm view at 24hrs

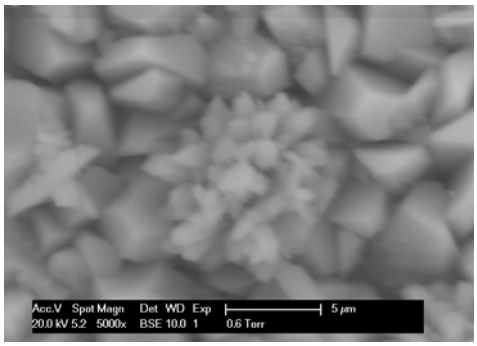

↔

Element	Weight%	Atomic%
C	14.08	21.37
O	57.95	66.02
Ca	27.15	12.35
Fe	0.82	0.27
Totals	100	

Figures 8.3-8.4 showing $CaCO_3$ at 5µm view and EDAX data of the Crystals at 24hrs

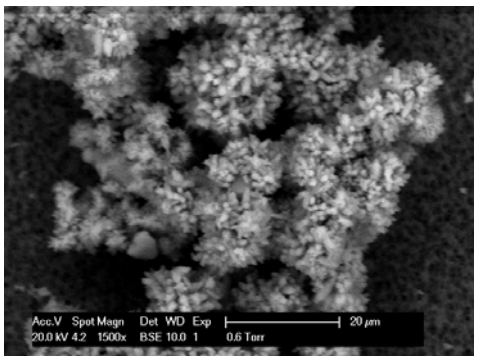

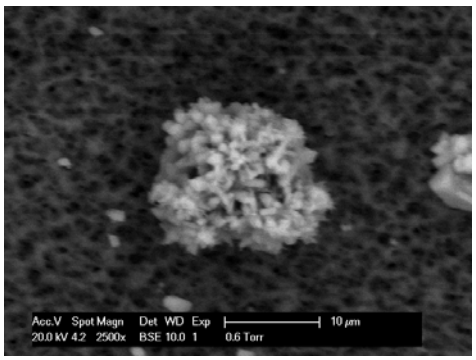

Figures 8.5-8.6 showing $CaCO_3$ crystals mass formed in the bulk solution at 24hrs

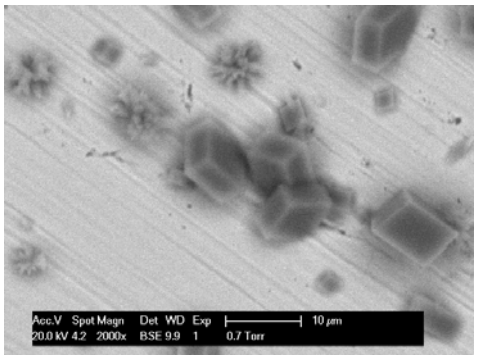

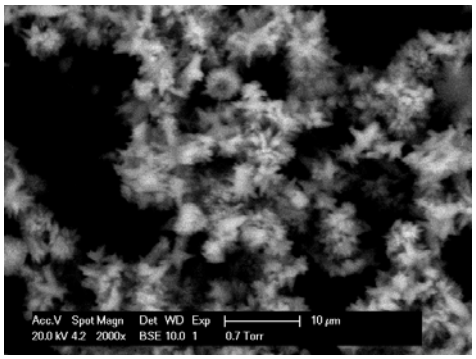

Figures 8.7-8.8 showing $CaCO_3$ crystals formed on the metal surface and in bulk solution at 2hrs

8.4.2 $CaCO_3$ Crystal Formation in the Presence of H_2S

Figures 8.9 and 8.10 show the $CaCO_3$ crystals formed using the brine composition in Table 8.2. These figures show the ESEM images and EDAX quantifications for the $CaCO_3$ crystals, formed on the active metal surface in the presence of H_2S. The $CaCO_3$ crystals formed on the metal surface are distorted with most crystals projecting outwards as thin crystals, appearing like spikes or as "*opening flower petals*" when they aggregate together. The figure also indicates that fewer crystals are deposited on the metal surface compared to the base case.

The EDAX quantification shows that $CaCO_3$ crystals were formed; [Fe], [Cr] and [Ni] indicated here represent the metal steel surface whose signal is more enhanced due to the less coverage of the metal surface by $CaCO_3$ crystals. Figure 8.12 shows the $CaCO_3$ crystals formed in the bulk solution in the presence of H_2S. These crystals form a mass of nucleated $CaCO_3$ with NaCl, but

are unable to form fully developed $CaCO_3$ crystals. The EDAX data show that $CaCO_3$ crystals with NaCl are the predominate ions in the bulk solution.

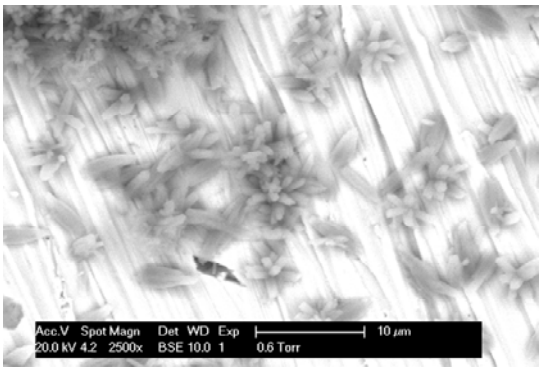

Element	Weight%	Atomic%
C	15.33	26.71
O	40.88	53.49
Ca	22.44	11.72
Cr	4.46	1.8
Fe	14.72	5.52
Ni	2.17	0.77
Totals	100	

Figures 8.9-8.10 ESEM image and the EDAX data of $CaCO_3$ crystals formed on the metal surface in the presence of H_2S at 24hrs.

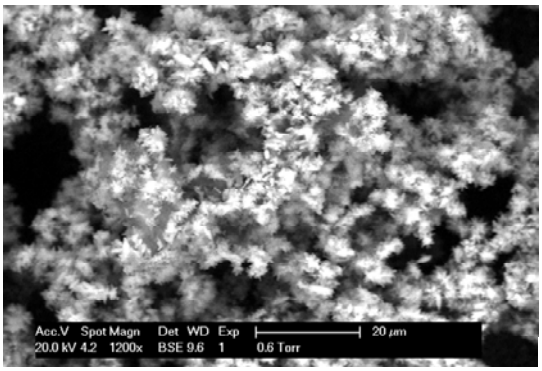

Element	Weight%	Atomic%
C	16.21	25.88
O	45.88	55.01
Na	1.97	1.65
Cl	4.23	2.29
Ca	31.71	15.17
Totals	100	

Figures 8.11-8.12 ESEM image and the EDAX data of $CaCO_3$ crystals formed in the bulk solution in the presence of H_2S at 24hrs.

8.4.3 $CaCO_3$ Crystal Formation in the Presence of Zn^{2+}

Figures 8.13-8.14 show ESEM image and EDAX data of the deposits formed on the surface of the metal in the presence of Zn^{2+}. The $CaCO_3$ crystals were formed using the brine composition in Table 8.3. The entire metal surface was without deposits and the only deposit is shown in Figure 8.14, this deposit is not characterised as $CaCO_3$ crystals. The EDAX quantification shows that the deposit is not $CaCO_3$ crystals, but rather $ZnCO_3$ which readily occurs in carbonate systems. Note that no deposit was formed on the metal surface, the Zn^{2+} may have formed

complexes with the carbonate, thereby the preventing the formation of $CaCO_3$ crystals on the metal surface. Figures 8.16-8.17 show the ESEM image and EDAX data of the deposits formed in the bulk solution in the presence of Zn^{2+}, the deposits shows a compact earthy, white solid precipitate.

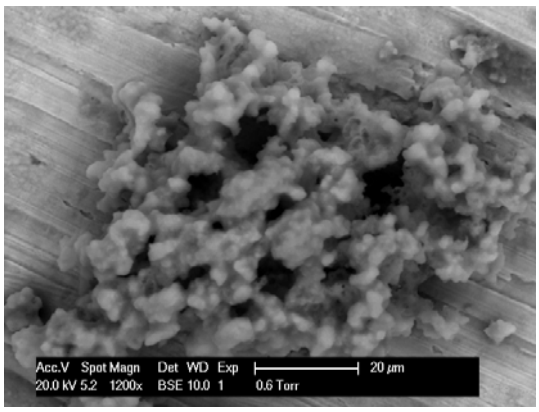

Element	Weight%	Atomic%
C	4.78	12.65
O	24.28	48.21
S	0.34	0.34
Ca	0.6	0.48
Cr	9.54	5.83
Mn	1.03	0.59
Fe	33.5	19.05
Ni	4.77	2.58
Zn	21.15	10.28
Totals	100	

Figures 8.13-8.14 ESEM image and the EDAX data of deposit formed on the metal surface in the presence of Zn at 24hrs.

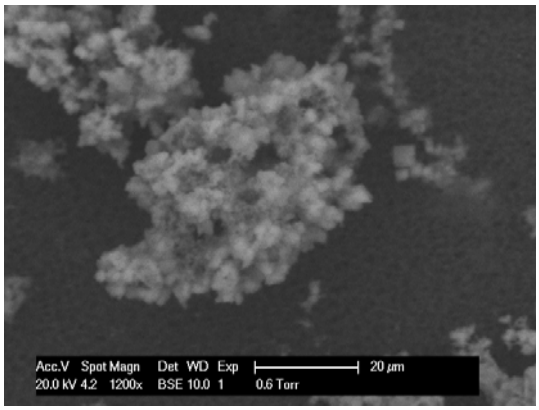

Element	Weight%	Atomic%
C	28.7	45.1
O	36.67	43.26
Cl	5.51	2.93
Ca	1.61	0.76
Zn	27.52	7.95
Totals	100	

Figures 8.15-8.16 ESEM image and the EDAX data of deposit formed in the bulk solution in the presence of Zn at 24hrs.

8.4.4 $CaCO_3$ Crystal Formation in the Presence of Pb^{2+}

Figures 8.18 to 7.19 show ESEM images and EDAX data for $CaCO_3$ crystals formed on the surface of the metal in the presence of Pb. The $CaCO_3$ crystals were formed on the metal surface using the brine composition in Table 8.4. $CaCO_3$ crystals deposited on the metal surface are a

mix of partially formed $CaCO_3$ crystals with some distorted crystals that appear to fuse together and fully developed $CaCO_3$ crystals. Note that the amount of crystals formed on the metal surface is less than in the base case for the 24hrs period. EDAX quantification shows that the deposits are $CaCO_3$ [Fe], [Cr] and [Ni] signals are from the stainless steel metal surface. Figure 8.20 shows the ESEM image of the deposits formed in the bulk solution using brine compositions in Table 8.4 These deposits appear as a mass of crystals with outward projecting crystals. The EDAX data indicates that the bulk crystals are $CaCO_3$.

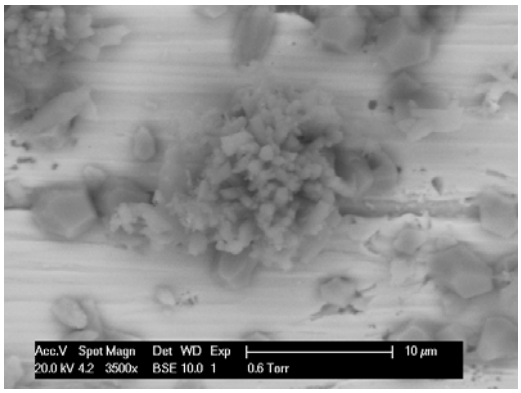

Element	Weight%	Atomic%
C	15.1	26.03
O	41.66	53.9
S	0.31	0.2
Ca	26.65	13.76
Cr	3.54	1.41
Fe	11.3	4.19
Ni	1.44	0.51
Totals	100	

Figures 8.17-8.18 ESEM image and the EDAX data of $CaCO_3$ crystals formed on the metal surface in the presence of Pb at 24hrs.

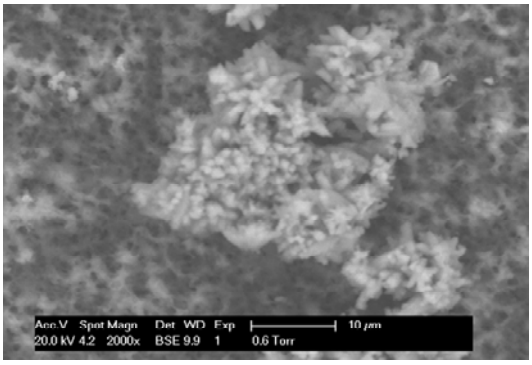

Element	Weight%	Atomic%
C	15.87	24.7
O	50.38	58.85
Na	1.54	1.25
Cl	2.92	1.54
Ca	29.3	13.66
Totals	100	

Figures 8.19-8.20 ESEM image and the EDAX data of deposit formed in the bulk solution in the presence of Pb at 24hrs.

8.4.5 $CaCO_3$ Co-precipitation with ZnS in Bulk and on Metal Surface

Figure 8.22 shows the morphology of the $CaCO_3$ crystals deposited on the active metal surface when co-precipitated with ZnS. The $CaCO_3$ crystals were formed using the brine composition in Table 8.5. The $CaCO_3$ crystals vary in size but are fully formed undistorted $CaCO_3$ crystals. Fewer crystals formed on the metal surface than in the base case at 24hrs. EDAX data in Figure 8.27 shows that it is $CaCO_3$ crystals which are are deposited on the metal surface. Figure 8.24 shows the $CaCO_3$ crystals formed in the bulk solution with elongated crystals in a fused mass. The EDAX data shows that both $CaCO_3$ crystals and ZnS are identified in the mixed scale in the bulk phase. However, ZnS was not identified in the EDAX of the scale on the metal surface. Although both scales ($CaCO_3$ and ZnS) form, there must be a difference in the degree of adhesion of these minerals to the metal surface.

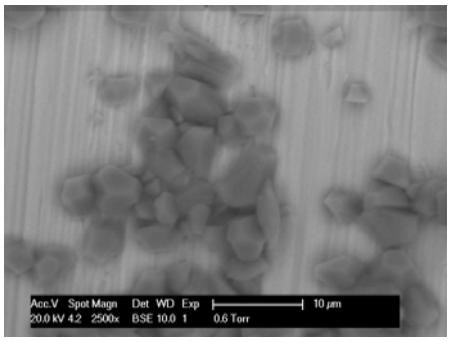

Element	Weight%	Atomic%
C	14.71	25.86
O	40.17	53.04
Mg	0.83	0.72
Ca	23.84	12.56
Cr	4.25	1.73
Fe	14.22	5.38
Ni	1.98	0.71
Totals	100	

Figures 8.21-8.22 Morphology and the EDAX data of $CaCO_3$ crystals co-precipitated with ZnS on metal surface at 24hrs.

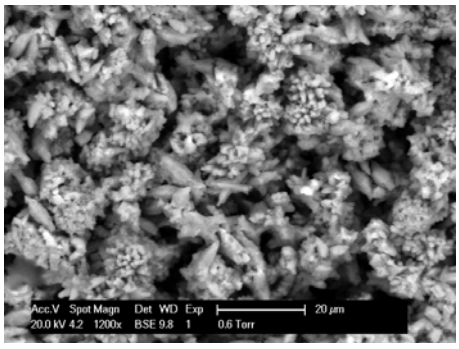

Element	Weight%	Atomic%
C	11.48	21.18
O	38.26	53.01
S	3.59	2.48
Cl	3.29	2.06
Ca	30.66	16.96
Zn	12.72	4.31
Totals	100	

Figures 8.23-8.24 Morphology and the EDAX data of $CaCO_3$ crystals co-precipitated with ZnS in bulk solution at 24hrs.

8.4.6 $CaCO_3$ Co-precipitation with PbS in Bulk and on Metal Surface

Figure 8.26 show the morphology of the $CaCO_3$ crystals deposited on the active metal surface when co-precipitated with PbS. The $CaCO_3$ crystals were formed using the brine composition in Table 8.6. The $CaCO_3$ crystals are distorted, with most crystals appearing to be quite thin, and projecting outwards, some crystals also bunched together giving a flower petal appearance. Figure 8.27 shows the EDAX data showing that $CaCO_3$ crystals were formed on the metal surface. Figure 8.28 show the morphology of the crystals formed in the bulk solution and the crystals shown here are fully formed crystals mix of $CaCO_3$ and $PbCO_3$. The $CaCO_3$ crystals formed are rhombohedral shaped, and the EDAX data shows that they are $CaCO_3$. In the bulk solution, PbS was spontaneously formed as the brines were mixed together. The scales formed appear as a brown gritty mix in the bulk solution. The low solubility of the PbS may have enhanced the full formation of the crystals by a heterogeneous precipitation process. This is the only experiment in this study where fully formed crystals were formed in the bulk solution.

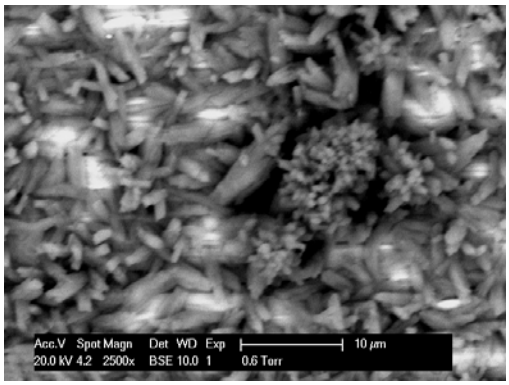

Element	Weight%	Atomic%
C	15.53	30.02
O	30.36	44.07
S	0.4	0.29
Ca	19.2	11.13
Cr	6.53	2.92
Mn	0.71	0.3
Fe	23.99	9.98
Ni	3.28	1.3
Totals	100	

Figures 8.25-8.26 Morphology and the EDAX data of $CaCO_3$ crystals co-precipitated with PbS on metal surface at 24hrs.

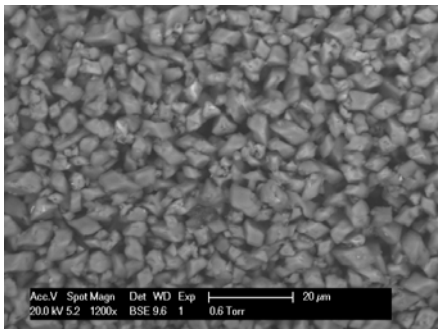

Element	Weight%	Atomic%
C	11.09	23.49
O	36.12	57.45
Ca	24.57	15.6
Pb	28.21	3.46
Totals	100	

Figures 8.27-8.28 Morphology and the EDAX data of crystals co-precipitated with PbS in bulk solution at 24hrs.

8.4.7 $CaCO_3$ Crystal Formation in the Presence of Pb^{2+} + Zn^{2+} (MVT)

Figure 8.30 shows the morphology of crystals deposited on the active metal surface when formed in the presence of Pb^{2+} + Zn^{2+}. The crystals were formed using the brine compositions in Table 8.7. Overall, less deposit was formed on the metal surface and the deposits formed consist of a cluster of spheres with globular external texture like a *bunch of grapes*. The EDAX data in Figure 8.31 shows that the deposit may possibly be $ZnCO_3$. Figure 8.32 show the morphology of deposits formed in the bulk solution in the presence of Pb^{2+} + Zn^{2+}, the deposits appear like a grit or crust. The EDAX data in Figure 8.33 indicates that $ZnCO_3$ is the principal deposit. This data also shows trace amount of Pb. The deposits formed on the metal surface and in the bulk solution in the presence of Pb and Zn are similar to the deposits formed in the presence of Zn only. $ZnCO_3$ is the principal product formed in both cases and the area of preference (i.e metal surface or bulk) and amount of deposit are also similar.

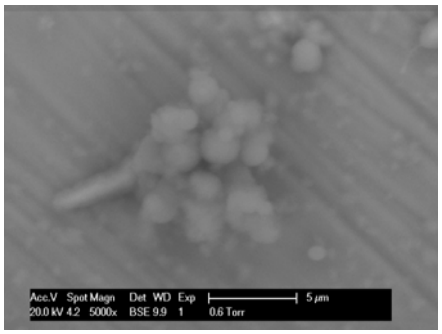

Element	Weight%	Atomic%
C	10.17	20.5
O	38.97	58.95
Ca	2.34	1.41
Cr	3.65	1.7
Fe	12.11	5.25
Ni	1.61	0.66
Zn	31.15	11.53
Totals	100	

Figures 8.29-8.30 ESEM image and the EDAX data of deposits formed on the metal surface in the presence of Pb and Zn at 24hrs.

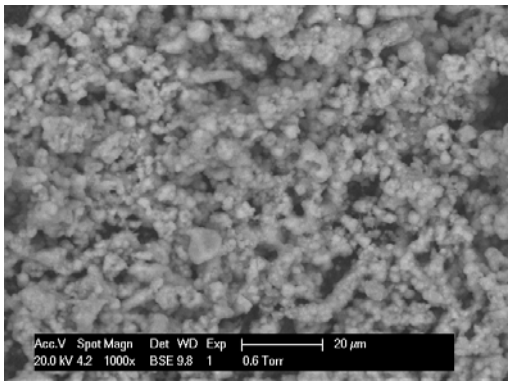

Element	Weight%	Atomic%
O	37.36	65.78
Cl	22.32	17.73
K	0.86	0.62
Ca	3.32	2.33
Zn	29.22	12.59
Pb	6.92	0.94
Totals	100	

Figures 8.31-8.32 ESEM image and the EDAX data of deposits formed in the bulk solution in the presence of Pb and Zn at 24hrs.

8.4.8 $CaCO_3$ Co-precipitation with ZnS + PbS in Bulk and on Metal Surface (MVT)

Figure 8.36 shows the morphology of the $CaCO_3$ crystals deposited on the active metal surface when co-precipitated with ZnS and PbS. The $CaCO_3$ crystals were formed using the brine composition in Table 8.8. Figure 8.36 shows that that are fewer crystals formed on the metal surface than in the base case. The $CaCO_3$ crystals formed on the metal surface are elongated, thin, pine leaf structures. The EDAX data indicates that $CaCO_3$ crystals are formed on the metal surface. [Fe], [Cr], [Ni] representing the stainless steel is also quantified as is [S] from the H_2S in the EDAX data. Figure 8.36 shows the morphology of the $CaCO_3$ crystals formed in the bulk solution, These crystals are in a scale mix of ZnS and $CaCO_3$ in a mass of cloudy crystals. The scale mix appears as a white flocculent precipitate over the $CaCO_3$ crystals. EDAX data indicates that $CaCO_3$ crystals were formed in the bulk solution.

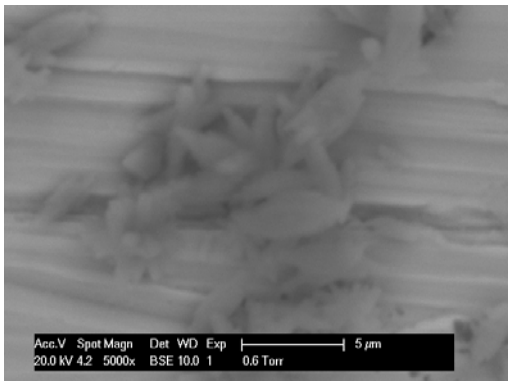

Element	Weight%	Atomic%
C	18.12	35.35
O	25.81	37.8
Si	0	0
S	0.45	0.33
Ca	18.37	10.74
Cr	7.63	3.44
Fe	25.59	10.74
Ni	4.03	1.61
Totals	100	

Figures 8.33-8.34 Morphology and the EDAX data of $CaCO_3$ crystals co-precipitated with ZnS PbS on the metal surface at 24hrs.

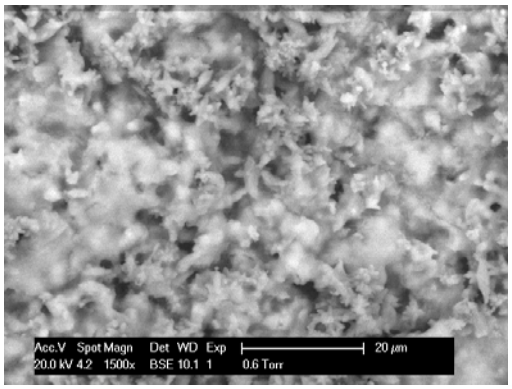

Element	Weight%	Atomic%
C	18.18	27.12
O	54	60.48
Cl	3.3	1.67
Ca	23.16	10.36
Zn	1.35	0.37
Totals	100	

Figures 8.35-8.36 Morphology and the EDAX data of $CaCO_3$ crystals co-precipitated with ZnS PbS in bulk solution at 24hrs.

8.5 $CaCO_3$ Co-precipitation with Sulphide Scales in the Presence of Scale Inhibitor

Experiments were performed with initial PPCA concentrations of 3ppm, 1ppm, 0.5ppm in the mixed brines. A base case experiment with $CaCO_3$ using the brine composition in Table 8.1 indicated that at 3ppm no $CaCO_3$ was formed in the brine or on the surface of the metal. However, as the [SI] was reduced tiny spots $CaCO_3$ crystals formed at 1ppm but they appeared unsual probably due to the [SI], Figures 8.37 and 8.38 shows the crystals formed on the metal surface in the presence of 1ppm PPCA and the EDAX quantification for the scale. When 0.5ppm of SI was present, the $CaCO_3$ crystals appear to be in the nucleaction stage and not in the same

quantity as in the base case, Figures 8.39 and 8.40 show the ESEM image and the corresponding EDAX data indicating $CaCO_3$ crystals in an early formation stage.

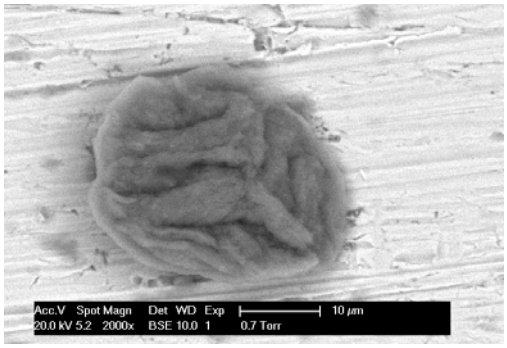

Element	Weight%	Weight%	Atomic%
C	20.65	2.55	34.56
O	37.46	2.29	47.08
Mg	1.15	0.2	0.95
Cl	0.43	0.13	0.24
Ca	18.14	0.86	9.1
Cr	4.59	0.35	1.77
Fe	15.43	0.82	5.55
Ni	2.14	0.33	0.73
Totals	100		

Figures 8.37-8.38 Morphology and the EDAX data of $CaCO_3$ formed on the metal surface in the presence of 1ppm PPCA at 24hrs.

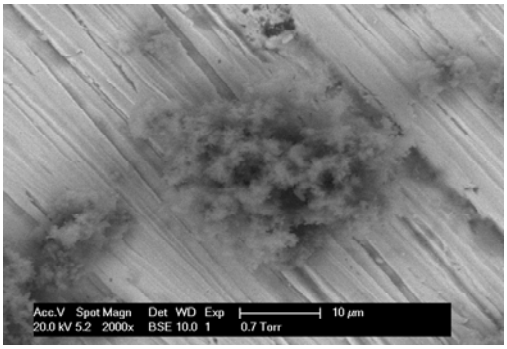

Element	Weight%	Weight%	Atomic%
C	11.85	2.17	23.62
O	31.68	3.9	47.41
Ca	27.5	1.72	16.43
Cr	5.7	0.49	2.63
Mn	0.97	0.28	0.42
Fe	19.39	1.3	8.31
Ni	2.92	0.44	1.19
Totals	100		

Figures 8.39-8.40 Morphology and the EDAX data of $CaCO_3$ formed on the metal surface in the presence of 0.5ppm PPCA at 24hrs.

8.5.1 $CaCO_3$ Co-precipitation with ZnS in the Presence of Scale Inhibitor

There were no $CaCO_3$crystals formed on the metal surface when 3ppm of the SI was applied. However, the $CaCO_3$ crystals formed in the bulk solution were similar to the crystals formed in the absence of the scale inhibitor. Figure 8.41 show the morphology of the $CaCO_3$ crystals deposited on the active metal surface when co-precipitated with ZnS, in the presence of 1ppm PPCA. Figure 8.42 show the $CaCO_3$ crystals at 0.5ppm which is very similar to the crystals formed without the SI. The $CaCO_3$ crystals formed in the bulk at 1ppm and 0.5ppm were similar to those formed in the absence of the scale inhibitor. The results demostrate that the SI was able

to stop the deposition of $CaCO_3$ scale on the metal surface, however the bulk precipitation was unaffected.

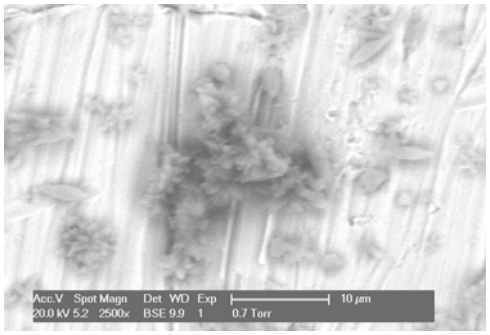

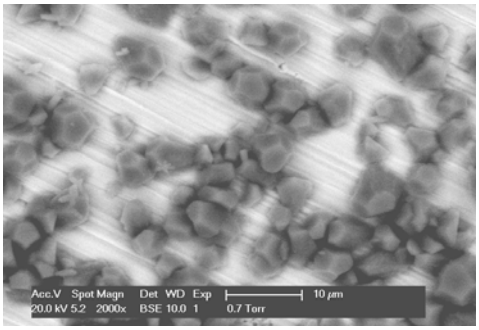

Figures 8.41-8.42 $CaCO_3$ crystals co-precipitated with ZnS in the presence of 1ppm and 0.5 ppm PPCA on the metal surface.

8.5.2 $CaCO_3$ Co-precipitation with PbS in the Presence of Scale Inhibitor

Again no $CaCO_3$ crystals were formed on the metal surface when 3ppm of the SI was applied. However the $CaCO_3$ crystals formed in the bulk solution were similar to those formed in the absence of the scale inhibitor. Figure 8.43 shows the morphology of the $CaCO_3$ crystals deposited on the active metal surface when co-precipitated with PbS, in the presence of 1ppm PPCA. Figure 8.44 shows the $CaCO_3$ crystals at 0.5ppm which are very similar to those formed without the SI. The $CaCO_3$ crystals formed in the bulk at 1ppm and 0.5ppm were similar to those formed in the absence of the scale inhibitor. The results, which are quite similar to the ZnS results, demostrate that the SI was able to stop the deposition of $CaCO_3$ scale on the metal surface, however the bulk precipitation was much less affected.

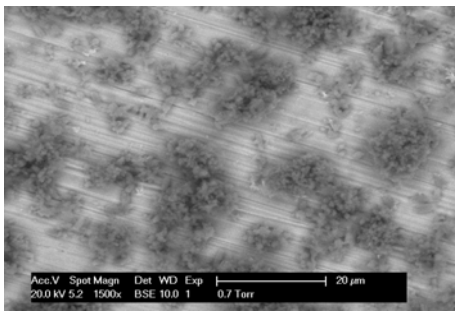

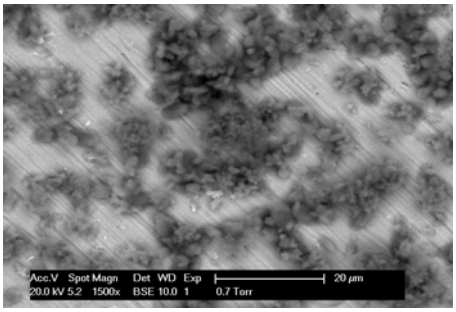

Figures 8.43-8.44 $CaCO_3$ crystals co-precipitated with PbS in the presence of 1ppm and 0.5 ppm PPCA on the metal surface.

8.5.3 $CaCO_3$ Co-precipitation with ZnS + PbS in the Presence of Scale Inhibitor

Figures 8.45 and 8.46 show the morphology of the $CaCO_3$ crystals deposited on the active metal surface when co-precipitated with ZnS and PbS, in the presence of 3ppm and 0.5ppm PPCA. Unlike the prevous PbS and ZnS cases described above, some of the $CaCO_3$ crystals deposited on the active metal surface. These $CaCO_3$ crystals were few and distorted and they also appeared to form clusters as thin spikes. The crystals for the 1ppm and 0.5ppm SI cases appeared to be similar to the $CaCO_3$ crystals formed in the 3ppm case but with more clusters of $CaCO_3$ crystals. The $CaCO_3$ crystals deposited in the bulk solution were similar to those deposited in the absence of the SI.

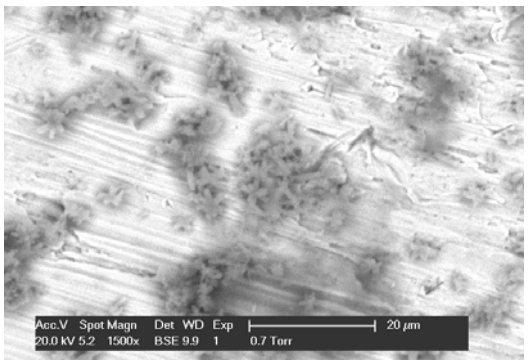

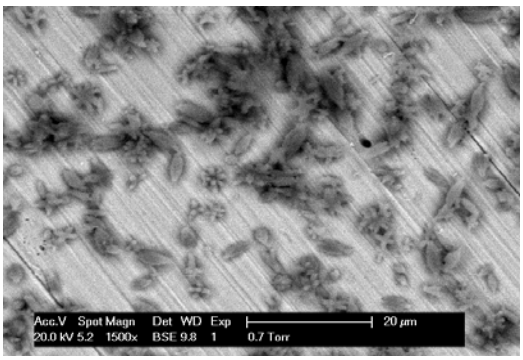

Figure 8.45-8.46 $CaCO_3$ crystals co-precipitated with ZnS and PbS in the presence of 3 ppm and 0.5ppm PPCA on the metal surface

8.6 Summary and Conclusions

Results are presented here showing the deposition of $CaCO_3$ crystals both in bulk and on a stainless steel metal surface. This is similar to the field conditions where $CaCO_3$ scales are deposited on metal surfaces as well as in the bulk solution. Sulphide scales have different effects on the type and medium (surface or bulk) for $CaCO_3$ scale deposition. Table 8.9 presents a summary of the data. Crystal habits were found to be sensitive to changes in the brine chemistry. The impact of sulphide scale co-precipitating with $CaCO_3$ scales has not been reported previously and this study shows the impact both on surface and bulk deposition. The effect of co-precipitated sulphide scales on the $CaCO_3$ crystals was also investigated, again in bulk solution and on metal surfaces. When $CaCO_3$ is co-precipitated with ZnS, less $CaCO_3$ crystals are deposited on the metal surface, while more $CaCO_3$ crystals are mixed with the ZnS flocculent precipitate. However, when $CaCO_3$ is co-precipitated with PbS, the $CaCO_3$ deposited on the metal surface shows distorted crystal forms (probably a polymorph) of those deposited in the base case. The corresponding crystals formed in the bulk, however, were a mix of fully formed $CaCO_3$ with $PbCO_3$ crystals. This suggests that the PbS-$CaCO_3$ scaling system may be more difficult to inhibit in the bulk than the ZnS-$CaCO_3$ scaling system. The precipitation of $CaCO_3$ crystals in the presence of [SI] demostrate that "MIC" levels appropriate for the metal surface and the bulk solution are quite different. However, in the presence of sulpides scales the bulk precipitaion is less affected than the metal surface preipitation. This study will help in designing better scale treatment programs as more information becomes available as to what precise scales occur, where and in what form these mixed scales occur. Such data will also help in determining the type of scale inhibitors to treat the different mixed sulphide/carbonate scaling scenarios.

Table 8.9 Summary of $CaCO_3$ Morphology Results

	SI	**$CaCO_3$ Crystal Morphology on Metal surface**	**Comment**
Blank $CaCO_3$	NO	Large amount of classic $CaCO_3$ trigonal rhombohedral crystals structure.	Bunched up crystal in the bulk solution
$CaCO_3$-[H_2S]	NO	Spiky elongated crystals – fewer crystals on metal surface.	Fewer crystals deposited on metal surface-
$CaCO_3$-[Pb]	NO	No change to $CaCO_3$ crystal structure-fewer crystals on metal surface	Some crystals appear to bunch up
$CaCO_3$-PbS	NO	Significant distortion to $CaCO_3$ crystal structure to elongated Orthorhombic structure-few crystal on metal surface	$PbCO_3$ crystals formed in the bulk and probably some $CaCO_3$ crystals
$CaCO_3$-[Zn]	NO	No deposit of $CaCO_3$ crystals-probable formation of $ZnCO_3$ crystal observed on metal surface	Mixed crystals of $CaCO_3$ and $ZnCO_3$
$CaCO_3$-ZnS	NO	Fewer $CaCO_3$ crystals on metal surface	Elongated crystals in ZnS flocculent formed in bulk solution

$CaCO_3$-[Pb]+[Zn]	NO	No $CaCO_3$ crystals on metal surface	Gritty mix of $CaCO_3$ and $ZnCO_3$ in the bulk solution
$CaCO_3$-PbS+ZnS	NO	Spiky elongated crystals – fewer crystals on metal surface.	Rhombohedral $CaCO_3$ crystal to Four pointed star structure
$CaCO_3$-Blank	Yes	distorted crystals in <1ppm (SI) early stages of	Tiny fine crystals on metal surface
$CaCO_3$-[PbS]	Yes	1ppm caused bunching up of crystals on metal surface	Distortion of $CaCO_3$ crystals on metal surface.
$CaCO_3$-ZnS	Yes	1ppm caused distortion of $CaCO_3$ crystals	Elongation of crystals into spike like crystals
$CaCO_3$-ZnS+PbS	Yes	At 3ppm $CaCO_3$ crystals was formed on the metal surface	Distorted $CaCO_3$ crystals on metal surface.

Chapter 9 Mixed Sulphide (ZnS and PbS) Formation, Deposition and Inhibition.

9.1 Introduction

Mixed zinc/lead sulphide scale appears to be common in HT/HP wells (Jordan *et al.* 2000) although research into the formation mechanisms of this mixed scale has been limited. The potential sources of Pb and Zn scaling cations have been discussed in Chapter1. This chapter looks at the formation mechanism, and the effects of a polymer SI on the formation of these mixed scales. The study tries to elucidate how these sulphides form and on the effect of scale inhibitors in preventing their formation. Before studying mixed scales of PbS and ZnS, each of these scales are first studied on their own. The scales PbS and ZnS were studied both in DW and in a moderate brine system.

9.2 Experimental details

The PbS scale experiments in DW were carried out at 20°C using the modified static bottle test method described in Chapter 3. The PbS is precipitated spontaneously by mixing solution A containing Pb^{2+} made by dissolving Lead Acetate [$Pb(CH_3COO)_2.3H_20$] in DW, (Lead Acetate was selected because of its solubility and stability) and solution B containing sodium sulphide ($Na_2S.3H_2O$) solution which was made in same way as the lead acetate. (Compositions are given in Table 3.4). The solutions are mixed in a 50:50 v/v ratio. The ZnS scale experiments in DW made were also carried out at 20°C using the same procedure. ZnS is precipitated spontaneously by mixing solution A containing Zn^{2+} made by dissolving Zinc Acetate [$Zn(CH_3COO_2)_2$] in DW, and solution B containing sodium sulphide ($Na_2S.3H_2O$). After mixing, the solutions are monitored very regularly to note any change in colour, deposits and turbidity. The analysis was performed using a spectrophotometer and ICP. The brine solutions were made up using the Nelson formation water and North Sea water (see Table 3.4 for brine composition). The deposition/formation of PbS was studied and its effects on $BaSO_4$ formation was also examined. A modified version of this experiment was also performed which included [$Pb(CH_3COO)_2.3H_2O$] and NaS. In this experiment a 50:50 mix of these solutions was selected to give a moderately severe PbS scaling regime. The mixed scales were prepared by the addition

of both Pb and Zn Acetate to the seawater and the NaS to the formation water. The brines are filtered through a 0.45µm filter paper and further degassed to minimize the presence of oxygen and therefore reduce the potential of oxidative (free radical) degradation. The resulting brine is a clear solution which when mixed produced scaling brines $BaSO_4$ and PbS or ZnS or a combination of both PbS and ZnS corresponding to the mixing case.

9.3 PbS formation, deposition and inhibition in DW

9.3.1 Effects of PbS Concentration on Formation and Inhibition

Figures 9.1 to 9.8 shows the static bottle test visual results at 2 hours and 22hrs after mixing PbS in DW at various scale inhibitor concentrations. The PbS concentration is 50ppm in the mix. (i.e. a 50:50 mix of a 100ppm solution of Lead acetate and a 100ppm solution of sodium sulphide). The reaction was instantaneous and brown coloured lead sulphide was formed immediately. Figures 9.1 and 9.2 show this experiment 2hours and 22hrs after mixing with PPCA, at low [SI] of 5, 10 &50ppm respectively. The visual results indicate the formation of PbS across the [SI] range including the blank (untreated samples). At 22hours there is deposition of PbS at the base of the sample bottles across the range including the blank, which indicates that the [SI] could not prevent the formation of PbS. Figures 9.3 and 9.4 show similar result using DETPMP. Figures 9.5 to 9.8 show the results of increased [PPCA] from 50ppm to 2000ppm, with inhibition occurring at 2000ppm. Figure 9.9 shows the fate of the [Pb^{2+}] along with the visual results when [Pb] concentration in mix was reduced from 50ppm to 25ppm. The figure indicates that PbS deposition does not occur at 3000-500ppm of PPCA scale inhibitor, compared to the previous experiment shown in Figures 9.5 to 9.8. Figure 9.10 shows the same result using DETPMP where the PbS is held in solution and the deposition of PbS that occurred with the 50ppm mix did not occur. However the solution changed from a clear solution to a light brown colour for the SI tested. The static inhibition efficiency and visual results are shown when the PbS concentration in the mix was reduced from 50ppm to 25ppm. The PbS is held in solution and the deposition of PbS that occurred with the 50ppm in the mix did not occur. However the solution changed from a clear solution to a light brown colour and this slight brownish coloration may be indicative of the formation of Pb(OH), or PbO. It was noted in the visual results that

PPCA was more effective at reducing PbS deposition and as a consequence PPCA was used in further PbS studies.

Figure 9.1 PbS in DW with [PPCA] at 2hours

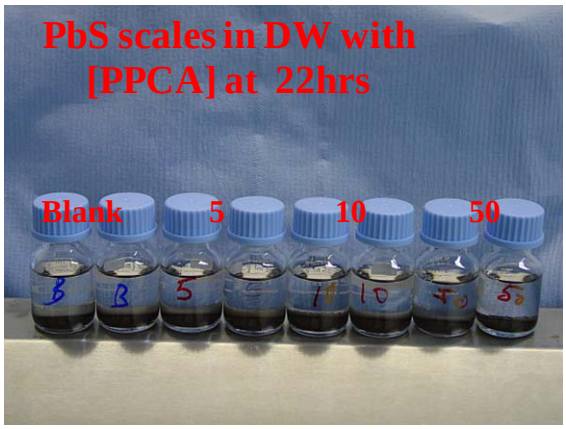

Figure 9.2 22hours of figure 9.1

Figure 9.3 PbS in DW with [DETPMP] at 2hours

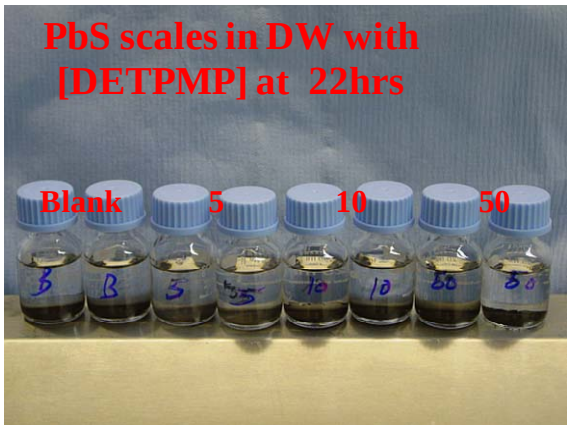

Figure 9.4 22hours of figure 9.3

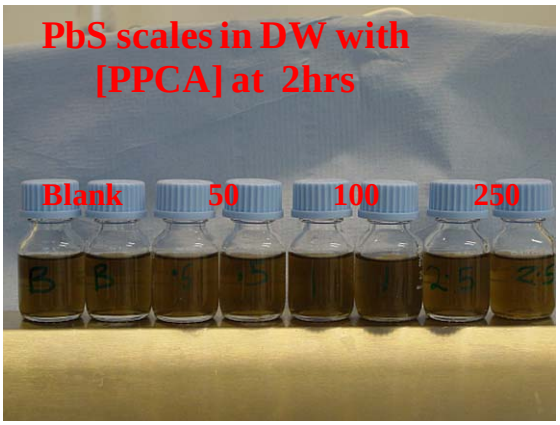

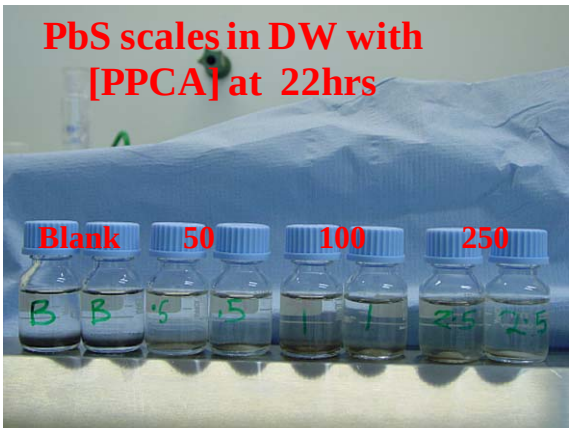

Figure 9.5 PbS in DW with [PPCA] at 2hours **Figure 9.6** 22hours of figure 9.5

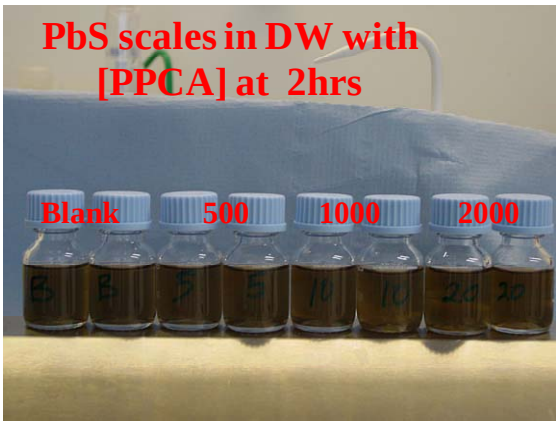

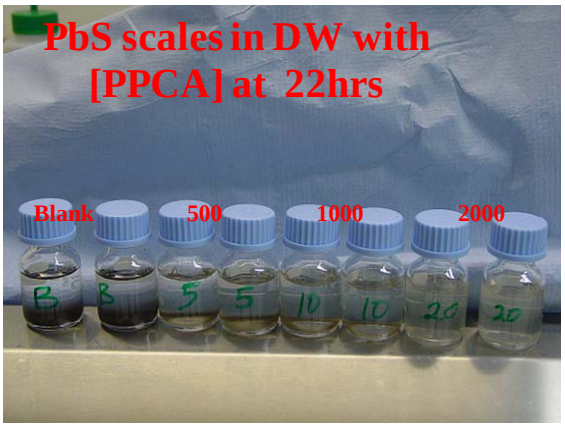

Figure 9.7 PbS in DW with [PPCA] at 2hours **Figure 9.8** 22hours of figure 9.7

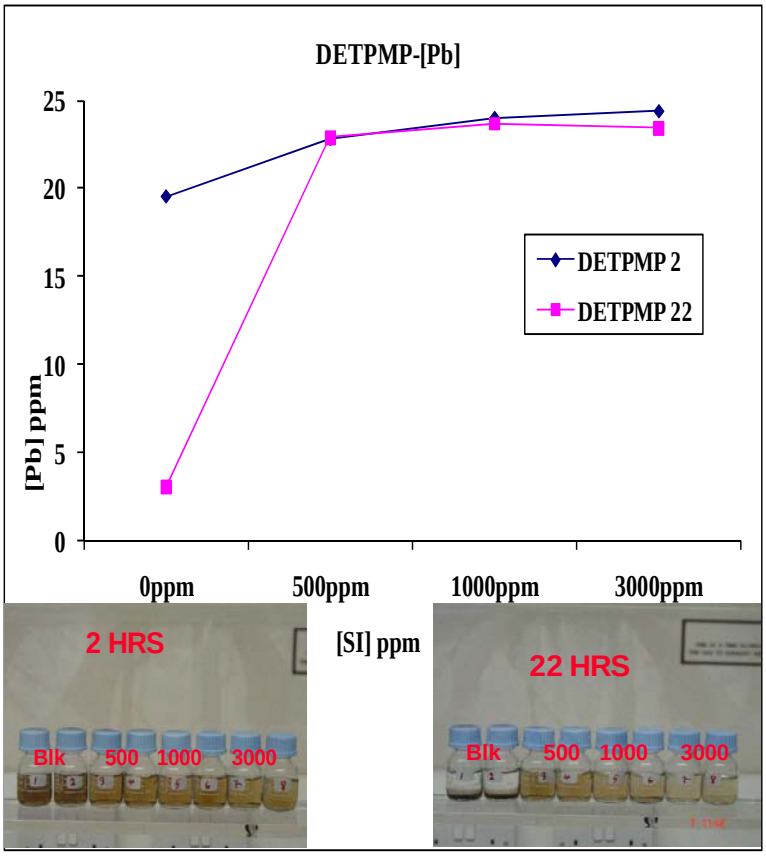

Figure 9.9 Fate of [Pb^{2+}] in PbS in DW with [DETPMP] at 2 & 22hours with the Visual results.

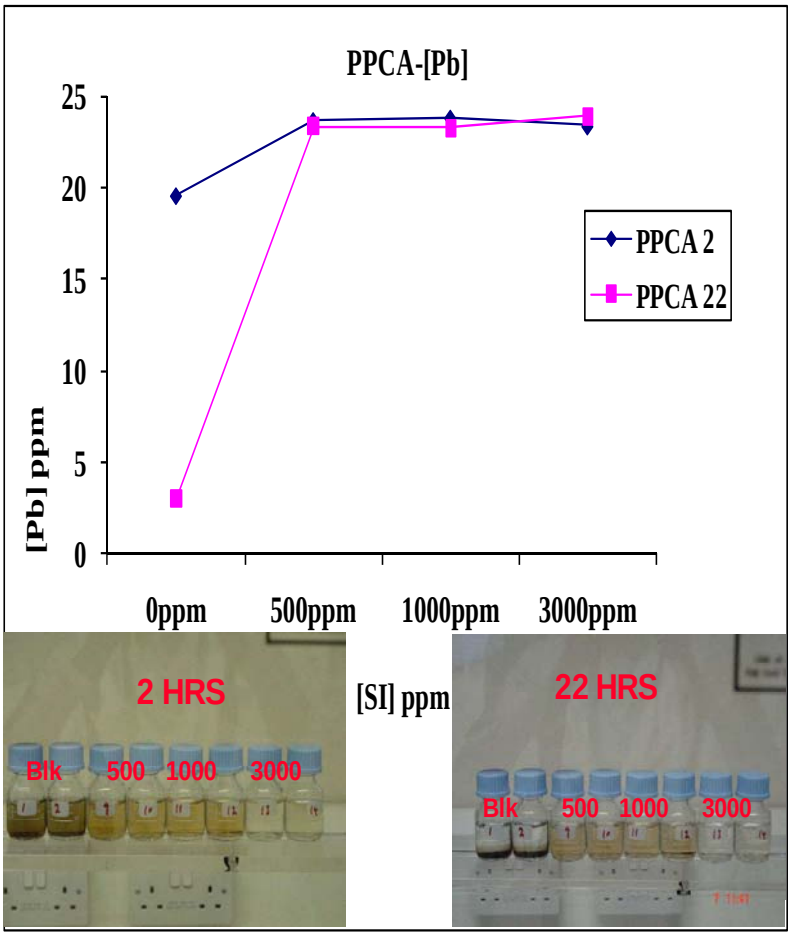

Figure 9.10 Fate of [Pb^{2+}] in PbS in DW with [PPCA] at 2 & 22hours with the Visual results

During the course of the study, the definition of "inhibition" was changed: if at 22hours after mixing there was no deposition, then it was considered inhibited even though it may appear to be coloured brown. This change of definition allowed the effective concentration of SI to be reduced from 3000 to 50ppm without causing deposition, as shown in Figures 9.11 to 9.22. This shows that both PPCA and DETPMP are capable of stopping the deposition of PbS. Figure 9.23 shows the ESEM image of PbS in DW, the PbS is like flakes of dried mud and the EDAX quantification indicate the presence of [Pb] and [S]. The study shows that [Pb] concentration has a significant impact on the formation and inhibition of PbS.

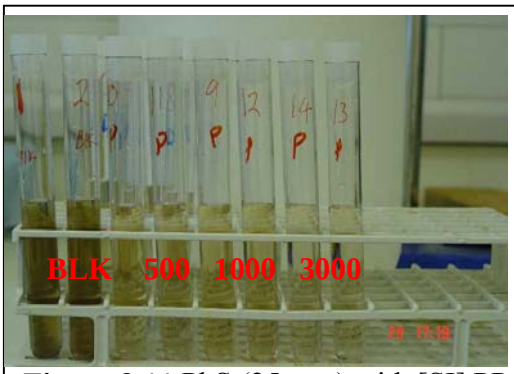

Figure 9.11 PbS (25ppm) with [SI] PPCA 2hr

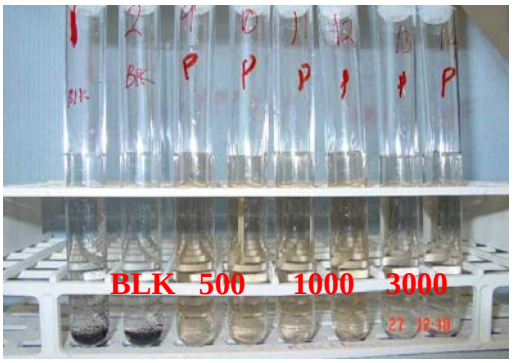

Figure 9.12 22 hrs of Figure 9.11

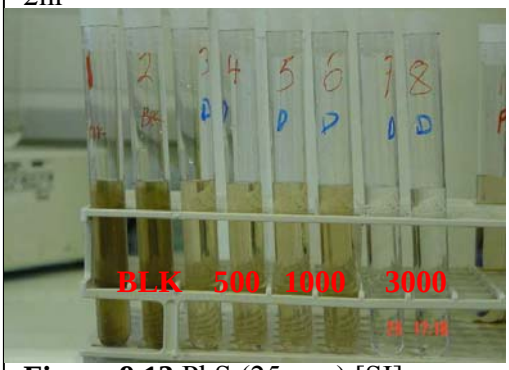

Figure 9.13 PbS (25ppm) [SI] DETPMP 2hr

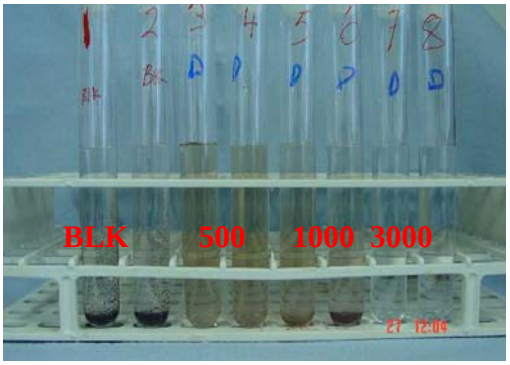

Figure 9.14 22 hrs of Figure 9.13

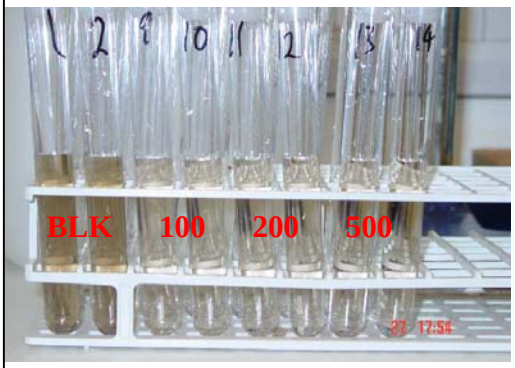

Figure 9.15 PbS (25ppm) [SI] DETPMP 2hr

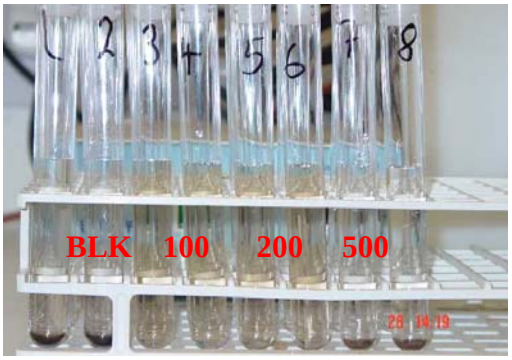

Figure 9.16 22 hrs of Figure 9.15

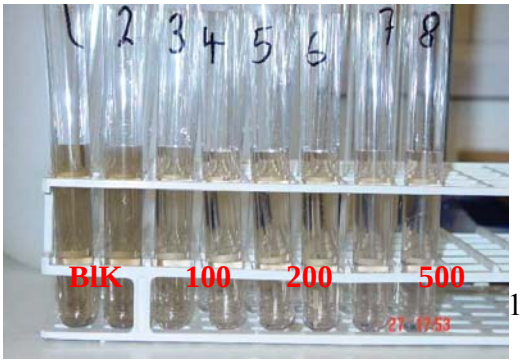

Figure 9.17 PbS (25ppm) with [SI] PPCA 2hr

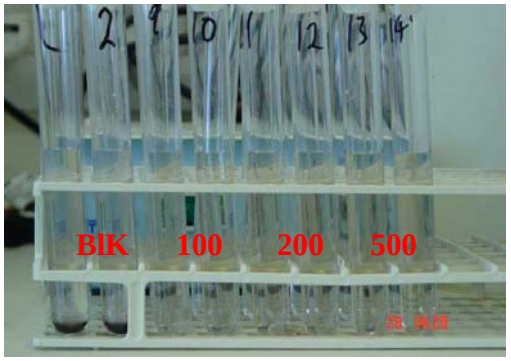

Figure 9.18 22 hrs of Figure 9.17

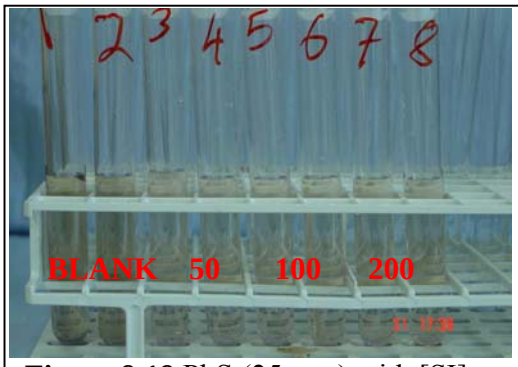

Figure 9.19 PbS (25ppm) with [SI] PPCA 2hr

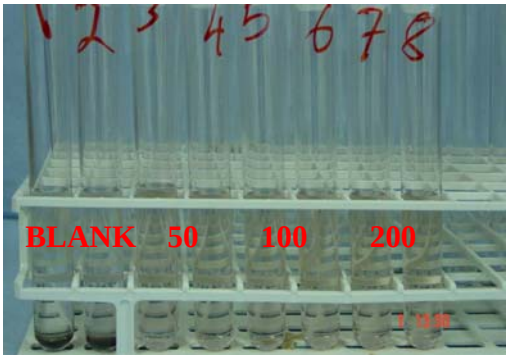

Figure 9.20 22 hrs of Figure 9.20

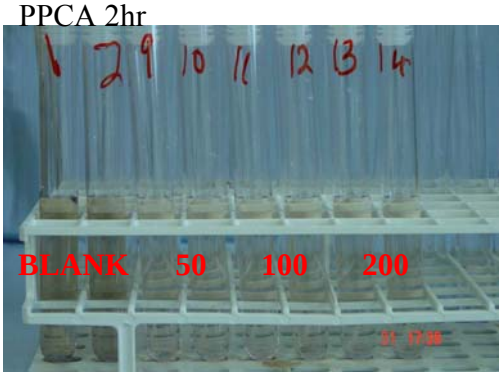

Figure 9.21 PbS (25ppm) with [SI] DETPMP 2hr

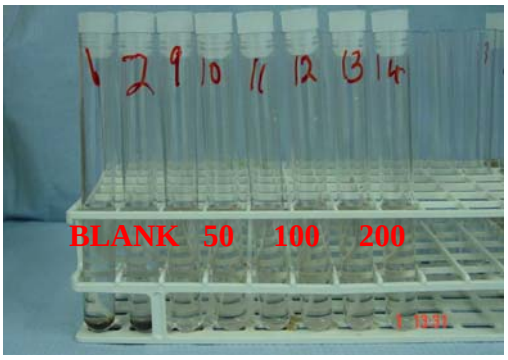

Figure 9.22 22 hrs of Figure 9.22

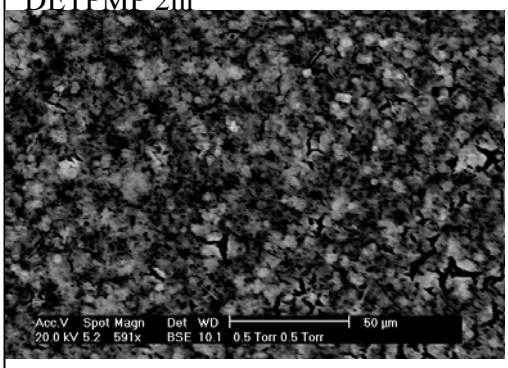

Figure 9.23 ESEM image of PbS in DW

Element	Wt %	At %
C K	26.43	70.05
O K	8.8	17.52
S K	2.94	2.92
PbL	61.82	9.5
Total	100	100

Figure 9.24 EDAX of Figure 9.23

9.4 ZnS Formation, Deposition and Inhibition in DW

Zinc Sulphide unlike PbS forms a white flocculent precipitate that settles over time but has a slower deposition time (about 24hrs in DW) than FeS and PbS). The Zn^{2+} concentration also affects the formation and deposition of ZnS similar to PbS in DW. Figures 9.25 to 9.28 shows the formation of ZnS in DW at 5000ppm (Figures 9.25-9.26) and 250ppm (Figures 9.27-9.28) respectively. The ZnS formed in DW from the 5000ppm solution appears as a white floculent precipitate, and the SI could not prevent its formation. Figure 9.25 indicates that PPCA and DETPMP of 3000ppm did not prevent the formation of ZnS. However when the ZnS concentration was reduced to 250ppm, Figure 9.26 and 9.27 indicate that at 2 and 22hours, ZnS was prevented from precipitating at 3000ppm SI. The blank solution shows immediate deposition of white ZnS as the two solutions are mixed. The 1000ppm sample shows that the ZnS has been held in solution at 2 hours. Although the white precipitate was formed just at 2hours, it deposited on the bottom of the testube at 22hours, thus suggesting that the "MIC" is between 1000-3000ppm. The ESEM image in Figure 9.28 shows the untreated (blank) ZnS as a dried sludge, while Figure 9.29 shows the EDAX quantification of ZnS indicating the presence of [Zn] and [S]. Figure 9.30 shows the ESEM image of the treated ZnS with 1000ppm of PPCA SI. The figures shows that the sludge has reduced but is still visible. The EDAX quantification shows the presence of Zinc and sulphur, indicating ZnS. The presence of phosphorus is also indicated in the EDAX quantification and this is probably from the SI. Figure 9.30 shows the absorbance results for 50ppm indicating that ZnS can be detected by turbidity. The use of turbidity to determine the formation of scales at low concentrations in the industry is quite common. In Figure 9.30, the visual diference between the untreated and treated samples is dificult to determine, unless a turbidty meter is used, in this case a spectophotometer is used to detemine the turbidity.

Figure 9.25 ZnS (5000pm) with varying [SI] at 22hrs showing floculent white precipitate.

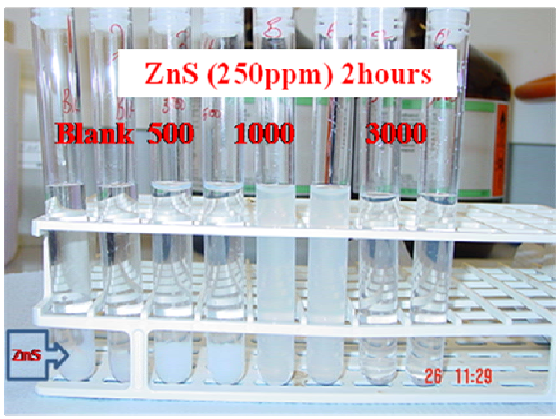

Figure 9.26-2.7 ZnS (250pm) with Varying [PPCA] at 2 & 22hrs showing floculent white precipitate

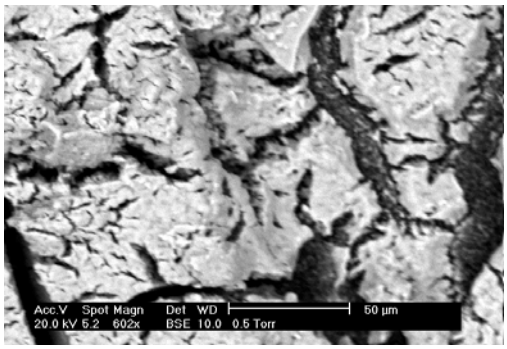

Element	Wt %	At %
C K	19.46	41.25
O K	14.48	23.05
S K	24.6	19.54
ZnK	41.46	16.15
Total	100	100

Figure 9.28-2.9 ESEM image and EDAX quantification of ZnS

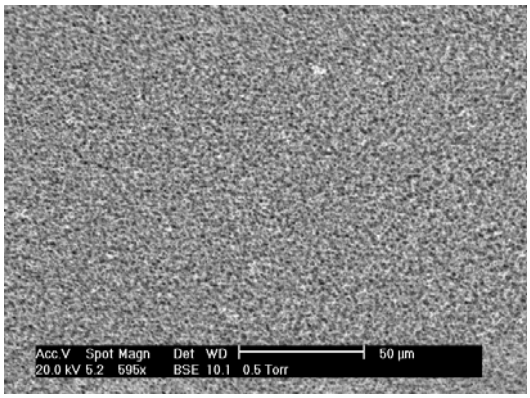

Element	Wt %	At %
C K	5.13	16.32
O K	5.86	13.99
P K	1.37	1.7
S K	27.56	32.86
ZnK	60.08	35.13
Total	100	100

Figure 9.28-2.9 ESEM image and EDAX quantification of ZnS with 1000ppm of PPCA

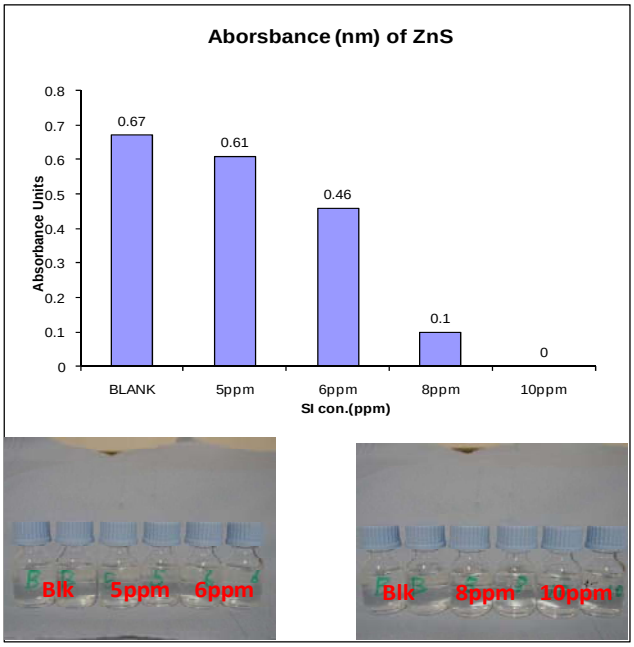

Figure 9.30 Absorbance data and visual results for ZnS (50ppm)

9.5 Mixed Scaling (PbS and ZnS) in DW

The purpose of this study is to understand the mechanism, rate and preference of formation/deposition of both ZnS and PbS. We know from field reports and literature that PbS and ZnS very frequently occur together, with PbS being the dominant sulphide. This study tries to elucidate how these sulphides combine and the effects it has on scale inhibitors during treatment or prevention.

The first experiment was performed in order to study the mixed scales in equal concentrations (100ppm Lead acetate and 100ppm Zinc acetate were mixed with Excess Sodium Sulphide) in Distilled water and the effects of high [SI] is shown in Figures 9.31 and 9.32. The results shown indicate that mixed scales of ZnS and PbS can be inhibited (although at [SI] levels which are probably too high). The rate of precipitation was very fast and as seen in Figure 9.30 which shows the blank dropping off, while the treated samples are held in solution. The precipitate was unlike the white fine powdery ZnS or the dark brown grainy PbS. This deposit was a rather lumpy, black mass, as shown in Figure 9.32. The result from the previous experiment led us to

redesign the subsequent experiments which tried to determine the "MIC" for the mixed solution of PbS and ZnS; lower ranges of [SI] were selected [10], [25], [50] ppm as shown in Figures 9.33 and 9.34. The results obtained from this study suggest that a mixed scaling system of PbS and ZnS is easier to inhibit than a lone case of either PbS or ZnS. The increased rate of precipitation for the untreated (blank) case is also noted. Figure 9.35 shows the ESEM image of the untreated mixed scale, which is a cross between the ZnS sludge and the grainy PbS. The EDAX quantification indicates the presence of [Pb] [S] and [Zn].

This implies that in field cases were both scales occur, the mixed scales will be easier to control than if only one of the scales occur. The exact mechanism is still unknown but the amorphous nature of ZnS and the low solubility of PbS appears to combine in a way that makes 50ppm able to hold the ions in solution, preventing the deposition of the mixed scales. To my knowledge this increased inhibition occurring with mixed scales, than with individual sulphide scale has not been reported before. The texture of the untreated mixed scale appears as a lumpy mass as seem in figure 9.31 which shows the mixed scales at 2hours after mix, and at 22hours shown in figure 9.32 compared to the flat dried mud of PbS or powdery look of ZnS.

The mixed scales have combined to form a sulphide complex which is easier for the scale inhibitor to hold in solution. One theory supplied (Peters 1985) is that the [SI] reduces the nucleating rate, but promoted the aggregation rate of larger ZnS particles thus eliminating a step off ZnS formation this was observed working with several complexing agents for sulphide precipitation (citrate, phosphate and EDTA). Another theory provided (Patrick 1998) was that the PbS sorbed unto the surface of ZnS particles preventing them from dropping out of the solution. This mechanism requires activation of the ZnS nucleating surface and two mechanisms have been proposed: (1) the formation of PbS directly on the surface by Pb ↔ Zn exchange (Houot 1992) and (2) the development of Zn—O—Pb species which are the product of complex interactions between $Pb(OH)^{+}$ and the ZnS surface (Bernasconi 1983). In either case a catalyst is needed to activate the ZnS in order to hold the PbS in solution, and this may be provided by the SI. Furthermore a certain amount is needed to sufficiently trigger this reaction, the untreated

samples with the lower [SI] (25ppm,10ppm) samples proves that without the [SI] at an MIC deposition will occur.

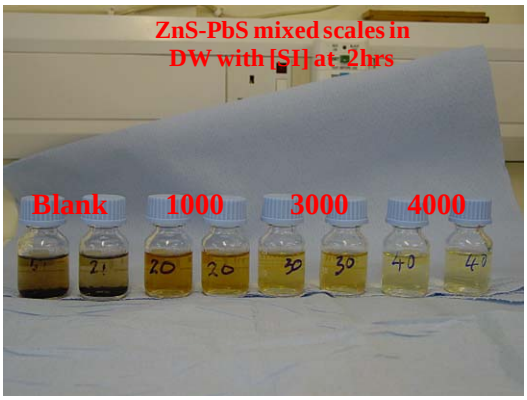

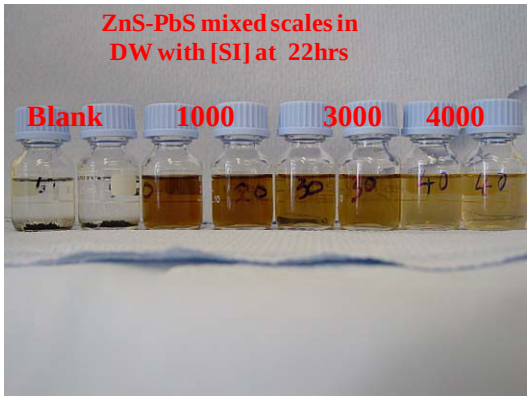

Figure 9.31 mixed scale with varying [SI] at 2hrs. **Figure 9.32** 22 hours of figure 9.31

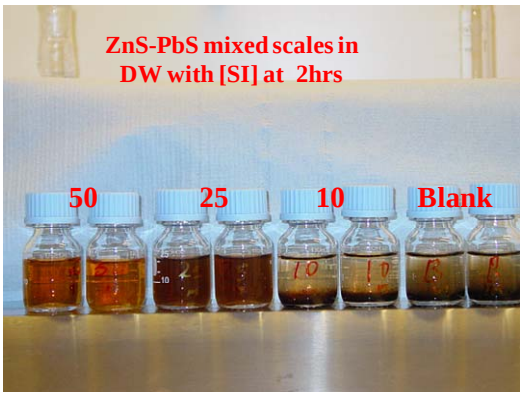

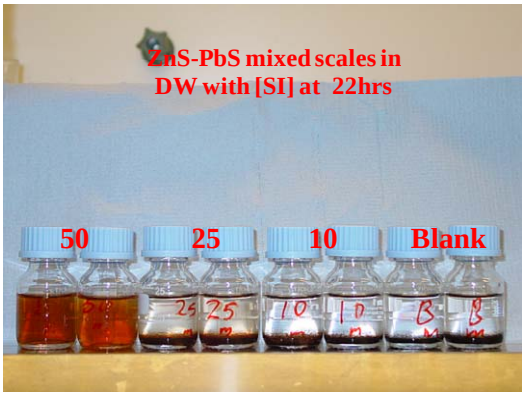

Figure 9.33 mixed scale with reduced [SI] at 2 hrs. **Figure 9.34** 22 hours of figure 9.33

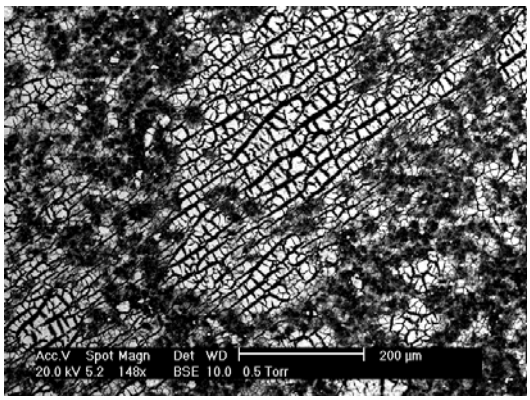

Element	Wt %	At %
C K	28.48	72.28
O K	5.42	10.33
SrL	1.41	0.49
S K	6.53	6.21
ZnK	6.67	3.11
PbL	51.49	7.58
Total	100	100

Figure 9.35-36 ESEM image and EDAX quantification of ZnS-PbS mixed scale (blank)

9.6 Mixed Scaling (PbS and ZnS) in Brine

The formation of mixed sulphide (ZnS and PbS) in a $BaSO_4$ forming brine system has been discussed in details in Chapter 2 and Chapter 6 and CaCO3 has also been studied in Chapter 7. The combination of PbS and ZnS may be formed along with $BaSO_4$ when two incompatible brines commingle and thus lead to the formation of mixed PbS, ZnS and $BaSO_4$ scales. In this section, results are shown on the fate of [Pb] and [Zn] along with the visual observations is presented here. These 3 scales will interact and, although the system is rather complex, some interesting features and observations emerge. Forties formation water and North Sea seawater were used as described in the experimental details of the brine compositions in Chapter 7. The objective of this study was (i) to observe and measure, the formation of PbS and ZnS in the final brine, (ii) likewise to observe/measure the formation of $BaSO_4$ in the brine mixture, (iii) to assess the performance /efficiencies of the SIs for PbS ZnS and BaSO4 in the mixture, and (iv) establish the fate of [Pb], [Zn] and [Ba] in the system with varying concentrations of [SI].

9.6.1 ZnS:PbS (50ppm:50ppm) Mixed Scaling in Moderate Brine Scaling

Figure 9.37 shows the inhibition efficiency of PPCA for $BaSO_4$ and its accompanying visual observations. Note the higher efficiencies of the SI at time 2 hrs is not reflected in the visual observations. Inhibition results show a steady improvement as the [SI] is increased at 2hr while at 22 hours the efficiencies drop, which can be seen as the precipitates have settled to the base of the sample bottles. At 22hrs, the blank samples, 25, 50, 100 and 500ppm samples show a settling/separation of a dark brown precipitate to the base of the bottle.

Also note the yellowish coloration of the 500ppm case at 5minutes after mixing. This coloration may have resulted as a product of the combination of the PbS + ZnS and SI. The precipitate was brown, grainy and looked more like PbS in DW, except lighter in colour.

Figure 9.38 shows the fate of the [Pb^{2+}] in the mixed system with Pb^{2+} showing a steady increase as the [SI] was increased at 2hrs while at 22 hours the measured Pb^{2+} levels in the system have dropped as shown in the figure, which corresponds to visual observations.

Note that the Pb^{2+} drops out with time as shown with the clear solution on top. It is also worth noting that the blank solution is not as dark as when distilled water was used in earlier experiments. At 22hrs, the Blank samples, 25, 50, 100 and 500ppm samples show a settling/separation to the base of the bottle of the formed precipitate.

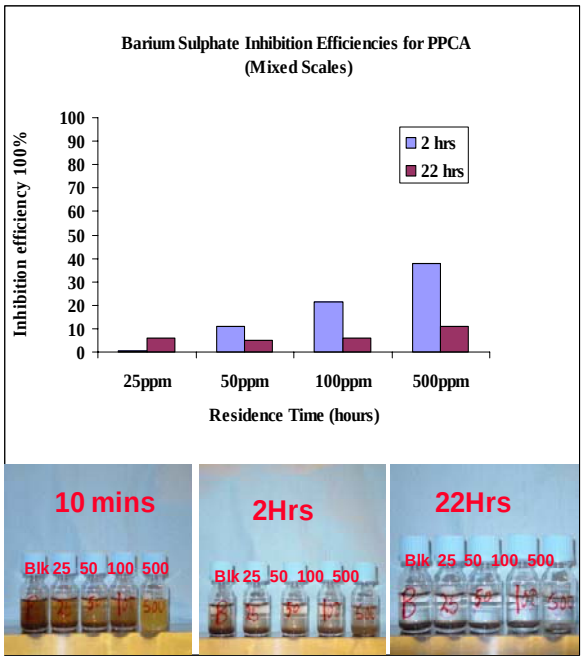

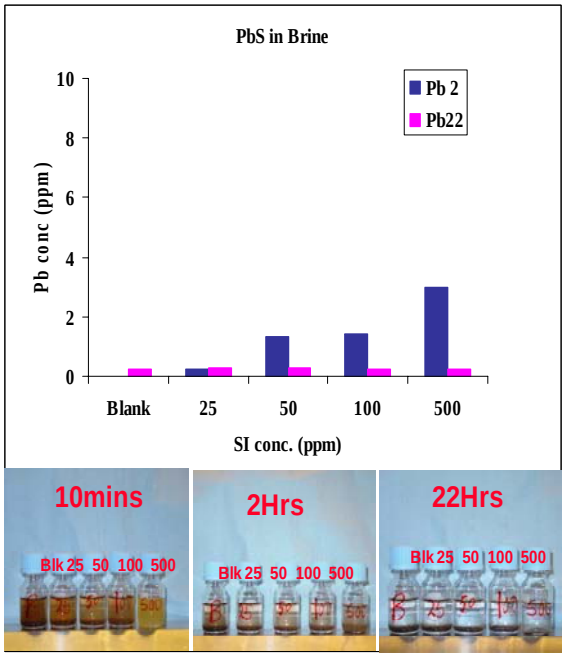

Figure 9.37: I.E% for PPCA in mixed scales. **Figure 9.38**: The fate of [Pb] in the mixed scales

9.6.2 ZnS:PbS (50ppm:50ppm) Mixed Scaling in Moderate Brine with Scaling Increased SI

Figures 9.39 and 9.40 shows the inhibition efficiency of PPCA for $BaSO_4$ and its accompanying visual observations when the [SI] was increased to 500, 750, 1000 and 2000ppm. The yellow coloration noticed in the previous experiment occurred in all of the [SI] samples, but the [2000] turned darker at two hours, probably due to the high [SI]. Note - at 22 hours the solutions clear up with visible precipitate at the base of the bottles as shown in Figures 9.39 and 9.40. Figure 9.40 shows the fate of [Pb] in the mixed system with the Pb^{2+} showing a steady increase as the [SI] was increased at 2hr, while at 22 hours the measured Pb^{2+} in the system started to drop out as shown in the figure and this corresponds to visual observations. At 22 hours, most of the Pb^{2+} can be seen to settle to the base of the bottle forming a rubbery dark brown film. At 22hrs, the

Blank samples, 500 and 750pppm, 1000ppm and 2000ppm samples show a settling/separation to the base of the bottle.

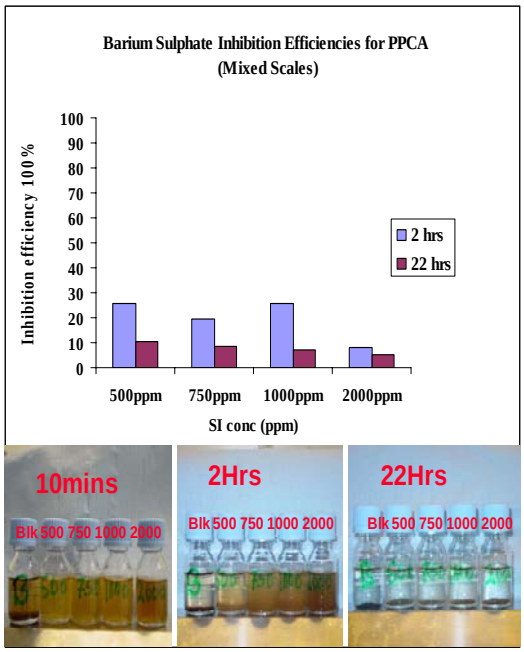

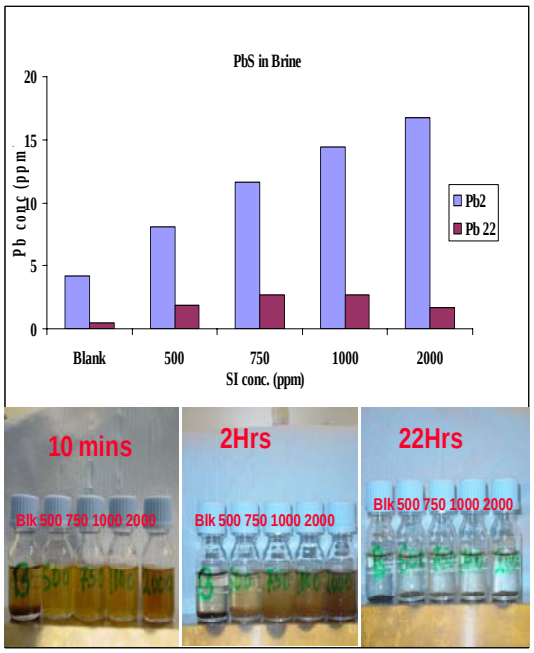

Figure 9.39: I.E% for PPCA in mixed scales. **Figure 9.40**: The fate of [Pb] in the mixed scales

9.6.3 ZnS:PbS (250ppm:50ppm) Mixed Scaling in Moderate Brine Scaling Increased Zn^{2+}

Figure 9.41 shows the inhibition efficiency for the PPCA for $BaSO_4$ and increased Zn^{2+} along with the visual observations and conditions. Note that the inhibition efficiency increased with an increase in [SI] from 500 to 2000ppm for the 2hr time which is higher than the previous experiments shown in Figures 9.37 to 9.40 (equal concentration of $[Zn^{2+}]$ and $[Pb^{2+}]$). We know that PPCA performs particularly well over shorter residence times and it is less significantly affected by brine composition (Boak et al. 2001). Across the board, there is an increase in efficiency at 22hrs compared to the previous experiments. Only the blank sample and the 500ppm samples show a settling/separation to the base of the bottle to form a dark brown precipitate compared to the last experiments. Note that at 22hrs there was a light brown amorphous precipitate which appears at the base of the 500, 1000 and 2000ppm samples. Figure 9.42 shows the fate of [Pb] in the mixed system with the Pb^{2+} showing a steady increase as the

[SI] was increased at 2hr. This also recurs at 22 hours where the measured Pb^{2+} in the system increased as shown in the figure and this also corresponds to visual observations.

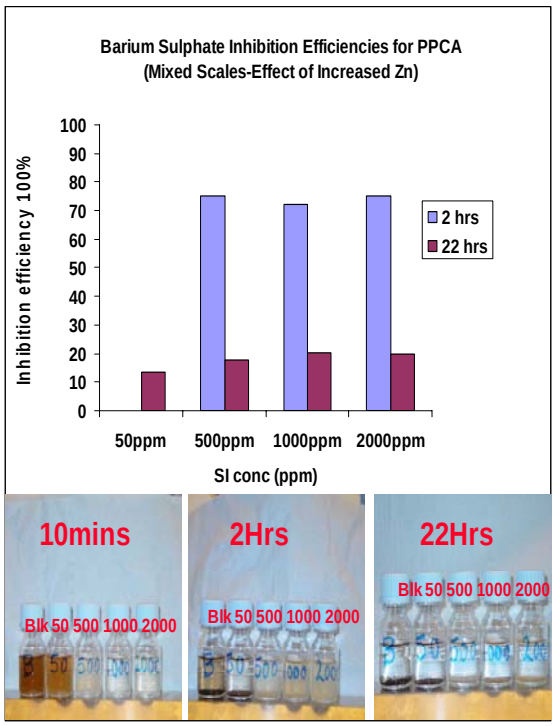

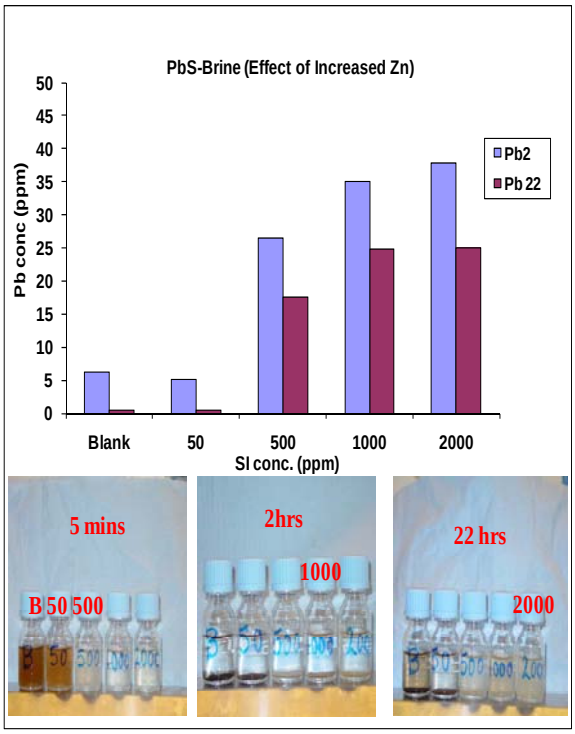

Figure 9.41: I.E% for PPCA in mixed scales. **Figure 9.42**: The fate of [Pb] in the mixed scales.

Figure 9.43 is a comparison of zinc, lead and iron sulphide solubility in a 1M NaCl brine by Collins and Jordan (Collins 2001) the figure shows the sulphides solubilities plotted against pH, it also indicates that ZnS is about 30-100 times more soluble than PbS. The mixed brine is at ~pH 5.72 and using the solubility in this graph the ZnS is more soluble than PbS which implies that PbS should have formed as seen in the previous experiment. This new interference by excess Zn has not to our knowledge previously been reported.

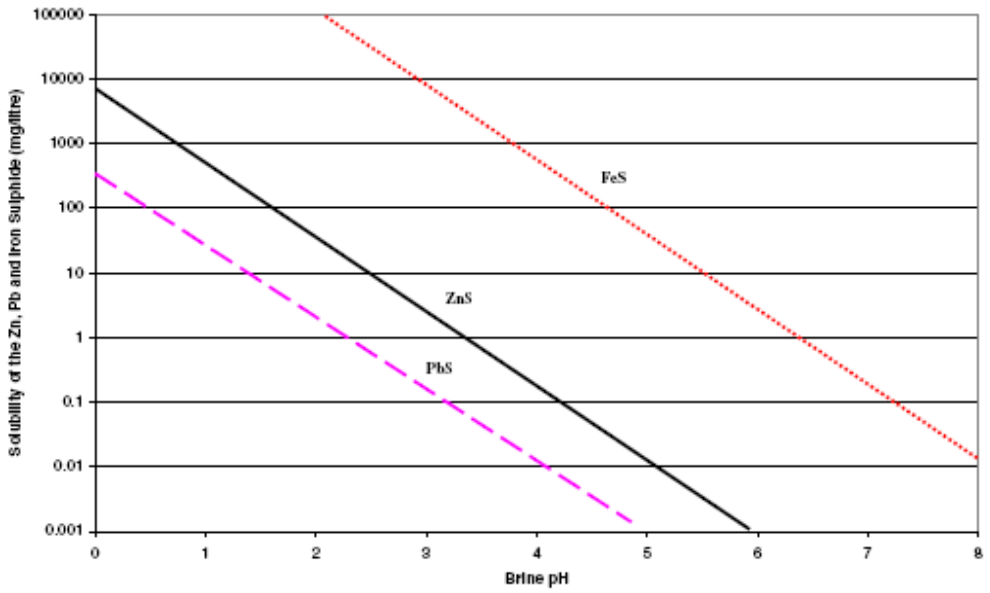

Figure 9.43 Comparison of zinc lead and iron sulphide solubility in 1M NaCl brine at 25°C – from Collins and Jordan (2000)

9.7 Summary

The sulphide loading has an important effect on the formation and inhibition mechanism of the mixed sulphide scales. Mixed sulphide scales (PbS and ZnS) are found to be easier to inhibit that either PbS or ZnS single scales. The resulting mixed scales required less SI to prevent precipitation. The influence of Zn^{2+} ions in enhancing the overall inhibition process is also recognized but the exact mechanism is not certain. This result corroborate what was observed in chapter 6 with Zn^{2+} ions playing a part in causing significant distortions to $BaSO_4$ crystals.

These results enhance our knowledge and understanding of mixed sulphide scales interactions and the role brine compositions on the SI inhibition mechanism.

Chapter 10 Conclusions and Future Work

10.1 Introduction

In this thesis, several aspects of sulphide scale formation are studied and the fundamental aspects of sulphide co-precipitation with both barium sulphate and calcium carbonate scale from bulk solution and on the metal surfaces are addressed. This study has focused on the following issues:

(1) Developing a sulphide scale prediction model that is validated by laboratory experiments.
(2) Development of a modified static bottle technique to study sulphide scale formation and inhibition mechanisms.
(3) The study of the effects of sulphide scales on the morphology of $BaSO_4$ scale formation, and inhibition.
(4) The effects of brine composition (specifically the role of Mg ion) on THPS in sulphide scale inhibition.
(5) The development of dynamic beaker test was used to understand the mechanisms of sulphide scale co-precipitation with calcium carbonate scale formation and inhibition.
(6) Devising an integrated experimental approach by combining a range of techniques such as bulk precipitation, surface deposition, ICP, SEM and EDX which has led to insights into the mechanisms of sulphide scaling co-precipitating with calcium carbonate scale formation and inhibition.

In this chapter, the conclusions are given for each part of this study.

10.2 Sulphide Scale Prediction Model

In Chapter 4, a sulphide prediction model is developed and tested experimentally. The model describes two processes, one involving a simple pH determination and another where full sulphide precipitation occurs. This model was used to investigate the sulphide precipitate mechanisms and a range of sensitive parameters has also been studied, including the fixed pH case. The main conclusions in this chapter are as follows:

i. The pH determination in sulphide systems is well predicted by the sulphide prediction model in that the model predictions agree very well with the experimental results.

ii. The model describes the complete sulphide system from NaS through to H_2S, S^{2-} and HS^-

iii. The model accurately predicts the mass of the sulphide scale precipitated and this agrees with measured experimental results.

iv. The model describes accurately for fixed pH scenarios the role that pH plays in the deposition and inhibition mechanisms.

10.3Modified Static Bottle Test (FeS)

A modified static bottle test technique was developed in conjunction with FeS particle size analysis, to study the formation and inhibition of FeS in Chapter 5. The purpose of this study is to elucidate the impact of the SI (DETPMP and PPCA) on the formation and inhibition of sulphide scales. It was demonstrated that:

i. Three types of visual behaviour were observed as the FeS interacted with the SI and they are be grouped together; as follows:

Behaviour type A - Black solution when scaling waters are mixed and remains black (e.g the blank uninhibited solutions).

Behaviour type B - Black solution when scaling waters are mixed then clarifies within 24 hours.

Behaviour type C - Clear solution when scaling waters are mixed and stays clear.

ii. Low concentrations of ***all*** scale inhibitors were found to significantly affect the particle size of FeS. The FeS is essentially prevented from agglomerating and growing, thus limiting the ability of the FeS to cause blockage and fouling as it passes through the system.

10.4 THPS Study

The mechanism of THPS inhibition was systematically studied in chapter 6 in order to elucidate the optimal conditions for FeS inhibition. THPS does not function as a threshold inhibitor since

high concentrations of THPS are required to inhibit/disperse FeS. Some novel and interesting observations have been made as follows:

i. THPS is more stable in brine than previously reported and is capable of inhibiting FeS for up to three weeks after mixing and exposure to the environment. This result is contrary to reports that THPS blended in brine solutions degrades rapidly (in minutes).

ii. THPS does not suffer from poisoning in the presence of mixed ZnS and PbS scaling, and it is capable of keeping [Fe] in solution. THPS blends tested were not capable of inhibiting ZnS and PbS in a mixed scaling system (it was never intended for this purpose).

iii. Mg^{2+} has a profound effect on the ability of THPS to inhibit FeS and our study demonstrates that THPS is significantly enhanced by the presence of Mg^{2+} which has more effect than any other ion.

10.5 Sulphide Scale Influence on $BaSO_4$ Morphology

In Chapter 7, the effect of sulphide scale on the morphology of conventional barium sulphate was studied using ESEM and EDAX techniques, and this has enabled some interesting aspects of mixed sulphide–sulphate scale inhibition to be elucidated. The important findings from this work are:

i. That there is little interaction between co-precipitating PbS and ZnS and barium sulphate and therefore their inhibition should be “additive” i.e. the barite crystal is unsubstituted (Zn^{2+} or $Pb^{2+)}$ and should still be just as difficult to inhibit;

ii. In contrast, co-precipitation of barite and FeS leads to quite significant interactions in terms of the barite crystal distortion which is observed. This *may*, in some circumstances, lead to a more easily inhibited barite situation.

iii. Scale inhibitors do retain their primary inhibition mechanism in dealing with barium sulphate scales in the presence of FeS, although they can be “poisoned” by the sulphide scales.

10.5 $CaCO_3$ and Sulphide Scale.

The interaction of calcite and sulphide scales was systematically studied in Chapter 8 using a newly developed dynamic/static technique with MVT-type brine compositions. The morphology of the calcite crystals was monitored and any changes to the crystal structure were recorded. The $CaCO_3$ crystals in both the bulk solution and on the metal surface were examined for changes in morphology. The effect of inhibitors on the morphology of the mixed scale was also studied both in the bulk solution and on the metal surface in supersaturated scale solutions at 20°C. This study has enabled some interesting and novel observations to be made, as follows:

i. Most of the $CaCO_3$ crystals are precipitated in bulk solution, rather than on the metal surface when ZnS is co-precipitated with $CaCO_3$. The $CaCO_3$ crystals in the bulk solution are coated with a flocculated ZnS mass.
ii. The $CaCO_3$ crystals formed when PbS is co-precipitated with $CaCO_3$ are distorted and are probably a polymorph of $CaCO_3$. However, in the bulk the $CaCO_3$ crystals are fully developed crystals.
iii. The mixed (MVT) sulphide scale produced less $CaCO_3$ crystals on the metal surface and these crystals were distorted. Most $CaCO_3$ crystals formed in the bulk solution in the presence of a ZnS flocculent mix.
iv. The inhibitor at 3ppm was able to stop metal deposition of $CaCO_3$ crystals in all cases except for the mixed scale (ZnS-PbS) case. $CaCO_3$ was produced in bulk solution for all inhibitor tested cases.

10.6 Mixed Sulphide Scale (ZnS and PbS)

Mixed sulphide scaling of ZnS and PbS is reported in Chapter 9 to be easier to inhibit than ZnS or PbS only scaling. The mixed scales combine to form a complex which makes inhibition easier. MVT-scaling is has been reported in the oil industry as a mixed scale problem, and proprietary inhibitors have been formulated to control it. This study systematically studies both scales (formation and inhibition) individually and in a typical mixed composition. The [SI] concentration needed to inhibit mixed scale is a fraction of what is needed to inhibit a single ZnS or PbS scale.

10.7 Industrial Applications of the Thesis Findings

This thesis has significant industrial applications to oilfield engineers and researchers. The relevance of this work to present day engineers working in the oil and gas industry and researchers in this field are presented as follows.

1. The experimental methods developed and described in this thesis can be confidently employed when selecting SI for a sulphide scale program, it is currently been used to test sulphide scale chemicals/inhibitors that will be used in a North Sea field. The experimental methodologies used to evaluate SI are vital for engineers in the oil and gas industry and other researchers in this field as they depend on being able to use the information from lab trials in assessing the field situations.
2. Reservoir models are developed to simulate the reactions that happen down in the formation and the associated effects it has on oil production and production equipments. The sulphide model developed in this thesis will enhance the ability of engineers in the oil and gas to predict the occurrence and rate of deposition of sulphide scales which is a useful tool in a scale treatment program.
3. SI effect on the particle size of FeS has a profound impact on the way engineers will respond to "black water" to understand the particle size experimental results, we should consider both bulk precipitation and scaling (colloidal) in the treated system. FeS is formed immediately as soon as the two solutions are mixed due to the high super-saturation. The FeS formed in the blank solution has a final particle size about that of coarse sand (~300μm) which could block filters, separators and other production equipment. The treated systems ***look like*** the untreated system but the actual sizes of the colloidal FeS has been greatly reduced from their original size to about ~0.5μm and this is observed for ***all*** the SIs. This reduced particle size should save on equipment downtime and prolong the life of filters ultimately impacting on OPEX.
4. The sulphide-$BaSO_4$/$CaCO_3$ studies give new insight to the mechanisms of sulphide co-precipitation with other conventional scales. In the field, scale co-precipitation occurs frequently, and this study provides new mechanisms which detail unique sulphide-

$BaSO_4$/$CaCO_3$ formation and dissolution mechanism. These insights will provide additional tools in scale treatment program.

5. The dynamic static inhibition studies will be very valuable for oil and gas industry and other researchers because it combines the static beaker test and dynamic tube blocking tests and this gives more information as they simulate scale formation in the reservoir and production equipments. Traditionally, static beaker test and dynamic tube blocking tests have been two separate techniques for inhibitor evaluation. However, they do not give enough data to fully understand the mechanisms of scale formation and inhibition. In this thesis, dynamic beaker tests were used to study sulphide scale formation, which can not only test the inhibition efficiency of scale inhibitors, but also give a novel insight into the mechanisms of scale formation. In the oil and gas industry, the surface deposition and bulk precipitation are in the same system and have correlation between each other. From this study, it was shown that surface deposition and bulk precipitation are two different processes in the same system. To fully understand the mechanism of scale formation in the oil and gas industry, both of them should be studied in the same system.
6. The new sulphide scale mechanisms detailed in this thesis is relevant to oilfield engineers in understanding sulphide scale depositions and responding accordingly. The effect of [Mg] on THPS will provide insights in optimizing THPS for FeS scale control. The enhanced effect described in this thesis is particularly relevant to chemical manufacturers as operators demand long lasting and efficient chemicals.

10.8 Future Work

This thesis has studied several aspects of sulphide scale formation and inhibition to be investigated. New insights into the mechanisms of sulphide scale formation and inhibition are given. However, to fully understand the mechanisms of sulphide scale formation and inhibition in industrial situation, like those experienced in the oil and gas industry is still a challenge. A number of recommendations for future work are listed below.

i. The sulphide model proposed here has been tested at a temperature of 25°C and at atmospheric pressure of 1bar. Higher ranges in temperature and pressure should be validated against the thermodynamic part of the model. However, such tests can only be performed if a HPHT facility is available for the experiments.

ii. Further studies on sulphide formation and inhibition should study the influence of more polymeric and phosphonate sulphide scale inhibitors in the formation of mixed sulphide and calcium carbonate scales and the impact of SI on surface deposition or more solid substrates.

iii. It is recommended that the FeS experiments be carried out in at higher temperatures at [SI] close to those reported in this thesis with Behaviour B (black to clear) and observe the visual changes. Phosphonate base SI used for the study should be compared with polymer or co-polymer SI.

iv. Mg^{2+} has been found to have a profound effect on the THPS blends tested in this thesis. However, all the test caried out with the THPS blends were performed using synthetic brines, and it is recommeneded that selected field brines should be used to test these THPS blends.

v. The impact of sulphides on barite scale was examined in this thesis, and the effect on the morphology of the barite crystals was reported. It is recommended that a study should be carried out to examine the impact on barite scale formation and inhibition when sulphides scales are co-precipitated with barite scale on a metal surface and on other solid substrates.

vi. The effects of mixed sulphide scales of calcite, zinc and lead sulphide was examined both in the bulk and on stainless steel metal surface. It is recommended that the studies conducted in this thesis be repeated using carbon steel to replicate the conditions found in the oil industry.

vii. The brine compositions used in this thesis was below 100,000 TDS. It is recommended that salinity bines of ~250,000 TDS be tested using similar conditions observed in

sulphide scaling fields. The high salinity brine can be tested for a range of conditions including.

- Temperature and pressure effects using HTHP equipments to simulate reservoir conditions, this should include in simulating fluid pressure and temperature history
- The use of dynamic tube blocking rig in elucidating the efficacy of sulphide SIs.
- The use of actual field brine produced with sulphide scale (or sulphide forming ions) and report how the effect of the components in the produce brine will affect particle size reduction reported in this thesis.

viii. It is recommended that the observed "dip" in [Fe] at 10 ppm, reported in Chapter 5 be investigated in a more systematic manner, including;

- A time phased sampling pattern of 10 ppm [SI] at 0, 10, 30, 45, 60, 90, 120, 150 and 180 mins after mix. This sampling pattern should elucidate the "dip" occurring at 10 ppm.
- To further elucidate the dip at 10 ppm, it is recommended that [SI] values on either side of 10 ppm such as 7, 8, 9, 11, 12 ppm be analysed to give a comprehensive picture of the mechanism for this drop in [Fe] values.

APPENDIX A: The Full Sulphide-Iron System and the Na_2s System

In this Appendix, the technical details of the calculation procedure for solving both the full sulphide scaling system and the simpler Na_2S system are given. These will only be of interest to the specialist who either wishes to recode the model or has a very specific interest in such details. It is also useful to archive such details for future researchers who may wish to continue this modelling work.

A.1 The Full Sulphide-Iron System

The sulphide-iron system considered in this work is as follows:

Summary of the Sulphide-Iron Scaling System

Equilibrium Equations		Notation
1. $H_2S_{(aq)} \rightleftarrows H^+ + HS^-$	$K_1 = \frac{x_2.x_3}{x_1}$	$x_1 = [H_2S]_{(aq)}$
$x_1 \quad x_2 \quad x_3$		$x_2 = [H^+]$
2. $HS^- \rightleftarrows H^+ + S^{2-}$	$K_2 = \frac{x_2.x_4}{x_3}$	$x_3 = [HS^-]$
$x_3 \quad x_2 \quad x_4$		$x_4 = [S^{2-}]$
3. $Fe^{2+} + S^{2-} \rightleftarrows FeS_{(s)}$	$K_{sp1} = x_5.x_4$	$x_5 = [Fe^{2+}]$
$x_5 \quad x_4 \quad x_7$		$x_6 = [OH^-]$
4. $H_2O \rightleftarrows H^+ + OH^-$	$K_w = x_2.x_6$	$x_7 = [FeS]_{(s)}$
$x_2 \quad x_6$		

Mass Balances (Sand Fe)

5. *Total Sulphur* (M), $X_S = x_1 + x_3 + x_4 + x_7$

6. *Total Fe* (M), $X_{Fe} = x_5 + x_7$

Charge Balance

7. *Total Charge* (M), $C = x_2 - x_3 - 2x_4 + 2x_5 - x_6$

The above equations can be manipulated algebraically to successively eliminate chosen variables. How this is done is a matter of choice and is usually suggested by the form of the

equations and algebraic convenience but it is elementary mathematics. Through such manipulation of the above equations, we can reduce the set of 7 equations to just 2 equations in x_2 ($[H^+]$) and x_5 ($[Fe^{2+}]$). The two equations to be solved are as follows:

$$F_1(x_2, x_5) = \left[\left(\frac{x_2^2}{x_5} \right) \left(\frac{K_{sp1}}{K_1 K_2} \right) + \left(\frac{x_2}{x_5} \right) \left(\frac{K_{sp1}}{K_2} \right) + \left(\frac{K_{sp1}}{x_5} \right) - x_5 + \left(X_{Fe} - X_S \right) \right] = 0$$

$$F_2(x_2, x_5) = \left[x_2 - \left(\frac{x_2}{x_5} \right) \left(\frac{K_{sp1}}{K_2} \right) - \left(\frac{2K_{sp1}}{x_5} \right) + 2x_5 - \left(\frac{K_w}{x_2} \right) - C \right] = 0$$

The above equations were solved in this work using the Newton-Raphson method, which is an iterative numerical method, and a solved example is shown below for illustration. As a practical point, these equations can often have several roots and generally only one of these is physical (e.g. all negative solution for x_2 ($[H^+]$) and x_5 ($[Fe^{2+}]$) are clearly unphysical). When x_2 and x_5 are found, the other unknowns are calculated by back substitution into the appropriate (eliminated) equations. For example, knowing x_2 and x_5 means that we can use Eq. 3 to obtain x_4 since $x_4 = \left(K_{sp1} / x_5 \right)$ etc.

The example below shows in outline how the sulphide prediction models works for a case where we input the sulphur (S) as $H_2S_{(aq)}$ ([H_2S] = 0.001M or 34.08ppm) and iron as Fe^{2+} ([Fe^{2+}] = 0.03M or 1675.5ppm). The 3 parts of the calculation can be seen as follows:

▲ **Part 1- Input Data** – which consists of the "fixed" data such as equilibrium constants for the system (K_1, K_2, K_{sp1} and K_w) and changing data such as [H_2S] and [Fe^{2+}] (i.e. X_{Fe} and X_S). Some intermediate constants are calculated for convenience which are used in the subsequent calculations in Part 2;

▲ **Part 2 - Iterative Solution** - of the equations $F_1(x_2, x_5) = 0$ and $F_2(x_2, x_5) = 0$ to calculate the primary variables, x_2 ($[H^+]$) and x_5 ($[Fe^{2+}]$). It is clearly seen that the iterations in Part 2 are fully converged in about 14 iterations (see below) and as the

remaining calculations proceed up to iteration 20, no further changes take place. The final [H+] = 6.146910E-06 M (i.e. pH = -$\log_{10}$[H+] = 5.211);

▲ **Part 3 - Back Substitution** - of the converged primary variables, x_2 ($[H^+]$) and x_5 ($[Fe^{2+}]$), is then carried out to calculate the other (eliminated) variables x_1, x_3, x_4, x_6 and x_7. This entire solution vector x_1 to x_7 then defined the equilibrium solution for this sulphide – iron system.

Sulphide model - KSS 15 dec. 2010
UPDATE 7th JAN 2011 - now solving 2 corrected equations for x2 (=[H+]) and x5 (=[Fe2+])

1. INPUT DATA

Equilibrium constants

K1 =	1.632E-08
K2 =	1.000E-17
Ksp1 =	1.290E-19
Kw =	1.000E-14

Initial Input

x10=[H2S]aq=	1.000E-03	M
x50=[Fe2+]aq=	3.000E-02	M

New constants

c1 =	7.90E+05
c2=	1.29E-02
c3 =	1.29E-19
c4=	0.029
c5=	0.06
c6	1.00E-14

34.08 ppm
1675.50 ppm

Notation		Newton Raphson notation
x1 =	[H2S](aq)	
x2=	[H+]	**z1**
x3=	[HS-]	
x4=	[S2-]	
x5=	**[Fe2+]**	**z2**
x6=	[FeS] (s)	

delta = 1.0000E-07

Molecular/Atomic weights

H=	1.0080E+00
S=	3.2064E+01
Fe =	5.5850E+01
H2S	3.4080E+01
HS-	3.3072E+01
FeS=	8.7914E+01

2. MAIN ITERATIVE CALCULATIONS SOLVING ;F1 = 0 AND F2 =0

	x2 = [H+]	x5 = [Fe2+]	F1(z1,z2)	F2(z1,z2)	
	x2=z1	x5=z2			
Iter. no	**z1**	**z2**	**Eff1**	**Eff2**	**pH**
0	1.000000E-07	1.000000E-06	3.819341E-02	-6.128800E-02	7.000
1	5.125856E-06	9.861049E-05	2.401821E-01	-6.046821E-02	5.290
2	2.909921E-04	1.118715E-02	6.001056E+00	-3.767024E-02	3.536
3	3.869516E-04	2.975122E-02	3.977538E+00	-2.783850E-04	3.412
4	1.947742E-04	2.994430E-02	1.000564E+00	-5.442952E-07	3.710
5	9.756878E-05	2.997219E-02	2.501271E-01	-3.907549E-08	4.011
6	4.899467E-05	2.998604E-02	6.231239E-02	-9.711116E-09	4.310
7	2.488333E-05	2.999291E-02	1.533583E-02	-2.474708E-09	4.604
8	1.319836E-05	2.999624E-02	3.599752E-03	-7.252353E-10	4.879
9	8.028907E-06	2.999771E-02	7.043526E-04	-3.000911E-10	5.095
10	6.367140E-06	2.999819E-02	7.277834E-05	-7.855398E-11	5.196
11	6.150712E-06	2.999825E-02	1.234753E-06	-2.088621E-12	5.211
12	6.146911E-06	2.999825E-02	3.868591E-10	-8.326673E-16	5.211
13	6.146910E-06	2.999825E-02	1.967176E-15	0.000000E+00	5.211
14	6.146910E-06	2.999825E-02	0.000000E+00	0.000000E+00	5.211
15	6.146910E-06	2.999825E-02	0.000000E+00	0.000000E+00	5.211
16	6.146910E-06	2.999825E-02	0.000000E+00	0.000000E+00	5.211
17	6.146910E-06	2.999825E-02	0.000000E+00	0.000000E+00	5.211
18	6.146910E-06	2.999825E-02	0.000000E+00	0.000000E+00	5.211
19	6.146910E-06	2.999825E-02	0.000000E+00	0.000000E+00	5.211
20	6.146910E-06	2.999825E-02	0.000000E+00	0.000000E+00	5.211

3. BACK SUBSTITUTION USING SOLVEDxX2 ([H+]) AND x5 ([Fe]) TO FIND REMAINING COMPONENTS

Back Substitution to obtain all species ..

Converged solution z1, z2

z1 = x2			pH	
= [H+]=	6.14691E-06	M	5.21	
z2 = x5				
[Fe2+]=	2.99982E-02	M	1675.40	ppm

Back substitute to obtain ..

x4 ={S2-]	4.30025E-18	M	Total S (M)	
			1.00000E-03	
x3=[HS-]	2.64333E-06	M		
x1=[H2S]	9.95606E-04	M		
x6=[OH-]	1.62683E-09	M		
x7 ={FeS]	1.75098E-06	M		
Mass FeS per Litre =	1.53936E-01	mg		

Sp_FeS = 1.00000E+00 after pptn.
4.07204E+11 before pptn..

A.2 The Na2S System – Solution B

As noted in the main text of this chapter, the actual sulphide blank test is performed by adding a solution of iron ($[Fe^{2+}]$) at a given pH ($[H^{+}]$) – Solution A – to a solution of Na_2S – Solution B. Solution A is simply fixed by adding the appropriate quantity of iron and the solution pH is adjusted; hence, we essentially fix $[Fe^{2+}]$ and $[H^{+}]$ experimentally in Solution A. However, Solution B is made up by adding Na_2S to distilled water (or a brine) and the S^{2-} ions will then re-speciate and the pH will change. Thus, we must calculate the equilibrium composition of Solution B. It was noted in the text that the appropriate subset of the sulphide system for Solution B is as follows:

Summary of the Na_2S System

1. $H_2S_{(aq)} \rightleftarrows H^+ + HS^-$ $\quad K_1 = \frac{x_2.x_3}{x_1}$

   x_1 $\quad x_2 \quad x_3$

2. $HS^- \rightleftarrows H^+ + S^{2-}$ $\quad K_2 = \frac{x_2.x_4}{x_3}$

   x_3 $\quad x_2 \quad x_4$

4. $H_2O \rightleftarrows H^+ + OH^-$ $\quad K_w = x_2.x_6$

   $x_2 \quad x_6$

Mass Balances (Sand Fe)

5. *Total Sulphur* (M), $X_S = x_1 + x_3 + x_4$

Charge Balance

7. *Total Charge* (M), $C = x_2 - x_3 - 2x_4 - x_6$

Similarly to the full sulphide-Fe system, we could choose to solve all of the above 5 equations for the 5 unknowns numerically but again we can reduce the equations by elimination. In this case, it turns out that this set of equations can be reduced to a *single* equation in x_2 only ($[H^+]$) as follows:

$$F_3(x_2) = \left[C - \left(\frac{x_1.K_1}{x_2} \right) + x_2 - \left(\frac{2x_1K_1K_2}{x_2^2} \right) - \frac{K_w}{x_2} \right] = 0$$

$$\textit{where } x_1 = \frac{x_{40}}{\left[1 + \frac{K_1}{x_2} + \frac{K_1K_2}{x_2^2} \right]}$$

Note that, the equation $F_3(x_2) = 0$ depends only on x_2 since x_1 is an explicit function of x_2 as shown above. This single equation for x_2 is easily solved numerically by the Newton-Raphson iterative method, and as before the remaining species are found by back substitution into the other eliminated equations.

A.3 The Fixed pH Sulphide-Iron System

For some purposes, we may wish to ***fix*** the pH in the sulphide system e.g. this may be buffered to a given pH by the reservoir. If we fix the pH, then we basically fix the $[H^+]$t o a given value denoted as $[H^+] = \bar{x}_2$ and the set of sulphide equations becomes the following:

Summary of the Sulphide-Iron Scaling System

Equilibrium Equations		Notation
1. $H_2S_{(aq)} \rightleftharpoons H^+ + HS^-$	$K_1 = \frac{\bar{x}_2.x_3}{x_1}$	$x_1 = [H_2S]_{(aq)}$
$x_1 \quad \bar{x}_2 \quad x_3$		$\bar{x}_2 = [H^+]$ – *now fixed*
2. $HS^- \rightleftharpoons H^+ + S^{2-}$	$K_2 = \frac{\bar{x}_2.x_4}{x_3}$	$x_3 = [HS^-]$
$x_3 \quad \bar{x}_2 \quad x_4$		$x_4 = [S^{2-}]$
3. $Fe^{2+} + S^{2-} \rightleftharpoons FeS_{(s)}$	$K_{sp1} = x_5.x_4$	$x_5 = [Fe^{2+}]$
$x_5 \quad x_4 \quad x_7$		$\bar{x}_6 = [OH^-]$ - *also fixed*
4. $H_2O \rightleftharpoons H^+ + OH^-$	$K_w = \bar{x}_2.\bar{x}_6$	$x_7 = [FeS]_{(s)}$
$\bar{x}_2 \quad \bar{x}_6$		

Mass Balances (Sand Fe)

5. *Total Sulphur* (M), $X_S = x_1 + x_3 + x_4 + x_7$

6. *Total Fe* (M), $X_{Fe} = x_5 + x_7$

Charge Balance

7. *Total Charge* (M), $C = \bar{x}_2 - x_3 - 2x_4 + 2x_5 - \bar{x}_6$

Note that the concentration of hydroxide is also automatically fixed as $[OH^-] = \bar{x}_6 = K_w / \bar{x}_2$ and these two variables are dropped from the above set of equations which is duly reduced. After some algebra, it turns out that the above equations can be reduced by elimination to a *single* equation in the variable $x_1 = [H_2S]_{(aq)}$ as follows:

$$x_1^2\left[1+\frac{K_1}{\overline{x_2}}+\frac{K_1.K_2}{\left(\overline{x_2}\right)^2}\right]+x_1\left[X_{Fe}-X_S\right]-\left[\frac{K_{sp1}.\left(\overline{x_2}\right)^2}{K_1.K_2}\right]=0$$

This is a simple quadratic equation which can be solved explicitly without the need for a numerical solution as in the full sulphide model (with pH as a free variable).

We solve this equation at a range of pH values for the following input data:

	K1 =	**9.632000E-08**	
	K2 =	**1.000000E-17**	
	Ksp1 =	**1.290000E-19**	
	Kw =	**1.000000E-14**	
	X_S =	6.237525E-04	M
	[S2-] =	**2.000000E+01**	ppm
	X_Fe=	8.9526E-05	
	[Fe2+]=	5	ppm
	[H+]=	3.16228E-06	
	pH =	5.5	
Charge			
-	**C =**	not required?	

Varying the pH from 2 to 12 for an initial $[Fe^{2+}]$= 5ppm and $[S^{2-}]$= 20ppm gives the output below. Plotting up the iron concentration gives the results shown in Figure 4.6. It is clear that Fe does not precipitate until the pH is about 6 for this case. This is as expected and we can observe that since there is a molar excess of S, then virtually all the iron is precipitated.

		A, B & C from the quadratic for the fixed					Back substitution..-->				filtered here	
	x2	pH case in notes 01/02/11 (notebook)			Sqrt	Two - roots						
pH	[H+]	A	B	C	(b^2-4ac)	x1=[H2S]aq	x3=[HS-]	x4=[S2-]	x5=[Fe2+]	x5 Fe(ppm)	x7=[Fe](s)
2.0	0.01	1.000010E+00	-5.34227E-04	-1.339286E+01	7.3193E+00	3.659875E+00	3.525191E-05	3.525191E-20	3.659376E+00	5.000000E+00	-3.659286E+00
2.5	0.003162	1.000030E+00	-5.34227E-04	-1.339286E+00	2.3146E+00	1.157525E+00	3.525711E-05	1.114928E-19	1.157026E+00	5.000000E+00	-1.156936E+00
3.0	0.001	1.000096E+00	-5.34227E-04	-1.339286E-01	7.3196E-01	3.662121E-01	3.527355E-05	3.527355E-19	3.657131E-01	5.000000E+00	-3.656236E-01
3.5	0.000316	1.000305E+00	-5.34227E-04	-1.339286E-02	2.3149E-01	1.159772E-01	3.532557E-05	1.117093E-18	1.154783E-01	5.000000E+00	-1.153888E-01
4.0	0.0001	1.000963E+00	-5.34227E-04	-1.339286E-03	7.3230E-02	3.684647E-02	3.549052E-05	3.549052E-18	3.634773E-02	5.000000E+00	-3.625821E-02
4.5	3.16E-05	1.003046E+00	-5.34227E-04	-1.339286E-04	2.3187E-02	1.182454E-02	3.601643E-05	1.138939E-17	1.132633E-02	5.000000E+00	-1.123680E-02
5.0	0.00001	1.009632E+00	-5.34227E-04	-1.339286E-05	7.3738E-03	3.916288E-03	3.772169E-05	3.772169E-17	3.419783E-03	5.000000E+00	-3.330258E-03
5.5	3.16E-06	1.030459E+00	-5.34227E-04	-1.339286E-06	2.4095E-03	1.428360E-03	4.350649E-05	1.375796E-16	9.376391E-04	5.000000E+00	-8.481135E-04
6.0	0.000001	1.096320E+00	-5.34227E-04	-1.339286E-07	9.3419E-04	6.697032E-04	6.450581E-05	6.450581E-16	1.999820E-04	5.000000E+00	-1.104565E-04
6.5	3.16E-07	1.304591E+00	-5.34227E-04	-1.339286E-08	5.9606E-04	4.331960E-04	1.319474E-04	4.172544E-15	3.091639E-05	1.726681E+00	5.860912E-05
7.0	1E-07	1.963200E+00	-5.34227E-04	-1.339286E-09	5.4398E-04	2.746048E-04	2.644993E-04	2.644993E-14	4.877139E-06	2.723882E-01	8.464838E-05
7.5	3.16E-08	4.045906E+00	-5.34227E-04	-1.339286E-10	5.3625E-04	1.322916E-04	4.029478E-04	1.274233E-13	1.012374E-06	5.654109E-02	8.851314E-05
8.0	1E-08	1.063200E+01	-5.34227E-04	-1.339286E-11	5.3476E-04	5.027214E-05	4.842212E-04	4.842212E-13	2.664071E-07	1.487884E-02	8.925911E-05
8.5	3.16E-09	3.145906E+01	-5.34227E-04	-1.339286E-12	5.3438E-04	1.698416E-05	5.173217E-04	1.635915E-12	7.885496E-08	4.404050E-03	8.944666E-05
9.0	1E-09	9.732000E+01	-5.34227E-04	-1.339286E-13	5.3428E-04	5.489636E-06	5.287617E-04	5.287617E-12	2.439662E-08	1.362551E-03	8.950112E-05
9.5	3.16E-10	3.055906E+02	-5.34227E-04	-1.339286E-14	5.3424E-04	1.748204E-06	5.324864E-04	1.683870E-11	7.660924E-09	4.278626E-04	8.951785E-05
10.0	1E-10	9.642001E+02	-5.34227E-04	-1.339286E-15	5.3423E-04	5.540649E-07	5.336753E-04	5.336753E-11	2.417200E-09	1.350006E-04	8.952310E-05
10.5	3.16E-11	3.046907E+03	-5.34227E-04	-1.339286E-16	5.3423E-04	1.753345E-07	5.340522E-04	1.688821E-10	7.638463E-10	4.266081E-05	8.952475E-05
11.0	1E-11	9.633010E+03	-5.34227E-04	-1.339286E-17	5.3423E-04	5.545798E-08	5.341712E-04	5.341712E-10	2.414956E-10	1.348753E-05	8.952527E-05
11.5	3.16E-12	3.046015E+04	-5.34227E-04	-1.339286E-18	5.3423E-04	1.753855E-08	5.342078E-04	1.689313E-09	7.636238E-11	4.264839E-06	8.952544E-05
12.0	1E-12	9.632196E+04	-5.34227E-04	-1.339286E-19	5.3423E-04	5.546264E-09	5.342161E-04	5.342161E-09	2.414753E-11	1.348640E-06	8.952549E-05

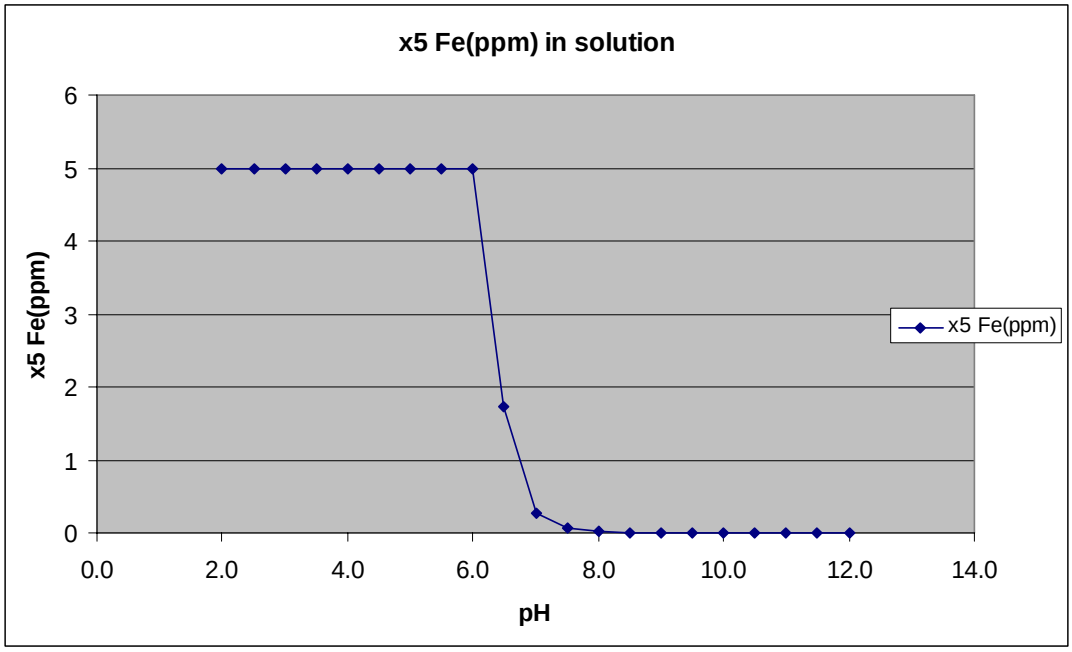

Figure 4.6 Plot of the iron concentration as a function of pH for the data above.

References

Akcil, A., Koldas, S. (2006). "Review article: Acid Mine Drainage (AMD): causes, treatment and case studies." Journal of Cleaner Production **14**: 1139-1145.

Al-Masri, M. S., Aba. A. (2005). "Distribution of scales containing NORM in different oilfields equipment." Applied Radiation and Isotopes **63**(4): 457-463

Alnes, K. F., Rohde, H.C., Vindenes, D., Nordland,K.A., Ramstad, K. (2009). Evaluation of "soft scale" deposits in oilfield process systems. Tekna 20th International oil field chemistry symposium, Geilo

Antonio, M. R., Karet,G.B., Guzowski, J.P. (2000). "Iron chemistry in petroleum production." Fuel **79**: 37-45.

Armstrong, R. D., and Hall, C. A. (1995). "The Corrosion of Metals in Contact with Ester Oils Containing Water at 60 and 150^{o}C." Electrochimica Acta **40**(9): 1135-1147.

Arots, J. B. (1980). "Laboratory Evaluation of Deposit Control Agents Via Heat Transfer in Corrosion Controlled Systems." Materials Performance **19**(1): 28-34.

Bahadori, A. and Zeidani, K. (2006). A New Correlation Predicting the Formation of Iron Sulfide Precipitation in Wastewater Disposal Wells. SPE 8th International Symposium on Oilfield Scale, Aberdeen, Scotland, UK, SPE.

Ball, C. L. and Frenier.,W.W (1984). An Improved Solvent for Iron Sulfide Deposits. New Orleans, LA, NACE.

Barnes, H. L. (1959). Ore solutions: the system ZnS-H2S-H2O., Carnegie Institution of Washington.

Barnes, H. L. (1960). "Sphalerite solubilities in sulfide solutions." Bull. Geol. Soc. Am. **71**(12): 1821.

Barnes, H. L., Helgeson, H. C., Ellis, A. J. (1966). Ionisation Constants in Aqueous Solutions. Handbook of Physical Constants. S.P.Clark**:** 402-413.

Barnes, H. L, and Czamanske, G. K. (1967). Solubilities and transport of ore minerals. In Geochemistry of Hydrothermal Ore Deposits. New York, Holt, Rinehart and Winston.

Barnes, I. and Back, W. (1964). Dolomite Solubility in Ground Water, US Geology Survey**:** D179-D180.

Barnes, I. and Clarke, F. E. (1969). Chemical Properties of Ground Water and Their Corrosion and Encrustation Effects on Wells, US Department of the Interior.

Barrett, T. J., Anderson, G. M. (1982). "The solubility of sphalerite and galena in NaCl brines." Econ. Geol.(77): 1923-1933.

Barrett, T. J., Anderson, G. M. (1988). "The solubility of sphalerite and galena in 1-5m NaCl solutions to 300C." Geochemica et Cosmochica Acta **52**: 813-820.

Bernasconi, P. (1983). lectronique de l'activation et de la dtsactivation de la blende (ZnS) en milieu complexant: influence de potentiel. . Etude ~D.E.A de Chimie Moldculaire, Laboratoire de Chimieet d'l~lectrochimie Analytique, . Nancy University de Nancy

Benning, L. G., Wilkin, R. T and Barnes, H. L. (2000). "Reaction pathways in the Fe-S below 100C,." Chemical Geology **167**: 25-51.

Berner, R. A. (1967). "Thermodynamic stability of sedimentary iron sulfides." Amercan Journal of Science.: 773-785.

Blount, C. W. (1977). "Barite solubilities and thermodynamic quantities up to 3008C and 1400 bars. ." American. Mineral. 62: 942-957.

Boak, L. S., Graham, G. M., Sorbie, K. S. (1999). The Influence of Divalent Cations on the Performance of $BaSO_4$ Scale Inhibitor Species (SPE 50771). SPE International Symposium on Oilfield Chemistry, Houston, Texas, USA, SPE.

Boak, L. S., Graham, G. M., Hobden, C. M (2001). The Effect of a Polymeric and a Phosphonate Scale Inhibitor on the Adherence and Growth of $BaSO_4$ on Hastelloy C276 (A1450, ICCG-13/ICVGE-11). 13th International Conference on Crystal Growth, Japan.

Bourne, H . M. Heath, S. M. Mackay, S. Fraser, J. Stott, L. Muller, S. (2000). Effective Treatment of Subsea Wells with a Solid Scale Inhibitor System (SPE 60207). 2nd International Symposium on Oilfield SCale, Aberdeen, UK, SPE.

Breen, P. J., Diel, B. N., Downs, H. H. (1990). Correlation of Scale Inhibitor Structure with Adsorption Thermodynamics and Performance in Inhibition of Barium Sulphate in Low-pH Environments (SPE 20688). 65th Annual Technical Conference and Exhibition of the SPE, Orleans, LA, SPE.

Campbell, H. S. (1971). "Corrosion, Water Composition and Water Treatment." Proc.Soc.Water Treat. & Exam. **20**: 11-34.

Carney, L. L., Jones, B. (1974). Practical Solutions to Combat the Detrimental Effects of Hydrogen Sulfide During Drilling Operations. SPE Symposium on Sour Gas and Crude, Tyler, Texas, USA.

Carpenter, A. B. (1978). Origin and Chemical Evolution of Brines in Sedimentary Basins. 53rd Annual Fall Technical Conference and Exhibition of the SPE of AIME, Houston, Texas, AIME.

Carpenter, A. B., Trout, M.L., and Pickett, E.E., (1974). "Report on the origin and chemical Evaluation of Lead and Zinc rich oilfield Brines in central Mississippi." Eccological Geology **69**: 1191-1206.

Carroll, J., Mather, A. E. (1989). "The solubility of hydrogen sulfide in water from 0 to 90oC and pressures to 1 MPa." Geochimica et Cosmochimica Acta **53**: 1163-1170.

Chen, T. (2005). New Insight into the Mechanisms of Calcium Carbonate Mineral Scale Formation and Inhibition. Chemical and Process Engineering. Edinburgh, Heriot-Watt University. **Ph.D**.

Chen, T., Neville, A., Yuan, M. (2006). "Influence of Mg^{2+}on the CaCO3 formation -bulk precipitation and surface deposition." Chemical Engineering Science **61**: 5318-5327.

Chen, T., Chen, P., Montgomerie,H., Hagen,T. Jeffrey,C. (2010). Development of test method and Inhibitors for lead sulfide deposited in oil and gas fields. International conference on oilfield scale Aberdeen U.K.

Choi, D.J., You, S.J., Kim, J. G. (2002). "Development of an environmentally safe corrosion, scale, and microorganism inhibitor for open recirculating cooling systems." Materials Science and Engineering **A335**: 228-236.

Collins, I. R., and Jordan, M.M, (2001). Occurance, Prediction and Prevention of Zinc Sulphide Scale within Gulf Coast and North Sea High Temperature/High Salinity Production Wells. International Symposium on Oilfield Scale, Aberdeen, Society of Petroleum Engineers.

DeBerry, D. W. and Viehbeck, A. (1988). "Inhibition of Pitting Corrosion of ASIS 304L Stainless Steel by Surface Active Compounds." Corrosion-NACE **44**(5): 299-305.

Daskalakis, K. D., Helz ,G. R. (1993). " The solubility of sphalerite (ZnS) in sulfidic solutions at 25°C and 1 atm pressure " Geochimica et Cosmochimica Acta **57**(20): 4923-4931.

Day, D. A., Underwood, A. L. (1991). Quantitative Analysis. Englewood Cliffs, NJ, Prentice-Hall.

Deshmukh, R. D., Mather, A.E. (1980). "A mathematical model for equilibrium solubility of hydrogen sulfide and carbon dioxide in aqueous alkanolamine solutions." Chemical Engineering Science,: 355-362.

Douabul, P. A. A., Riley, J. P. (1979). "The solubility of gases in distilled water and seawater - V. hydrogen sulphide." Deep Sea Research **26** (A): 259-268.

Downward, B. L., Talbot, R.E., Haack.T.K. (1997). "A New Biocide With low Environmetal Toxcity " NACE.

Doyle, R. W. (1968). "Identification and solubility of iron sulfide in anaerobic lake sediment." Amercan Journal of Science. **266** 980-984.

Dyer, S. J. (2000). The Influence of Iron on Scale Inhibitor Performance and Carbonate Scale Formation The 11th International Oil Field Chemicals Symposium

Dyer, S. J., Orski, K., Menezes, C., Heath, S., MacPherson, C., Simpson, C., Graham, G. (2006). Development of Appropriate Test Methodologies for the Selection and Application of Lead and Zinc Sulfide Inhibitors for the Elgin/Franklin Field SPE International Oilfield Scale Symposium, Aberdeen, UK, SPE.

Dyer, S. J., Orski, K., Menezes, C., Heath, S., MacPherson, C., Simpson, C., Graham, G. (2006). Prediction and optimisation of Pb/Zn/Fe sulphide scales in gas production fields. 17th International Oil Field Chemistry Symposium, Geilo, Norway.

Dyer, S. Orski. K. Menezes, C, Heath, S., MacPherson, C., Simpson, C., Graham, G.M. (2006). Development of Appropriate Test Methodologies for the Selection and Application of Lead and Zinc Sulfide Inhibitors for the Elgin/Franklin Field SPE International Oilfield Scale Symposium, Aberdeen, UK, SPE.

Edwards, A., Osborne, C. G., Webster, S., Klenerman, D., Ostovar, P., Doyle, M., Joseph, M. (1993). "Mechanistic Studies of the Corrosion Inhibitor Oleic Imidazoline." Corrosion Science **36**(2): 1-13.

Ellis, A. J. and Giggenbach, W. Hydrogen sulfide ionization and sulfur hydrolysis in high temperature solution, Geochim Cosmochim. Acta, 35 (1971) 247-260.

Emmons, D. and Chestnut, G.R. (1998). The Utilization of Hydroxyethylacrylate/arcrylic Acid Copolymer as Zinc sulphide scale inhibitor in oil well production process."

Evans, H. T. (1970). "Lunar troilite: Crystallography. Science **167**: 621-623.

Flaschka, H. A., Barnard, A. J. Jr. and Starrock, P. E. (1980). Quantitative Analytical Chemistry. Boston, MA, Willard Grant Press,

Feitler, H. (1975). Critical pH Scaling Indexes (Paper 144). The International Corrosion Forum Devoted Exclusively to the Protection and Performance of Materials, Toronto, Canada.

Fidoe, S., Talbot. R., Jones, C. (2002). Treatment of Iron Sulphide Deposits. World Intellectual Property Organisation International bureau. W. I. P. O. I. bureau. World wide, Rhodia Consumer Specialities Limited. **PCT/GB01/03139**.

Finan, M. A. Harris, A., Marshall, A. (1980). "The Prevention of Scale and Corrosion in Industrial Cooling Water Systems." Chimia **34**(1): 32-38.

Fleming, N., Stokkan, J. A., Mathisen, A. M., Ramstad, K., Tydal, T. (2003). Maintaining Well Productivity Through Deployment of a Gas Lift Scale Inhibitor: Laboratory and Field Challenges (SPE 80374). 5th SPE Oilfield Scale Symposium, Aberdeen, UK.

Frenier, W., W., and Ziauddin, Murtaza, (2008). Formation, Removal, and Inhibition of Inorganic scale in the oilfield Environment, SPE.

Fu, G., Kan, A. T., Mason, B. T., (2009). Enhanced Effect of Transition Metal Ions on Inhibitor Squeeze Treatments. SPE International Symposium on Oilfield Chemistry.

Garland C.R. (1993). Miller Field: reservoir stratigraphy and its impact on development. . Petroleum Geology of Northwest Europe 4th Conference.Geological Society,, London.

Graham, G. M., L. S. Boak, et al. (1997). The Influence of Formation Calcium on the Effectiveness of Generically Different Barium Sulphate Oilfield Scale Inhibitors (SPE 37273). SPE International Symposium on Oilfield Chemistry, Houston, Texas, USA, SPE.

Giggenbach, W. Optical Spectra of Highly Alkaline Sulfide Solutions and the Second Dissociation Constant of Hydrogen Sulfide, Inorganic Chemistry, 10 (1971) 1333-1338.

Gilbert, P. D., Talbot, R. E., Veale, M. A., Hernandez, K. A. (2002.). Tetrakishydroxymethylphosphonium Sulfate (THPS) For Dissolving Iron Sulfides Downhole And Topside - A Study Of The Chemistry Influencing Dissolution. NACE 2002, Houston Texas.

Giordano, T., H. (2002). "Transport of Pb and Zn by carboxylate complexes in basinal ore fluids and related petroleum-field brines at 100°C: the influence of pH and oxygen fugacity " Geochemical Transactions(3): 56-72.

Glixelli, S. (1907). "Zur theorie der H2S-fa¨llung der metalle. Die einwirkung von schwefelwasserstoff auf zinksalze." Anorganische und Allgemeine Chemie **55**: 297-320.

Godoy, J. M., Carvalho, F., Cordilha,A., Matta, L.E. Godoy, M.L. (2005). "^{210}Pb content in natural gas pipeline residues ("black-powder") and its correlation with the chemical composition." Journal of Environmental Radioactivity **83**(1): 101-111.

Gutjahr, A., H. Dabringhaus, et al. (1996). "Studies of the growth and dissolution kinetics of the CaCO3 polymorphs calcite and aragonite II. The influence of divalent cation additives on the growth and dissolution rates." Journal of Crystal Growth **158**: 310-315.

Giordano, T., H. (2002). "Transport of Pb and Zn by carboxylate complexes in basinal ore fluids and related petroleum-field brines at 100°C: the influence of pH and oxygen fugacity " Geochemical Transactions (3): 56-72.

Graham, G. M., Wattie, I., Mackay, E. J., Boak, L. S. (2001). Examination of the Effect of Generically Different Scale Inhibitor Species (PPCA and DETPMP) on the Adherence and Growth of Barium Sulphate Scale on Metal Surfaces (SPE 68298). 3rd SPE International Symposium on Oilfield Scale, Aberdeen, UK.

Graham, G. M., Sorbie, K. S., Jordan, M. M. (1997). The Influence of Formation Calcium on the Effectiveness of Generically Different Barium Sulphate Oilfield Scale Inhibitors (SPE 37273). SPE International Symposium on Oilfield Chemistry, Houston, Texas, USA, SPE.

Graham, G. M. Frigo, D. M., McCracken, I. R., Graham, G. C., Davidson, W. J., Kapusta, S., Shone, P. (2001). The Influence of Corrosion Inhibitor/ Scale Inhibitor Interference on the Selection of Chemical Treatments Under Harsh (HP/HT/HS) Reservoir Conditions (SPE 68330). SPE International Symposium on Oilfield Scale), Aberdeen, UK.

Graham, G. M., Mackay, E. J. (2002) The Challenges for Scale Control in Deepwater Production Systems: Chemical Inhibition and Placement, Paper No. 02316. Annual Spring Meeting of NACE International, CORROSION/2002, Denver, Colorado.

Graham, G. (1994). A Mechanistic Examination of the Factors Influencing Downhole $BaSO_4$ Oilfield Scale Inhibitors and the Design of New Species. Department of Petroleum Engineering, Heriot-Watt University.

Harmandas, N. G., Navarro Fernandez, E., Koutsoukos, P. G. (1998). "Crystal Growth of Pyrite in Aqueous Solutions. Inhibition by Organophosphorus Compounds." Langmuir (*14*,): 1250-1255.

Harmandas, N. G., Koutsoukos,P. G. (1996). "The formation of iron sulfides in aqueous solutions. Journal of Crystal Growth **167**: 719-724.

Hartman, P., Strom. C. S. (1989). "Structural morphology of crystals with the barite ($BaSO_4$) structure: A revision and extension." Journal of Crystal Growth 97: 502-512.

Hartog, F. A., Jonkers,G., Schmidt, A.P., Schuiling, R.D., (2002). " Lead Deposits in Dutch Natural Gas Systems." Journal SPE Production & Facilities **17**(2): 122-128

Hasson D.B. D., Limoni-Relis B., Semiat R., (1996). " Influence of the flow system on the inhibitor action of CaCO3 scale prevention additives,." Desalination **108,**: 67-79.

Heath, S. M., Samuelsen, E. H., Frederiksen, R. A., Thornton, A. R., Sim, M., Arefjord, A., McAra, E.K. (2009). Downhole Scale Control Through Continuous Injection of Scale Inhibitor in the Water Injection - A Field Case. International Oilfield Chemistry Symposium Geilo, Norway.

Helgeson, H.C. Thermodynamics of hydrothermal systems at elevated temperature and pressures, American Journal of Science 267 (1969) 729-804.

Hitchon, B. (2006). "Lead and zinc in formation waters, Alberta Basin, Canada: Their relation to the Pine Point ore fluid." Applied Geochemistry **21**(1): 109-133

Houot, R., Ravenau, P. (1992). "Activation of sphalerite flotation in the presence of lead ions." International Journal of Mineral processes **35**: 253-271.

Jairo, L., Solares, J. R., Nasr-El-Din, H.A., Franco, C., Garzon, F., Marri, H. M., Aqeel, S.A., Izquierdo, G., (2007). A Systematic Approach To Remove Iron Sulphide Scale: A Case History. SPE Middle East Oil and Gas Show and Conference, Kingdom of Bahrain.

Jefferey, J. C., Odell, B., Stevens, N., Talbot, R. (2000). "Self assembly of a novel water soluble iron(II) macrocyclic phosphine complex from tetrakis(hydroxymethyl)phosphonium

sulfate and iron(II) ammonium sulfate: single crystal X-ray structure of the complex [Fe(H2O)2{RP(CH2N(CH2PR2)CH2)2PR}]SO4·4H2O (R = CH2OH) " Chemical Communication(1): 101-102.

Johnson, D. B., Hallberg, K. B. (2005). " Acid mine drainage remediation options: a review." Science of the Total Environment **3- 14** (338).

Jordan, M. M., Edgerton, M., Mackay, E. J. (1999). Application of Computer Simulation Techniques and Solid Divertor to Improve Inhibitor Squeeze Treatments in Horizontal Wells (SPE 50713). SPE International Symposium on Oilfield Chemistry, Houston, Texas, SPE.

Jordan, M. M., Mackin, K., Johnston, C. J., Feasey, N. D. (2004). Control of Hydrogen Sulphide Scavenger Induced Scale and the Associated Challenge of Sulphide Scale Formation Within a North Sea High Temperature/High Salinity Fields Production Wells. Laboratory Evaluation to Field Application (SPE 87433). SPE 6th International Symposium on Oilfield Scale, Aberdeen, UK.

Jordan, M. M., Collins, I.R (2001). Occurance, Prediction and Prevention of Zinc Sulphide Scale within Gulf Coast and North Sea High Temperature/High Salinity Production Wells. International Symposium on Oilfield Scale, Aberdeen, Society of Petroleum Engineers.

Jordan, M. M., Sjursaether, K., Edgerton, M. C., Bruce, R. (2000). Inhibition of Lead and Zinc Sulphide Scale Deposits formed during Production from High Temperature Oil and Condensate Reservoirs. SPE Asia Pacific Oil and Gas Conference and Exhibition, Brisbane, Australia, SPE.

Jordan, M. M., Collins, I.R (2001). Occurance, Prediction and Prevention of Zinc Sulphide Scale within Gulf Coast and North Sea High Temperature/High Salinity Production Wells. International Symposium on Oilfield Scale, Aberdeen, Society of Petroleum Engineers.

Jordan, M. M., Archibald, I., Donaldson, L., Stevens, K., Kemp, S. (2003). Deployment, Monitoring and Optimization of a Combined Scale/Corrosion Inhibitor Within a Subsea

Facility in the North Sea Basin (SPE 80214). SPE International Symposium on Oilfield Chemistry, Houston, Texas, USA.

Jones, E. N. (1951). "Corrosion and Scale Control." World Oil: 204, 208, 210.

Kelland, M. (2009). Production chemicals for the gas and oil industry. New York, CRC press.

Kaplan, R., I (1992). Scale Deposition Inhibitor. United States, United States. **5,171,459**.

Kharaka, Y. K. (1986). Origin and evolution of water and solutes in sedimentary basins, in Hydrogeology of Sedimentary Basins: Applications to Exploration and Exploitation. Third Canadian/American Conference on Hydrogeology., Dublin, National Water Well Association.

Kharaka, Y. K., Maest, A. S., Carothers, W. W., Law, L. M., Lamothe, P. J., Fries, T. L. (1987). "Geochemistry of metal-rich brines from central Mississippi Salt Dome Basin, USA." Appl. Geochem.(2): 543-561.

Kharaka, Y. K., Maest, A. S., Fries, T. A., Law, L. M., Carothers, W. W., (1986). Geochemistry of Pb and Zn in oil field brines: Central Mississippi Salt Dome Basin revisited. Conference on Genesis of Stratiform Sediment-Hosted Pb-Zn Deposits, Stanford Stanford University.

Kharaka, Y. K. and M. S. Lico (1979). Corrosion and Scale-Formation Properties of Geopressurised Geothermal Waters from the Northern Gluf of Mexico Basin (SPE 7866). SPE of AIME International Symposium on Oilfield and Geothermal Chemistry, Houston, Texas, USA.

Kharaka, Y. K. (1986). Origin and evolution of water and solutes in sedimentary basins, in Hydrogeology of Sedimentary Basins: Applications to Exploration and Exploitation. Third Canadian/American Conference on Hydrogeology., Dublin, National Water Well Association.

Kharaka, Y. K., Maest, A. S., Carothers, W. W., Law, L. M., Lamothe, P. J., Fries, T. L. (1987). "Geochemistry of metal-rich brines from central Mississippi Salt Dome Basin, USA." Appl. Geochem.(2): 543-561.

Kharaka, Y. K., Maest, A. S., Fries,T. A., Law, L. M., Carothers, W. W., (1986). Geochemistry of Pb and Zn in oil field brines: Central Mississippi Salt Dome Basin revisited. Conference on Genesis of Stratiform Sediment-Hosted Pb-Zn Deposits, Stanford Stanford University.

Kostov, I. (1982). "Sulfide Minerals: Crystal Chemistry, Parageneses and Systematics." Inst. Geo: pp. 11-31.

Laing, N. (2006). The Performance and Mechanisms of Selected Barium Sulphate Scale Inhibitors under Various Conditions of Brine Composition and Temperature. Petroleum Engineering. Edinburgh, Heriot-Watt University. **Ph.D.** .

Leach, D. L., Bradley, D.C., Lewchuck, M., Symons, D.T.A., Brannon J., and De Miirsily, G., (2001). " Mississippi Valley-type lead-zinc deposits through geological time: Implications from recent age-dating research. ." Mineralium *Deposita* **39**: 711-740.

Leach, D. L., Sangster, D.F. (1993). "Mississippi Valley-type lead-zinc deposits." Geological Association of Canada Special Paper(40): 289-314. .

Lee, K. J. (2004). A Mechanistic modelling of CO_2 corrosion of mild steel in the presnce of H_2S. Fritz J. Dolores H. Russ college of Engineering and Technology Ohio, University of Ohio. **PhD**.

Lewis, A. E. (2010). "Review of metal sulphide precipitation." Hydrometallurgy **104**(2): 222-234.

Leach, D. L., Bradley, D.C., Lewchuck, M., Symons, D.T.A., Brannon J., and De Miirsily, G., (2001). " Mississippi Valley-type lead-zinc deposits through geological time: Implications from recent age-dating research. ." Mineralium *Deposita* **39**: 711-740.

Leach, D. L., Sangster, D.F. (1993). "Mississippi Valley-type lead-zinc deposits." Geological Association of Canada Special Paper(40): 289-314. .

Lee, K. J. (2004). A Mechanistic modelling of CO_2 corrosion of mild steel in the presnce of H_2S. Fritz J. Dolores H. Russ college of Engineering and Technology Ohio, University of Ohio. **PhD**.

Lehmann, M., Firouzkouhi,F. (2008). A New Chemical Treatment to inhibit Iron sulphide Deposition. SPE International Oilfield Scale Conference Aberdeen 2008, SPE.

Lopez, T. H., Yuan, M., Williamson, D.A., Przbylinski, J.L. (2005). Comparing Efficacy of scale inhibitors for Inhibition of zinc sulfide and lead sulfide scales. SPE international Symposium on oilfield scale Aberdeen.

Lu, J. (2008). CO2 interaction with aquifer and seal on geological timescales: the Miller oilfield, UK North Sea. Department of Geoscience Edinburgh, University of Edinburgh. **PhD:** 200.

Luther, G. W. (1991). "Pyrite synthesis via polysulfide compounds. ." Geochimica et Cosmochimica Acta **55** (10): 2839-2849.

Luther III, G. W., Theberge, S.M., Rickard, D.T. (1999). "Evidence for aqueous clusters as intermediates during zinc sulfide formation." Geochimica et Cosmochimica Acta **63**(19-20): 3159-3169

Mackay, E. J., I. R. Collins, et al. (2003). PWRI: Scale Formation Risk Assessment and Management (SPE 80385). 5th SPE International Symposium on Oilfield Scale, Aberdeen, UK.

Matlock, M. M., Howerton, B. S., Atwood, D. A. (2002). "Chemical precipitation of heavy metals from acid mine drainage." Water Research **36**: 4757-4764.

Mougin, P., Lamoureux-Var, V., Bariteau, A., Huc, A.,Y. (2007). "Thermodynamic of thermochemical sulphate reduction." Journal of Petroleum Science and Engineering **58** 413-427.

Malandrino, A., M. D. Yuan, et al. (1995). Mechanistic Study and Modelling of Precipitation Scale Inhibitor Squeeze Problems (SPE 29001). SPE International Symposium on Oilfield Chemistry, San Antonio, Texas, USA.

Mannhardt, K., L. L. Schramm, et al. (1990). Effect of Rock Type and Brine Composition on Adsorption of Two Foam-Forming Surfactants. 65th Annual Technical Conference and Exhibition of the SPE, New Orleans, LA, SPE.

Meyer, F. H., Riggs, O.L., .McGlasson, R.L., Sudbury, J.D., (1958). "Corrosion of mild steel in H_2S environments." Corrosion **14**: 109.

McRae, J. A., S. M. Heath, et al. (2004). Development of a degradable, solid scale inhibitor and it's application in a low pressure, sub-sea well. 15th International Oil Field Chemistry Symposium, Geilo, Norway.

Misra, K. C. (1999). Understanding mineral deposits. Boston, Academic Publishers.

Morse, J. W., Millero,F. J., Cornwell,J. C. and Richard,D. T. (1987). "he chemistry of the hydrogen sulfide and iron sulfide systems in natural waters." Earth Science Reviews **24**: 1-42.

Misra, K. C. (1999). Understanding mineral deposits. Boston, Academic Publishers.

Naona, H. (1967). "The Effect of Triphosphate on the Crystallisation of Strontium Sulfate." Bull. Chem. Soc. Japan **40**: 1104-1110.

Nasr-El-Din, H., A., Al-Humaidan, A., Y. (2001). Iron Sulphide Scale: Formation, Removal and Prevention. International Symposium on Olifield Scale SPE. Aberdeen U.K, SPE.

Nasr-El-Din, H., A., Al-Humaidan, A., Y. (2001). Iron Sulphide Scale: Formation, Removal and Prevention. International Symposium on Olifield Scale SPE. Aberdeen U.K, SPE.

Nasr-El-Din, H. A., Al-Humaidan, A., Mohammed, S.K., Salman, A. (2001). Iron Sulfide Scale Formation in Water Supply Wells with Gas Lift. SPE Oilfield Chemistry. SPE. Houston, TX,, SPE.

Nyborg, R. (2003). "Corrosion Control in Oil and Gas Pipelines." The Oil and Gas Review 2003 **2**: 79-82.

Oriski, K., Grimbert, B., Menezes, C., Quin, E. (2007). Fighting Lead and Zinc Sulphide Scales on a North Sea HP/HT Field. European Formation Damage Conference, Scheveningen The Nertherlands, SPE.

Okocha, C., Sorbie, K.S., and Boak, L.S. (2008) Inhibition Mechanisms for Sulphide Scales. SPE International Symposium and Exhibition on Formation Damage Control, Lafayette, Louisiana, U.S.A., 13–15 February 2008.

Okocha, C. and Sorbie, K. S. (2010) Effects of sulphide scales (PbS, ZnS & FeS) on $BaSO_4$ Crystal growth and dissolution. SPE International conference on oilfield scale, Aberdeen, U.K 26-27 May 2010.

Patrick, R. A. D., Charnock, J.M., England, K,E.R ,Mosselmans, J.F.W., Wright, K. (1998). "Lead sortion on the surface of ZnS with relevance to flotation: A flourence reflex AFS study " Minerals Engineering **11**(11): 1025-1033.

Peters, R. W., Ku, Y. (1985). " Batch precipitation studies for heavy metal removal by sulphide precipitation." AIChE Symposium Series **243**(81): 9-27.

Peters, R. W., Ku, Y., Chang, T.K. (1984). "Heavy metal crystallization kinetics in an MSMPR crystallizer employing sulphide precipitation." AIChE Symposium Series-Advances in Crystallization from Solutions **240**(80): 55-75.

Poggesi, G., Hurtevent, C., Brazy, J. L. (2001). Scale Inhibitor Injection Via the Gas Lift System in High Temperature Block 3 Fields in Angola. International Symposium on Oilfield Scale, Aberdeen, United Kingdom, Society of Petroleum Engineers.

Przybylinski, J. L. (2001). Iron sulfide scale deposit formation and prevention under Anaerobic conditions typically found in the oil field (SPE65030). SPE Internation symposium Houston, Texas, SPE.

Przybylinski, J. L. (2003). Ferrous Sulfide Solid Formation and Inhibition at Oxidation-Reduction Potentials and Scaling Indices Like Those That Occur in the Oil Field (SPE 80260). SPE International Symposium on Oilfield Chemistry, Houston, Texas, USA.

Rakovan, J. (2006). "Mississippi Valley-Type Deposits." Rocks & Minerals **8**(1).

Ragulin, V. V., A. Mikhailov, et al. (2004). Scale Management of Production Wells via Inhibitor Application in Supporting Injection Wells (SPE 87462). SPE 6th International Symposium on Oilfield Scale, Aberdeen, UK.

Rakovan, J. (2006). "Mississippi Valley-Type Deposits." Rocks & Minerals **8**(1).

Ramsay Jr., H. J. (1964). "Use of Carbon Dioxide for Water Injectivity Improvement." Journal Journal of Petroleum Technology **16**.

Ramsdell, L. S. (1925). "The crystal structures of some metallic sulfides." American Mineralogist **10**: 281-304.

Rickard, D. (1974). "Kinetics and mechanism of the sulfidation of goethite." American Journal of Science **274**: 941- 952.

Rickard, D., Morse,J. W. (2005). "Acid volatile sulfide (AVS)." Marine Chemistry **97**: 141-197.

Rickard, D. T. (1969). "The chemistry of iron sulfide formation at low temperatures." Stockholm Cont. Geology **20**: 67-95.

Rickard, D. T. (1975). " Kinetics and mechanisms of pyrite formation at low temperatures." American Journal of Science **275**: 636-652.

Rickard, D. (1995). "Kinetics of FeS precipitation: part 1. competing reaction mechanisms." Geochimica et Cosmochimica Acta. **59**: 4367-4379.

Rickard, D., Butler,I. B., Oldroyd, A. (2001). "A novel iron sulphide mineral switch and its implications for Earth and planetary science." Earth and Planetary Science Letters **189** 85-91.

Rincon, P. R., McKee,J.P.,Tarazon,C.A., Guevera,L.A. (2004). Biocide Stimulation in oilwells for downhole corrosion and control and increasing production Ist International Symposium on oilfield corrosion Aberdeen United Kingdom, SPE.

Roberts, B. E. (1985). "Vapor liquid equilibrium calculations for dilute aqueous solutions of CO2, H2S, NH3 and NaOH to 300oC." The Canadian Journal of Chemical Engineering, **63**: 294-300.

Ronngren, L., Sjoberg,S., Sun, Z. (1993). "Surface reactions of Sulfide Ions at the ZnS-H_2O and PbS-H_2O Interfaces." Colliods and Interface Science **162**: 227-235.

Salma, T. (2000). Cost effective removal of Iron sulphide and hyrdgen sulphide from water using Acrolein. SPE Permian Basin oil and gas recovery Midland Texas, SPE.

Sangster, D. F. (1995). Mississippi Valley-type lead-zinc In *Geology of Canadian mineral deposit types*. Ottawa, Geological Survey of Canada.

Sanghvi, G. J., D. A. Garcia, et al. (2003). Large Scale Laboratory Investigation of Corrosion Inhibitor Containing Emulsion Placement in Wells (SPE 80215). SPE International Symposium on Oilfield Chemistry, Houston, Texas, USA.

Saurbier, K., J. W. Schultze, et al. (1994). "Temporary Inhibitors of Corrosion in Wet Atmosphere: Electrochemical Investigations of the Mechanism and Efficiency." Electrochimica Acta **39**(8/9): 1171-1178.

Schoonen, M. A. A., Barnes, H. L. (1991). "Reactions forming pyrite and marcasite from solution: II. Via FeS precursors below 100°C " Geochimica et Cosmochimica Acta **55**(6): 1505-1514.

Sekine, I., M. Sanbongi, et al. (1992). "Corrosion Inhibtion of Mild Steel by Cationic and Anionic Polymers in Cooling Water System." J.Electrochem.Soc **139**(11): 3167-3173.

Shoesmith, D. W., Taylor, P., Bailey, M.G., Owen, D.G. (1980). "The formation of ferrous monosulfide polymorphs during the corrosion of iron by aqueous hydrogen sulfide at 21C. ." Journal of the Electrochemical Society **127**: 1007-1015.

Skinner, B. J. (1961). "Unit-cell edges of natural and synthetic sphalerites." American Mineralogist **46**: 1399-1411.

Simpson, C. M. E., R. Stalker, et al. (2004). CO_2 Corrosion Inhibitor Performance Measurements in OIW Emulsion Systems - Importance of Test Methodology for Effective Inhibitor Ranking. 15th International Oil Field Chemistry Symposium, Geilo, Norway.

Sohnel, O., Garside J. (1992). Precipitation, Basic principles and industrial application. , Butterworth/Heineman.

Sorbie, K. S., G. M. Graham, et al. (2000). How Scale Inhibitors Work and How this Affects Test Methodology. 4th Chemistry in Industry Conference & Exhibition, Bahrain.

Sorbie, K. S., P. Jiang, et al. (1993). The Effect of pH, Calcium, and Temperature on the Adsorption of Phosphonate Inhibitor Onto Consolidated and Crushed Sandstone (SPE 26605). 68th Annual Technical Conference and Exhibition of the SPE, Houston, Texas.

Sorbie, K. S. and E. J. Mackay (2007). Oilfield Scale Management in the 21st Century. 7th International Conference and Exhibition on Chemistry in Industry, Manama, Bahrain.

Sorbie, K. S. (1991). The Improved Design of Scale Inhibitor Squeeze Treatments. Water Management Offshore Conference, Aberdeen.

Sorbie, K. S., G. M. Graham, et al. (2000). How Scale Inhibitors Work and How this Affects Test Methodology. 4th Chemistry in Industry Conference & Exhibition, Bahrain.

Sorbie, K. S., M. M. Jordan, et al. (1995). Scale Inhibitor Treatments in Horizontal Wells. IBC Ltd Conference, "Solving Oilfield Scaling Problems", Aberdeen, Scotland.

Sorbie, K. S., Wat, R. M. S.,Todd, A. C., McClosky, T (1991). Derivation of Scale Inhibitors Adsorption Isotherms for Oil Reservoir Squeeze Treatments. Royal Society of Chemistry Symposium: Session "Chemicals in the Oil Industry", Imperial College, London, RSC.

Sorbie, K. S., M. D. Yuan, et al. (1992). Appropriate Laboratory Evaluation of Oilfield Scale Inhibitors. Advances in Solving Oilfield Scaling Problems, Aberdeen, UK.

Suleimenov, O. M., Krupp, R. E. (1994). "Solubility of hydrogen sulfide in pure water and in NaCl solutions, from 20 to 320oC and at saturation pressures. ." Geochimica et Cosmochimica Acta **58**: 2433-2444.

Suleimenov, O. M., Seward, T. M. (1997). "A spectrophotometric study of hydrogen sulfide ionization in aqueous solutions to 350oC." Geochimica et Cosmochimica Acta Chemica Scandinavica **61** 5187-5198.

Tagirov, B. R., Seward, T.M. (2010). " Hydrosulfide/Sulfide complexes of zinc to 250 C and the thermodynamic properties of sphalerite." Chemical Geology **269**: 301-311.

Tagirov, B. R., Suleimenov, O.M., Seward, T.M. (2007). "Zinc complexation in aqueous sulphide solutions: determination of the stoichiometry and stability of complexes via ZnS(cr) solubility measurements at 100 °C and 150 bars." Geochim. Cosmochim. Acta **71**: 4942-4953.

Talbot, R., Jones, C. (2005). Syenergistic compositions World Intellectual Property Organisation International Bureau. W. I. P. O. I. Bureau. world wide, Rhodia Consumer Specialities Limited. **PCT/GB2005/000373**.

Taylor, K. C., A. H. Al-Ghamdi, et al. (2003). Effect of Rock Type and Acidizing Additives on Acid Reaction Rates Using the Rotating Disk Instrument (SPE 80256). SPE International Symposium on Oilfield Chemistry, Houston, Texas, USA.

Van Den Leeden, M.,C., G. M. V. R. (1995). "Adsorption behavior of polyelectrolytes on barium sulfate crystals " Colloid and Interface Science 171: 142-149.

Vaughan, D. J. (2005). Sulphides. Minerals Mancahester, Elsevier**:** 574-586.

Videla, H. A. (2002). "Prevention and control of biocorrosion " International Biodeterioration & Biodegradation **49**(4): 259-270.

Vorholz, J., Rumpf, B., Maurer, G. (2002). "Prediction of the vapor-liquid phase equilibrium of hydrogen sulfide and the binary system water-hydrogen sulfide by molecular simulation." Physical Chemistry 4449-4457.

Wang, K.-S., Y. Tang, et al. (2002). Effects of Scale Dissolvers on Barium Sulfate Deposits: A Macroscopic and Microscopic Study. NACE International Conference/CORROSION2002.

Wei, S. (2006). KINETICS OF IRON CARBONATE AND IRON SULFIDE SCALE FORMATION IN CO2/H2S CORROSION. Russ College of Engineering and Technology of Ohio University, Ohio University. **PhD**.

Weiss, R. F. (1970). "The solubility of nitrogen, oxygen and argon in water and seawater." Deep Sea Research **17**: 721-735.

WHO (2000). "Flame Retardants." http://www.inchem.org/documents/ehc/ehc/ehc218.htm,

Worden, R. H., Manning, D.A.C., Lythgoe, P.R (2000). "The origin and production geochemistry of radioactive lead (210Pb) in NORM-contaminated formation waters " Journal of Geochemical Exploration **69-70**: 695-699

Xu, Y. N., Ching, W. Y. (1993). "Electronic, optical, and structural properties of some wurtzite crystals." Physical Review **48**(B): 4335-4351.

Yuan, M. D., Jamieson, E., et al. (1998). Investigation of Scaling and Inhibition Mechanisms and The Influencing Factors in Static and Dynamic Inhibition Tests. NACE Annual Conference and Exposition: Corrosion 98, San Diego, California, USA.

Zhang, Y. and Dawe, R. A. (2000). "Influence of Mg^{2+} on the kinetics of calcite preciptiation and calcite crystal morphology." Chemical Geology **13**: 129-138.

Zhao, K., Wen, T., Gu, T., Kopliku, A., Cruz, I. (2008). "Mechanistic Modeling of Anaerobic THPS Degradation in seawater under various conditions." NACE.